Modelling and Analysis of Transient Temperature in Gas Reservoir-Well Systems

Akindolu Oluwakanyinsola Dada

Submitted for the degree of Doctor of Philosophy

Heriot-Watt University
School of Energy Geoscience Infrastructure and Society
Institute of Petroleum Engineering

August, 2018

Abstract

The need for more efficient production operations has resulted in a push for greater control and monitoring of wells and reservoirs. This need along with the development of better downhole sensors has resulted in the availability of vast amounts of downhole data. However, data analysis methods have not developed at the same pace as data acquisition, resulting in large amounts of operational data that are left in data silos and never used for any value added activity.

Transient pressure and temperature are one of the most commonly measured downhole parameters, and have been proven to be quite valuable. For a long time transient pressure has been used for reservoir characterization and near wellbore analysis, however, transient temperature data has been demonstrated to quite valuable as well, in that it can be used to characterize a formation, provide more detailed near-wellbore analysis and also discriminate between produced fluids. While pressure transient analysis (PTA) methods are quite mature, the same cannot be said of temperature transient analysis (TTA). The major advancements in TTA methods occurred over the last two decades, but have mostly been for slightly compressible fluids. This leaves a knowledge gap, in the area of TTA for gases (i.e. highly compressible fluids) and this work focuses on this.

This thesis presents novel transient sandface temperature solutions and methods for analysing the measured transient temperature. Further, since the transient temperature is rarely measured at the mid-perforation point, but at some distance from the mid perforation point, it has to be corrected for the effect of heat transmission in the wellbore before applying the sandface temperature analysis methods. A method for correcting the measured gauge temperature (a process called sandface temperature reconstruction) was presented as well. These methods developed for sandface temperature reconstruction and for analysing the resulting reconstructed sandface temperature were developed for gas producing wells. However, in certain situations these methods can also be applied to liquid producing wells.

The combination of the developed sandface TTA methods (for gases) with methods for handling the distant gauge problem makes TTA applicable to a wide range of wells, let alone this can further be combined with the existing liquid TTA methods for a robust multiphase TTA methodology.

Dedication

This work is dedicated to the glory of God and the benefit of mankind

Acknowledgement

I want to express my sincere gratitude to all those who have contributed to the success of my doctoral programme.

I sincerely appreciate my supervisors Dr. Khafiz Muradov and Prof. David Davies, thank you for betting on my abilities and hiring me for this position despite having no prior training or experience in petroleum engineering, and for supporting me all through the programme. I hope I didn't let you down. I also thank Dr. Kokou Dadzie for his support while developing the vertical well temperature solution.

I appreciate the support of the sponsors of the Value from Advanced Wells (VAWE) Joint Industry Project (JIP), for providing financial support, data, and valuable discussions and suggestions throughout my programme.

I am grateful to the developers of OpenFOAM and the entire community of users for making the source codes, documentation and an extensive knowledgebase available.

I thank my colleagues, members of the VAWE JIP at Heriot-Watt for valuable discussions and my former classmates, students of the year 2000 graduating set of LSMCM for emotional support, by providing a place to relax from the "stress" of research. I also appreciate the efforts of Hong Wang, for discovering the limitations of the analytical wellbore model inversion.

Finally I thank my parents Mr and Mrs Dada for teaching me the value of hard-work, and their unflinching support and encouragement. None of these would have been possible without your support.

ACADEMIC REGISTRY
Research Thesis Submission

Name*:*	Akindolu Oluwakanyinsola Dada		
School/PGI:	Energy Geoscience Infrastructure and Society/ Institute of Petroleum Engineering		
Version: *(i.e. First, Resubmission, Final)*	Final	Degree Sought (Award and Subject area)	PhD in Petroleum Engineering

Declaration

In accordance with the appropriate regulations I hereby submit my thesis and I declare that:

1) The thesis embodies the results of my own work and has been composed by myself
2) Where appropriate, I have made acknowledgement of the work of others and have made reference to work carried out in collaboration with other persons
3) The thesis is the correct version of the thesis for submission and is the same version as any electronic versions submitted*.
4) My thesis for the award referred to, deposited in the Heriot-Watt University Library, should be made available for loan or photocopying and be available via the Institutional Repository, subject to such conditions as the Librarian may require
5) I understand that as a student of the University I am required to abide by the Regulations of the University and to conform to its discipline.

* *Please note that it is the responsibility of the candidate to ensure that the correct version of the thesis is submitted.*

Signature of Candidate*:*		Date:	

Submission

Submitted By *(name in capitals):*	
Signature of Individual Submitting:	
Date Submitted:	

For Completion in the Student Service Centre (SSC)

Received in the SSC by *(name in capitals):*			
1.1 Method of Submission (Handed in to SSC; posted through internal/external mail):			
1.2 E-thesis Submitted (mandatory for final theses)			
Signature:		Date:	

Table of Contents

Publications by the Candidate

Journal Papers

1. Akindolu Dada., Khafiz Muradov., Kokou Dadzie & David Davies. Numerical and analytical modelling of sandface temperature in a dry gas producing well. Journal of Natural Gas Science and Engineering Volume 40, Pages 189-207.

2. Akindolu Dada., Khafiz Muradov & David Davies. Temperature transient analysis models and workflows for vertical dry gas wells. Journal of Natural Gas Science and Engineering Volume 45, pages 207-229.

Conference Papers

1. Akindolu Dada., Khafiz Muradov & David Davies. Novel Solutions and Interpretation Methods for Transient, Sandface Temperature in Vertical, Dry Gas Producing Wells. SPE Intelligent Energy International Conference and Exhibition September 2016.

2. Akindolu Dada., Khafiz Muradov & David Davies. Transient, Sandface Temperature Solutions for Horizontal Wells Producing Dry Gas. EAGE St Petersburg 2018 Conference, April 2018.

3. Akindolu Dada., Khafiz Muradov., Hong Wang., Ehsan Nikjoo., Edsson Villarreal & David Davies. Mitigation of the Remote Gauge Problem in Temperature Transient Analysis. SPE Europec featured at 80th EAGE Annual Conference & Exhibition, June 2018

Chapter 1: Introduction

The recent development of modern downhole, real-time temperature sensors has led to the abundant availability of high precision, downhole temperature measurements. This in turn has driven the active development of downhole temperature transient analysis (TTA) methodology in the past two decades. The information that can be obtained from TTA has been shown to be either complementary to that obtained from the well-developed pressure transient analysis (PTA), or well testing, or the TTA could provide information which is difficult to obtain (or even impossible) from PTA.

The added value from TTA stems from the following; firstly, the transient temperature signal travels several orders of magnitude slower than the transient pressure signal. This makes it possible to carry out detailed analysis of the near wellbore region as TTA provides more data than PTA for the same distance of propagation of the transient signal. The second unique characteristic of TTA is that unlike PTA, the Joule-Thomson effect contributing to the temperature change is different in liquids and gases, thereby creating distinct and different transient temperature signals. This distinct trends can be used to discriminate flowing fluid phases in multiphase production, and could also be applied in soft multiphase metering. Finally, unlike the pressure signal which is essentially measuring the average reservoir properties throughout the whole of the production or injection interval of the wellbore, therefore making it difficult to discriminate zones, the temperature signal measured at multiple depths does discriminate the inflow or outflow zones making it possible to characterise the reservoir at a higher level of detail.

These unique features of the transient temperature signal has made TTA a very attractive and active area of research recently. TTA can also make virtual, multiphase flow metering possible in many wells by using existing low cost temperature (and pressure) gauges in them, and saving costs or eliminating the need for frequent production logging or the installation of physical flowmeters downhole. Fully developed TTA methods could also make zonal monitoring possible, and this would be invaluable both in advanced wells completed with intelligent completions, and in conventional wells requiring workover, because an interpretation algorithm can be added to the monitoring capabilities for little additional cost, since the necessary sensors and downhole valves often have already been installed in these wells.

The development of robust and accurate interpretation methods for transient temperature involves having methods that can be applied to different types of fluids (e.g. liquids and/or gases), different well configurations (e.g. vertical, horizontal or highly deviated wells) and different flow conditions (e.g. constant flow and variable flow conditions). Most of the work done (and published) so far has focused mainly on liquids (both horizontal and vertical well configurations), this leaves a gap in the development of a robust interpretation method for interpreting gas well transient temperature. Another area of interest is the impact of the thermal wellbore effects, as it has been observed that it can degrade the transient temperature signal considerably in situations where the temperature gauge is installed at a distance from the producing zone, therefore mitigation methods would also be necessary to extend the application of TTA interpretation to such wells (i.e. wells with distant gauges).

This work focuses on these gaps and tries to proffer solutions for them in a bid to ultimately developing a full-fledged TTA interpretation method which can handle different well configurations, both liquid and gas phases and wells where the gauge is distant from the sandface.

1.1 Research Questions

The following questions were answered in the course of this research, and the methodology used and results obtained were guided by these questions:

- How is transient temperature in dry gas producing reservoirs different from liquid producing ones?

- What are the factors that affect transient temperature in gas producing reservoirs?

- How much do these factors affect the transient temperature, and which of these factors can be ignored?

- Is it possible to use the sandface temperature in gas producing wells for TTA (i.e. to understand the properties of the formation)?

- Can numerical models be developed to predict transient sandface temperature?

- Can complete analytical solutions be developed for sandface temperature in dry gas producing wells? If not, can useful asymptotic solutions be obtained?

- What is the effect of wellbore heat transmission on TTA analysis developed using sandface temperature models and solutions?

- Can the effect of wellbore heat losses during the temperature signal transmission degrade TTA in the case of a distant gauge?

- If this effect of wellbore heat transmission cannot be (always) eliminated, is it possible to correct for this effect during TTA?

- How can the developed transient sandface temperature solutions be adapted to analyse transient temperature data in dry gas producing wells?

- What problems would be encountered in applying the developed methods to real data, and how can these problems be overcome?

1.2 Objectives

- Develop numerical models for predicting transient sandface temperature in gas producing wells. These model would be used as a tool in obtaining analytical solutions and inverse methods for use in TTA.

- Develop analytical models which can be used for predicting sandface temperature.

- Develop transient temperature interpretation workflows based on the analytical and (or) numerical solutions.

- Investigate the effects of wellbore heat transmission on the application of the developed workflows and suggest ways of mitigating these effects.

1.3 Scope

This work is mainly focused on TTA for natural gas producing wells in the context of the petroleum industry, as such the models and case studies used would focus on this. However, the application of some of the developed analytical solutions can go further than natural gas producing wells and should be applicable to any system with gas flow in porous media. Secondly, the thermal wellbore models were also developed initially for gas wells, but could also be extended to liquids and multiphase flow scenarios as well.

1.4 Thesis Layout

The layout of this thesis is presented below. In broad terms, this work presents the analytical solutions for transient sandface temperature, and then the analysis workflows based on these solutions and finally methods for correcting the measured gauge temperature for the wellbore heat transmission effect.

Chapter 2: provides an introduction to advanced well monitoring systems. It discusses the various types of measurements and then goes into details of the two most relevant measurements (pressure and temperature) in this work. The different types of well control systems are also discussed and the role of monitoring in respect to control is mentioned. Finally a review of temperature transient analysis, the modelling approaches and challenges are discussed for both the reservoir and the wellbore.

Chapter 3: This chapter goes into details as regards the modelling of transient sandface temperature for a dry gas producing vertical well. An analytical solution for transient temperature is presented for a dry gas producing well. The analytical solution was developed with the aid of numerical models and details of the solution approach, the assumptions used, validation of the solution and case studies (real and synthetic) are presented. Finally, some of the limitations of the derived analytical solution are discussed.

Chapter 4: presents the linearized form of the analytical solution developed in Chapter 3. This linearized sandface temperature solution was then used to develop a transient sandface temperature interpretation workflow for estimating permeability-thickness, rate and for near wellbore analysis (i.e. determining the depth and permeability-thickness of the damaged zone). The impact of non-step change in flow rate on TTA was further investigated, and a rule of thumb to ensure this impact is minimal is presented. Non-Darcy

effects were also investigated and the error introduced into the TTA analysis due to this was quantified. Finally, the developed workflow was applied to synthetic and real data and the results presented.

Chapter 5: presents analytical solutions of sandface temperature for flow of gas into a planar sink (i.e. a representation of an infinitely conductive vertical fracture); simplified forms of these solutions are also presented along with synthetic case studies applying the developed solutions. This chapter also discusses the limitations in applying the developed planar sink solution to a real well.

Chapter 6: discusses the distant gauge problem, then proposes a method for mitigating this problem and also for the reconstruction of the sandface transient temperature signal from the measured gauge temperature. Different wellbore models (numerical and analytical) are investigated and limitations and benefits identified. Methods of history-matching the wellbore model and reconstructing the sandface temperature are presented. Case studies applying this method are also presented, for the reconstruction of the sandface temperature and then using the reconstructed sandface temperature for TTA. A comparison of the TTA results obtained by using the reconstructed temperature and that obtained by using the actual sandface temperature is presented as well.

Chapter 7: Summarizes the results of the previous chapters and provides recommendations for further work.

Chapter 2: Literature Review

This work focuses on the development of TTA methods for gas, which can be used independently to analyse transient temperature from dry gas wells or in conjunction with existing liquid TTA methods to analyse multi-phase flow wells.

While TTA is merely an analysis method that makes use of measured transient temperature data, the application of these methods can vary greatly and can be split into two broad categories, the first being monitoring while the second is testing. While the applications seem different, the underlying physics are the same in these two categories. Monitoring seeks to provide a continuous assessment of the conditions of a well or formation, while testing provides snapshots at a given time.

While TTA can be applied to any well with a bottomhole temperature sensor installed (either temporary or permanent), it is most often applied to wells having permanent down-hole gauges installed (part of a broad category of wells called advanced wells). A review these types of wells would be presented, as they could potentially derive the greatest benefit from TTA at the lowest cost and with the least risk, because no shut-down or intervention is required to gather data. A review of the existing TTA solutions and methods along with some TTA applications cases is also presented. The different wellbore heat transmission models and solutions will be reviewed because the wellbore thermal effect has a significant impact on the quality of the measured transient temperature signal and its accuracy when used for TTA. Finally, some methods for modelling gas properties (in particular gas thermal properties) at high pressure will be presented; as this is quite important for developing accurate TTA models, solutions and / or workflows.

2.1 Intelligent Well Monitoring and Control

In most cases well monitoring is usually of greatest value in situations where there is ancillary equipment capable of changing the behaviour of the well in response to the information obtained from the monitoring process (i.e. in situations where well control is available). One category of wells with such capabilities are advanced wells, and when the monitoring and control capabilities are integrated into the well, it is called a smart or intelligent well (Bellarby 2009). Though these smart wells are rarely autonomous (this is

could be due to the ownership of risk / liability in the event of an incident), but they can provide enough information about the downhole conditions to aid the engineer take a more informed decision by using the well's control capabilities. Over time, the sophistication (and trustworthiness) of these condition monitoring systems will increase followed by limited autonomy {i.e. closed loops control systems (Going et al. 2006)}. However to the best of the author's knowledge, till date there is currently no intelligent well with a closed loop feedback control system.

A smart or intelligent well consists of a monitoring system and a control system (along with other elements of a conventional well completion). The monitoring part of the well is involved in measuring, transmitting and analysing the measured data to provide actionable information. Figure 2-1 shows an example of different monitoring systems that can be found in a modern well. Different types of sensors or transducers can be used, and these typically measure the physical parameters and then convert it to another form (usually electrical or optical) before transmitting it to a logging device where it is either stored or used directly for analysis. This research focuses on the development of analysis methods for the measured transient temperature data, therefore it should be relevant regardless of the measurement system used, provided the measurement accuracy and precision are high enough.

2.1.1 Well Monitoring Systems

There are different types of downhole parameters that can be measured in a producing well, by using different sensors or transducers. Some of these measurements are (but not limited to) temperature, pressure, rate, density, and acoustic signals. These measurements can be used to monitor both the conditions of the well and integrity of the completion, the produced fluids or the flow capability of the reservoir. Temperature and pressure measurements are of paramount importance in this work as this work is mainly about temperature analysis and pressure is the main driver for temperature changes in the reservoir, such the two cannot be separated.

There are currently different types of downhole gauges commonly used in wells to measure temperature and pressure. In most cases pressure data is the primary measurement of interest, however, the temperature is also measured in order to either compensate for the change in fluid property (e.g. density) due to the fluid temperature as

this has been shown to have a considerable effect on the pressure measurement in some cases (Izgec et al. 2007). Installation of a permanent downhole gauge in a moderate or high rate well can easily be justified (Bellarby 2009) and having temperature measurement along with pressure is beneficial in that it makes the pressure measurement more accurate. The inclusion of temperature measurement to complement pressure provides additional temperature data for stand-alone temperature analysis, therefore having an analysis method for temperature measurement is a natural choice.

Permanent downhole gauges can either be electronic or optical; the electronic gauges could be quartz crystals, sapphire or strain gauges with the quartz type offering the highest accuracy and precision (for pressure and temperature measurement) (Bellarby 2009). Though the quartz gauges provide the best precision and accuracy, they are less reliable than optical gauges because of the presence of downhole electronic components, as the failure rate of these electronic components increase as temperature increases (van Gisbergen & Vandeweijer 1999). Optical gauges on the other hand do not have any electronic component installed in the well as all the electronics are located in the surface acquisition system and they have been used as a reliable alternative to electronic gauges (especially in high temperature wells) (Kragas et al. 2002). However, the first generations of optical gauges were strongly susceptible to hydrogen darkening, which leads to attenuation of the signal, and as such the optic fibre should be properly protected to prevent this (Bellarby 2009). Another important factor that can affect the reliability of monitoring systems (both optical and electronic alike) is the installation procedure as considerable differences in reliability were observed for installations by different service companies, which can partly be traced to failure in the fibre or cable and splices in the system, and a lot of these were shown to have occurred during or shortly after installation (van Gisbergen & Vandeweijer 1999).

Since different measurement systems (or technologies) have their pros and cons, a cost benefit analysis should be carried out in order to choose a suitable measurement system for a well, as this would ensure the best system is selected for the specific monitoring needs (or requirements) and the prevailing conditions in the well.

2.1.1.1 Quartz Permanent Downhole Gauges

The quartz gauge is the most common electronic permanent downhole gauge. It uses a piezoelectric quartz oscillator (originally used in frequency control), and the

measurement system works based on resonant frequency shift in the oscillator which occurs in response to changes in its environment (EerNisse et al. 1988). These sensors provide advantages of high resolution, accuracy and stability (EerNisse 2001). Since the fundamental operating principle of the quartz temperature sensor is quite similar to the pressure sensor (both pressure and temperature changes result in a change of the resonant frequency of the quartz crystal), it is relatively easy to implement pressure and temperature measurement in the same gauge, and most times temperature measurement is included in order to calibrate the pressure measurement or in-situ fluid properties. The resolution of quartz temperature gauges can be as high as 0.005 K (Schlumberger 2008). This feature (high resolution) makes these gauges very valuable for TTA as they can accurately resolve small changes in temperature, typical of what you would expect in a lot of oil and gas wells.

2.1.1.2 Fibre Optic Permanent Downhole Gauges

Most fibre optic sensor technologies rely on the modulation of one or more properties of light in the optic fibre. Some of the major existing technologies and topologies are; single point sensors based on the Fabry-Perot interferometers which operates based on the phase difference between two light waves; multi-point Fibre Bragg grating sensors that operate based on the frequency of light interfering with a periodic structure; and finally the distributed sensors which are based on backscattering (in Rayleigh, Raman and Brillouin spectra) (NI 2011). A summary of the different fibre optic technologies and topologies is listed in Table 2-1 obtained from (NI 2011).

Table 2-1: Comparison of Optical Sensing Technologies (distances are approximate)

Technology	**Topology**	**Range**	**Temperature**	**Strain**	**Pressure**	**Vibration**
Fabry-Perot	Single-Point	< 10 km	Yes	Yes	Yes	Yes
FBG	Multi-Point	< 50 km	Yes	Yes	Yes	Yes
Rayleigh	Distributed	< 70 m	Yes	Yes	No	No
Raman	Distributed	< 20 km	Yes	No	No	No
Brillouin	Distributed	< 50 km	Yes	Yes	No	No

Just like in quartz gauges, it is also relatively easy to implement pressure and temperature measurements in an optic fibre based measurement system, therefore making the availability of temperature measurements almost ubiquitous with pressure measurements in modern permanent downhole gauges.

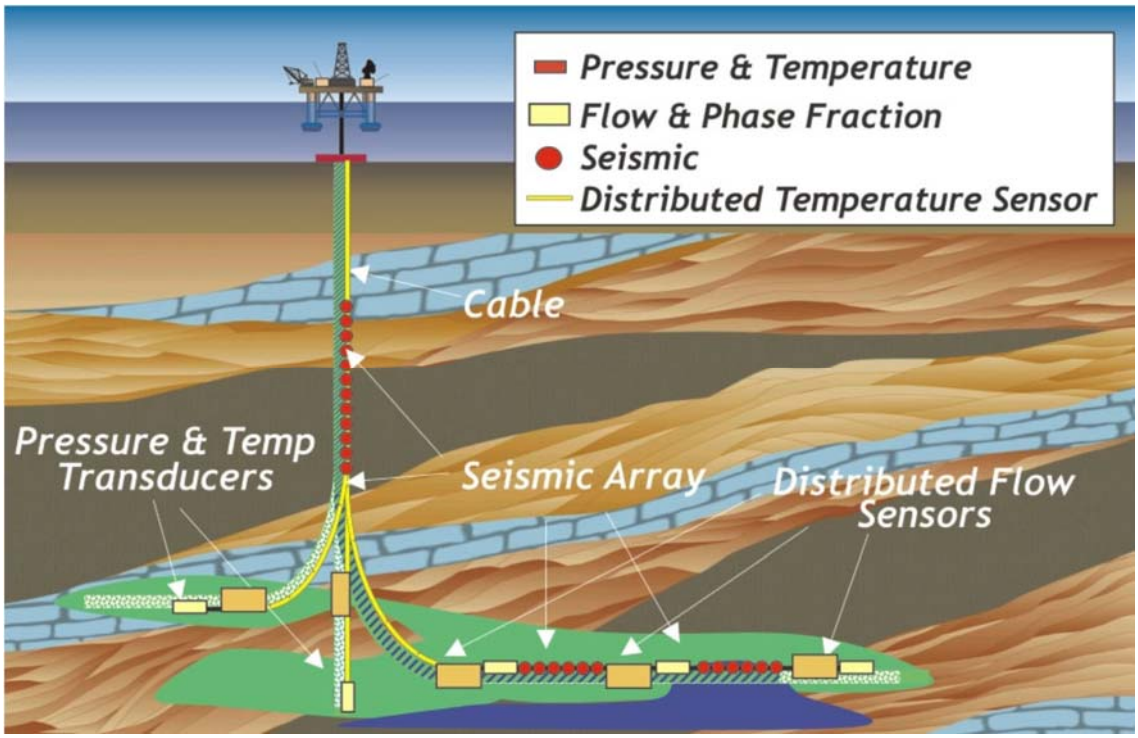

Figure 2-1: Intelligent well monitoring system (Bostick III 2003)

2.1.2 Well Control Systems

While this work focuses on monitoring, it would still be beneficial to highlight the control possibilities available in advanced wells and the different components of this system. Doing this would accentuate the benefits of monitoring as a complement to well control and reservoir management.

One of the major challenges facing all production wells is premature breakthrough of unwanted fluids (water in both oil and gas wells producing wells, and gas in oil producing wells). While in injection wells, uneven outflow distribution is the major challenge. These challenges can be caused (or exacerbated) by reservoir heterogeneity, frictional effects (especially in extended reach wells), variation of fluid properties (both in the reservoir and the wellbore), and variation of reservoir pressure. Advanced well completions

employing Downhole Flow Control technologies provide a practical solution to all these challenges (Al-Khelaiwi 2013).

The first down hole control device (in this case Inflow Control Device or ICD) installed in a horizontal well was installed in Troll field in the early 90's (Brekke & Lien 1994), this was done to mitigate the heel-toe effect (i.e. uneven production from a long horizontal well or lateral due to frictional pressure drop in the tubing) in a long horizontal well (about 500m reservoir contact) placed in a thin oil rim (about 2m thickness). ICDs equalize the flow into a horizontal section by creating additional pressure drops closer to the heel of the horizontal well segment. This flow equalization encourages uniform sweep and delays water or gas breakthrough near the heel of the well (as a result of coning). The delayed breakthrough in such wells increases recovery and the economic viability of the well. The increase in economic viability is due to delayed water treatment cost or increased revenue earlier on in the life of the field, these both have a positive impact on the NPV of the project.

The use of ICDs in the Troll field served as an invaluable proof-of-concept, and was shown to produce an increase of 50% in the plateau rate and 214% increase in the plateau period. This study (using ICD completions) was carried out after proving that horizontal well technology provided a viable technology for producing oil from the thin oil column in the Troll field by producing at least four times the vertical alternative (Lien et al. 1991) and also discovering that the frictional losses in the horizontal section of the well would lead to earlier gas breakthrough at the heel of the well (Haug 1992).

This demonstration of the value of flow control in horizontal wells opened the way for the development of several other inflow equalizing and control devices, and since then the use of ICDs (and other downhole flow control devices) in horizontal production and injection wells has increased. Another area of application of well control is for controlling the production from different layers in a bid to efficiently manage the reservoir and optimize recovery from one or more zones

2.1.3 Types of Well Control Devices

Downhole flow control devices can be grouped into three broad categories, namely, passive, active or reactive devices (Eltaher 2017). The passive devices provide a constant

choking effect which usually cannot be altered once the device is installed while the active devices provide a variable choking (on/off, discrete or continuous control) which is usually controlled from the surface (Grebenkin 2013) and the reactive devices react to the type of fluid flowing through them by providing different levels of choking for different types of fluids.

2.1.3.1 Passive Flow Control Devices (Inflow Control Devices)

These devices create a constant choking effect which cannot be altered once the device is installed. The choking effect is achieved by using several mechanisms such as; labyrinths, helical channels, slots, tubes nozzles and orifices; to create flow restrictions. A summary of several ICD types is given in (Eltaher 2017) and a more detailed description of the different types can be found in (Al-Khelaiwi 2013). The intensity of the choking effect (or flow restriction) is usually specified by a parameter called the ICD strength, this is a constant parameter which relates the square of the rate (through the device) to the pressure drop experienced across the device (Birchenko 2010). The ICD strength provides a uniform method of comparing different ICDs which might be based on different technologies, and this helps in standardizing the modelling methods used for these devices.

2.1.3.2 Active Flow Control Devices (Interval Control Valves)

Active flow control devices have the ability to alter the choking on the device, and these can be done in an on/off, discrete or continuous fashion. This control feature requires some sort of actuation (power and control) to move the valve and sometimes feedback to provide information about the current valve position. The valve actuation can be by electric, hydraulic or electro-hydraulic (i.e. hydraulic actuation and electric control) methods (Shaw 2011). Each actuation method has its pros and cons, for example the electric and electro-hydraulic actuation methods use fewer control lines than hydraulic ones but they have reliability issues because of the presence of downhole electronics. The all-hydraulic system provides a greater reliability as it eliminates downhole electronics, however, it requires multiple control lines (usually a minimum of n+1 control lines, where n is the number of ICVs installed), there have been recent technological advancements (e.g. All-Hydraulic Multiplexing, J-Latch Multiplexing and Digital Hydraulic Multiplexing) which has tried to reduce the number of required control lines (Shaw 2011). The type of actuation has been shown to greatly affect the reliability of these devices and

this is discussed in (Shaw 2011) and real case studies of these devices are presented in (Al-Shammari 2014) and (Ibeh et al. 2015)

Monitoring is particularly useful in wells with active flow control devices installed, as these devices provide the possibility of carrying out actions in response to the measured changes (occurring independently of, or due to the imposed control action), thereby creating a feed-back control system.

Table 2-2: Comparison of different types of well control devices

	Passive	**Active**	**Reactive**
Cost	Cheap	Expensive	Moderate
Reliability	High	Moderate	Relatively new technology, not enough information available
Flow equalization	High equalization and resolution possible	High equalization possible but with low resolution, due to limitation on the number of control lines installed per well	High equalization and resolution possible
Fluid discrimination	Not possible	Possible, but relies on use of ancillary monitoring and analysis equipment	Automatic
Choking effect	Constant, once set at installation	On/off, discrete or continuously variable	Discreet or continuously variable
Complexity	Low	High	Moderate

2.1.3.3 Reactive Flow Control Devices (Autonomous Flow Control Devices)

While ICDs (or other passive flow control devices) are beneficial for inflow equalization, they offer no advantage after breakthrough as they can't differently react to flow of the unwanted fluid across the device. Autonomous Flow Control Devices combine the benefits of active control which provides varying pressure drops across the device with the simplicity of passive devices as they don't need any form of telemetry or surface controlled actuation but rather operate based on the changes in property of the fluid

flowing through the device. They therefore provide the advantage of being able to choke unwanted fluid after breakthrough. The devices technology is relatively new and as such the behaviour of these devices in different reservoir conditions and scenarios is yet to be fully understood (Eltaher et al. 2014).

2.2 Thermal Processes in the Subsurface

The thermal effects of fluid flow in porous media in the subsurface has been studied and applied to processes such as geothermal energy extraction, thermal recovery of hydrocarbons and temperature transient analysis, which is the subject of this thesis. Though thermal recovery and geothermal energy extraction covers a broad range of processes the ones of interest in this work are those where the produced (or injected) fluid has been in direct contact with the rock because the physics in such situations are closely related to that of TTA.

Though this field is quite mature the use of thermal effects in the reservoir for well testing (i.e. TTA) is relatively new and the "important" physics are slightly different from those of thermal recovery, for instance. The reason for this is because in processes like thermal recovery or geothermal energy generation a fluid having a very large temperature difference from that in the reservoir is injected, while in TTA reservoir fluid at near isothermal (neglecting slight temperature differences due to geothermal gradient) conditions is produced and this results in temperature changes which can be monitored and analysed. In thermal recovery or geothermal energy extraction, the parameter of interest is the temperature difference between the reservoir fluid and the injected fluid as this enables sufficient heat transfer between the two, while in TTA the transient temperature changes, in the initially "isothermal" reservoir fluid, due to production is the parameter of interest.

In thermal recovery or geothermal energy extraction the heat transfer between the injected fluid and the reservoir masks other temperature effects like the Joule-Thomson effect or adiabatic fluid expansion. Consequently, the models used to describe processes such as geothermal energy extraction and thermal recovery are different from those used to describe the transient temperature change during conventional production processes. In most cases the models used to describe geothermal energy extraction (Franco & Vaccaro, 2014; Chen et al., 2018 and Pruess et al., 1999) and thermal recovery (Zhu et al., 2009

and Schlumberger 2014) only include the effects of heat convection and conduction, while that used in TTA include the adiabatic expansion effect and Joule-Thomson effect as well as heat conduction and convection (Weibo Sui et al. 2008).

These differences between the existing thermal models, used in the fields of thermal recovery and geothermal energy extraction, makes most of them inappropriate for TTA. It is therefore necessary to confirm that a thermal model or simulator includes the necessary physics before using it for TTA studies. A suitable model for TTA is that by Weibo Sui et al. (2008) and the commercial non-isothermal compositional simulator CMG-GEM (2012) also includes the necessary physics required for TTA, these would be used later in this study to develop and test analytical solutions, analysis workflows and to carry out TTA case studies.

2.3 Temperature Transient Analysis

TTA algorithms are inverse algorithms that are used to estimate the parameters of the formation and the fluid or flow conditions by using the measured sandface temperature. The development of these inverse algorithms depend on having an accurate forward model of the sandface temperature or solution. Since temperature changes in the sandface and formation are a direct result of fluid flow and pressure changes, it is imperative to first have pressure solutions in order to subsequently derive solutions for temperature.

2.3.1 Transient Pressure Solutions

Pressure solutions for flow in porous media are usually derived from the diffusivity equation for pressure which is equivalent to the heat conduction equation in solids. This makes it possible to apply existing transient (heat) conduction solutions to derive transient pressure solutions and this can be seen in the derivation of pressure solutions (Gringarten & Ramey 1973). Conduction solutions (Carslaw & Jaeger 1959) have been used extensively this way in the field of petroleum engineering.

However, in situations where the diffusivity coefficient is nonlinear (i.e. pressure dependent) for example in highly compressible fluids, i.e. gases, the derivation of the pressure solution from the diffusivity solution becomes non-trivial. Several methods have been developed to cater for the derivation of the pressure solution in compressible fluids,

for example, the pressure approximation method which is applicable for high pressure gas reservoirs, above 3,000 psi, or pressure-squared approximation method, applicable for low pressures less than 2,000 psi; and the pseudo-pressure method which is applicable for intermediate pressures between 2,000 psi and 3,000 psi (Ahmed 2006) and (Al-Hussainy et al. 1966). Of the three methods mentioned above, the pseudo-pressure gives the most accurate results and would therefore be employed in this work.

The pseudo-pressure approach combines the pressure dependent terms (P - pressure; mu - viscosity and z - real gas compressibility) of the diffusivity equation into a single pseudo-pressure term (defined by letter ψ), thereby linearizing the diffusivity equation and making it possible to apply the existing linear solutions of the diffusivity equation in terms of pseudo-pressure (Al-Hussainy et al. 1966).

While this pseudo-pressure method solves the pressure dependence problem in highly compressible fluids it still does not cater for all the nonlinearity in gas flow, specifically the "turbulent" flow effect which is significant in most gas wells (Firoozabadi 1979). This effect and its impact on TTA for gas wells is very important as (in some situations) it could account for a considerable portion of the total pressure drop (Firoozabadi 1979). While there has been controversy over the nomenclature used to describe this phenomenon, or the mechanism responsible for the observed increased pressure drop, there have also been numerous empirical relations which can be used to estimate the magnitude of this additional pressure drop while using Forchheimer's equation. The Forchheimer equation is similar to the Darcy's equation but with an extra pressure drop term which is a quadratic function of velocity (see Equation 2-1). This equation is widely used for modelling the non-Darcy behaviour experienced in high rate wells and a summary of some of the available correlations for estimating the Forchheimer parameter is given by Wang & Economides (2009).

$$-\nabla P = \frac{\mu}{k}\boldsymbol{v} + \beta\rho|\boldsymbol{v}|\boldsymbol{v} \qquad (2\text{-}1)$$

2.3.2 The Value of Transient Temperature Signal

The general consensus in conventional pressure transient analysis is that the reservoir is isothermal. While this is not true (the reservoir temperature changes during production, especially near the wellbore) the assumption produces results that are accurate enough to

be of practical value. The reason is because temperature changes in the reservoir are quite small and in most cases its effects on the fluid properties and consequently on the pressure response is usually negligible (Duru & Horne 2008).

While the temperature changes do not usually have any significant effect on the pressure response; that does not mean the temperature signal is useless, but the contrary is the case as it contains valuable information. The transient temperature signal has been shown to contain information about the formation, the type of fluids produced and the production rate. These features of the transient temperature signal have been utilized to characterize the formation (Duru & Horne, 2010; Onur & Çinar, 2016 and Muradov et al., 2017), for near wellbore analysis (Muradov et al., 2017; Ramazanov et al., 2010; Onur & Çinar, 2016 and Mao & Zeidouni, 2017b) for detection of water or gas breakthrough (Yoshioka et al. 2006) and for flow rate allocation (Malakooti 2015).

As discussed above, the transient temperature signal contains valuable information, however the method of analysis used to extract this information varies widely, and the approach used is usually determined by the available models or solutions. Generally, a forward model capable of predicting transient sandface temperature (when fluid, flow and formation properties are known) is required, this model can then be inverted to determine the fluid, flow or formation properties from the measured transient sandface temperature data.

2.3.3 Transient Sandface Temperature Modelling and Solutions

A PDE (Equation 2-2) for temperature in porous media was proposed by Weibo Sui et al. (2008) and applied this model to study the effect of skin and permeability on the transient bottomhole temperature in a multilayer co-mingled vertical well. According to Muradov et al. (2017) this model was first proposed by Chekalyuk (1965). This model has been used in several studies to investigate the behaviour of transient temperature in oil and gas producing reservoirs. It has also been employed in carrying out inverse studies when the measured (or simulated) sandface temperature is known and information about the reservoir or produced fluids is required.

$$\overline{\rho C_P}\,\frac{\partial T}{\partial t} - \emptyset\beta_T T\frac{\partial P}{\partial t} - \emptyset C_f\left(P + \rho_r C_{Pr} T\right)\frac{\partial P}{\partial t} = -\rho \boldsymbol{v} C_P \cdot \nabla T + \beta_T T \boldsymbol{v} \cdot \nabla P - \boldsymbol{v} \cdot \nabla P + K_T \nabla^2 T \qquad (2\text{-}2)$$

The strength of this model lies in the fact that it includes most of the practically significant temperature effects (effects that create a measureable temperature change, given the resolution of modern sensors); namely conduction, convection, expansion and Joule-Thomson effects. This PDE is normally solved to obtain a temporally varying temperature solution, which can either be spatially varying (although more difficult) or obtained at a single point of investigation (usually at the sandface). To a large extent the solution method and the temperature effects included in the model determine the type of solution obtained. Numerical methods usually give full solutions which are both temporally and spatially varying, while the analytical methods usually give approximate or asymptotic solutions and these have been shown to be accurate enough to be of practical value in TTA (Ramazanov et al. 2010) and (Muradov & Davies 2012a).

Some of the major finding in TTA research are summarised in Table 2-3. This summary covers a broad range of solution methods, well configuration and produced fluid phases. From this summary it is obvious that analytical solutions and workflows for gas producing wells have only recently been published.

One of the early works in TTA was by W. Sui et al. (2008) and this demonstrated the value in transient temperature data by using layer temperatures to estimate layer properties and also properties of the damage zone. As at the time of this publication, analytical solutions for transient sandface temperature were not as prevalent as they are now, as a result this work used numerical forward models which were then inverted by using the Levenberg-Marquardt regression algorithm in order to estimate the formation properties. Using this algorithm resulted in relatively accurate results for the four layers simulated, with errors of <1% for the estimated permeability of the clean formation and the permeability and depth of the damage region.

Table 2-3: Major findings in TTA research

Author, year	**Problem conditions**	**Numerical / Analytical**	**Major findings**
(W. Sui et al. 2008)	Multilayer system with liquid production	Numerical	Testing workflow for pressure and temperature in multi-layered system. Estimated skin and layer properties
(Ramazanov et al. 2010)	Vertical oil producing wells with thermal wellbore storage	Analytical	Developed analytical solutions for vertical liquid producing wells
(Sui et al. 2010)	Multilayer system with gas production	Numerical	Estimated skin, and layer properties in a multi-layered well-reservoir system, by using numerical inversion techniques
(Duru & Horne 2010)	Single and multiphase (oil and gas) flow, 1D radial flow	Semi analytical (operator splitting)	Semi analytical transient temperature solution, estimation of formation and fluid properties using real and synthetic data
(App & Yoshioka 2011)	Oil and gas flow in vertical wells	Analytical / Numerical	Effect of Peclet number on flowing temperature change, and relationship to layer properties.
(Muradov & Davies 2012a)	Horizontal liquid producing well	Analytical	Developed analytical solutions for transient sandface temperature in liquid producing horizontal wells
(Muradov & Davies 2012b)	Horizontal liquid producing wells	Analytical	Workflows for TTA for liquids in horizontal wells
(Muradov & Davies 2013)	Horizontal liquid (oil and water) producing wells	Analytical	Case studies for pressure and temperature transient analysis for liquid producing wells
(Chevarunotai et al. 2015)	Vertical oil producing wells	Analytical	Transient temperature solutions for oil producing wells with large drawdowns
(Onur & Çinar 2016)	Drawdown and build-up in vertical liquid producing well	Analytical / Numerical	Developed analytical transient temperature solutions for liquid drawdown and build-up
(Mao & Zeidouni 2017b)	Vertical liquid or gas producing wells	Analytical	Developed analytical transient temperature solutions for dry gas producing wells

After the publication by W. Sui et al. (2008) there was a significant increase in publications in the area of TTA as it had shown, as a proof-of-concept, that it is possible to use transient temperature data for analysis which would not only complement pressure, but possibly provide more information than can be obtained from pressure transient analysis.

Though there has been a surge in publications of TTA solutions and workflows since 2008, it is still nowhere as mature as PTA, and there is a relative shortage of available solutions and modelling tools, especially for gas wells.

2.3.4 Near Wellbore Analysis using TTA

Quantifying formation damage near the wellbore is an important aspect of well-test because this type of damage can have a considerable impact on the productivity of a well. The classical method of quantifying near wellbore damage (skin) is done by PTA and this only gives a lumped skin parameter, which is good enough to estimate the additional pressure drop or the reduction in productivity due to the damage. However it can also be important to know the depth of damage and the permeability of the damage region in order to design a proper well stimulation program, and these are parameters which cannot be determined from PTA.

One of the first attempts at using temperature to analyse the near wellbore region was carried out by Ramazanov et al. (2010), Sui et al. (2010) and W. Sui et al. (2008); these demonstrated the value of using transient temperature for near wellbore analysis, as it has the possibility of resolving both the permeability and the depth of damage. The work by Sui et al. (2010) and W. Sui et al. (2008) used a numerical model and nonlinear regression to match the layer parameters while the work by Ramazanov et al. (2010) developed a simple analytical solution (based on the method of characteristics) which can be used to estimate the depth of damage from the measured transient temperature signal. The method by Ramazanov et al. (2010) provides a fast and accurate method of carrying out near wellbore analysis.

Since the early works by Ramazanov et al. (2010), there have been other publications which developed analytical solutions for carrying out near wellbore analysis using

measured transient temperature. Out of these, some of the notable ones are Onur & Çinar (2016) and Mao & Zeidouni (2017b).

The unique property of transient temperature that makes it possible to use it for near wellbore analysis is the slow speed of propagation of the transient temperature signal through the formation. The speed of propagation of the transient temperature signal is several orders of magnitude less than that of pressure, therefore, while it takes a few seconds for the pressure wave to travel through the damage region near the wellbore, it takes the temperature wave a few hours to travel the same distance. This means there is more temperature data available to carry out near-wellbore analysis than pressure, and the prolonged duration of the temperature data available for analysis also means there is less chance that the data would be completely masked by wellbore storage effect.

2.3.5 Fluid Property Estimation for TTA

As mentioned earlier analytical solutions provide a fast and easy to implement TTA workflow, however, these solutions rely greatly on assumptions and one of these is that of constant fluid properties. While these assumptions have been demonstrated to provide accurate (for practical applications) results (Ramazanov et al., 2010; Mao & Zeidouni, 2017b and Onur & Çinar, 2016), the accuracy is highly dependent on the condition at which the fluid property is estimated. This assumption of constant fluid properties has minimal effect on the analysis when the fluid is a liquid at moderate drawdowns, however for gases and liquids with high drawdowns the condition at which the fluid property is estimated has to be chosen carefully.

The effect of fluid property variation on analytical transient temperature estimation was also investigated by Mao & Zeidouni (2017a) and a fluid property correction was proposed. The proposed fluid property correction uses a time averaged fluid property estimate for specific, mass heat capacity (i.e. the product of specific, volume heat capacity and density) and the product of viscosity and Joule-Thomson coefficient. While a linear time average was used for heat capacity, the product of viscosity and Joule-Thomson effect used a logarithmic time averaging method. The fluid property correction was observed to give a better transient temperature estimate when used in analytical solutions derived by Mao & Zeidouni (2017b). While the property correction method increased the accuracy of the TTA workflow presented in Mao & Zeidouni (2017b) the method was

only demonstrated for slightly compressible fluids, hence the accuracy of this method for highly compressible fluids is yet to be proven.

2.3.6 Non-Darcy Effect in TTA

As explained in a previous section (on pressure solutions)**,** the flow of high rate oil and gas in porous media does not obey Darcy's law and as such is better modelled by using Forchheimer's equation. This effect does not only result in additional pressure drop, but also affects the temperature transient as well, as the temperature changes occur due to the flow (driven by pressure gradient) and changes in pressure. Therefore, it is important to take this effect into account when carrying out TTA while using solutions based on the assumption that the flow obeys Darcy's law.

The effect of non-Darcy flow on the estimated transient temperature for slightly compressible fluids was investigated by Mao & Zeidouni (2017c), and a method of correcting for this effect was proposed. The proposed correction method involved correcting the fluid properties for non-Darcy effect by using a method developed by Mao & Zeidouni (2017a) which corrects the fluid property for the additional pressure drop due to the non-Darcy effect. This approach was proven to be sufficiently accurate, and the method was further simplified by applying it to viscosity alone. The result obtained from this study is expected as viscosity is the main fluid property responsible for the pressure drawdown in slightly compressible fluid flow (as the density is relatively constant).

2.4 Wellbore Temperature Modelling

TTA relies on the measured transient temperature and analysis workflows which are mostly based on transient sandface temperature solutions. However, the transient temperature is rarely measured at the sandface (but at some distance away from it) because of the practical limitations involved in installing the gauge at or near the mid-perforation point. Therefore, in order to accurately apply the developed workflows the thermal effects of the wellbore on the measured transient temperature has to be accounted for.

Some of these wellbore effects have been identified in Chapter 6 as the initial warmup effect and the attenuation of the transient wellbore temperature signal. The initial warmup

effect is due to warm fluid (at the geothermal temperature) flowing up to the gauge at well start-up, thereby causing an increasing trend in the measured temperature at early times, before the temperature front from the sandface reaches the gauge. The second effect is due to the heat transfer from the fluid to the well completions and the formation, this effect results in attenuation of the transient temperature signal thereby making it difficult (or at times impossible) to analyse the measured transient temperature.

In certain conditions measured transient temperature needs to be corrected for the wellbore effects for the TTA analysis to be accurate, and this would make the application of TTA more robust, being applicable to a wider range of wells and production scenarios. Correcting for the wellbore effect requires an accurate wellbore model and this can either be an analytical or numerical model, with each one having its unique advantage and disadvantage. For the use of TTA, analytical models would be preferred over numerical models because they offer an advantage in terms of speed.

One of the early works on wellbore heat transmission was by Ramey Jr. (1962), in this work an analytical solution for calculating transient wellhead temperature for a constant well inflow temperature was presented. This model (and similar ones) can be used to back-calculate the sandface temperature when the wellhead temperature is known for a given wellbore model. Since this model can be used to calculate the fluid temperature at any distance from the sandface (or wellhead) it can equally be used to back-calculate the sandface temperature from the temperature measured at the gauge location. This same method of back-calculating (or reconstructing) the sandface temperature from the measured gauge temperature can also be applied to other analytical or numerical wellbore models.

Since the work by Ramey Jr. (1962), there have been several works published which addresses the heat transmission in the wellbore. The works of Hasan et al. (2005), Izgec et al. (2006), Duru & Horne (2010) and Hagoort (2004) are of importance as they all try to address limitations in the original work by Ramey Jr. (1962). The works by Duru & Horne (2010) and Hagoort (2004) are the most important for this study as they include the effect of changing bottomhole flowing temperature (an important premise for TTA) in their models, while the others are based on a constant bottomhole temperature.

The wellbore model developed by Duru & Horne (2010) was developed by modifying the analytical solution by Izgec et al. (2006) which is similar to the analytical solution by Ramey Jr. (1962). Izgec et al. (2006) also proposed a semi-analytical solution, which updates the near temperature of the surrounding formation with time. While this addition might seem important, it is unnecessary as the original solution by Ramey Jr. (1962) models conduction in the formation as conduction in a semi-infinite radial domain with the internal boundary being the outer surface of the cement, and the outer boundary condition being the undisturbed earth temperature. The undisturbed earth temperature is assumed to be at a radial distance infinitely far from the wellbore, and the change in temperature of the surrounding formation is therefore accounted for in this conduction model.

Hagoort (2004) developed a rigorous solution for wellbore heat transmission and this was compared with the Solution by Ramey Jr. (1962), the rigorous solution was shown to be more accurate at early times as Ramey's model overestimated the wellhead temperature at early transient period (low values of Fourier time), although the two solutions converge at late time periods. It was also observed that the duration of the transient period is directly proportional to the Graetz number, and as such a large Graetz number results in a longer time before the two solutions converge.

2.5 Properties of Highly Compressible Fluids at High Pressure (i.e. gases)

The thermal model by Weibo Sui et al. (2008) is a function of properties of the fluid. The fluid properties included in the thermal model (explicitly or implicitly through pressure) are density, viscosity, specific heat capacity, thermal expansion coefficient and the Joule-Thomson and adiabatic expansion coefficient (the latter two can usually be derived from the former).

While the properties of liquids can usually be assumed constant for most practical applications, the same does not apply to gases as the properties vary greatly with pressure. Also, it has been shown that at high pressures (similar to those in a reservoir) the behaviour of gases depart from that of the ideal gas. This deviation has been studied extensively for density and is normally accounted for by adding a compressibility factor (sometimes called Z-factor) to the ideal gas equation (Elfrink et al. 1949). Accurate estimation of natural gas density is important for estimating gas reserves, calculating

pressure changes in the reservoir, pressure gradients in wells and pipelines and also for metering (Standing & Katz 1942). The estimation of the compressibility factor (Z-factor) for natural gas is either carried out by using correlations or fitting equation of states to experimental data, for instance Dranchuk & Abou-Kassem (1975) fitted the Starling Equation-of-State to the Standing and Katz Z-factor correlation. Using Equations-of-State makes it easier to implement the calculation of Z-factor using a computer as done by P M Dranchuk et al. (1973).

Since the experimental data used for correlations or equation of states is based on a specific composition, and there are an infinitely large number of possible fluid compositions, this approach of using correlations would have been of very little value. However, a similarity was observed in the behaviour of pure substances and a generalisation of this is called *"The Law of Corresponding States"*.

"The ratio of the value of any intensive property to the value of that property at the critical state is related to the ratios of the prevailing absolute temperature and pressure to the critical temperature and pressure by the same function for all similar substances"(Sage & Lace 1941)

The importance of this law is that experimental data for a given substance can be used to estimate the properties of another substance by using the pseudo-reduced (i.e. ratio of absolute to critical values) pressure and temperature, therefore greatly reducing the amount of experimental data required for different compositions of hydrocarbon fluids. Another important fluid property necessary for flow calculations is the viscosity and a good estimation of this can be obtained by using Carr et al. (1954) which covers practical ranges of temperature and pressure for phase compositions encountered in surface and subsurface conditions.

While the fluid properties like viscosity and density are normally included in most reservoir modelling tools, the thermal properties are not (due to the isothermal assumption in reservoirs). However, since these properties have a significant impact on the predicted sandface temperature it is important to estimate their values accurately. The important thermal properties to be considered are the specific heat capacity and thermal expansion coefficient of the gas.

The specific heat capacity, defined as the amount of heat required to change the temperature of a unit mass of a substance by 1 Kelvin, varies with pressure and for high pressures (similar to those in reservoirs) this property deviates significantly from that of an ideal gas. Estimation of the specific heat capacity at such conditions (i.e. high pressure) require the estimation of the ideal specific heat capacity and the heat-capacity departure at high pressure (Abou-Kassem & Dranchuk 1982). The thermal expansion coefficient can be derived from thermodynamic relations and the equation-of-state.

It is possible to use equations-of-state that have been fitted to some experimental data, to estimate the molal density, which can then be used to calculate the other gas properties, including the thermal properties. This approach would be used in this work and the selected equation of state to be used is the Benedict-Webb-Rubin equation-of-state (Benedict et al. 1942)

Chapter 3: Analytical Solution for Transient Sandface Temperature in Vertical Dry Gas Well

3.1 Introduction

The "business-pull" for Temperature Transient Analysis (TTA) research has increased in recent years due to the introduction and wide spread application of sensors of sufficient sensitivity that can detect the small temperature changes associated with TTA. The development of a comprehensive PTA/TTA data analysis framework will allow the full "Added Value" to be reaped from providing the measured data to the engineer's desk-top in real-time. Reliable real-time reservoir monitoring and management, in its turn, is a long-awaited goal able to make a notable difference to the efficiency and impact of hydrocarbon production.

The development and application of TTA solutions for flow rate allocation in oil wells has been reported as early as 2012 by Muradov & Davies (2012b) for horizontal wells and Ramazanov et al. (2010) for vertical wells. Transient temperature was also numerically proven to be able to estimate the formation parameters (Sui et al., 2010 and Duru & Horne, 2010) as well as to determine the presence of an hydraulic fracture (App et al. 2013). The application of the TTA workflow description by Muradov & Davies (2012b) was later illustrated by examples using real-well data (Muradov & Davies 2013). The combination of TTA and PTA allows the full reconstruction of zonal reservoir properties and flow rates after a small fraction of the complete transient period has elapsed.

TTA requires a comprehensive model of heat and mass transfer in porous media. Bird et al. (2007) proposed a thermal model which has been adapted for porous media flow; allowing analytical and numerical liquid solutions based on this or similar models to be obtained by Muradov & Davies (2012a), Duru & Horne (2010), Ramazanov et al. (2010) etc. Predicted temperatures derived from these thermal models were successfully compared to real-well data by Muradov & Davies (2013) and Duru & Horne (2010).

Most of the work done in the area of transient sandface temperature modelling has been limited to slightly compressible fluids (i.e. liquids). This limitation allowed the introduction of simplifying assumptions to the thermal models. However, extending their

application to gasses (i.e. compressible fluids) results in a highly non-linear mathematical problem which is more difficult to solve. This explains why there are only a few publications on TTA for gas producing wells. For example, Sui et al. (2010) coupled a wellbore model to a numerical, multilayer, gas reservoir model. They used transient temperature data from the forward model to determine the layer permeability and skin properties. The inversion of the forward model was accomplished by running multiple numerical simulations and minimizing the objective function by nonlinear regression.

Numerical inversion solvers have the capability to solve many inverse problems. However, these methods do not provide the valuable insights into the problem that an analytical model provides. Analytical solutions have the additional advantage of providing a unique solution more quickly, and with reduced computational resources, than is required by the numerical approach to solving an inverse problem. This work develops analytical models for prediction of downhole transient sandface temperatures of gas producing wells. It forms one step in the development of a comprehensive TTA workflow.

3.2 Governing Equations

3.2.1 The Pressure Model

Flow in porous media is usually described by combining the empirical Darcy's law equation (Equation 3-1) with the continuity equation (Equation 3-2), this would give the diffusivity equation (Equation 3-3). The Darcy's law is a form of momentum balance for fluid flow in porous media. Though the Darcy's law was derived empirically, it has been shown that it can also be derived from the Navier Stokes equation (Hubbert 1957), hence the Darcy's equation is the momentum equation used in place of the Navier Stokes equation in the developed numerical solver (discussed in Section 3.3 with further details given in Appendix C)

$$\boldsymbol{v} = -\frac{\bar{\bar{K}}}{\mu}\nabla P \qquad (3\text{-}1)$$

$$\underset{\substack{rate\ of\ increase\\ of\ mass\\ per\ unit\ volume}}{\frac{\partial}{\partial t}(\phi\rho)} + \underset{\substack{net\ rate\ pf\ mass\\ addition\ per\ unit\ volume\\ by\ convection}}{\nabla\cdot(\rho\boldsymbol{v})} = 0 \qquad (3\text{-}2)$$

$$\frac{\partial}{\partial t}(\phi\rho) + \nabla\cdot\left(-\rho\frac{\bar{\bar{\boldsymbol{K}}}}{\mu}\nabla P\right) = 0 \qquad (3\text{-}3)$$

Using an appropriate equation of state (EOS) to express density as a function of pressure (e.g. $\rho = \frac{P}{ZRT}$), Equation 3-3 can be expressed explicitly as a function of pressure.

$$\frac{\partial}{\partial t}\left(\phi\frac{P}{ZRT}\right) + \nabla\cdot\left(-\rho\frac{\bar{\bar{\boldsymbol{K}}}}{\mu}\nabla P\right) = 0 \qquad (3\text{-}4)$$

Where $\boldsymbol{v}$ is the flow velocity, ρ is the density, ϕ is the porosity, P is the pressure, μ is the viscosity, R is the specific gas constant, T is the temperature, Z is the gas compressibility factor and $\bar{\bar{\boldsymbol{K}}}$ is the permeability tensor.

Equation 3-4, the basic diffusivity equation used to calculate pressure, can be solved by numerical methods. However, the flow behaviour departs from the Darcy's law at high flow velocities, where the fundamental assumption of laminar flow is no longer valid. Geertsma (1974) provided the limits for applying Darcy's law in gas and high rate oil wells.

Traditionally used analytical pressure solutions assume that Darcy's Law, with its laminar flow assumption, is valid. Initially, the non-Darcy (inertial) effects will not be included in the numerical simulations. This will ensure consistency with the assumptions behind the analytical solutions. The boundaries of the region in which non-Darcy effects can be neglected would be defined in a later section.

3.2.2 The Thermal Model:

An energy balance formulation (Equation 3-7) for non-isothermal systems is given in Bird et al. (2007). This equation is used as the starting point of the thermal model which

describes the change in temperature in porous media making it possible to solve directly for temperature which is the property of interest in this thesis.

$$\underset{\substack{\text{rate of increase of}\\ \text{kinetic energy}\\ \text{per unit volume}}}{\frac{\partial}{\partial t}\left(\frac{1}{2}\rho v^2\right)} = \underset{\substack{\text{rate of addition of}\\ \text{kinetic energy by}\\ \text{convection per unit volume}}}{-\left(\nabla\cdot\frac{1}{2}\rho v^2\boldsymbol{v}\right)} \underset{\substack{\text{rate of work done by}\\ \text{pressure of surroundings}\\ \text{on the fluid}}}{-(\nabla\cdot P\boldsymbol{v})} \underset{\substack{\text{rate of reversible}\\ \text{conversion of kinetic}\\ \text{energy to internal energy}}}{-P(-\nabla\cdot\boldsymbol{v})} \underset{\substack{\text{rate of work done}\\ \text{by viscous forces}\\ \text{on the fluid}}}{-(\nabla\cdot[\tau\cdot\boldsymbol{v}])} \underset{\substack{\text{rate of irreversible}\\ \text{conversion}\\ \text{from kinetic to}\\ \text{internal energy}}}{-(-\tau\colon\nabla\boldsymbol{v})} \underset{\substack{\text{rate of work}\\ \text{by external force}\\ \text{on the fluid}}}{+\rho(\boldsymbol{v}\cdot g)}$$

(3-5)

$$\underset{\substack{\text{rate of increase of}\\ \text{energy per unit}\\ \text{volume}}}{\frac{\partial}{\partial t}\left(\frac{1}{2}\rho v^2+\rho\widehat{U}\right)} = \underset{\substack{\text{rate of energy addition}\\ \text{per unit volume by}\\ \text{convective transport}}}{-\left(\nabla\cdot\left(\frac{1}{2}\rho v^2+\rho\widehat{U}\right)\boldsymbol{v}\right)} \underset{\substack{\text{rate of energy addition}\\ \text{per unit of volume by}\\ \text{heat conduction}}}{-(\nabla\cdot q)} \underset{\substack{\text{rate of work done on}\\ \text{fluid per unit volume}\\ \text{by pressure forces}}}{-(\nabla\cdot P\boldsymbol{v})} \underset{\substack{\text{rate of work done on}\\ \text{fluid per unit volume}\\ \text{by viscous forces}}}{-(\nabla\cdot[\tau\cdot\boldsymbol{v}])} \underset{\substack{\text{rate of work done on}\\ \text{fluid per unit volume}\\ \text{by external forces}}}{+\rho(\boldsymbol{v}\cdot g)}$$

(3-6)

$$\underset{\substack{\text{rate of increase}\\ \text{of internal}\\ \text{energy per unit}\\ \text{volume}}}{\frac{\partial}{\partial t}\rho\widehat{U}} = \underset{\substack{\text{net rate of addition}\\ \text{of internal energy}\\ \text{by convective transport}\\ \text{per unit volume}}}{-\left(\nabla\cdot\rho\widehat{U}\boldsymbol{v}\right)} \underset{\substack{\text{rate of internal}\\ \text{energy addition}\\ \text{per unit of volume}\\ \text{by heat conduction}}}{-(\nabla\cdot q)} \underset{\substack{\text{reversible rate of}\\ \text{internal energy increase}\\ \text{per unit volume}\\ \text{by compression}}}{-P(\nabla\cdot\boldsymbol{v})} \underset{\substack{\text{irreversible rate of}\\ \text{internal energy increase}\\ \text{per unit volume}\\ \text{by viscous dissipation}}}{-(\tau\colon\nabla\boldsymbol{v})}$$

(3-7)

The equation of change for internal energy (Equation 3-7) is obtained by subtracting the "mechanical energy equation" (Equation 3-5) from the "energy equation" (Equation 3-6).

The thermal model (Equation 3-8) proposed by Weibo Sui et al. (2008), is obtained from the equation of change for internal energy (Equation 3-7). The model derivation and the assumptions made are presented in Appendix A. The thermal model (Equation 3-8) includes temperature changes in porous media due to transient fluid expansion, Joule-Thomson effect, heat conduction and convection.

$$\overline{\rho C_P}\,\frac{\partial T}{\partial t} - \emptyset\beta_T T\frac{\partial P}{\partial t} - \emptyset C_f\left(P + \rho_r C_{Pr} T\right)\frac{\partial P}{\partial t} = -\rho \boldsymbol{v} C_P \cdot \nabla T + \beta_T T \boldsymbol{v} \cdot \nabla P - \boldsymbol{v} \cdot \nabla P + K_T \nabla^2 T \qquad (3\text{-}8)$$

Where: C_P and C_{Pr} are the specific heat capacity of the gas and formation rock respectively, ρ_r is the density of the formation rock C_f is the formation compressibility, $\boldsymbol{v}$ is velocity, β_T is the thermal expansion coefficient, K_T is the thermal conductivity, T is the temperature and $\overline{\rho C_P}$ is the mean formation heat capacity.

3.3 Numerical Modelling

OpenFOAM, an open source library for numerical simulations in continuum mechanics using the finite volume method, was chosen for this work. Using an open-source library makes it possible to modify existing solvers or create new solvers which use existing library components (Jasak et al. 2007). OpenFOAM provides the flexibility needed.

3.3.1 Solver Modification

An existing solver "rhoPimpleFoam" (OpenFOAM Foundation 2014), -originally designed to simulate transient laminar or turbulent flow of compressible fluids- was customized to simulate transient compressible flow in porous media as follows:

1. Adding the ability to read gas property tables allows the inclusion of the actual pressure-temperature dependence for the properties of different gasses (see Appendix B for details).

2. Changing the momentum equation to Darcy's Equation (Equation 3-1).

3. Modifying the continuity equation for porous media flow (Equation 3-2).

4. Altering the energy equation to the thermal model (Equation 3-8) published by (Weibo Sui et al. 2008).

An auxiliary library, "swak4foam", is used alongside OpenFOAM to set the variable properties for each element in the mesh. Figure 3-1 is a flowchart of the solution procedure followed by the solver.

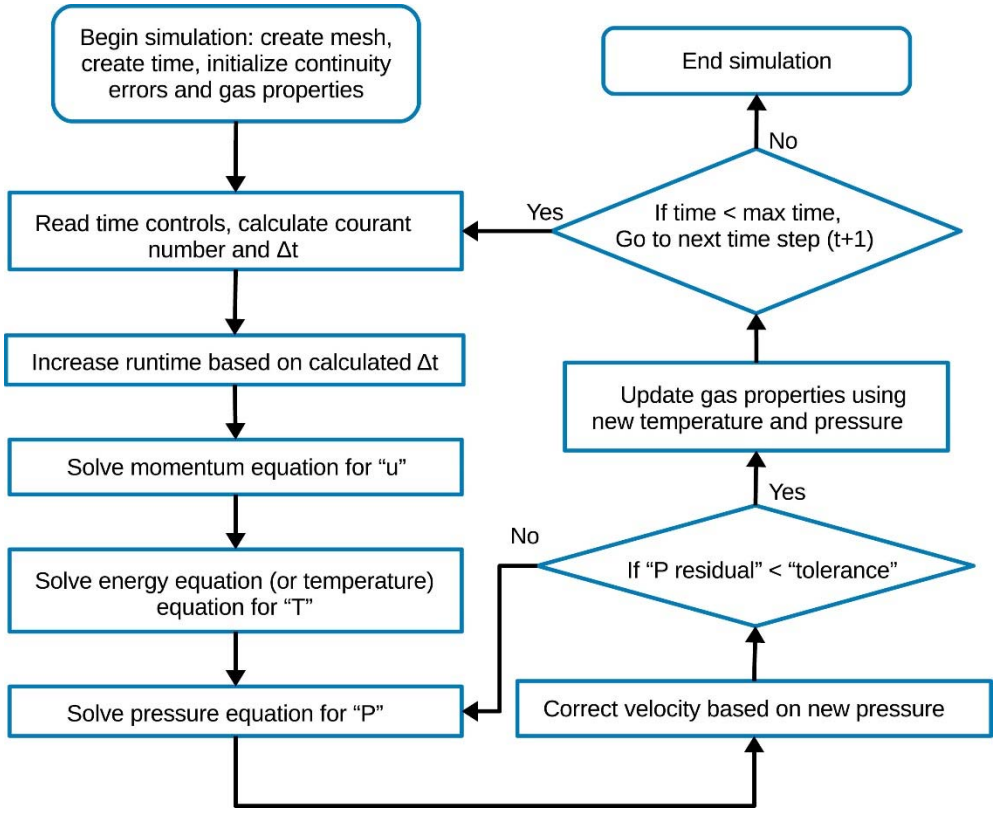

Figure 3-1: Flowchart for numerical simulation

3.3.2 Simulation Setup

A quarter symmetry element of a cylindrical numerical simulation model of a vertical, open-hole wellbore situated in the cetre of a cicular, horizontal reservoir was prepared (Figure 3-2). The numerical mesh employed grid refinement in the radial direction near the wellbore, since the transient effect is greatest in the near-wellbore region. The

gridding was prepared using OpenFOAM's "simpleGrading" method. This method emplys a uniform expansion ratio that is based on the ratio between the first to the last element lengths (the well radius and the boundary radius respectively).

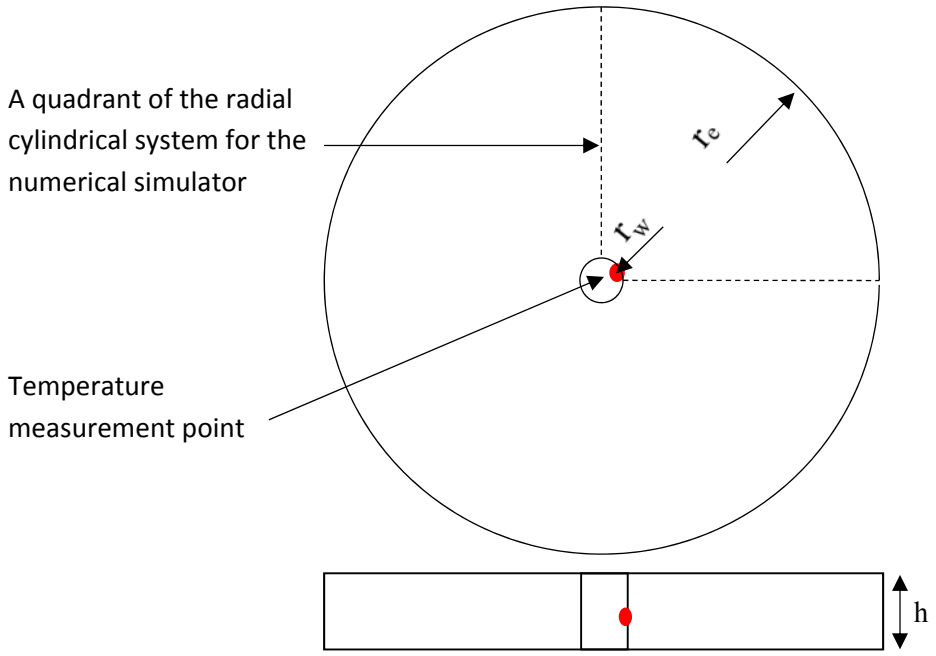

Figures 3-2: Radial cylindrical system, showing quadrant for numerical simulation and temperature probe.

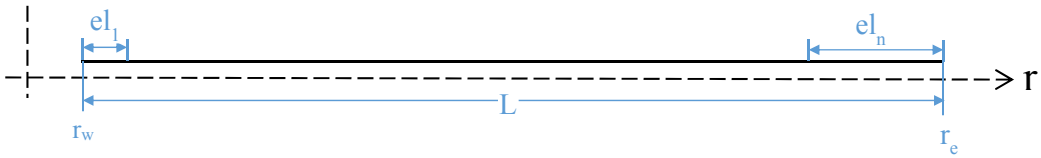

Figures 3-3: Radial direction showing first and last element lengths.

The expansion ratio "ER" is calculated from Equation 3-9

$$ER = \frac{el_1}{el_n} \qquad (3\text{-}9)$$

$$L = r_e - r_w = \sum_{i=1}^{n} el_i = \frac{el_1(1-\varepsilon^n)}{(1-\varepsilon)} \qquad (3\text{-}10)$$

$$el_i = el_1(\varepsilon^{i-1}) \qquad (3\text{-}11)$$

Where n is number of radial mesh elements, L is the radial length, r_e is the exterior radius of reservoir boundary, r_w is the well radius, el_i is the radial length of the i^{th} element.

$$\varepsilon = \frac{el_{i+1}}{el_i} \qquad (3\text{-}12)$$

The model was divided into 40 grid blocks in the z-direction. Only radial fluid flow is consdered in the model. A vertical, geothermal gradient of 0.025K/m was imposed across the model, allowing heat conduction to occur in this direction. Heat exchange with the underlying and overlying formations was not modelled. It was assumed that it has a negligible impact at early times, as observed by Muradov & Davies (2012a).

Most, if not all, gas reservoirs have a temperature greater than the critical temperature for the chosen natural gas composition. The fluid will thus exist purely in the gaseous state regardless of the reservoir pressure. Appendix B lists the gas property equations and correlations used.

The density of a gas is a function of the pressure (Equation 3-13) while Equation 3-14 gives the gas hydrostatic head at the bottom of the reservoir and Equation 3-15 is the relative magnitude of hydrostatic head to the reservoir pressure. A reservoir thicknesses of about 200 m together with the (Appendix B) natural gas properties indicates a ~ 2% change in pressure across the height of the reservoir; allowing a constant reservoir pressure assumed for all elements with sufficient accuracy.

$$\rho = \frac{P}{ZRT} \qquad (3\text{-}13)$$

$$P_h = \rho g \Delta z \qquad (3\text{-}14)$$

$$\frac{P_h}{P} = \frac{g\Delta z}{ZRT} \qquad (3\text{-}15)$$

Where P_h is the hydrostatic pressure, R is the specific gas constant, T is temperature, Δz is reservoir thickness and Z is the real gas compressibility factor.

3.3.3 Model Testing and Verification

3.3.3.1 Verification of the Pressure Solution:

The above numerical model can be compared with the analytical Line Source pressure Solution (LSS) for an infinitely acting reservoir with a constant, laminar flow, production rate in a radial system (Al-Hussainy et al. 1966). Their solution uses "pseudo-pressure", a term that combines the pressure, the viscosity and the gas compressibility, or Z-factor, into one equation (Equation 3-16). Equation 3-17 is pseudo-pressure solution by Al-Hussainy et al. (1966).

$$\psi = \int_{Pref}^{P} \left(\frac{2P}{\mu Z}\right) dp \qquad (3\text{-}16)$$

$$\psi = \psi_i - \frac{\psi_i Q_d}{2} Ei\left(\frac{\varphi \mu c r^2}{4\lambda k t}\right) \qquad (3\text{-}17)$$

$$Q_d = \frac{\Gamma T Q_{sc}}{kh\psi_i} \qquad (3\text{-}18)$$

Where: Q_d is the dimensionless rate, Γ is a constant multiplication factor, k is the permeability, h is the reservoir thickness and ψ_i is the pseudo-pressure at initial reservoir conditions.

Figure 3-4 is a comparison of the numerical and analytical solutions for the model parameters described in Appendix D. A close match is observed for both the radial pressure distribution and the transient wellbore pressures.

The reservoir temperature decreases as the well starts producing at a constant mass flow rate of gas (Figure 3-5). This is due to (1) the cooling due to transient gas expansion (a dominant effect initially that quickly disappears, as confirmed by the analytical solution) and (2) the Joule-Thomson cooling (a nearly constant effect that acts as a non-uniformly distributed heat sink). Heat conduction, as will be discussed later, is negligible compared to heat convection.

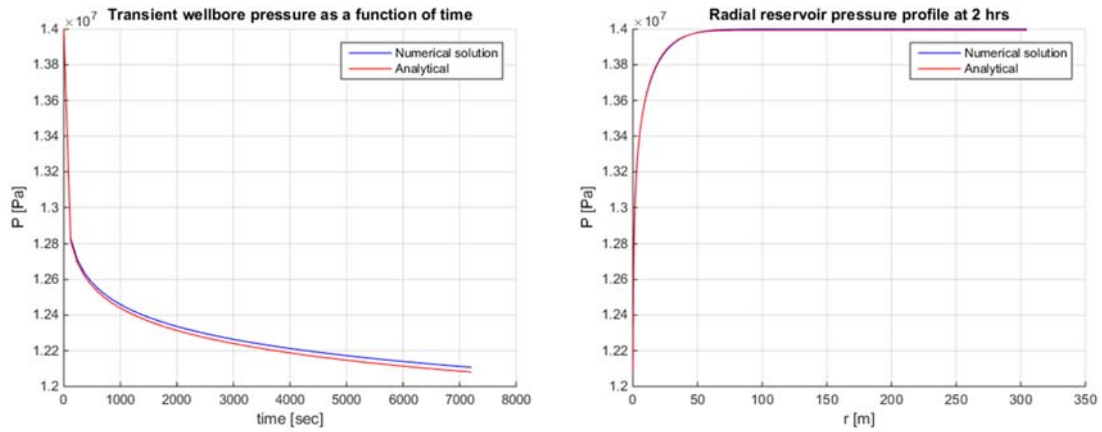

Figures 3-4: Plot of numerical and analytical solution (a) Transient wellbore pressure, (b) Radial reservoir pressure

3.3.3.2 Verification that the Mesh Refinement and Time Step Size are Sufficient

Figures 3-5 and 3-6 illustrate the sensitivity of the numerical solution to the size of the time step and the mesh (using the case study in Appendix D). As expected, the mesh size had the greatest effect on the solution accuracy (see Figure 3-6 and Table 3-2). This occurs because the solver automatically adjusts the time step to ensure convergence even when large time steps are used (see Figure 3-5 and Table 3-1).

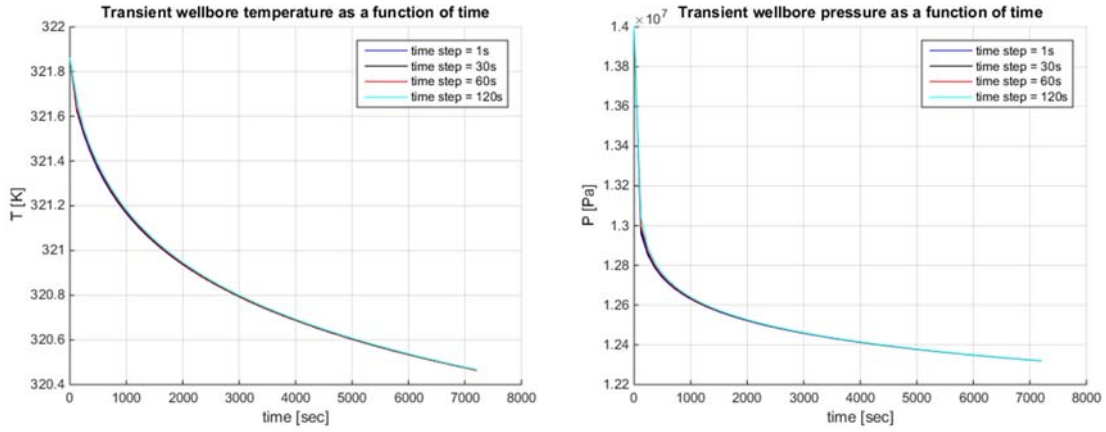

Figure 3-5: Plot of wellbore pressure and temperature for different time-step size (a) Transient wellbore temperature, (b) Transient wellbore pressure

Table 3-1: Effect of time step size on simulation time

Time step (seconds)	1	30	60	120
Simulation time (seconds)	34,171	3,154	2,309	1,233

.

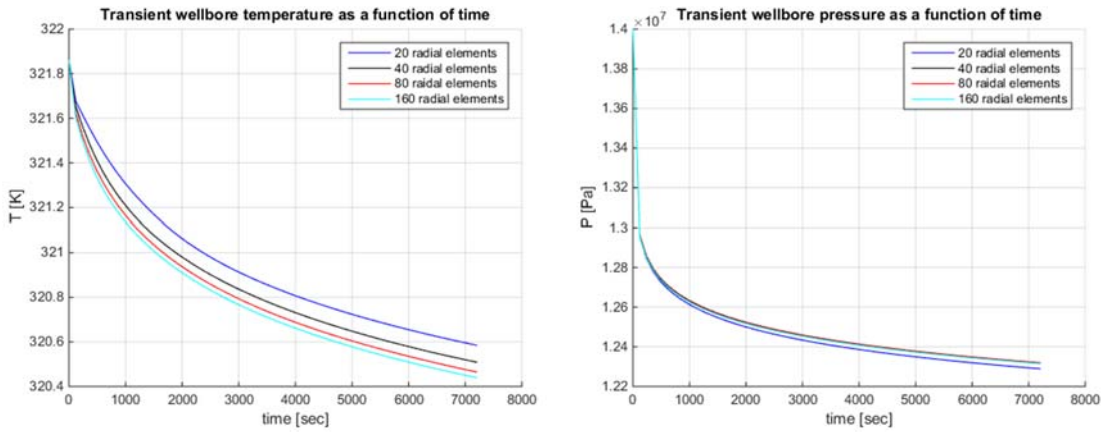

Figure 3-6: Plot of wellbore pressure and temperature for different number of element (a) Transient wellbore temperature, (b) Transient wellbore pressure

Table 3-2: Effect of element size (or number of elements) on simulation time

Radial elements	20	40	80	160
Simulation time (seconds)	360	2,857	33,416	133,116

The solutions converge as the number of mesh elements increase (Figure 3-6). The selected mesh size and time step corresponds to the converging cases, namely: the mesh with 80 radial elements and a time step of 1 second.

3.4 Analytical Modelling

Knowledge of the pressure distribution in the zone of interest is required when using the thermal model (Equation. 3-8) to develop an analytical solution. Developing this analytical solution requires a number of assumptions and a combination of numerical simulations and existing solutions. First, a scaling analysis is carried out to determine the order of magnitude of the terms in the thermal model, and also determine if there are any negligible terms. The case study described in Appendix D is then used to study and validate the derived analytical solution.

3.4.1 Scaling Analysis

A scaling analysis is carried out to investigate the order of magnitude of the terms in the thermal model.

The following dimensionless parameters are defined and used to non-dimensionalize the thermal model using a method by Krantz et al. (2007) and Kopaygorodsky et al. (2001).

$$r_D = \frac{r - r_r}{r_s} \tag{3-19}$$

$$t_D = \frac{t - t_r}{t_s} \tag{3-20}$$

$$P_D = \frac{P_r - P}{P_s} \tag{3-21}$$

$$T_D = \frac{T_r - T}{T_s} \tag{3-22}$$

Using the thermal model in Equation. 3-8 and the boundary and initial conditions defined in Equation 3-23 to Equation 3-28, the dimensionless parameters defined above are scaled, so their absolute values are bounded between zero and one.

Initial conditions ($t = 0, r_w \leq r \leq r_e$):

$$P = P_i \tag{3-23}$$

$$T = T_i \tag{3-24}$$

Boundary conditions at the well ($r = r_w, 0 \leq t \leq t_{stab} = \frac{\varphi \mu c r_e^2}{4\lambda k}$):

$$\frac{\partial T}{\partial r} = 0 \tag{3-25}$$

$$\frac{\partial P}{\partial r} = -\frac{v\mu}{k} \tag{3-26}$$

Boundary conditions at the reservoir lateral boundary ($r = r_e, 0 \leq t \leq t_{stab} = \frac{\varphi \mu c r_e^2}{4\lambda k}$):

$$P = P_i \tag{3-27}$$

$$T = T_i \qquad (3\text{-}28)$$

The reference value r_r can be determined by setting the dimensionless radius $r_D = 0$ at the wellbore, while the scale value is determined by setting $r_D = 1$ at the reservoir's lateral boundary

$$r_D = \frac{r_w - r_r}{r_s} = 0 \qquad (3\text{-}29)$$

$$r_D = \frac{r_e - r_r}{r_s} = 1 \qquad (3\text{-}30)$$

$$\therefore r_D = \frac{r - r_w}{r_e - r_w} \qquad (3\text{-}31)$$

The reference and scale values for time, i.e. t_r and t_s respectively, can be determined by setting $t_D = 0$ at the initial time $t = 0$ and $t_D = 1$ at the stabilization time $t_{st} = \frac{\varphi \mu c r_e^2}{4\lambda k}$.

$$t_D = \frac{0 - t_r}{t_s} = 0 \qquad (3\text{-}32)$$

$$t_D = \frac{t_{st} - t_r}{t_s} = 1 \qquad (3\text{-}33)$$

$$\therefore t_D = \frac{t}{t_{st}} \qquad (3\text{-}34)$$

The scale and reference values for P_D can be obtained by setting $P_D = 0$ at the initial condition when $P(r,t) = P_i$ and $P_D = 1$ at full drawdown, i.e. when $P(r,t) = 0$

$$P_D = \frac{P_r - P_i}{P_s} = 0 \qquad (3\text{-}35)$$

$$P_D = \frac{P_r - 0}{P_s} = 1 \qquad (3\text{-}36)$$

$$\therefore P_D = \frac{P_i - P}{P_i} \qquad (3\text{-}37)$$

Finally, the scale and reference values for T_D can be obtained by setting $T_D = 0$ at the initial condition when, $T(r,t) = T_i$ and $T_D = 1$ at full drawdown, i.e. when $T(r,t) = 0$

$$T_D = \frac{T_r - T_i}{T_s} = 0 \qquad (3\text{-}38)$$

$$T_D = \frac{T_r - 0}{T_s} = 1 \qquad (3\text{-}39)$$

$$\therefore T_D = \frac{T_i - T}{T_i} \qquad (3\text{-}40)$$

The dimensionless variables defined above are substituted into the thermal model to give Equation 3-41 below.

$$\frac{\overline{\rho C_P}(r_e - r_w)^2}{K_T t_{st}} \frac{\partial T_D}{\partial t_D} - \frac{\varphi \eta \rho C_P P_i (r_e - r_w)^2}{K_T t_{st} T_i} \frac{\partial P_D}{\partial t_D} = -\frac{\rho v C_P (r_e - r_w)}{K_T} \frac{\partial T_D}{\partial r_D} + \frac{\varepsilon \rho v C_P P_i (r_e - r_w)}{K_T T_i} \frac{\partial P_D}{\partial r_D} + \frac{\partial^2 T_D}{\partial r_D^2} + \frac{(r_e - r_w)}{[(r_e - r_w) r_D + r_w]} \frac{\partial T_D}{\partial r_D} \qquad (3\text{-}41)$$

The following dimensionless groups can be derived from the non-dimensionalized thermal model.

$$\frac{\overline{\rho C_P}(r_e - r_w)^2}{K_T t_{st}} = \frac{1}{Fo_f} \qquad (3\text{-}42)$$

$$\frac{\rho C_P (r_e - r_w)^2}{K_T t_{st}} = \frac{1}{Fo_g} \qquad (3\text{-}43)$$

$$\frac{\rho v C_P (r_e - r_w)}{K_T} = Pe \qquad (3\text{-}44)$$

$$\frac{\varepsilon P_i}{T_i} = \varepsilon_D \qquad (3\text{-}45)$$

$$\frac{\eta P_i}{T_i} = \eta_D \qquad (3\text{-}46)$$

$$\frac{(r_e - r_w)}{[(r_e - r_w)r_D + r_w]} = G_D \qquad (3\text{-}47)$$

The non-dimensionalized thermal model can be reformulated as Equation 3-48

$$\frac{1}{Fo_f}\frac{\partial T_D}{\partial t_D} - \frac{\varphi\eta_D}{Fo_g}\frac{\partial P_D}{\partial t_D} = -Pe\frac{\partial T_D}{\partial r_D} + \varepsilon_D Pe\frac{\partial P_D}{\partial r_D} + \frac{\partial^2 T_D}{\partial r_D^2} + G_D\frac{\partial T_D}{\partial r_D} \qquad (3\text{-}48)$$

Table 3-3: Scaling analysis

Dimensionless parameters	Scale	Dimensionless coefficients	Scale
Fo_f	4.235×10^{-6}	$\frac{1}{Fo_f}$	2.361×10^{5}
Fo_g	2.98×10^{-5}	$\frac{\varphi\eta_D}{Fo_g}$	1.283×10^{3}
φ	0.15	Pe	9.7909×10^{4}
η_D	0.2549	$\varepsilon_D Pe$	9.7909×10^{3}
ε_D	0.1018	1	1
Pe	9.7909×10^{4}	G_D	0.9996
G_D	0.9996		

The results of the scaling analysis is presented in Table 3-3. It shows that heat convection is the most important effect, followed by the Joule-Thomson effect and then the adiabatic expansion, while heat conduction effect can be ignored since it is about three orders of magnitude less than the other ones, this result is similar to the assumptions made by Ramazanov et al. (2010) and Onur & Çinar (2016). The scaling analysis was carried out for the infinite acting radial flow case, which in most cases is considered long enough for transient temperature analysis.

3.4.2 Assumptions Made in the Analytical Model

The following observations made it possible to simplify the thermal model sufficiently to obtain an asymptotic solution for the temperature at early times.

3.4.2.1 Temperature Independence of the Pressure Solution

The assumption that small temperature change does not significantly affect the pressure solution was confirmed by comparing the solution of the combined pressure and temperature equations and the equivalent pressure solution at a constant temperature. Very little pressure difference (~0.2% in Figure 3-7) is observed between the two solutions.

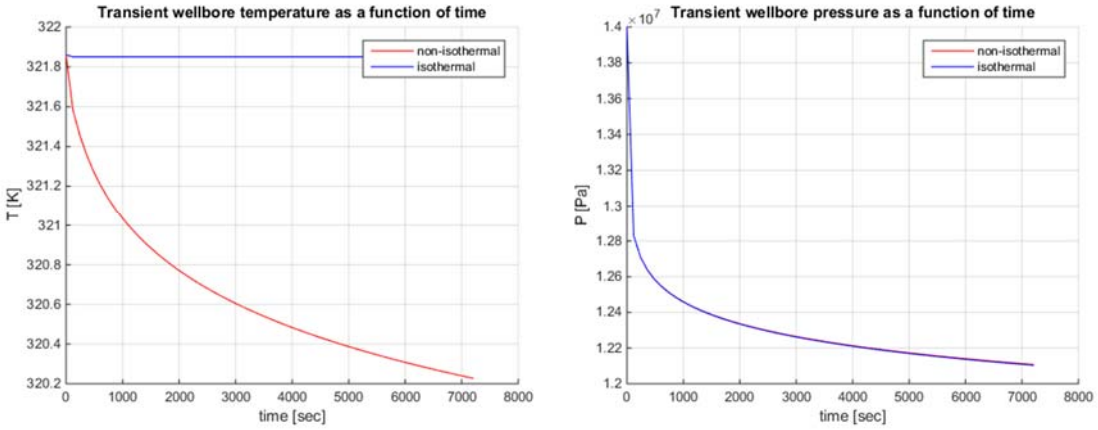

Figure 3-7: Plot of wellbore pressure and temperature for isothermal and non-isothermal conditions (a) Transient wellbore pressure, (b) Transient wellbore temperature

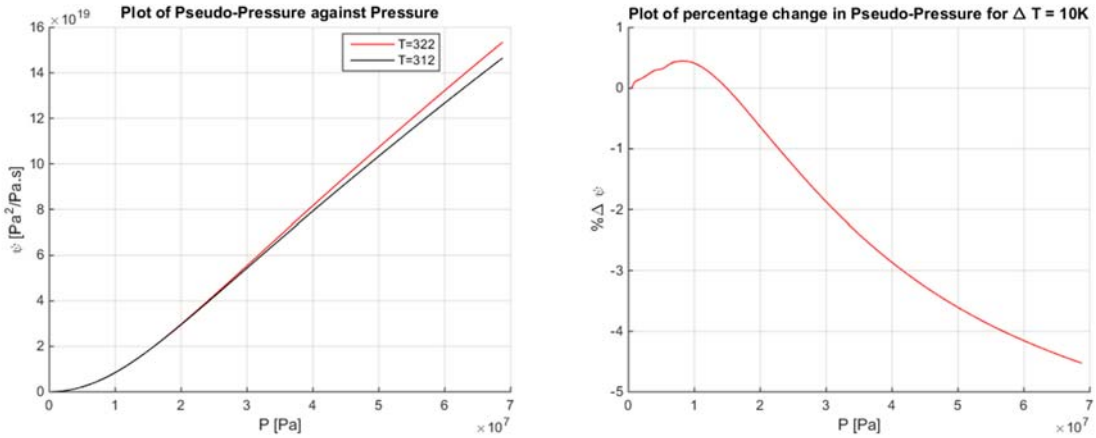

Figure 3-8: Plot of (a) Pseudo-pressure against pressure, (b) Percentage change in pseudo-pressure for $\Delta T = 10℃$

Similarly, the variation in the pseudo-pressure for a natural gas can be shown to be negligible (Figure 3-8) by considering the effect of the relatively small ($\Delta T \leq 10K$) temperature change. It is expected that changes in the pressure solution will also be negligible since it can also be expressed as a function of pseudo-pressure. A reasonable conclusion is that it is not necessary to account for the effect of temperature change when using the existing pressure solution in the thermal model for such relatively small

formation temperature changes. This assumption simplifies the problem's solution by allowing the pressure to be decoupled from the temperature.

3.4.2.2 The Negligible Effect of Heat Conduction

The observation that heat conduction has very little effect on transient temperature at early times has also been verified numerically (Figure 3-9) by comparing simulations which included and neglected the thermal conductivity. The contribution of heat conduction to the transient temperature response at early times was found to be small (< 4% with a maximum temperature change of 0.03K). It also had virtually no effect on the pressure response.

Conduction can thus be neglected (for drawdown sandface transient temperature) without significantly affecting the accuracy of the solution. This has also been shown in the scaling analysis and other TTA studies (Onur & Çinar 2016).

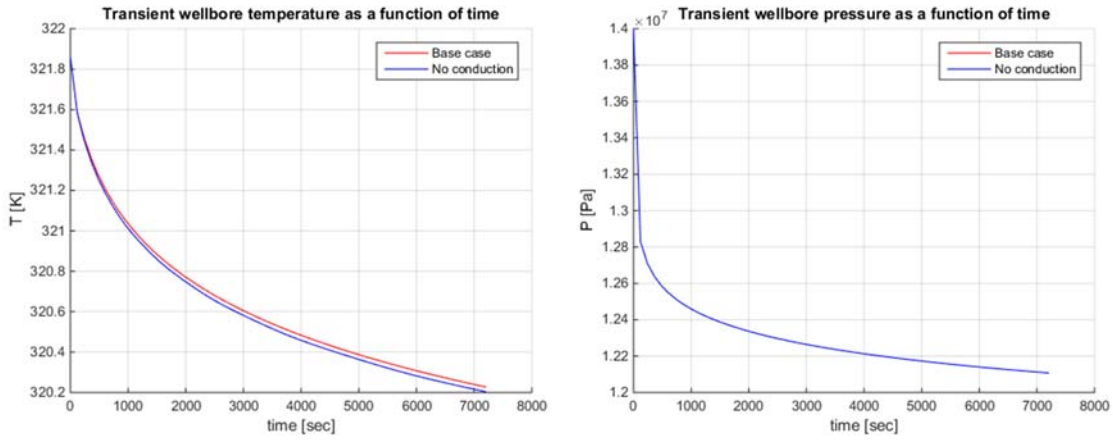

Figure 3-9: Plot of wellbore pressure and temperature for base case and case with conduction effects neglected (a) Transient wellbore pressure, (b) Transient wellbore temperature

Equation 3-49 simplifies the thermal model by eliminating the conduction term:

$$\overline{\rho C_P}\,\frac{\partial T}{\partial t} - \emptyset\beta_T T\frac{\partial P}{\partial t} - \emptyset C_f\left(P + \rho_r C_{Pr} T\right)\frac{\partial P}{\partial t} = -\rho \boldsymbol{v} C_p \cdot \nabla T + \beta_T T \boldsymbol{v} \cdot \nabla P - \boldsymbol{v} \cdot \nabla P \qquad (3\text{-}49)$$

N.B. App & Yoshioka (2011) showed that, when the Peclet number approaches zero, the conduction effect can become dominant. An example is a tight, very low permeability,

formation with low flow velocities. For production from conventional reservoirs (similar to what is being studied) the Peclet number is usually high enough to ignore conduction effects.

3.4.3 Identification of the Value of the Constant Parameters in Equation 3-49

The value of some of the coefficients in the simplified thermal model (with conduction elliminated) has been investigated by modelling a one-dimensional, radial system with a constant production rate and infinite acting boundaries. Equation 3-49 can be written in a different form:

$$K1\frac{\partial T}{\partial t} - K2\frac{\partial P}{\partial t} = K3 \cdot \frac{\partial P}{\partial r} \cdot \frac{\partial T}{\partial r} - K4\left(\frac{\partial P}{\partial r}\right)^2 \qquad (3\text{-}50)$$

The coefficients K1, K2, K3 and K4 can be defined by comparing Equation 3-50 with Equation 3-49:

$$K1 = \overline{\rho C_P} = \phi\rho C_p + (1-\phi)\rho_r C_{pr} \qquad (3\text{-}51)$$

$$K2 = \emptyset\beta_T T + \emptyset C_f\left(P + \rho_r C_{Pr} T\right) \qquad (3\text{-}52)$$

$$K3 = \frac{\rho C_p k}{\mu} \qquad (3\text{-}53)$$

$$K4 = \frac{(\beta_T T - 1)k}{\mu} \qquad (3\text{-}54)$$

The values of K1, K2, K3 and K4 may be calculated based on the numerical simulation results for the case considered. The relative change in the values of K1, K2, K3 and K4 over the pressure and temperatre changes considered were 0.36%, 1.5%, 12.06% and 0.94% respectively. K1, K2 and K4 may be assumed to be constant, further simplifying the derivation of the analytical solutions.

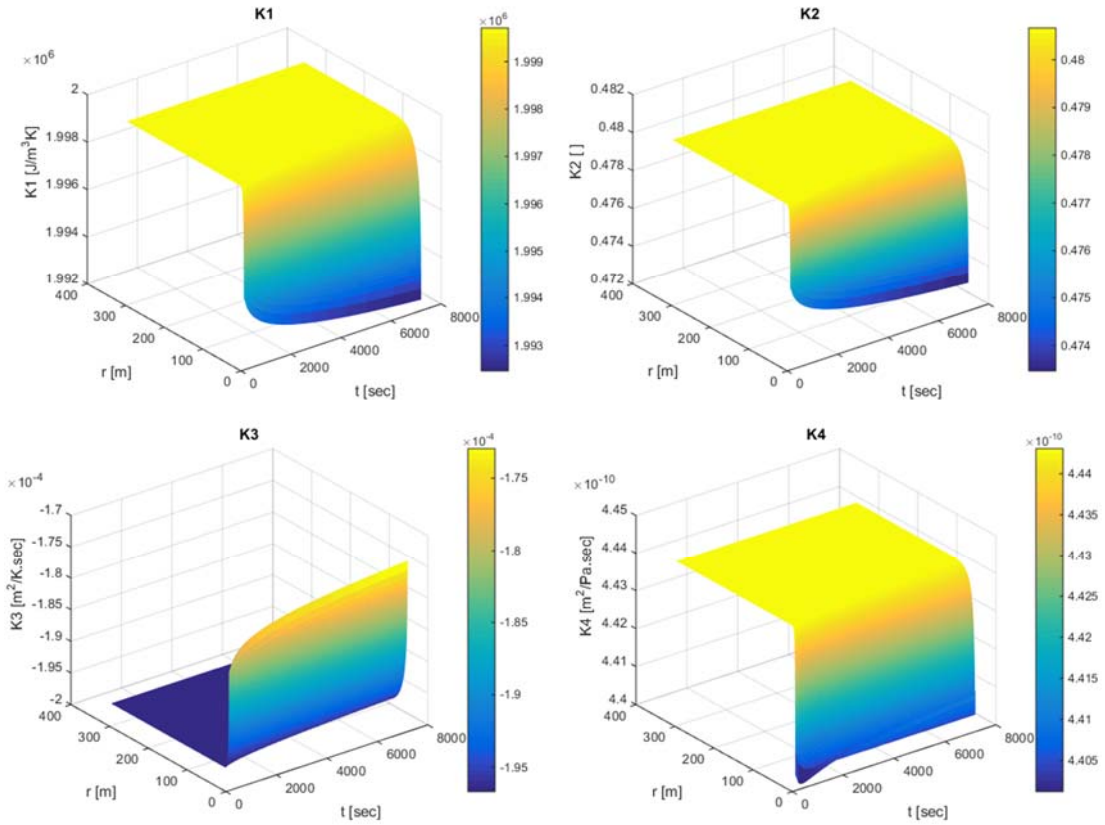

Figure 3-10: Plot of coefficients of Equation 3-50 (a) Coefficient K1, (b) Coefficient K2, (c) Coefficient K3, (d) Coefficient K4

3.4.4 Solution of the Simplified Thermal Model

3.4.4.1 Assumptions:

The following assumptions were made in arriving at the early-time solution:

1. Conduction and heat exchange with the surrounding rocks effects are negligible.

2. The existing Line Source Pressure Solution (at constant temperature) for gas flow in porous media can be used to calculate pressure.

3. The relationship between pressure and pseudo-pressure can be represented by a straight line. This is normally valid within the range of pressure between the initial reservoir pressure and the bottomhole flowing pressure (measured for the period of the analysis).

4. The term $exp\left(-\frac{\varphi\mu cr^2}{4\lambda kt}\right)$ can be assumed to equal unity for r < 3 m (a typical investigation distance in TTA) if very early times (t < 0.5 hrs) are excluded. This is shown graphically in Figure 3-12. $exp\left(-\frac{\varphi\mu cr^2}{4\lambda kt}\right) = exp\left(-\frac{\alpha r^2}{t}\right) \approx 1$

5. Non-Darcy effects are neglected[1].

6. There is instantaneous thermal equilibrium between the rock and the flowing fluid.

Further assumptions about the gas properties are as follows;

7. The reservoir and well temperature are always higher than the critical temperature of the gas and below the Joule-Thomson inversion temperature.

8. The gas behaviour can be adequately modelled using the real gas compressibility factor (z-factor).

The following assumptions are required when using the line source, pressure solution (Ahmed 2006):

9. The reservoir is infinitely acting.

10. The well is producing at a constant flow rate.

11. The wellbore, radius r_w, is situated at the centre of the reservoir.

3.4.4.2 Solution Method:

A linear relationship between pressure and pseudo-pressure was derived. This was obtained for a specific gas by calculating the gradient (or fitting a straight line) of the pressure pseudo-pressure curve between the value at the initial reservoir pressure and the

[1] The effect of this assumption is discussed in the literature review and in a subsequent section of this chapter and the next chapter.

lowest expected flowing bottomhole pressure. This relationship can be obtained from the gas PVT data or by using appropriate correlations.

$$P = A + B\psi \qquad (3\text{-}55)$$

$$dP/d\psi = B \qquad (3\text{-}56)$$

The above relationship was derived around the initial temperature and pressure of the reservoir, as required by the thermal model. This relationship, determined from Figure 2-4 of (ERCB 1979), enables us to convert the pseudo-pressure solution to the pressure. Figure 3-11 is the plot of the pressure versus the pseudo-pressure. There is an approximately linear correlation between these two parameters in the area of interest indicated (indicated by a red box).

Where: $= 6 \times 10^{6}\ [Pa]$, $B = 0.5 \times 10^{-12}\ [Pa/(Pa^2/Pa.s)]$, $\psi: Pseudo - pressure\ [(Pa^2/Pa.s)]$, $P: Pressure\ [Pa]$

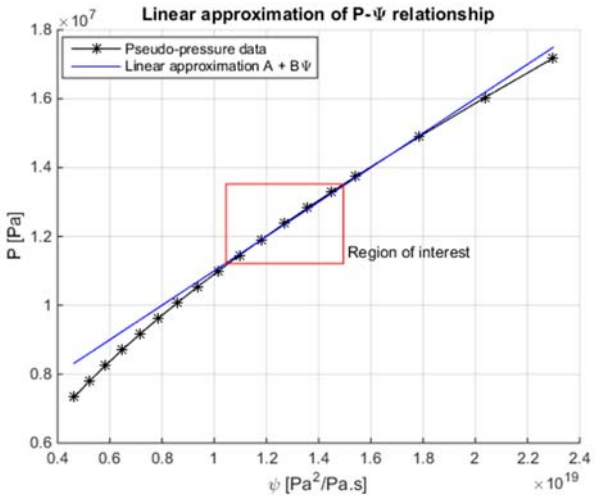

Figure 3-11: Plot showing linear approximation of pressure pseudo-pressure relationship

The pressure drawdown satisfies the Darcy assumption when there is a linear relationship between pressure and pseudo-pressure for all values and at most times between the bottomhole pressure and the reservoir pressure.

Using the existing Line Source Pressure Solution (LSS) for gas flow in porous media:

$$\psi = \psi_i \mp \frac{\psi_i Q_d}{2} Ei\left(-\frac{\varphi\mu C_t r^2}{4\lambda kt}\right) \quad (3\text{-}57)$$

$$d\psi/_{dr} = \frac{\psi_i Q_d}{2}\left[\frac{exp\left(-\frac{\varphi\mu C_t r^2}{4\lambda kt}\right)}{\left(\frac{\varphi\mu C_t}{4\lambda kt}\right)}\right]\left(\frac{2\varphi\mu C_t r}{4\lambda kt}\right) = \psi_i Q_d\left[\frac{exp\left(-\frac{\varphi\mu C_t r^2}{4\lambda kt}\right)}{r}\right] \quad (3\text{-}58)$$

$$d\psi/_{dt} = \frac{\psi_i Q_d}{2}\left[-\frac{exp\left(-\frac{\varphi\mu C_t r^2}{4\lambda kt}\right)}{\left(\frac{\varphi\mu C_t r^2}{4\lambda kt}\right)}\right]\left(\frac{-\varphi\mu C_t r^2}{4\lambda kt^2}\right) = -\frac{\psi_i Q_d}{2}\left[\frac{exp\left(-\frac{\varphi\mu C_t r^2}{4\lambda kt}\right)}{t}\right] \quad (3\text{-}59)$$

The solution for pressure as a function of radial position and time is obtained by combining the relationship between the pressure and the pseudo-pressure as described below:

$$P = A + B\left[\psi_i + \frac{\psi_i Q_d}{2} Ei\left(-\frac{\varphi\mu C_t r^2}{4\lambda kt}\right)\right] \quad (3\text{-}60)$$

$$dP/_{dr} = B\psi_i Q_d\left[\frac{exp\left(-\frac{\varphi\mu C_t r^2}{4\lambda kt}\right)}{r}\right] \quad (3\text{-}61)$$

$$dP/_{dt} = -\frac{B\psi_i Q_d}{2}\left[\frac{exp\left(-\frac{\varphi\mu C_t r^2}{4\lambda kt}\right)}{t}\right] \quad (3\text{-}62)$$

Excluding early times (t < 0.5 hr) and investigating near-wellbore zone (r < 3 m) gives: $exp\left(-\frac{\varphi\mu C_t r^2}{4\lambda kt}\right) = exp\left(-\frac{\alpha r^2}{t}\right) \approx 1$. Where $\alpha = \frac{\varphi\mu C_t}{4\lambda k} = 4.84182\ sec/m^2$

$$dP/_{dr} = B\frac{\psi_i Q_d}{r} \quad (3\text{-}63)$$

$$dP/_{dt} = -B\frac{\psi_i Q_d}{2t} \quad (3\text{-}64)$$

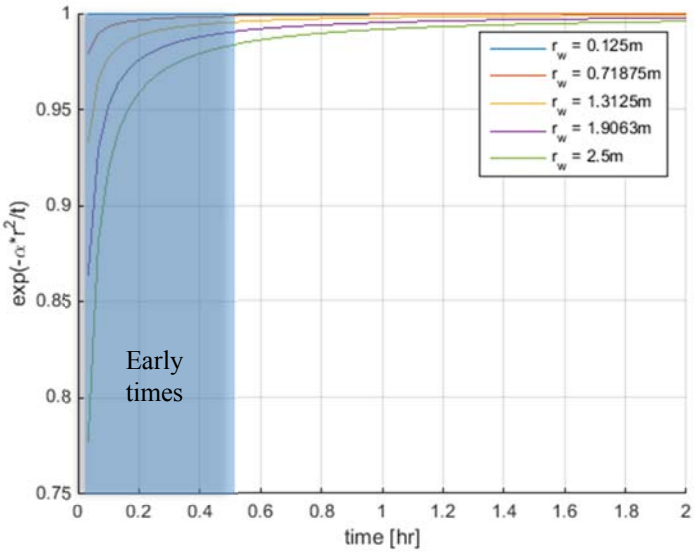

Figure 3-12: Plot of $exp\left(-\frac{\alpha r^2}{t}\right)$ showing approximation to unity

The assumption $exp\left(-\frac{\alpha r^2}{t}\right) \approx 1$ (Figure 3-12) gives a result equivalent to the log approximation of the line source solution for pressure.

The simplified thermal model Equation 3-57 can be expressed as Equation 3-65 below

$$\frac{\partial T}{\partial t} - \frac{K3}{K1} \cdot \frac{\partial P}{\partial r} \cdot \frac{\partial T}{\partial r} = \frac{K2}{K1}\frac{\partial P}{\partial t} - \frac{K4}{K1}\left(\frac{\partial P}{\partial r}\right)^2 \qquad (3\text{-}65)$$

Applying the method of characteristics to Equation 3-65, let $t = t(\tau)$ and $r = r(\tau)$

$$\frac{\partial t}{\partial \tau} = 1 \qquad (3\text{-}66)$$

$$\frac{\partial r}{\partial \tau} = -\frac{K3}{K1}\frac{\partial P}{\partial r} \qquad (3\text{-}67)$$

Equation 3-65 can be written in the form below.

$$\frac{\partial T}{\partial t}\frac{\partial t}{\partial \tau} + \frac{\partial T}{\partial r}\frac{\partial r}{\partial \tau} = \frac{\partial T}{\partial \tau} = \frac{K2}{K1}\frac{\partial P}{\partial t} - \frac{K4}{K1}\left(\frac{\partial P}{\partial r}\right)^2 \qquad (3\text{-}68)$$

Substitute Equation 3-66 and 3-67 into Equation 3-68

$$\frac{\partial T}{\partial \tau} = \frac{K2}{K1}\frac{\partial P}{\partial \tau} + \frac{K4}{K3}\frac{\partial P}{\partial \tau} \qquad (3\text{-}69)$$

$$\frac{K2}{K1} = \frac{\emptyset\beta_T T + \emptyset C_f\left(P + \rho_r C_{Pr} T\right)}{\overline{\rho C_P}} \qquad (3\text{-}70)$$

But for most practical cases the formation compressibility C_f can be assumed negligible, i.e. $C_f = 0$

$$\frac{K2}{K1} = \frac{\emptyset\beta_T T}{\overline{\rho C_P}} = \eta^* \qquad (3\text{-}71)$$

$$\frac{K4}{K3} = \frac{(\beta_T T - 1)}{\rho C_p} = -\varepsilon \qquad (3\text{-}72)$$

$$\frac{\partial T}{\partial \tau} = -\varepsilon\frac{\partial P}{\partial \tau} + \eta^*\frac{\partial P}{\partial \tau} \qquad (3\text{-}73)$$

Equation 3-73 is similar to that derived by Ramazanov et al. (2010), therefore it is possible to use a similar solution method as that used in their work.The solution was obtained by solving Equation 3-73 along the characteristic of the problem (to be determined later).

$$T_{wb}(t) = T_i(t) + \varepsilon\left[P_{(r=r_T)} - P_{wf}(t)\right] + \eta^* \int_0^t \frac{dP}{d\tau}_{(r=r_T)} d\tau\ ; \qquad (3\text{-}74)$$

Next consider the characteristic of this problem, by solving Equation 3-66 and 3-67. Integrating Equation 3-66 gives the following result.

$$t = \tau + C_1 \qquad (3\text{-}75)$$

But $\frac{\partial P}{\partial r} = \frac{B\psi_i Q_d}{r}$, therefore $\frac{\partial r}{\partial \tau} = -\frac{K3B\psi_i Q_d}{K1r}$, integration of this gives

$$\frac{K1r^2}{2 \cdot K3 \cdot B\psi_i Q_d} = -\tau + C_2 \qquad (3\text{-}76)$$

Applying the following boundary conditions; $t(0) = 0$ and $r(0) = s$ results in $t = t(\tau, s)$ and $r = r(\tau, s)$

$$t = \tau \tag{3-77}$$

$$r^2 = \frac{-2 \cdot K3 \cdot B\psi_i Q_d \tau}{K1} + S^2 \tag{3-78}$$

Which can also be expressed as $\tau = \tau(t, r)$ and $s = s(t, r)$

$$\tau = t \tag{3-79}$$

$$s = \sqrt{r^2 + \frac{2 \cdot K3 \cdot B\psi_i Q_d t}{K1}} \tag{3-80}$$

Equation 3-80 can be written in terms of U_o as defined by (Ramazanov et al. 2010)

$$s = \sqrt{r^2 + 2U_o t} \tag{3-81}$$

Where $U_o = \frac{K3}{K1} \cdot B\psi_i Q_d = \frac{\rho C_p k}{\overline{\rho C_P} \cdot \mu} \cdot r \frac{\partial P}{\partial r}$

From the charactersitics in Equation 3-77 and 3-78 the same result as that defined by Ramazanov et al. (2010) is obtained. Therefore it is possible to use a similar solution as that obtained by Ramazanov et al. (2010).

$$s = r_T = \sqrt{{r_w}^2 + 2U_o t} \tag{3-82}$$

The transient expansion term for gas, which is represented by the third term in Equation. 3-74, can be redefined using the $\frac{dP}{dt}$ term obtained from the LSS. The $\frac{dP}{dt}$ term is given by Equation 3-62

Therefore the integral in the third term of the solution given in Equation 3-74 is shown in Equation 3-83.

$$\int_0^t \frac{dP}{d\tau}_{(r=r_T)} d\tau = \int_0^t -B\frac{\psi_i Q_d}{2}\left[\frac{exp\left[\frac{-\alpha\left(r_w{}^2+2U_o K1\cdot\tau\right)}{K1\cdot\tau}\right]}{\tau}\right]d\tau \quad (3\text{-}83)$$

$$\int_0^t \frac{dP}{d\tau}_{(r=r_T)} d\tau = -B\frac{\psi_i Q_d}{2} exp(-2\alpha U_o)\int_0^t \left[\frac{exp\left(\frac{-\alpha r_w{}^2}{K1\cdot\tau}\right)}{\tau}\right]d\tau \quad (3\text{-}84)$$

Let $\tau = \frac{1}{X}$

$$\int_0^t \frac{dP}{d\tau}_{(r=r_T)} d\tau = -B\frac{\psi_i Q_d}{2} exp(-2\alpha U_o)\left(-\int_{\frac{1}{t}}^{\infty}\left[\frac{exp\left(\frac{-\alpha r_w{}^2 X}{K1}\right)}{X}\right]dX\right) \quad (3\text{-}85)$$

Let $Y = \frac{\alpha r_w{}^2 X}{K1}$

$$\int_0^t \frac{dP}{d\tau}_{(r=r_T)} d\tau = -B\frac{\psi_i Q_d}{2} exp(-2\alpha U_o)\left(-\int_{\left(\frac{\alpha r_w{}^2}{K1\cdot\tau}\right)}^{\infty}\left[\frac{exp(-Y)}{Y}\right]dY\right) \quad (3\text{-}86)$$

$$-\int_{\left(\frac{\alpha r_w{}^2}{K1\cdot\tau}\right)}^{\infty}\left[\frac{exp(-Y)}{Y}\right]dY = Ei\left(-\frac{\alpha r_w{}^2}{K1\cdot\tau}\right) = Ei\left(-\frac{\alpha r_w{}^2}{t}\right) \quad (3\text{-}87)$$

$$\int_0^t \frac{dP}{d\tau}_{(r=r_T)} d\tau = -B\frac{\psi_i Q_d}{2} Ei\left(-\frac{\alpha r_w{}^2}{t}\right) exp(-2\alpha U_o) \quad (3\text{-}88)$$

$$-B\frac{\psi_i Q_d}{2} Ei\left(-\frac{\alpha r_w{}^2}{t}\right) = P_{wf}(t) - P_i \quad (3\text{-}89)$$

$$\therefore T_{wb}(t) = T_i(t) + \varepsilon\left[P_{(r=r_T)} - P_{wf}(t)\right] + \eta^* e^{(-2\alpha U_o)}\left[P_{wf}(t) - P_i\right] \quad (3\text{-}90)$$

$$\therefore T_{wb}(t) = T_i + \varepsilon\left[P_{(r=r_T)} - P_{wf}(t)\right] + \eta^{**}\left[P_{wf}(t) - P_i\right] \quad (3\text{-}91)$$

Where: $r_T = \sqrt{({r_w}^2 + 2U_o t)}$; $\alpha = \frac{\varphi \mu C_t}{4\lambda k}$; $Q_d = \frac{\Gamma T Q_{sc}}{kh\psi_i}$; $U_o = cv(r,t)r$; $v(r,t) = \frac{k}{\mu}\frac{dP}{dr}$; $c = \frac{C_p \rho}{C_t}$; $C_t = \overline{\rho C_P} = \phi C_p \rho + (1-\phi) C_{pr} \rho_r$; $\varepsilon = \frac{1-\beta_T T}{C_p \rho}$; $\eta^{**} = \eta^* e^{(-2\alpha U_o)}$; $\eta^* = \phi c \eta$; $\eta = \frac{\beta_T T}{C_p \rho}$

The exponential integral function can be represented using the logarithmic approximation for most practical cases. $P_{(r=r_T)}$, $P_{wf}(t)$ and P_i can be represented as:

$$P_{(r=r_T)} = A + B\left(\psi_i + \frac{\psi_i Q_d}{2}\left[\gamma + ln\left(\frac{\varphi \mu C_t r_T^2}{4\lambda k t}\right)\right]\right) \quad (3\text{-}92)$$

$$P_{wf}(t) = A + B\left(\psi_i + \frac{\psi_i Q_d}{2}\left[\gamma + ln\left(\frac{\varphi \mu C_t r_w^2}{4\lambda k t}\right)\right]\right) \quad (3\text{-}93)$$

$$P_i = A + B\psi_i \quad (3\text{-}94)$$

Equation 3-91 can now be written as shown below:

$$T_{wb}(t) = T_i + \varepsilon\left(B\frac{\psi_i Q_d}{2}\left[ln\left(\frac{r_T^2}{r_w^2}\right)\right]\right) + \eta^{**}\left(B\frac{\psi_i Q_d}{2}\left[\gamma + ln\left(\frac{\varphi \mu C_t r_w^2}{4\lambda k t}\right)\right]\right) \quad (3\text{-}95)$$

Equation 3-95 can be expressed explicitly as a function of time, as shown in Equation 3-96

$$T_{wb}(t) = T_i + \frac{B\Gamma T Q_{sc}}{2kh}\left(\frac{1-\beta_T T}{C_p \rho}\left[ln\left(\frac{\left({r_w}^2 + 2\left[\frac{C_p \rho B \Gamma T Q_{sc}}{\overline{\rho C_P}\mu h}\right]t\right)}{r_w^2}\right)\right]\right) +$$
$$\frac{B\Gamma T Q_{sc}}{2kh}\left(\frac{\phi \beta_T T}{\overline{\rho C_P}} exp^{\left(-\frac{2\alpha C_p \rho B \Gamma T Q_{sc}}{\overline{\rho C_P}\mu h}\right)}\left[\gamma + ln\left(\frac{\varphi \mu C_t r_w^2}{4\lambda k t}\right)\right]\right) \quad (3\text{-}96)$$

3.4.5 Comparison of Different Solution Methods with the Full Numerical Solution

Two analytical solutions have been investigated: (1) with and (2) without transient expansion effects. The case described in Appendix D was used to compare the full analytical solution with the numerical solution that had been solved using the finite volume method implemented in OpenFOAM.

Numerical: Full numerical solution

Analytical 1: Current analytical solution with expansion term

$$T_{wb}(t) = T_i + \varepsilon\left[P_{(r=r_T)} - P_{wf}(t)\right] + \eta^{**}\left[P_{wf}(t) - P_i\right] \qquad (3\text{-}97)$$

Analytical 2: Analytical solution without expansion term as used on the oil production studies by Ramazanov et al. (2010):

$$T_{wb}(t) = T_i + \varepsilon\left[P_{(r=r_T)} - P_{wf}(t)\right] \qquad (3\text{-}98)$$

A close match between the Analytical 1 solution and the numerical results was obtained, while the Analytical 2 solution was significantly different. This indicates that neglecting the effect of transient expansion of gas on the sand-face temperature would significantly increase the error. Not surprisingly, an opposite conclusion for oil flow was made by Ramazanov et al. (2010).

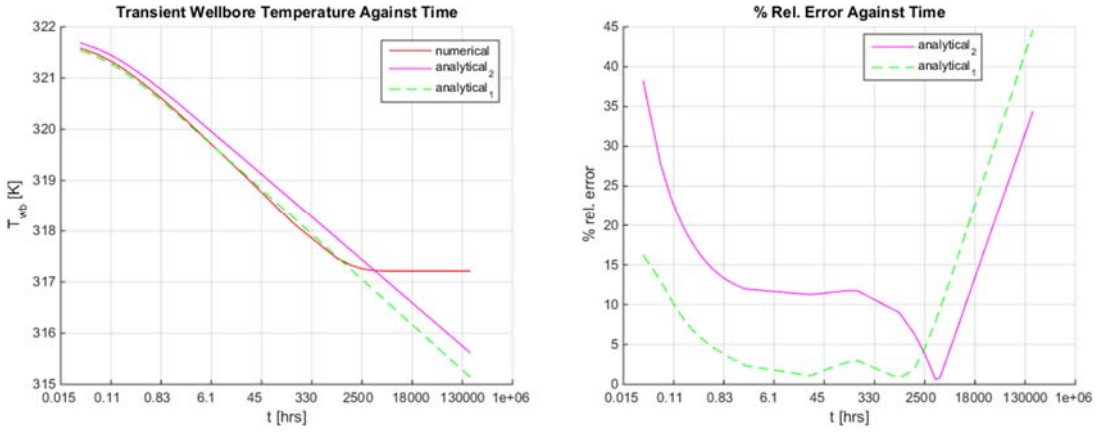

Figure 3-13: (a) Plot of transient wellbore temperature for numerical and analytical solutions, (b) Plot of percentage relative errors for the analytical solution methods

Figure 3-13(a) compares the three scenarios while Figure 3-13(b) shows the error between the analytical1 and numerical solution defined by Equation 3-99. The analytical solution began to diverge from the numerical in the late time region. This is due to the reservoir boundary effect so that IARF LSS no longer applies.

$$\%Rel.Error = \frac{\sqrt{\left(\Delta T_{wb,analytical} - \Delta T_{wb,numerical}\right)^2}}{\Delta T_{wb,numerical}} \quad (3\text{-}99)$$

3.4.6 Sensitivity Analysis

3.4.6.1 Sensitivity to Gas Properties:

An analysis was carried out to determine the sensitivity of the transient temperature response to changes in the properties of the gas (Table 3-4). The thermal expansion coefficient had the greatest effect on the predicted sand-face temperature. Hence a more precise value of the thermal expansion coefficient will lead to a more accurate estimation of the sand-face temperature.

Table 3-4: Sensitivity of transient temperature solution to variation in the properties of the gas

% change in parameter	**Resulting % change in temperature transient due to specified parameter**			
	Viscosity	**Thermal expansion coefficient**	**Specific heat capacity**	**Density**
+50	+13.0	-114.3	+19.3	+19.3
-50	-23.7	+114.3	-42.2	-42.2

3.4.6.2 Appropriate Gas Property Estimation:

It is important to determine the conditions at which the gas properties should be estimated since accurate gas property values have a considerable effect on the results.

1. The effect of temperature change may be neglected for the following reasons. Firstly, the temperature changes are small compared to pressure changes which is expected to be dominant. Further, since the temperature solution is being derived, hence it is logical to, at least initially, assume that the temperature change is an unknown in the analysis.
2. Three possible definitions of the pressure are the:
   a) Initial reservoir pressure.
   b) Stabilized bottomhole pressure.

c) Volumetrically average reservoir pressure.

The stabilized pressure is the pressure at which (i) the radius of investigation equals the external reservoir radius or (ii) when the transient pressure effect is felt at the reservoir boundary (ERCB 1979). The time required for stabilization can be determined from the equation $t_s = \frac{\varphi \mu c r^2}{4\lambda k}$. It is about 121 hours for the case considered. The bottomhole pressure at this time is about 11.4 MPa.

Table 3-5: Gas property values for simulation

Gas Properties	**At Initial Pressure**	**At Stabilized Pressure**	**At Average Pressure**	**Units**
Specific heat capacity	3111	2967	3041	J/kg K
Density	95.78	77.004	86.3737	kg/m^3
Viscosity	0.01515	0.01416	0.01465	cP
Thermal expansion coefficient	0.005198	0.004969	0.0051	K^{-1}

The average pressure is given by Equation 3-100, while the errors are calculated using Equation 3-101

$$P_{avg} = \frac{P_i + P_s}{2} \qquad (3\text{-}100)$$

$$\%Error = \left|\frac{\Delta T - \Delta T_{numerical}}{\Delta T_{numerical}}\right| \qquad (3\text{-}101)$$

Where $\Delta T = T - T_i$ and $\Delta T_{numerical} = T_{numerical} - T_i$

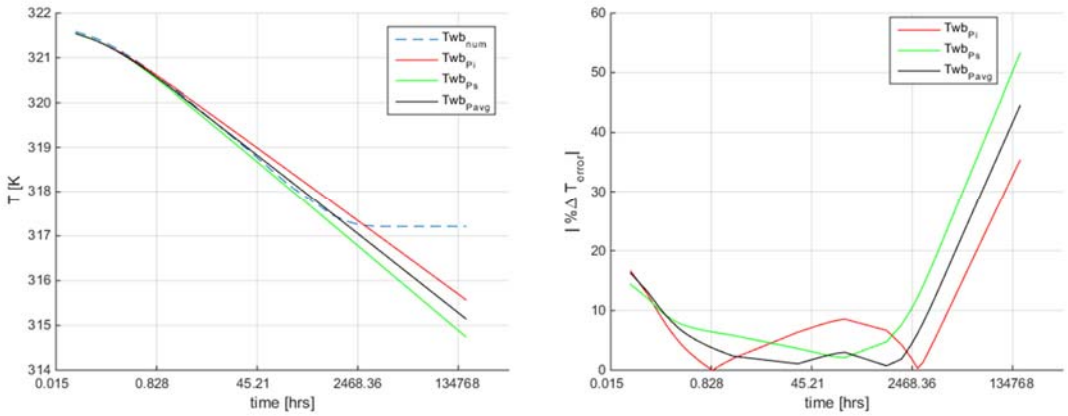

Figure 3-14: (a) Plot of analytical transient wellbore temperatures for four pressure conditions, (b) Plot of % relative errors of the analytical transient wellbore temperature for three pressure conditions

Figure 3-14 indicates the errors associated with the volumetrically averaged properties are consistently lower than when the alternative definitions of the pressure are used. Hence the volumetrically averaged properties provide the closest match to the numerical solution for the case considered.

3.5 Limitations Due to Non-Darcy Effects

The analytical solution in this work was derived based on the assumption that the gas flow obeys Darcy's law. However, it is well known that the gas flow deviates from Darcy's law as flow velocity increases. Forchheimer's equation, (Equation 3-102), describes this effect by adding an additional pressure drop term { $\beta\rho|\boldsymbol{v}|\boldsymbol{v}$ (Wang & Economides 2009)} to Darcy's equation that represents inertial effects.

$$-\nabla P = \frac{\mu}{k}\boldsymbol{v} + \beta\rho|\boldsymbol{v}|\boldsymbol{v} \qquad (3\text{-}102)$$

A dimensionless number r_{nD} can be defined (Equation 3.103) from Forchheimer's equation. r_{nD} represents the ratio of the pressure gradients due to the non-Darcy and the Darcy effects.

$$r_{nD} = \frac{\beta\rho|\boldsymbol{v}|k}{\mu} \qquad (3\text{-}103)$$

It is possible to estimate the velocities at which the non-Darcy effect is negligible (i.e. $r_{nD} \ll 1$). $r_{nD(crit)}$ can be defined as the critical non-Darcy ratio at which the pressure drops can be assumed to be mainly due to Darcy effects. It is therefore possible to obtain a corresponding critical flow velocity below which the non-Darcy effects can be neglected.

$$\left|\boldsymbol{v}_{(\boldsymbol{crit})}\right| = \frac{\mu r_{nD(crit)}}{\beta \rho k} \qquad (3\text{-}104)$$

Our analytical solution may thus be applied to velocities smaller than $\boldsymbol{v}_{(\boldsymbol{crit})}$. It is also possible to express this critical condition in terms of the surface flowrates when the well geometry is known (i.e. well radius, r_w, and well length, L_w, are known) (Equation 3-105).

$$Q_{sc(crit)} = \frac{\mu r_{nD(crit)} 2\pi r_w L_w}{\beta \rho_{sc} k} \qquad (3\text{-}105)$$

The limits of application of the analytical solution are determined by $Q_{sc(crit)}$ for a given well geometry and reservoir formation. This is calculated based on choosing a value of $r_{nD(crit)}$ at which the resulting errors are still acceptable. However, accurate estimation of $Q_{sc(crit)}$ depends on having a good knowledge of the value of β. Different correlations have been developed to estimate the value of the non-Darcy coefficient, some of which were published by Wang & Economides (2009).

Alternatively, the effect of non-Darcy flow on transient temperature can be investigated by considering the relationship between r_{nD} and the additional transient temperature drawdown due to non-Darcy flow.

$$r_{nD} = \frac{Q_{sc}\rho_{sc}\beta k}{2\pi r_w L_w \mu} \qquad (3\text{-}106)$$

$$r_{nD} = \frac{Q_{sc}\rho_{sc}}{2\pi r_w L_w} \cdot \frac{\beta k}{\mu} \qquad (3\text{-}107)$$

Where $\frac{Q_{sc}\rho_{sc}}{2\pi r_w L_w}$ is the mass flux at the well, β is usually expressed as a function of permeability "k" and porosity "$\emptyset$".

The dimensionless number T_{nD} is the ratio of the additional temperature drawdown due to the non-Darcy flow effect to the temperature drawdown due to Darcy flow.

$$T_{nD} = \frac{T_{w\,(Darcy)} - T_{w\,(non-Darcy)}}{T_i - T_{w\,(Darcy)}} \qquad (3\text{-}108)$$

Figure 3-15 illustrates the effect of non-Darcy flow on the transient well temperature and pressure for the Appendix D case study. It clearly shows that the non-Darcy effect cannot always be neglected when applying the transient temperature solutions. Application of the analytical solutions with a reasonable accuracy therefore requires verification that the non-Darcy effects is negligible.

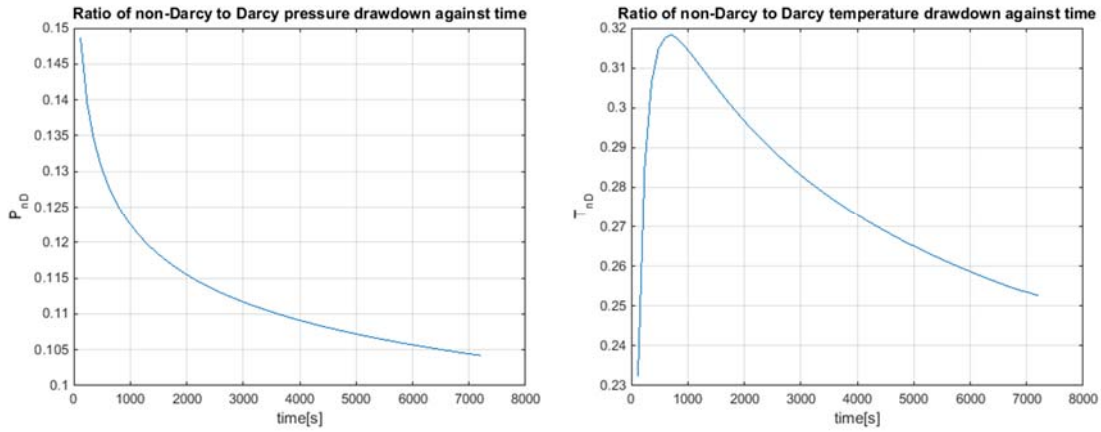

Figure 3-15: (a) Plot of ratio of non-Darcy to Darcy pressure drawdown, (b) Plot of ratio of non-Darcy to Darcy temperature drawdown

The values of T_{nD} for different values of r_{nD} were determined from numerical simulations (Figure 3-16). The plots show that r_{nD} should be < 10% if the error in T_{nD} is to be < 5%, surface flowrates corresponding to this value of r_{nD} can be estimated and used as a guide when applying the analytical solution. N.B. The value of r_{nD} can be changed by changing the permeability k or the mass flux (or surface rate Q_{sc}) at the well. The curves of $r_{nD}(k)$ were obtained by changing the permeability from that of the base case, while the curves of $r_{nD}(Q)$ were obtained by changing the rate from that of the base case.

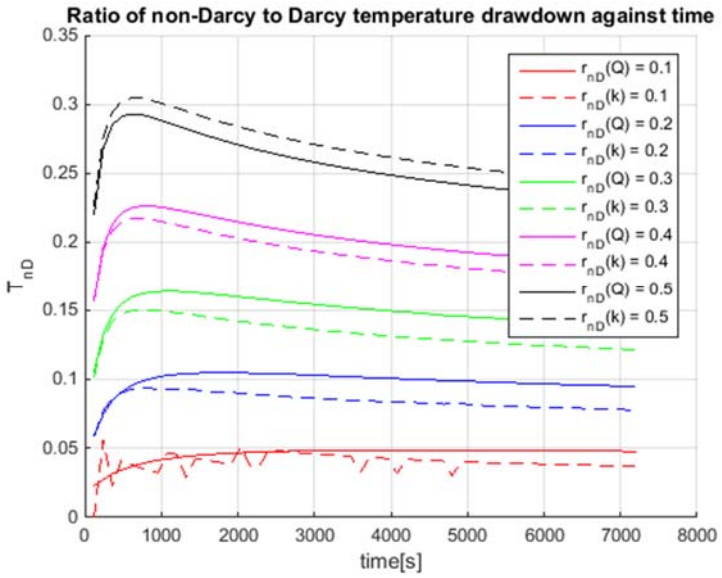

Figure 3-16: Curves of T_{nD} for different values of r_{nD},

A better way of representing the critical surface flowrate is by expressing it as the rate per unit well-reservoir contact area. This term can then be applied to different well geometries and reservoir thicknesses.

$$Q_{scn(crit)} = \frac{Q_{sc(crit)}}{2\pi r_w L_w} = \frac{\mu r_{nD(crit)}}{\beta \rho_{sc} k} \qquad (3\text{-}109)$$

3.6 Case Studies

The synthetic and real case studies presented below demonstrate the applicability of the derived analytical solution for analysing the transient, sandface temperature. The synthetic model used is similar to the one used for validating the analytical solution in Section 3.4, but with different formation thickness, permeability and surface production rates values (Table 3-6). The real case is based on the downhole data measured in a gas production well in the Norwegian sector of the North Sea.

3.6.1 Synthetic Models

Three models are considered to compare the numerical and analytical solutions. Their formation thickness, permeability and surface production rates values are listed in Table 3.5. Full details for setting up each model are provided in Table D-2 of Appendix D.

Table 3-6: Case study description

Property	**Symbol**	**Case Study 1**	**Case Study 2**	**Case Study 3**	**Unit**
Formation thickness	h	30	30	60	m
Surface production rate	Qsc	2.3	16.1	34.5	m^3/s
Permeability	k	10	100	100	$\times 10^{-15} m^2$

The prediction of the transient sandface temperature using the derived analytical solution (Equation 3-96) was carried out for each case and compared with the accurate, numerical prediction. The results are shown in (Figure 3-17, 3-18 & 3-19). The parameters used in the analytical equations are listed in Table D-3 of Appendix D.

As can be seen, for the initial, 'infinitely-acting reservoir' time period (i.e. until the boundary effects start impacting the numerical model and pressure and temperature start to stabilise) the numerical and analytical match very well in all three cases.

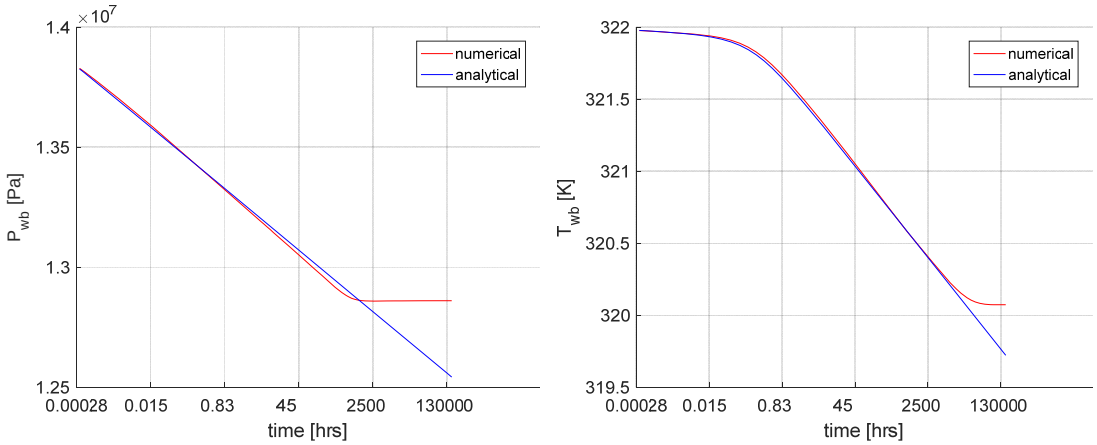

Figure 3-17: Case Study 1 (a) Plot of transient wellbore pressure, (b) Plot of transient wellbore temperature

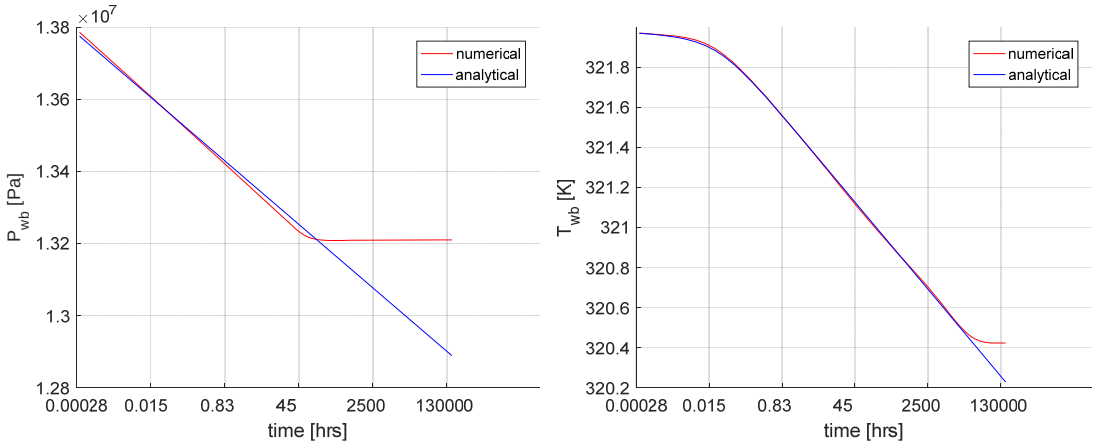

Figure 3-18: Case Study 2 (a) Plot of transient wellbore pressure, (b) Plot of transient wellbore temperature

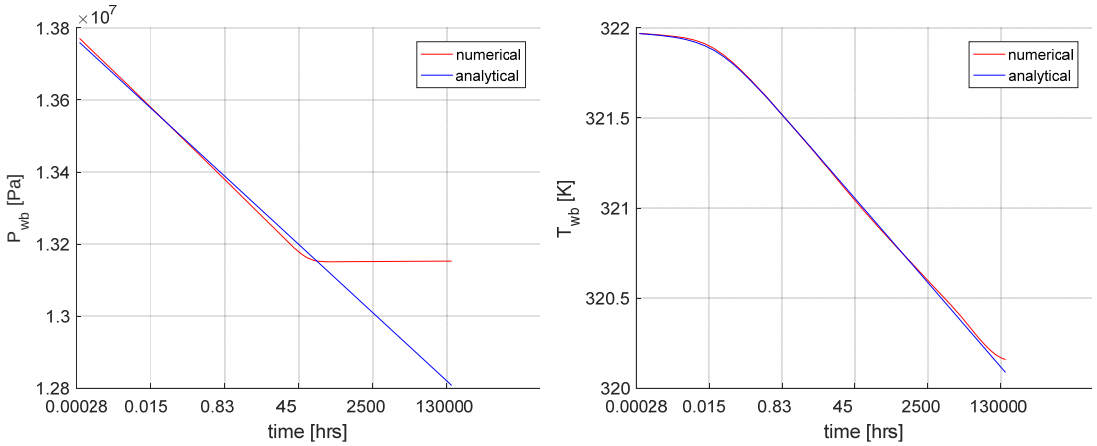

Figure 3-19: Case Study 3 (a) Plot of transient wellbore pressure, (b) Plot of transient wellbore temperature

3.6.2 Real Well Case Study

The data presented in this section were measured downhole in a vertical, gas producing well. Table D-4 of Appendix D lists the fluid and formation properties. Figure 3-20 shows the well rate and pressure data. The drawdown events (highlighted by red dots) are used in this section. This case study is presented and analysed in detail in Dada et al. (2016).

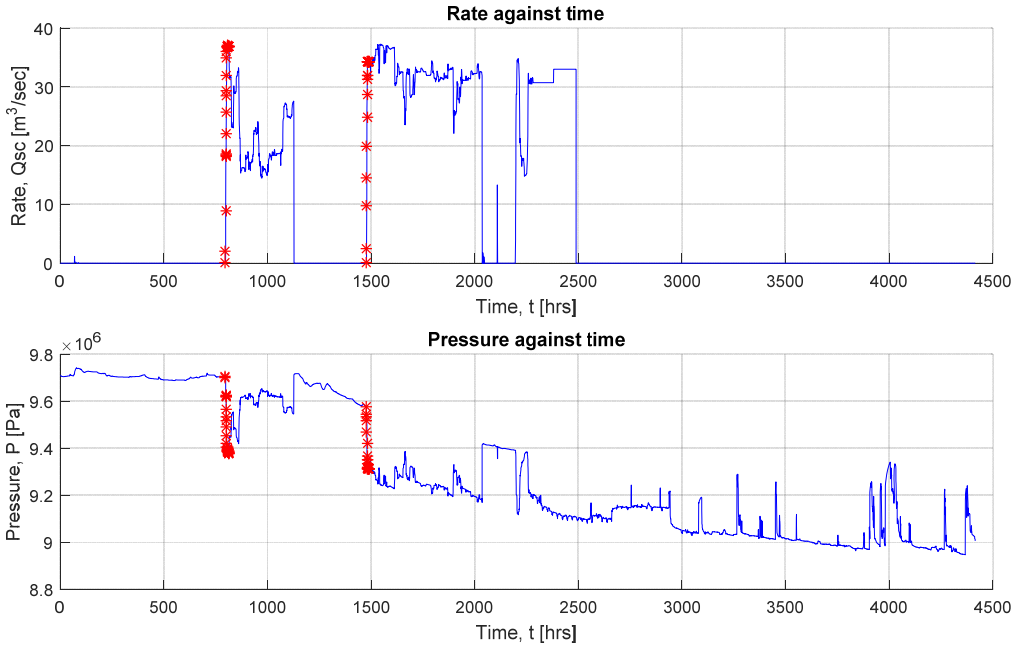

Figure 3-20: Real Well Case Study: Plot of surface rate and pressure.

Pressure Transient Analysis of the Build-up test was inconclusive, presumably because the well shut-in was not perfect. Rate Transient Analysis of the draw-down period has resulted in the estimate of the reservoir permeability*thickness product kh of 40,900 mD.ft (1.23×10^{-11} m^3). Using this value in the analytical solution (Equation 3-96) it is possible to predict the transient temperature in the steadily declining temperature region (Figure 3-21). As can be seen, the predicted and real temperature data match reasonably well. It was impossible to model the very early period (first 6 hours) because of the well gradual opening and clean-up effects masking the pure sandface temperature response. The work to tackle these effects is ongoing.

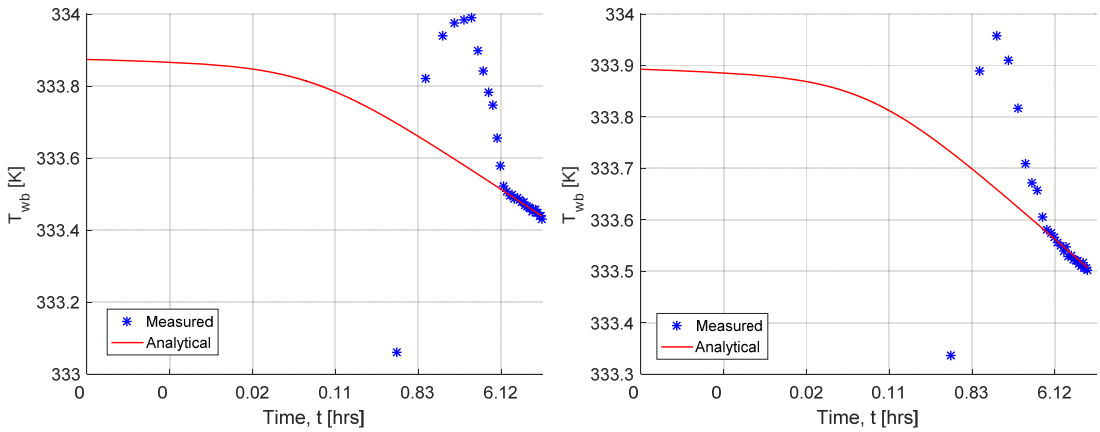

Figure 3-21: Real Well Case Study: (a) Plot of transient wellbore temperature for drawdown 1. (b) Plot of transient wellbore temperature for drawdown 2.

3.7 Conclusions

Transient temperature data from producing wells can be invaluable for analysis and monitoring purposes. Robust models need to be available for analysis and interpretation; these models should be able to handle single and multiphase flows of liquids and gases. However, very little work has been published on TTA for gases, and in particular there seems to be no analytical model existing for this.

This chapter tries to fill the existing gap in the development of robust TTA methods by developing an analytical solution which can be used to predict transient sandface temperature of gas producing wells, as this solution can then be inverted for use in TTA. The solution was validated by comparing against numerical simulations and a close match was observed at times prior to the pressure transient arriving at the reservoir boundary. The derivation method for the analytical solution was described, along with the necessary assumptions and simplifications.

Recommendations were also made about the pressure and temperature conditions to be used when estimating the gas properties to be used in the solution since the choice of these values affects the accuracy of the results. The limitations of this solution due to non-Darcy effects are discussed and recommendations made on where the solution is applicable. Finally synthetic and real well case studies were presented to illustrate the application of the analytical solution derived.

3.8 Nomenclature

β: Non-Darcy coefficient $[m^{-1}]$

β_T: Thermal expansion coefficient $[K^{-1}]$

ε: Joule-Thomson coefficient $[K/Pa]$

η: Adiabatic coefficient $[K/Pa]$

η^*: Formation averaged adiabatic coefficient $[K/Pa]$

μ: Viscosity of fluid $[Pa.s]$

ρ: Density of fluid $[kg/m^3]$

ρ_r: Density of rock $[kg/m^3]$

ϕ: Porosity [ ]

ψ: Pseudo-pressure $[Pa^2/Pa.s]$

ψ_i: Pseudo-pressure at initial conditions $[Pa^2/Pa.s]$

c: Ratio of gas heat capacity to averaged formation heat capacity. [ ]

d: Molal density $[mol/m^3]$

γ: Euler-Mascheroni constant [ ]

k: Permeability $[m^2]$

r: Radius $[m]$

r_{nD}: Ratio of non-Darcy pressure drop component to Darcy pressure drop component [ ]

r_T: Thermal radius of investigation $[m]$

t: Time $[s]$

t_j: Time at which transient temperature becomes linear $[s]$

υ: Kinematic viscosity $[m^2/s]$

$\boldsymbol{v}$: Velocity $[m/s]$

A: Constant term in pressure pseudo-pressure relationship $[Pa]$

B: Coefficient in pressure pseudo-pressure relationship $[s]$

C_p: Specific heat capacity of fluid $[J/kgK]$

C_{pr}: Specific heat capacity of rock $[J/kgK]$

C_t: Total formation compressibility $[Pa^{-1}]$

P: Pressure $[Pa]$

Q_d: Dimensionless pressure [ ]

R: Specific gas constant $[J/kgK]$

T: Temperature $[K]$

T_{nD}: Ratio of temperature change due to non-Darcy effect to temperature change due to Darcy effect [ ]

3.9 Subscripts

$crit$: Critical condition

f: Formation

g: Gas

i: Initial conditions

r: Rock

t: Time

sc: Surface conditions

T: Thermal

w: Well

wb: Wellbore

wf: Well flowing

Chapter 4: Transient Temperature Analysis Workflows for Vertical Dry Gas Wells

4.1 Introduction

The regular determination of a well's inflow performance is one of the key well surveillance tasks in production engineering. The well inflow performance depends on the permeability-thickness (kh) product contacted by the completion and the condition of the near-wellbore zone. Estimation of the permeability-thickness (kh) and the skin values is one of the most important results from well test analysis.

Another important task of the production engineer involves monitoring the produced fluid phases and their flow rates from the combined well-reservoir system (well production allocation) as required for production optimisation, reservoir management and reporting of well reserves. Flow rate estimation involves quantifying the total volume and phase fraction of produced fluid, while production allocation determines the fraction of the total production contributed by each reservoir zone (or layer). Several methods have been developed for flow estimation, including production logging, permanent downhole flow meters, pressure drop measurement across flow constrictions, multi-rate tests, virtual flow-metering and thermal modelling (both steady state and TTA) (Konopczynski et al. 2003). Thermal modelling has great potential as a low-cost, low-risk method of obtaining this information. Further, the temperature signal propagates at a much slower rate than the traditional pressure signal. This gives TTA the unique advantage of being able to accurately probe the near-wellbore zone or profile the reservoir/inflow properties along the production interval.

High resolution downhole temperature sensors that can resolve small temperature changes for well surveillance purposes were developed in the 1970s (Schlumberger 2008), with fibre optic technology extending the range of possible completion designs. The measurement required for TTA are now available at a reasonable cost.

However, accurate thermal models are essential when predicting the transient temperature change in the reservoir and at the sandface, during TTA. This thermal model is the basis for most analytical or numerical solutions for TTA. It is usually a partial differential equation (PDE) which describes the relationship between the fluid and rock properties

and the pressure and temperature changes in the porous media. Derivation of the thermal model used to estimate the transient sandface temperature can be found in e.g. Weibo Sui et al. (2008), which is itself based on the model by Bird et al. (2007). This thermal model shows that the measured transient temperature change in porous media is a function of the fluid expansion, Joule-Thomson effect, heat convection and conduction. This, or similar models, were used by Muradov & Davies (2012a), Duru & Horne (2010) and Ramazanov et al. (2010) to estimate the transient sandface temperature analytically or numerically. The authors obtained realistic estimates of sandface temperature. Muradov & Davies (2013) and Duru & Horne (2010) compared their results obtained from analytical and/or numerical solutions (based on this model) with real well data.

Numerical solutions for TTA are normally used directly in inversion workflows for characterizing a formation, allocating flow rate or carrying out a near wellbore analysis. They are usually case specific, and do not produce a general solution while the analytical TTA solutions are faster and more general, as well as providing valuable insights into the problem. Table 4-1 lists some of the TTA publications along with their area of application.

Table 4-1: Major findings in TTA research

Author, year	**Problem conditions**	**Numerical / Analytical**	**Major findings**
(Mao & Zeidouni 2017b)	Vertical liquid or gas producing wells	Analytical	Developed analytical transient temperature solutions for dry gas producing wells
(Akindolu. Dada et al. 2017)	Vertical gas producing wells	Analytical	Developed TTA workflows for vertical gas producing wells
(Akindolu Dada et al. 2017)	Vertical gas producing wells	Analytical	Developed analytical transient sandface temperature solutions for dry gas producing wells
(Onur & Çinar 2016)	Drawdown and build-up in vertical liquid producing well	Analytical / Numerical	Developed analytical transient temperature solutions for liquid drawdown and build-up
(Chevarunotai et al. 2015)	Vertical oil producing wells	Analytical	Transient temperature solutions for oil producing wells with large drawdowns

(Muradov & Davies 2013)	Horizontal liquid (oil and water) producing wells	Analytical	Case studies for pressure and temperature transient analysis for liquid producing wells
(Muradov & Davies 2012b)	Horizontal liquid producing wells	Analytical	Workflows for TTA for liquids in horizontal wells
(Muradov & Davies 2012a)	Horizontal liquid producing well	Analytical	Developed analytical solutions for transient sandface temperature in liquid producing horizontal wells
(App & Yoshioka 2011)	Oil and gas flow in vertical wells	Analytical / Numerical	Effect of Peclet number on flowing temperature change, and relationship to layer properties.
(Duru & Horne 2010)	Single and multiphase (oil and gas) flow, 1D radial flow	Semi-analytical (operator splitting)	Semi-analytical transient temperature solution, estimation of formation and fluid properties using real and synthetic data
(Sui et al. 2010)	Multilayer system with gas production	Numerical	Estimated skin, and layer properties in a multi-layered well-reservoir system, by using numerical inversion techniques
(Ramazanov et al. 2010)	Vertical oil producing wells with thermal wellbore storage	Analytical	Developed analytical solutions for vertical liquid producing wells
(W. Sui et al. 2008)	Multilayer system with liquid production	Numerical	Well test workflow for pressure and temperature in multi-layered system. Estimated skin and layer properties

The estimation of zonal production rates, formation properties and the identification of the produced phases requires inversion of the forward TTA solution. This inversion is easy and fast for analytical solutions; but is slower for numerical solutions as it requires some form of optimization to minimize an objective function. Sui et al. (2010), for example, performed the inversion by nonlinear regression using the Levenberg-Marquardt algorithm. Another advantage of an analytical solution for a system is that it explicitly describes the nature of the system's behaviour and how its parameters relate and affect the system's response. However, most of the analytical solutions and inversion methods developed to-date refer to liquid producing wells. This chapter reports the work carried out to characterize a dry gas producing reservoir by development of inversion workflows for TTA data.

Analytical solutions were previously developed for predicting the transient sandface temperature in a vertical dry gas producing well. This solution would now be used for characterizing a reservoir; i.e. by determining the permeability-thickness product and skin. This method is used in conjunction with the well-developed PTA workflow. The combination of PTA and RTA (Rate Transient Analysis) is further used to validate the results obtained from TTA of a real-well data.

The following sections show how to linearize the analytical solution (in log-time scale) for vertical dry gas producing wells. This linear form of the equation is then used for characterizing the reservoir and analysing the near wellbore reservoir properties. The limits of the method stemming from the assumption of laminar flow are discussed. The developed method was further successfully applied to both synthetic and real case studies, showing that it can be applied to many field situations.

4.2 Analysis of the Problem

Equation 4-1 is the analytical solution for the sandface temperature of a vertical dry gas well producing at a constant rate after a period of shut-in (or a step change in the flow rate). Equation 4-1 was derived for a dry gas well producing at a constant, non-zero rate and with an infinite acting boundary condition. Chapter 3 details how the solution was derived and the assumptions used in its derivation.

$$T_{wb}(t) - T_i(t) = \varepsilon\left[P_{(r=r_T)} - P_{wf}(t)\right] + \eta^* e^{(-2\alpha U_o)}\left[P_{wf}(t) - P_i\right] \qquad (4\text{-}1)$$

Note: Equation. 4-1 is normally used to describe a "drawdown" test where the production rate is instantaneously increased from one constant value to a second, higher value. The derivation often assumes a zero initial rate; describing the case when well production starts after a shut-in. However, the solution is also applicable to any rate change as long as the initial temperature term in Equation. 4-1 is accurate and the final flow rate is non-zero. This covers a well being placed on production and a positive or negative flow rate change, as long as the well is ***not*** *shut-in. The full analytical solution for a well shut-in, or "build-up" test, is not currently available.*

Gas properties are strongly temperature and pressure dependent. However, their combinations that appear in Equation 4-1 may be assumed to be constant for thermal analysis. They are estimated at the initial temperature and the average pressure "P_{avg}" (midway between the initial wellbore pressure and the final, stabilized wellbore pressure). *Note this assumption is not valid for the equivalent pressure solution for a gas well since gas properties used in the pressure model are very sensitive to the changes in pressure observed in field application. That is why an accurate, classical gas well pressure solution is used in this work (pressure is part of thermal Equation. 4-1) as far as the pressure model is concerned.*

Equation. 4-1 shows that the temperature change is a combination of the Joule-Thomson effect (term 1 on RHS) and the transient fluid expansion (term 2 on RHS) plus the heat convection term due to the resulting temperature gradient. Also, $2\alpha U_o \ll 1$ for most practical purposes, therefore $e^{(-2\alpha U_o)} \approx 1$.

The above allows Equation. 4-1 to be reformulated as:

$$T_{wb}(t) - T_i(t) = \varepsilon\left[P_{(r=r_T)} - P_{wf}(t)\right] + \eta^*\left[P_{wf}(t) - P_i\right] \qquad (4\text{-}2)$$

The pseudo-pressure method developed for gas wells by Al-Hussainy et al. (1966) was used to obtain the pressure solution. A linear pressure - pseudo-pressure relationship (Equation 4-3) is sufficiently accurate for most well production conditions. It can be combined with the line source solution and the logarithmic approximation for an infinite acting reservoir producing at a constant rate (Equation 4-4) (Al-Hussainy et al. 1966)}.

$$P = A + B\psi \qquad (4\text{-}3)$$

$$\psi = \psi_i - \frac{\psi_i Q_d}{2}\left[\gamma + ln\left(\frac{\phi\mu c r^2}{4\lambda kt}\right)\right] \qquad (4\text{-}4)$$

Where "γ" is the Euler-Mascheroni constant.

The constants "A" and "B" in Equation 4-3 are case-specific and should be found by matching P and ψ for a given fluid composition. They can be obtained from PVT

measurements of the produced fluids or calculated from its Equation-of-State as explained in Chapter 3.

$$\therefore\ T_{wb}(t) - T_i(t) = -\varepsilon B \frac{\psi_i Q_d}{2}\left[ln\left(\frac{{r_w}^2+2U_o t}{r_w^2}\right)\right] - \eta^* B \frac{\psi_i Q_d}{2}\left[\gamma + ln\left(\frac{\phi\mu c r_w^2}{4\lambda k t}\right)\right] \quad (4\text{-}5)$$

Equation. 4-5 can be expressed explicitly as a function of time, as shown in Equation 4-6

$$T_{wb}(t) = T_i - \frac{B\Gamma T Q_{sc}}{2kh}\left(\frac{1-\beta_T T}{C_p\rho}\left[ln\left(\frac{\left({r_w}^2+2\left[\frac{C_p\rho B\Gamma T Q_{sc}}{\overline{\rho C_P}\mu h}\right]t\right)}{r_w^2}\right)\right]\right) +$$
$$\left(\frac{\phi\beta_T T}{\overline{\rho C_P}} e^{\left(-\frac{2\alpha C_p\rho B\Gamma T Q_{sc}}{\overline{\rho C_P}\mu h}\right)}\left[\gamma + ln\left(\frac{\phi\mu c r_w^2}{4\lambda k t}\right)\right]\right) \quad (4\text{-}6)$$

A plot of the transient temperature calculated from Equation 4-5 w.r.t log time is initially a curve followed by a linear portion (see Figure 4-1(a), taken from the case study described in Appendix E). An equation that accurately represents the linear portion of Equation 4-5 {Figure 4-1(a)} is obtained by plotting the two terms in Equation 4-5 – i.e. fluid compression and Joule-Thomson effects - on a logarithmic scale {Figure 4-1(b)} to determine when each term is dominant.

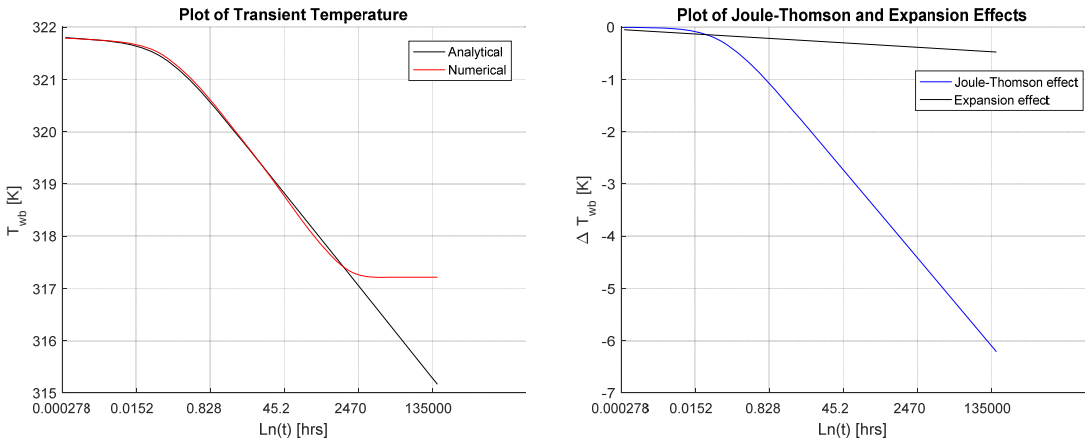

Figure 4-1 (a) Plot of numerical and analytical transient wellbore temperature (b) Plot of temperature change due to Joule-Thomson and expansion effect

Mathematical speaking, the initial nonlinear behaviour is due to the term $\left(\frac{{r_w}^2+2U_o t}{r_w^2}\right)$ at early times. However, the derivative of $ln\left(\frac{{r_w}^2+2U_o t}{r_w^2}\right)$ approaches that of $ln(t)$ as time increases. Its value can be approximated as shown below.

$$\lim_{t\to\infty}\left[ln\left(\frac{{r_w}^2+2U_o t}{r_w^2}\right)\right] = ln(t) + \Delta \qquad (4\text{-}7)$$

Where Δ is a shift added to $ln(t)$. $\Longrightarrow \lim_{t\to\infty}\frac{d}{dt}\left(ln\left[\frac{{r_w}^2+2U_o t}{r_w^2}\right]\right) = \frac{d}{dt}(ln[t])$. However for practical purposes, it is possible to obtain a time $t_j \neq \infty$ at which the value of $\frac{d}{dt}\left(ln\left[\frac{{r_w}^2+2U_o t}{r_w^2}\right]\right)$ is sufficiently close to that of $\frac{d}{dt}(ln[t])$. A time t_j is determined such that the percentage difference between these two is less than δ (where $\delta \leq 1\%$) i.e. $\frac{d}{dt}\left(ln\left[\frac{{r_w}^2+2U_o t}{r_w^2}\right]\right) = \frac{2U_o}{{r_w}^2+2U_o t}$ and $\frac{d}{dt}(ln[t]) = \frac{1}{t}$

For a time $t \geq t_j$

$$\therefore t_j = \frac{{r_w}^2(100+\delta)}{2U_o\delta} \qquad (4\text{-}8)$$

Combining Equation 4-7 & 4-8 the value of the shift Δ at time t_j can be determined.

$$\Delta = \left|ln\left(\frac{{r_w}^2+2U_o t}{r_w^2}\right) - ln(t)\right|_{t=t_j} = ln\left[\frac{200U_o\delta}{{r_w}^2(100+\delta)}\right] \qquad (4\text{-}9)$$

From Equation 4-7 it can be safely assumed that when $t \geq t_j$, $ln\left(\frac{{r_w}^2+2U_o t}{r_w^2}\right)$ is given by Equation 4-10

$$ln\left(\frac{{r_w}^2+2U_o t}{r_w^2}\right) \cong ln(t) + ln\left[\frac{200U_o\delta}{{r_w}^2(100+\delta)}\right] \qquad (4\text{-}10)$$

A suitable accuracy of the δ term above is taken as 5%. Equation 4-11, obtained by substituting Equation 4-10 into Equation 4-5, describes the linear portion of Equation 4-5.

$$T_{wb}(t) = T_i(t) - \varepsilon B \frac{\psi_i Q_d}{2}\left[ln(t) + ln\left(\frac{200U_o\delta}{{r_w}^2(100+\delta)}\right)\right] - \eta^* B \frac{\psi_i Q_d}{2}\left[\gamma + ln\left(\frac{\phi\mu c r_w^2}{4\lambda k t}\right)\right] \quad t \geq t_j \qquad (4\text{-}11)$$

where $Q_d = \frac{\Gamma T Q_{sc}}{kh\psi_i}$. Equation 4-12 will now be used to develop workflows for characterizing transient temperature data.

$$T_{wb}(t) = T_i + \frac{B\Gamma T_i Q_{sc}}{2kh}[\eta^* - \varepsilon]ln(t) - \frac{B\Gamma T_i Q_{sc}}{2kh}\left[\eta^* ln\left(\frac{\phi\mu c r_w^2}{4\lambda k}\right) + \varepsilon ln\left(\frac{200U_o\delta}{{r_w}^2(100+\delta)}\right) + \eta^*\gamma\right] \qquad (4\text{-}12)$$

Where: $r_T = \sqrt{({r_w}^2 + 2U_o t)}$; $\alpha = \frac{\phi\mu c}{4\lambda k}$; $C = \frac{C_p\rho}{C_t}$; $C_t = \overline{\rho C_P} = \phi C_p\rho + (1-\phi)C_{pr}\rho_r$;

$U_o = Cv(r,t)r$; $v(r,t) = \frac{k}{\mu}\frac{dP}{dr}$; $\eta^{**} = \eta^* e^{(-2\alpha U_o)}$;$\eta = \frac{\beta_T T_i}{C_p\rho}$; $\varepsilon = \frac{1-\beta_T T_i}{C_p\rho}$;$\eta^* = \phi C\eta$;

4.3 Reservoir Characterization and Near-Wellbore Analysis

Equation 4-13 is the gradient of the linearized form of the transient temperature solution on a semi-log scale Equation 4-12, and Equation 4-14 is the intercept. The semilog slope and intercept of the transient temperature signal can be estimated by fitting a straight line (of the form "$T = aln(t) + b$") to the transient temperature signal (Figure 4-2).

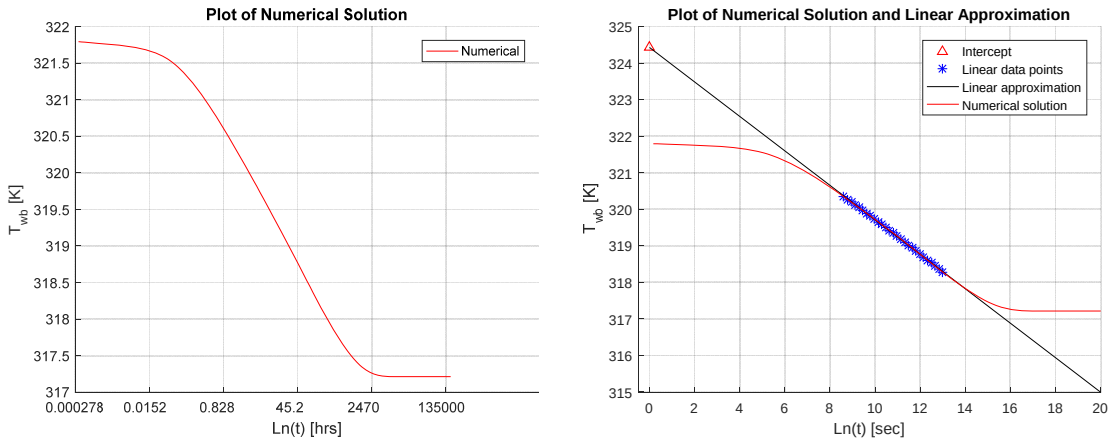

Figure 4-2 (a) Plot of numerical transient wellbore temperature (b) Plot of numerical transient wellbore temperature showing linear portion with slope and intercept

$$slope\ (a) = \frac{B\Gamma T Q_{sc}}{2kh}[\eta^* - \varepsilon] \qquad (4\text{-}13)$$

$$intercept\ (b) = T_i(t) - \frac{B\Gamma TQ_{sc}}{2kh}\left[\eta^* ln\left(\frac{\phi\mu c r_w^2}{4\lambda k}\right) + \varepsilon ln\left(\frac{200U_o\delta}{{r_w}^2(100+\delta)}\right) + \eta^*\gamma\right] \quad (4\text{-}14)$$

Equation 4-13, the slope of Equation 4-12, determines the permeability-thickness "kh" and the rate "Q", while the intercept (Equation 4-14) evaluates the permeability "k". Unfortunately, determining the permeability from the intercept is susceptible to large errors (described in Section 4.7), a similar effect is observed in PTA.

4.3.1 Workflow for Estimating Permeability-thickness or Rate

The value of the permeability-thickness or the production rate is estimated as follows:

1. Calculate the values of the fitting coefficient "B" from the PVT data or an appropriate Equation-of-State.

2. Determine "ψ_i", the pseudo-pressure at initial reservoir conditions.

3. Determine "η^*" & "ε" from Equation 4-12 at T_i and P_{avg}.

4. Identify the linear portion of the transient temperature profile.

5. *Optional:* Estimate the value of the prediction uncertainty "δ" (Equation 4-8) using the value of "t_j" (step 4) and "U_o" (Equation 4-12).

6. Determine the slope of the transient temperature data from the semi-log plot.

7. Calculate Q_{sc} or kh from Equation 4-13. Q_{sc} is calculated if an estimated value of kh is available OR kh may be calculated if $Q_{sc}$is measured.

8. *Optional:* An approximate value of k may also be estimated by substituting either Q_{sc} or kh in Equation 4-14 after determining the intercept of the straight line fitted to the linear portion of the transient temperature signal (following steps 1 to 8 above).

4.3.2 Workflow for Near-Wellbore Analysis

The thermal radius of investigation, r_T (Equation 4-15), is the distance the temperature signal has travelled in the reservoir at the velocity of convective heat transfer (Ramazanov et al. 2010).

$$r_T = \sqrt{(r_w{}^2 + 2U_o t)} \qquad (4\text{-}15)$$

The permeability and the radius of the damage zone can be determined from TTA. The damage zone permeability k_{skin} is solely responsible for the temperature response at early times when the thermal radius of investigation r_T is confined to the damage zone. The damage radius, r_d, is determined from Equation 4-15 once "t_d", the transition time at which the transient temperature signal slope changes due to a change in permeability, is identified {see Figure 4-3(a)}.

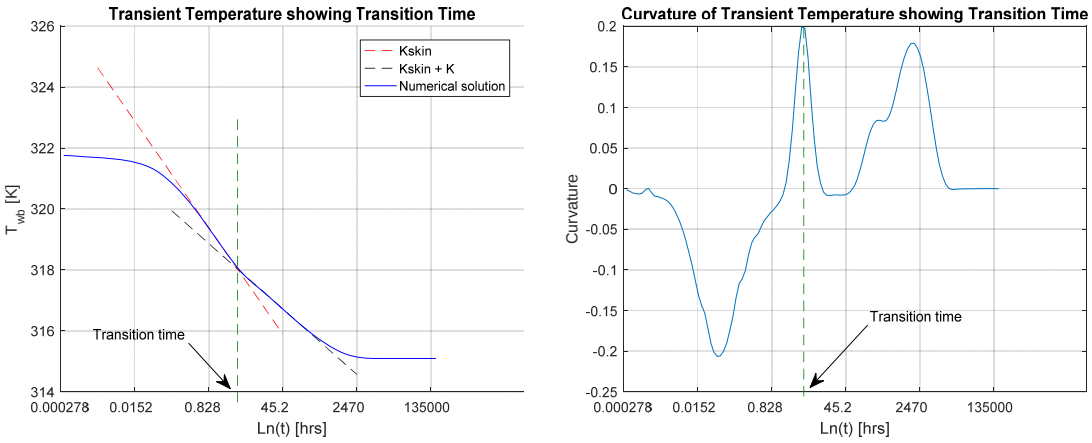

Figure 4-3 (a) Plot of transient temperature showing transition time. (b) Plot of curvature of transient temperature showing local maximum at transition time.

The procedure for carrying out near-wellbore analysis is shown below. This is similar to the workflow for estimating kh for the virgin formation, but it also estimates the damage radius.

1. Calculate the values of the fitting coefficient "B" from the PVT data or from appropriate Equation-of-State.

2. Determine "ψ_i", the pseudo-pressure at initial reservoir conditions.

3. Determine "η^*" & "ε" from Equation 4-12 at T_i and P_{avg}.

4. Identify the linear portions of the transient temperature profile and estimate the transition time "t_d" corresponding to their intercept.

5. *Optional:* Estimate the value of "δ" (Equation 4-8) with the value of "t_j" from step 4 and "U_o" (Equation 4-12).

6. Determine the slope of the transient temperature data between "t_j" and "t_d". This slope relates to the damage zone.

7. Evaluate the rate Q_{sc} if the value of $k_{skin}h$ is known from Equation 4-13 and the slope calculated in step 6. Alternatively, estimate $k_{skin}h$ if the value of $Q_{sc}$is known.

8. Calculate the damage radius r_d from the value of t_d calculated in step 4 and Equation 4-15.

9. *Optional:* Estimate the damage skin from the Hawkins formula if the "kh" of the damaged and virgin formation's and the damage radius have been calculated.

4.4 Comparison of Developed Solution to Numerical Result from a Commercial Simulator

The developed analytical solution has been compared with the numerical model developed in OpenFOAM. The solution would also be compared with the results from a commercial simulator.

The selected numerical simulator to be used is CMG-GEM. CMG-GEM is a compositional non-isothermal reservoir simulator and can model the transient temperature changes in the formation and the sandface. A model (based on the case study in Appendix E but with slightly different properties, as defined in Table 4-2) was created using this simulator and the transient sandface temperature (i.e. well bottomhole temperature) was extracted. The fluid properties used in the model was generated using

WinProp software (part of the CMG suite of software). Using the PVT properties generated by WinProp meant the required properties to be used in the developed solution had to be extracted, either from the PVT data or from the fluid properties in the numerical model. The latter approach was chosen as it is representative of the condition of the production period. Muradov & Davies (2013) demonstrated that the ratio of the measured pressure and temperature derivatives can be used to determine the Joule-Thomson coefficient; this method will be used here. The thermal expansion coefficient and adiabatic expansion coefficient is also determined from the Joule-Thomson coefficient, to ensure the fluid properties used in the analysis is consistent.

Table 4-2: Parameters for GMG-GEM simulation

Property	**Symbol**	**Value**	**Unit**
Thermal conductivity	K_T	1.73	W/mK
Specific heat capacity of rock	Cp_r	885.77	J/kgK
Density of rock	ρ_r	2650	kg/m^3
Gas flow rate at standard conditions	Qsc	2,000,000	m^3/day
Initial reservoir pressure	P_i	1.4×10^7	Pa
Initial reservoir temperature	T_i	321.4	K
Reservoir permeability	k	10×10^{-15}	m^2
Relative permeability to gas	k_{rg}	0.7	
Reservoir thickness	h	100	m
Thermal expansivity of gas	β_T	0.0054	K^{-1}

$$\mu_{JT} = \frac{\frac{dT}{dt}}{\frac{dP}{dt}} \qquad (4\text{-}16)$$

Figure 4-4 compares the transient temperature signal from the CMG-GEM with that of the analytical solution for the same condition. A significant difference is observed

between the two signals and it was impossible to match the numerical results using the developed analytical solution and the specified properties in the CMG-GEM simulator.

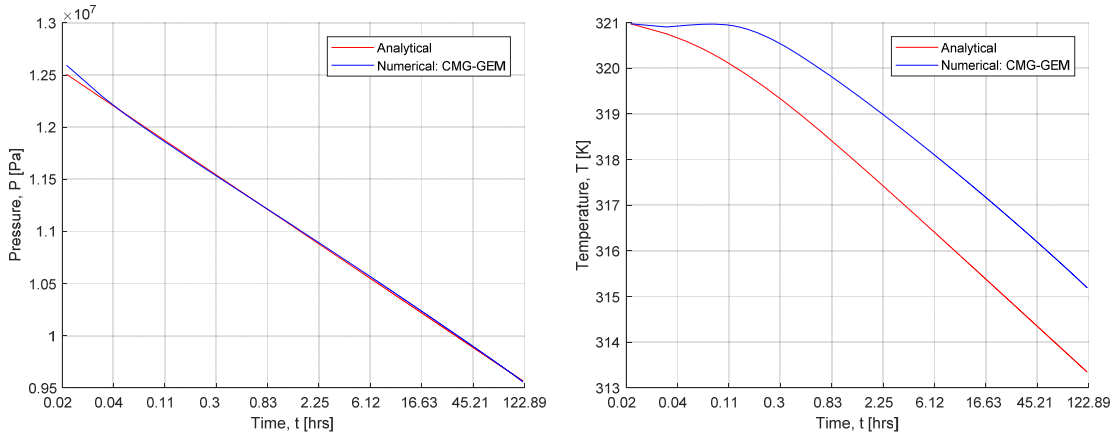

Figure 4-4: (a) Plot of transient bottomhole pressure for a case in CMG-GEM (b) Plot of transient bottomhole temperature a case in CMG-GEM

The reason why this was impossible is because the analytical solution was developed using the infinite acting constant radial flow with a step change in rate i.e. the surface production rate, or mass flux is produced from a well with an infinitesimal radius located at the centre of a cylindrical domain (i.e. the region of influence). While CMG-GEM models the infinitesimal wellbore in the centre of a cylindrical domain, the constant surface production rate, or mass flux assumption is met in the simulator. It was observed that, despite a constant surface flow condition being imposed, the mass flux in CMG-GEM is not constant but increases gradually at the start of production, with a range of about $76{,}000\, m^3/day$, this value is quite large compared to the range of less than $1\, m^3/day$ for the production rate in OpenFOAM. Consequently, the analytical solution matches the numerical results from OpenFOAM better, because the OpenFOAM model is a better representation of the step rate-change assumptions used to develop the analytical solution.

The gradual rate increase at the early time results in a smaller slope at early time relative to the case with a step rate-change. Even though the early time period of the analytical solution and the GEM simulation do not match (and this also affects the match of the late period), the slope at the later period are similar; about $-1.0511\, K/log_e\, cycle$ for the GEM model and $-1.0335\, K/log_e\, cycle$ for the analytical solution. This means that the

workflow which uses the constant slope of the late period can be applied to the CMG-GEM results as demonstrated in Section 4.5.

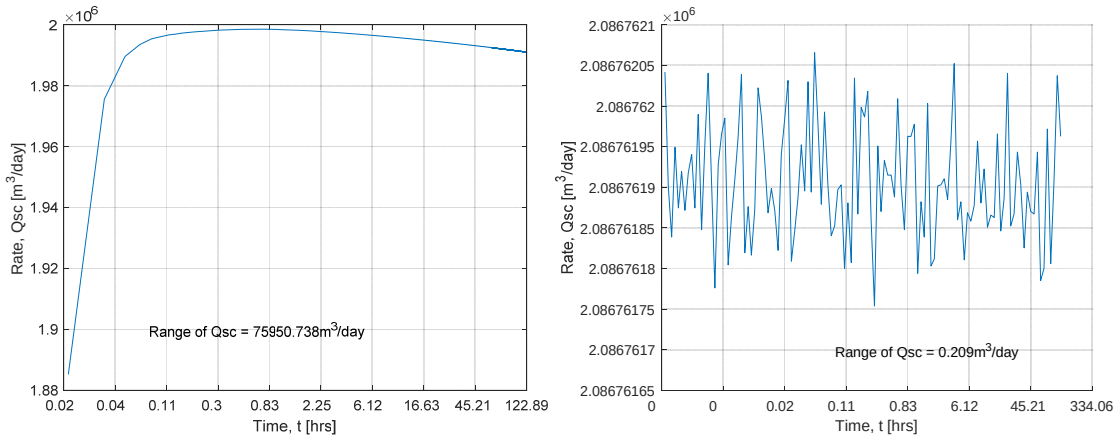

Figure 4-5: (a) Plot of sandface rate for a CMG-GEM simulation (b) Plot of sandface rate for a simulation using the developed solver in OpenFOAM.

4.5 Validation of Developed Workflow Using a Commercial Simulator

The developed analytical transient sandface temperature solutions and interpretation workflows can be used for analysis of real transient temperature measurements or in other situations for well completion design case studies which can be carried out for different purposes. Since the majority of design case studies carried out by practicing engineers are done using commercial numerical simulators it is important to demonstrate the possibility of applying the developed methods on data obtained from these simulators.

To carry out this analysis using CMG-GEM, the fluid properties are first determined. After determining the fluid properties required for the analysis (i.e. the adiabatic expansion coefficient, and the Joule-Thomson coefficient), it were then used in Equation 4-13 to obtain the permeability-thickness "kh" from the slope. The result is shown in Table 4-3 for two cases, case 1 has permeability of 10 mD, case 2 has permeability of 20 mD and the thickness for both cases is the same (100m).

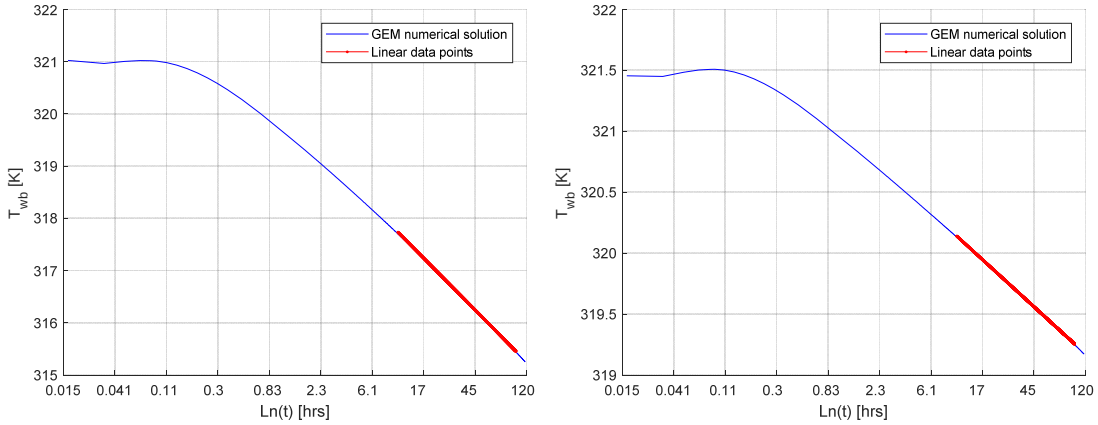

Figure 4-6: (a) Plot of transient bottomhole temperature for Case 1 with permeability of 10 mD (b) Plot of transient bottomhole temperature for case 2 with permeability of 20 mD

Table 4-3: Results of the TTA for both cases

	Actual permeability	**Relative permeability**	**Actual Effective permeability**	**Estimated permeability**
Case 1	10 mD	0.7	7 mD	6.51 mD
Case 2	20 mD	0.7	14 mD	13.36 mD

4.6 Improving the TTA Estimation Using Pressure Data

Chapter 3 (Section 3.4.4) explained the process of estimating the coefficients ("A" and "B" of Equation 3-55 of the linear pressure pseudo-pressure relationship from correlations or PVT properties of the produced fluid. An alternative way of doing this is by history-matching the pressure data, where an accurate measurement of pressure data is available. This can potentially improve the estimation accuracy of these values thereby improving the accuracy of the TTA.

4.7 Estimation of Virgin Formation KH In The Presence of Near-Wellbore Damage

Section 4.3 presented the estimation of the properties of the near wellbore damage zone using TTA and also the estimation of the properties of the virgin formation without near wellbore damage. While it is possible to estimate these two properties, it was observed that estimation of the properties of the virgin formation in the presence of near wellbore damage results in errors. This reason for this is that the transient temperature signal after the transition time is due to combined effect of flow through the damage zone and the virgin formation.

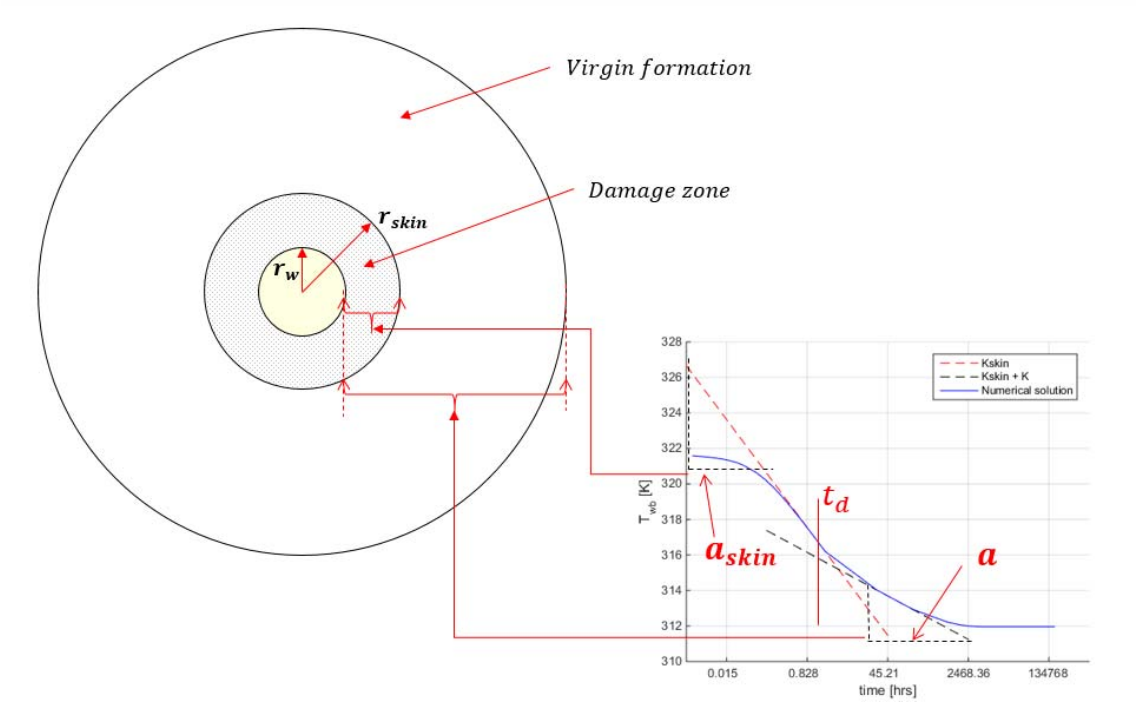

Figure 4-7: Illustration of transient temperature slopes for the damage zone and clean formation

Figure 4-7 Illustrates this, a_{skin} is the slope of the transient temperature signal for the damage zone while a is for the virgin formation. In reality, the value of the slope "a" is due to a combined effect of both the virgin formation and damage zone. Therefore, carrying out TTA to determine the permeability thickness by using the slope a would result in an effective value of permeability thickness and not the true value for the virgin formation.

This effect is further illustrated by considering several cases with the same virgin formation permeability and formation thickness, but with different damage zone permeability. The four cases considered are:

1. Case 1, a formation with no near wellbore damage

2. Case 2, a formation with a damage zone permeability of 1 mD

3. Case 3, a formation with a damage zone permeability of 3 mD

4. Case 4, a formation with a damage zone permeability of 5 mD

It can be seen that (Figure 4-8) the transient temperature slope after the transition time is different even though the permeability of the virgin formation are the same for the four cases considered {shown in the plot of transient temperature {Figure 4-8(a)} and its derivative {Figure 4-8(b)}. The radius of damage in the four cases are the same (0.5m) and this is evident as the transition time for the four cases are approximately equal.

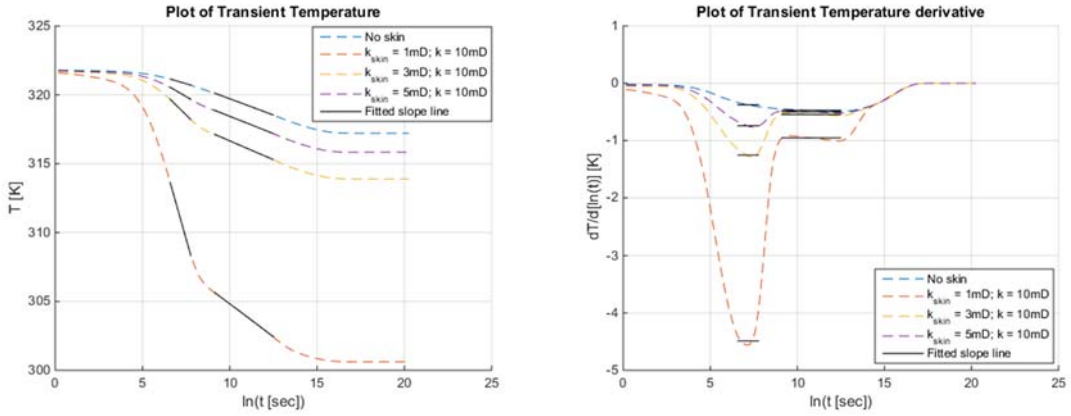

Figure 4-8: (a) Plot of transient sandface temperature for Case 1 to 4 with different damage zone permeability. (b) Plot of transient sandface temperature derivative for Case 1 to 4 with different damage zone permeability

4.8 Sensitivity to Errors

4.8.1 Errors in Measured Temperature Data

The temperature measurement used to determine the rate, permeability-thickness (kh), damage permeability and damage radius will be subject to some degree of error. A sensitivity study was therefore carried out to determine how an error of up to $\pm 10\%$ in the measurement translates into an error in the value of the slope and hence the values of the derived parameters.

1. The error of estimating kh and/or measuring Qsc are almost linearly related to error in the slope (for small errors in the slope) e.g. between 0 and ± 10% (Figure 4-4(a) and Equation 4-17). The sensitivity of the temperature sensor, rather than its absolute accuracy, is thus the parameter that determines the accuracy of the kh value.

2. The error of estimating k alone using secondary logarithms in Equation 4-12 increases exponentially with the error in the intercept (Figure 4-9(b) and Equation 4-19). Errors of –0.001% or +0.001% in the intercept result in errors of -14 and +16 % in the estimated permeability. Determination of the intercept is also subjected to increased errors because it involves extrapolation from the measured results. Systematic sensor errors (e.g. drift) further increase the error, so the direct estimation of k from Equation 4-12 is not recommended. This is normally not a problem, because k is (traditionally) best determined from the kh value if the formation thickness is known from well logs.

3. The error in damage permeability (or permeability-thickness) is similar to that described in "1" and "2" above. This is because the estimation of permeability-thickness kh is similar to that of the virgin formation, albeit, using a different portion of the transient temperature signal. The distinct source of error in near-wellbore analysis is from the estimation of the transition time "t_d", and this depends on the sensitivity of the gauge and the temporal resolution used in the measurement. The higher the temporal resolution the more accurate the value of "t_d".

$$\Delta kh = \frac{B\Gamma TQ_{sc}}{2\Delta a}[\eta^* - \varepsilon] \qquad (4\text{-}17)$$

$$\Delta Q_{sc} = \frac{2kh\Delta a}{B\Gamma T[\eta^* - \varepsilon]} \qquad (4\text{-}18)$$

$$\Delta k = \frac{\phi\mu c r_w^2}{4} exp - \left[\left(\frac{(T_i - \Delta b)2kh}{\eta^* \Gamma TQ_{sc}B}\right) - \frac{\varepsilon}{\eta^*} ln\left(\frac{200U_o\delta}{r_w{}^2(100+\delta)}\right) - \gamma\right] \qquad (4\text{-}19)$$

Where "a" is the slope and "b" is the intercept.

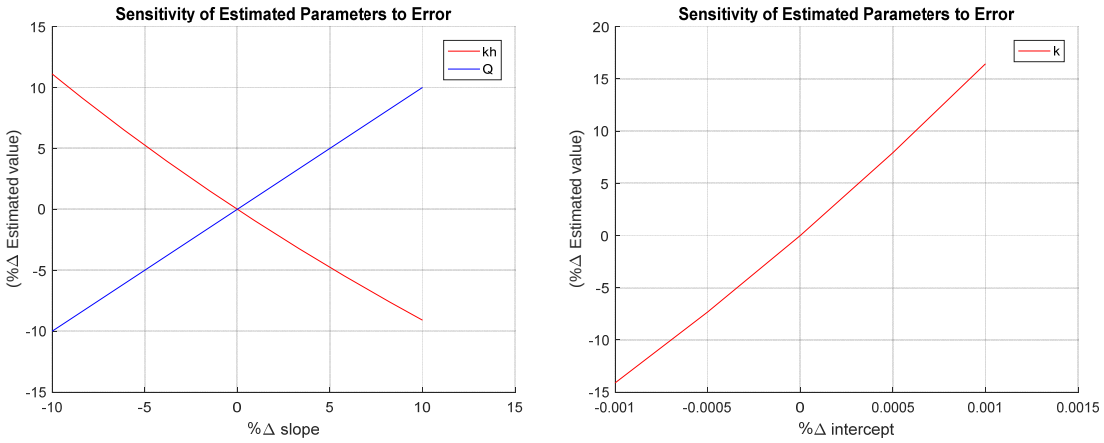

Figure 4-9 (a) Plot showing sensitivity of permeability- thickness and rate estimation to errors in the slope. (b) Plot showing sensitivity of permeability alone estimation to errors in the intercept.

4.8.2 Errors in Other Input Parameters

The analysis carried out using the workflows described above depends on inputs from several sources, e.g. sensor measurements for transient temperature, pressure and rate data, PVT lab reports or correlations for fluid properties, well logs or well test data for formation properties. All such measurements have some degree of uncertainty associated with them. It is important to quantify how the uncertainties in the inputs translate into the results of the TTA.

The effect of the uncertainty in the thermal properties, the Joule-Thomson coefficient, "ε", and the adiabatic expansion coefficient, "η^*", on the estimation of kh and flow rate is described by Equation 4-20 and Equation 4-21 respectively. These thermal properties are themselves a function of other fluid and formation properties. The Figure 4-10 spider

plot illustrates the sensitivity of the various input parameters on the estimated values of kh and Q_{sc}. The initial temperature, T_i, and the thermal expansion coefficient, β_T, have the greatest impact on the kh and Q_{sc} estimates. The gas density, ρ, gas specific heat capacity, C_p, pressure-pseudo pressure slope, B, and TTA slope, a, have a lower, linear effect on estimated values of kh and Q_{sc}. The rock density, ρ_r, rock specific heat capacity, C_{pr}, and porosity, ϕ, have a negligible impact.

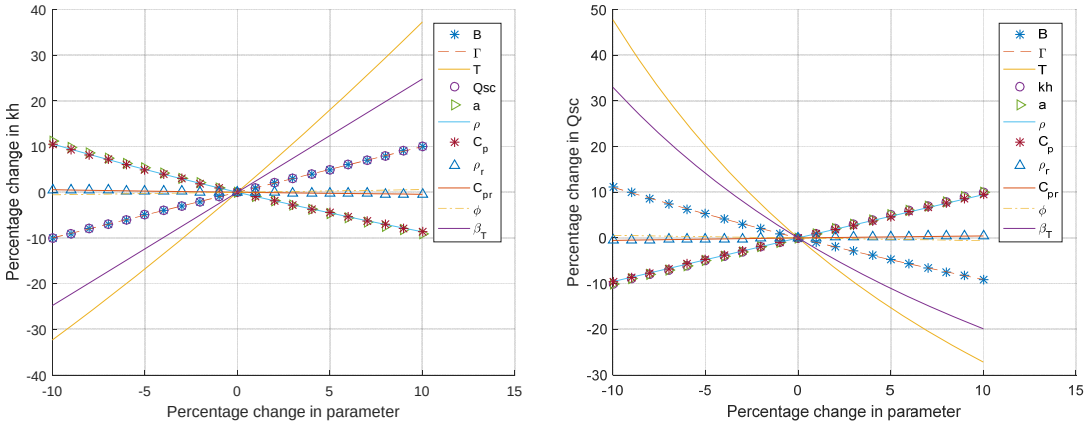

Figure 4-10 (a) Plot showing sensitivity of permeability- thickness to different input parameters. (b) Plot showing sensitivity of rate to different input parameters.

$$kh = \frac{B\Gamma T_i Q_{sc}}{2a}[\eta^* - \varepsilon] \qquad (4\text{-}20)$$

$$Q_{sc} = \frac{2akh}{B\Gamma T_i[\eta^* - \varepsilon]} \qquad (4\text{-}21)$$

The Monte-Carlo method and the linearized form of the analytical equation {the semi-log slope, "a", from (Equation 4-13) could also be used to prepare an uncertainty analysis. A random sample is chosen from a normal distribution of ε and η^* and the distribution of the estimated kh values calculated, as described in Section 4.11.4.

4.9 The Effect of a Gradual Change in the Flow Rate

The change in the sandface production rate will not always be instantaneous, despite the TTA solutions assuming a step-like change in the flow rate. This assumption is regularly violated by:

1. Gradual opening or closing a valve or choke.

2. Wellbore storage effects when the well is controlled by a surface choke.

These effects last between a few minutes and hours. Example 1 can be minimized by operating the valve at the highest allowed rate while example 2 cannot be changed and is case specific.

The comprehensive numerical model of mass and heat transfer around a wellbore (described in Chapter 3 and Appendix C) was used to generate the data required for studying the variable rate effect. The variable rate effect produces a transient temperature signal which has a similar appearance to the skin effect (Figure 4-11). This presents difficulties when carrying out a near-wellbore analysis, making it necessary to differentiate whether a particular feature is caused by a rate variation, the skin effect or a combination of both. Figure 4-11 shows that the transient temperature signal returns to the base (step rate change) value after a time period that is proportional to the duration of the rate change. The time required for measuring data suitable for carrying out a meaningful TTA depends on the rapidity with which the change to the sandface flowrate is achieved.

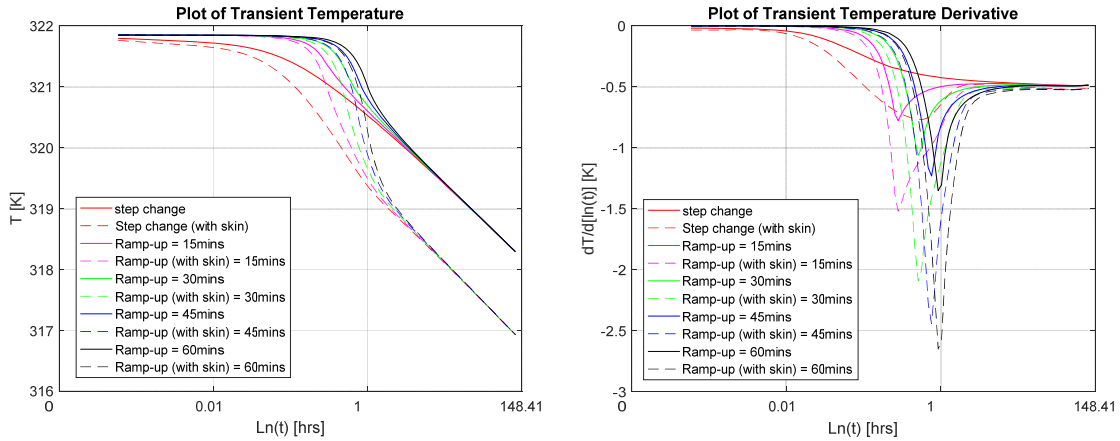

Figure 4-11 Plot of (a) The transient temperature (b) Its derivative versus time

Figure 4-12(a) shows the relative change in transient temperature derivative (Equation 4-22) for different ramp-up times (the time required for the change in sandface rate to occur). The relative differences between the derivatives compared to that for a step rate change reduces with time. Figure 4-12(b), a plot of the settling time (the time it takes for

the relative error in the slope to reduce to 5%) shows that it is ~ 12 times greater than the ramp-up time. An allowable relative error of 5% was chosen since the TTA is more sensitive to errors in other parameters, such as the PVT properties and surface rate measurement.

$$rel.error = \frac{\left(\frac{dT}{d[ln(t)]_{ramp}} - \frac{dT}{d[ln(t)]_{step}}\right)}{\frac{dT}{d[ln(t)]_{step}}} \qquad (4\text{-}22)$$

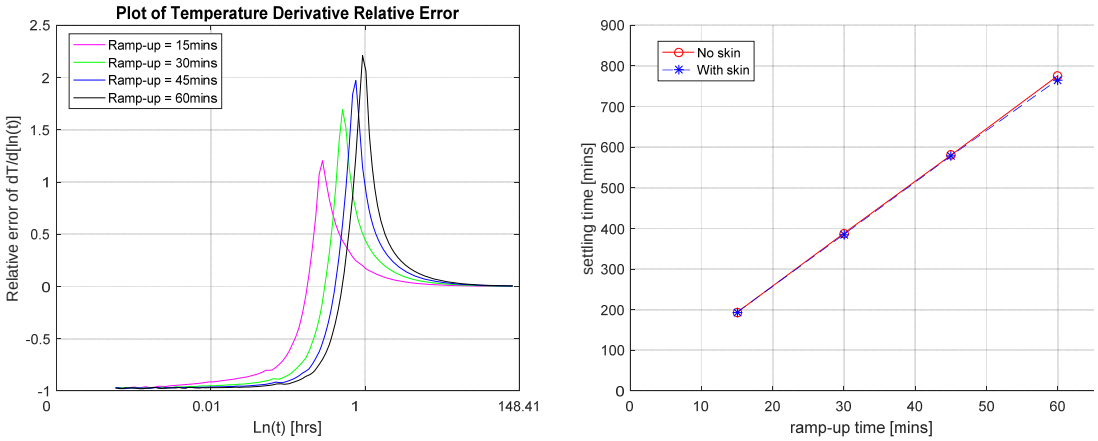

Figure 4-12 (a) Plot of relative change between transient temperature and base case (b) Plot of settling time against ramp-up time

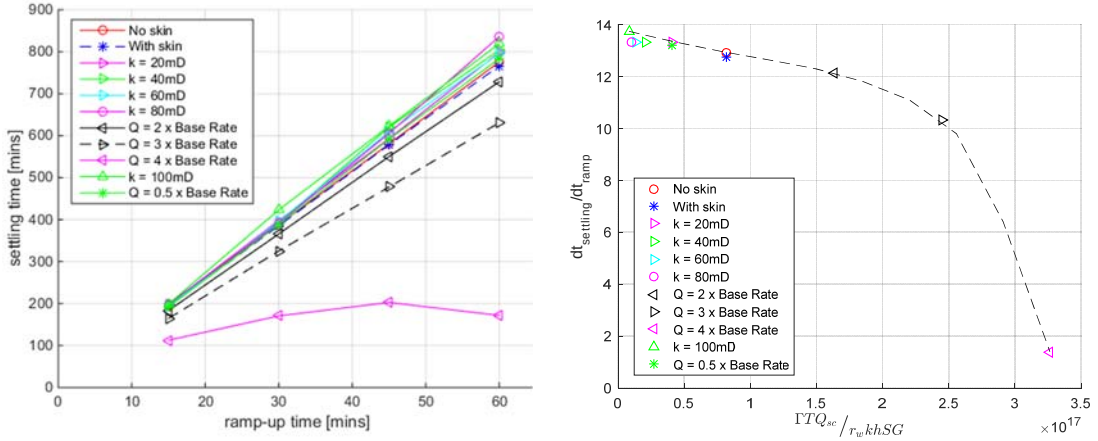

Figure 4-13 (a) Plot of settling time against ramp-up time (b) Plot of slope of Figure 4-13(a) against $\frac{\Gamma TQ_{sc}}{r_w kh \cdot SG}$

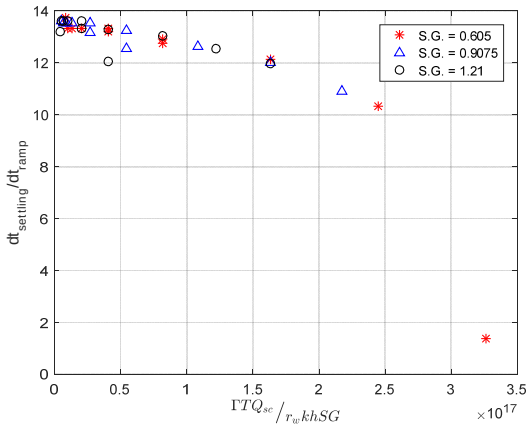

Figure 4-13(c) Plot of slope of Figure 4-13(a) against $\frac{\Gamma TQ_{sc}}{r_w kh \cdot SG}$ for different gas properties

It was observed that the slope of the plots in Figure 4-13(a) showed a downward trend with increasing $\frac{\Gamma TQ_{sc}}{r_w kh \cdot SG}$. The settling time (for the ramp-up effect to stop masking the step-like rate change solution) can be estimated by using this trend {Figure 4-13(b)} if an estimate of $\frac{\Gamma TQ_{sc}}{r_w kh \cdot SG}$ is also available. Note that Figure 4-13(b) refers to the specific gas properties chosen, but a similar trend is observed for other gas properties {Figure 4-13(c)}.

The settling time in a particular case can be quantified from the product of $\frac{dt_{settling}}{dt_{ramp}}$ {read off the y-axis of Figure 4-13(b)} and t_{ramp}. More qualitatively, Figure 4-13(b) indicates that the settling time of the TTA slope is less than 15 times the ramp-up time for the example chosen. Therefore, TTA requires that:

1. The duration of data measurement must be sufficiently long so that the transient temperature signal has unambiguously (within a relative error < 5%) returned to the base value.

2. Investigation of the near-wellbore skin effect requires that the ramp-up time must be short enough for the transient signal to return to the base value within the time it takes for the transient temperature disturbance to travel out of the near-wellbore region. This time can be estimated with Equation 4-15.

Note that the "Ramp-Up Time" as used here refers to the time for the sand face flow rate to stabilise. This may be very different from the actual stroke time required to move a surface choke.

4.10 Limitations Due to Non-Darcy Effects

Our analytical solution assumes the gas flow obeys Darcy's law. However, inertial effects which lead to the gas flow deviating from Darcy's law at the higher velocities are often observed in the field. Sui et al. (2010) included this non-Darcy effect in their numerical models while the analytical Forchheimer's equation (Equation 4-23) adds an additional pressure drop term { $\beta\rho|\boldsymbol{v}|\boldsymbol{v}$ - see e.g. (Wang & Economides 2009)} to Darcy's equation.

$$-\nabla P = \frac{\mu}{k}\boldsymbol{v} + \beta\rho|\boldsymbol{v}|\boldsymbol{v} \qquad (4\text{-}23)$$

Equation 4-24 defines a dimensionless number (r_{nD}) that represents the relative importance of the non-Darcy effect (the ratio of the pressure gradients due to the non-Darcy and the Darcy flow). Note that r_{nD} is defined here in terms of the gas flow rate measured at standard conditions.

$$r_{nD} = \frac{\beta\rho|v|k}{\mu} \qquad (4\text{-}24)$$

$$r_{nD} = \frac{Q_{sc}\rho_{sc}}{2\pi r_w L_w} \cdot \frac{\beta k}{\mu} \qquad (4\text{-}25)$$

$r_{nD(crit)}$ is the critical non-Darcy ratio at which the resulting errors are still acceptable compared to the errors in other input parameters). An acceptable error of 5% in the TTA slope is suggested. The corresponding critical Darcy velocity ($\boldsymbol{v}_{(crit)}$, Equation 4-26) and critical Darcy surface rate ($Q_{sc(crit)}$ Equation 4-27) below which the non-Darcy effects can be neglected are:

$$\left|\boldsymbol{v}_{(crit)}\right| = \frac{\mu r_{nD(crit)}}{\beta\rho k} \qquad (4\text{-}26)$$

$$Q_{sc(crit)} = \frac{\mu r_{nD(crit)} 2\pi r_w L_w}{\beta\rho_{sc} k} \qquad (4\text{-}27)$$

Our analysis methods may thus be confidently applied to velocities or surface flow rates smaller than $\boldsymbol{v}_{(\boldsymbol{crit})}$ and $Q_{sc(crit)}$ respectively. The valid application area of the developed TTA methodology is well specific. It depends on the completion geometry and the reservoir properties. An accurate estimation of $Q_{sc(crit)}$ also depends on a good knowledge of the value of β. Wang & Economides (2009) have published a compilation of non-Darcy coefficient correlations.

An approach that will be useful to well surveillance engineers is to calculate the specific critical surface flowrate by dividing $Q_{sc(crit)}$ by the length of the well's completion or the thicknesses of the reservoir sand. This term can then be applied to different wells within the same field/reservoir.

$$Q_{scn(crit)} = \frac{Q_{sc(crit)}}{2\pi r_w L_w} = \frac{\mu r_{nD(crit)}}{\beta \rho_{sc} k} \qquad (4\text{-}28)$$

Alternatively, the effect of non-Darcy flow on transient temperature can be investigated by considering the relationship between r_{nD} and the additional transient temperature drawdown due to non-Darcy flow. The dimensionless number T_{nD} is the ratio of the additional temperature drawdown due to the non-Darcy flow effect to the temperature drawdown due to Darcy flow.

$$T_{nD} = \frac{T_{w\,(Darcy)} - T_{w\,(non-Darcy)}}{T_i - T_{w\,(Darcy)}} \qquad (4\text{-}29a)$$

$$P_{nD} = \frac{P_{w\,(Darcy)} - P_{w\,(non-Darcy)}}{P_i - P_{w\,(Darcy)}} \qquad (4\text{-}29b)$$

Figure 4-14 illustrates the effect of non-Darcy flow on the transient well temperature and pressure for the case study described in Appendix E. It clearly shows that the non-Darcy effect cannot always be neglected during TTA as it is responsible for between 10% - 30% of the measured temperature change. Application of the analytical solutions with a reasonable accuracy therefore requires verification that the non-Darcy effect is either negligible or can be corrected for.

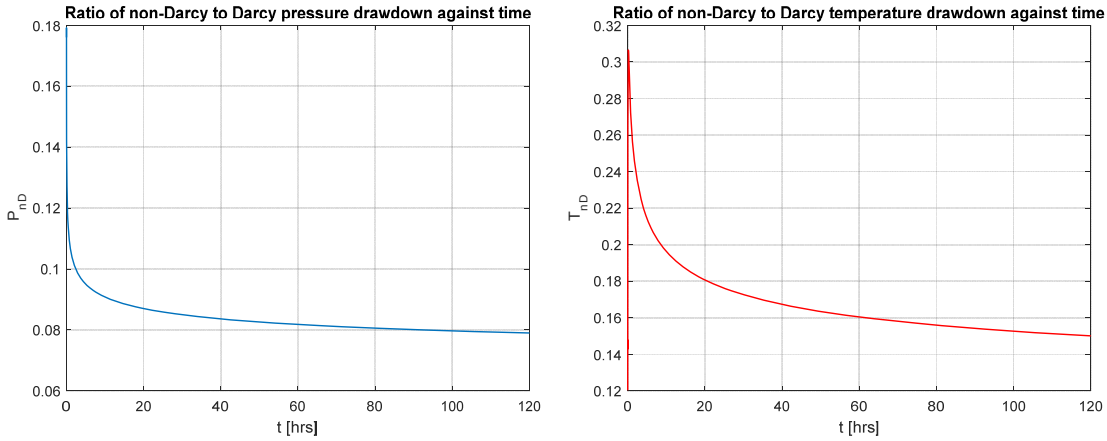

Figure 4-14: (a) Plot of ratio of non-Darcy to Darcy drawdown drawdown pressure (b) Plot of ratio of non-Darcy to Darcy temperature

It is important to note that in all cases the effect on the slope of the transient temperature signal due to non-Darcy flow is relatively small. Hence the developed TTA methodology (of estimating kh from the slope) is valid in many practical applications, even if the critical rate is by far exceeded. For example, Figure 4-15(b) shows that the error in the slope of the transient temperature is about one order of magnitude less than the value of r_{nD}.

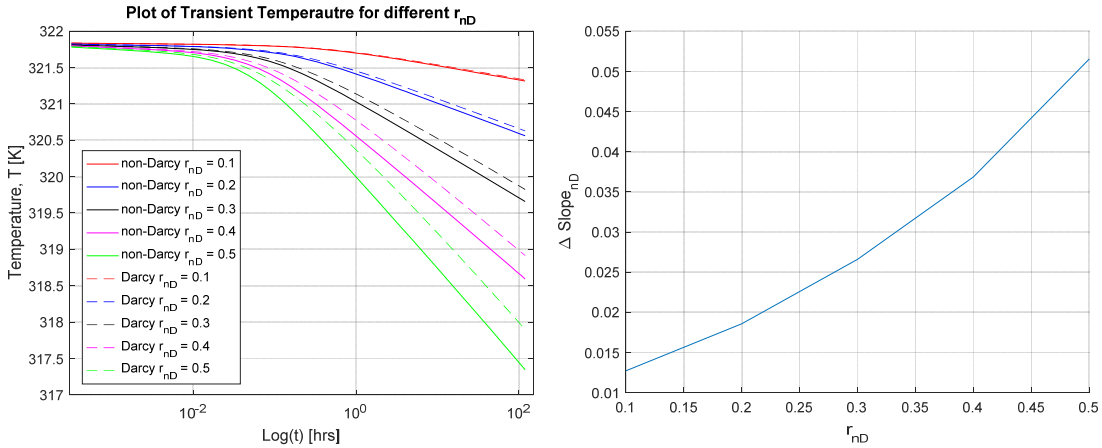

Figure 4-15: (a) Plot of transient temperature for temperature different values of r_{nD} (b) Plot of relative error in transient slope against r_{nD}.

How the non-Darcy flow affects the transition time between the damaged and virgin formation was also studied. The Appendix E case study with the addition of a damaged zone of reduced permeability was used. Figure 4-16 shows that the transition time is independent of the non-Darcy effect despite there being a significantly greater change in temperature in the non-Darcy case {Figure 4-16(b)}.

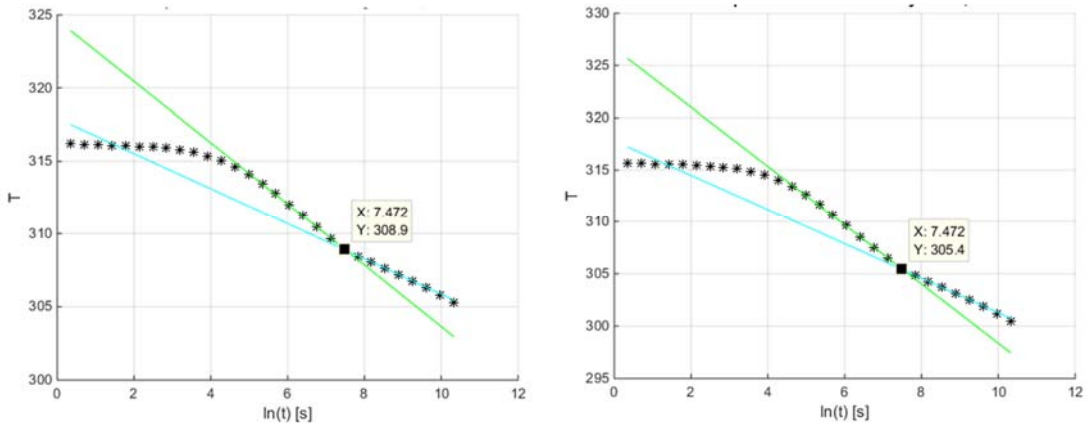

Figure 4-16: (a) Plot of transient temperature showing the transition time for pure Darcy flow (b) Plot of transient temperature showing the transition time for non-Darcy flow

This means it is possible to determine the damage radius using the Darcy's law TTA solution without loss of accuracy due to the non-Darcy effect. The transition time was also shown to be independent of the value of β.

4.11 Case Studies

4.11.1 A Synthetic Well Model

This synthetic case history concerns the application of TTA to constant rate production from a vertical dry gas production well. The TTA data [Figure 4-17(a)] was generated by a developed numerical simulator described in Chapter 3 and Appendix C, using the model parameters of Appendix E. Two of these case studies are discussed in this section, refer to Appendix E for details of the other case studies.

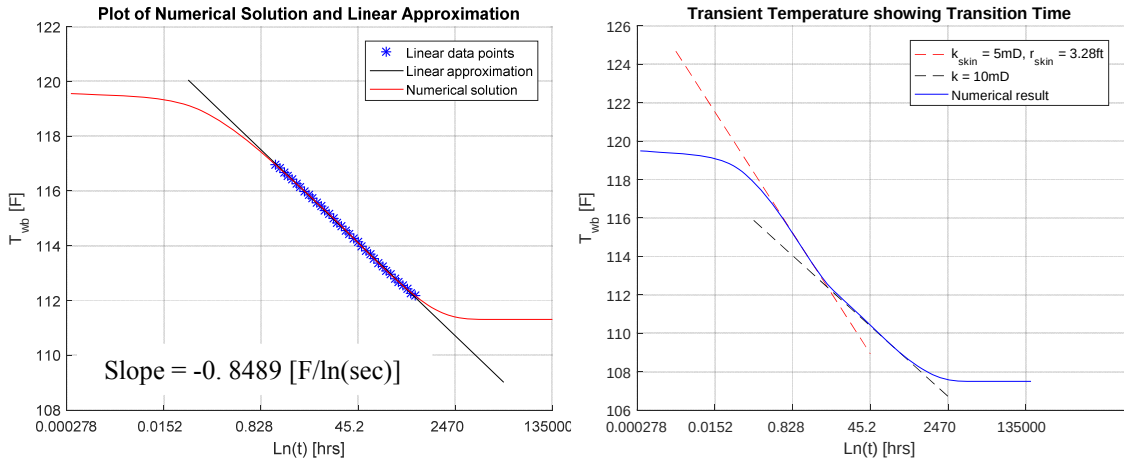

Figure 4-17 Transient temperature (a) with the linear interval and slope highlighted. (b) with slope of damage region and clean formation indicated

4.11.1.1 Estimating the Rate and Permeability Thickness

Figure 4-17(a) is a semi-log plot of the transient, downhole temperature versus time (Case study 1, full details in Table E-4 and E-5 of Appendix E). The first and last data points (blue stars) of the well-fitted ($R^2 = 0.9998$) straight line are $t_j = 1.5\,hr.$ and $t_s = 120\,hr$ respectively. The analysis can thus be applied a few hours after the rate change. t_j can be estimated using Equation 4-8 for different test conditions, but a short duration well test not only requires a low value of t_j, but also requires good quality data (lack of noise etc.). However, a longer test period will normally ensure a more accurate value for the slope.

The estimated values of either $kh = 380\,mD.ft$ or Flow Rate $= 7.37\,MMScf/day$ are within 5% of the Appendix E input values of $kh = 390\,mD.ft$ and Flow Rate = $7.02\,MMScf/day$.

4.11.1.2 Estimating the Magnitude of a Near-Wellbore Damaged Zone

A near-wellbore formation damage zone with a 50% reduction in permeability for a distance of 2.89 ft from the wellbore wall was added to the Appendix E numerical model (Case study 1, full details given in Table E-6 and E-7 of Appendix E) i.e. $r_d = 3.28\,ft$ and $k_{skin}h = 195\,mD.ft$. TTA using the skin estimation workflow (Section 4.3.2) utilising the temperature derivatives and the thermal investigation radius, gave estimates within 6% of the above input values {estimated $k_{skin}h = 202.4\,mD.ft$ and estimated $r_d = 3.08\,ft$}.

Figure 4-18(a) illustrates the sensitivity of the transient temperature signal for formation damage radii of 1.5 ft and 3.0 ft. The radius of the formation damage, the time at which the slope of the transient temperature changes, is even more conspicuous in the derivative plot {Figure 4-18(b)}.

The TTA signal increases as the level of formation damage increases. This case history illustrates how the TTA signal travels through the formation damage zone at a rate that is several orders of magnitude smaller (4.2 hr) than the corresponding pressure signal (10 s). This slow transmission of the transient temperature signal gives TTA its unique ability to recognise permeability changes in the near wellbore formation; information which cannot be obtained from PTA.

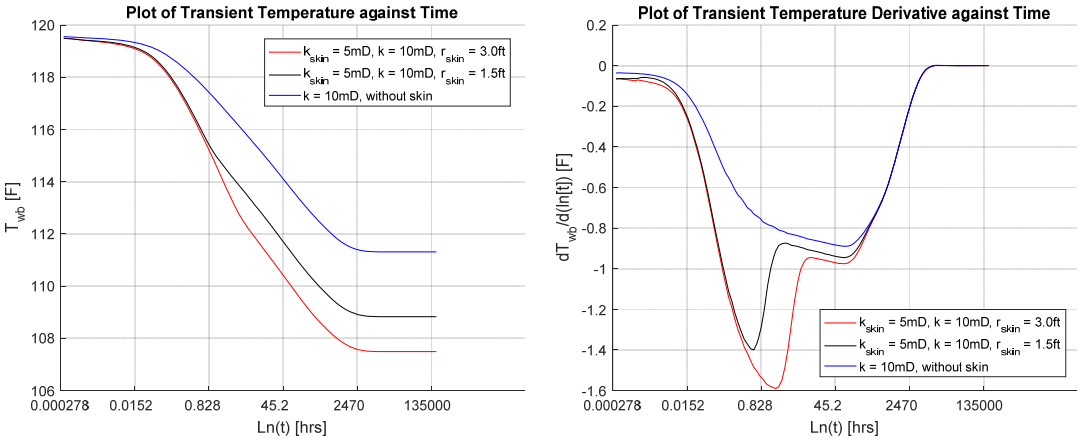

Figure 4-18 Impact of damage radius on (a) the Transient temperature and (b) its derivative

4.11.2 Analysis of Real-Field Data

This section applies the workflows developed to transient temperature downhole data recorded in a real, vertical, gas producing well (Figure 4-19 and Table 4-4) producing ~100 MMscf/day. A permanent downhole gauge installed some distance above the producing layer measures pressure, temperature and surface production rate is measured every 30 minutes. There are 3 well start-ups during the 3½ month data acquisition period (Figure 4-19). Two usable drawdown periods (highlighted in red) were identified from the raw, production measurements.

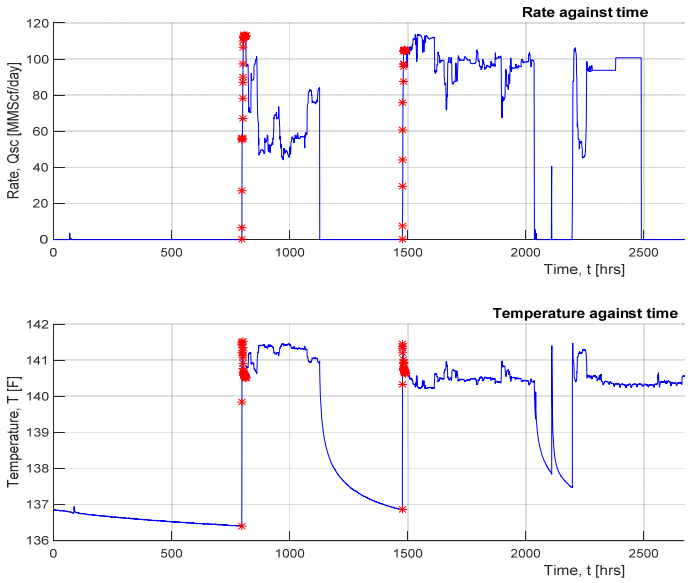

Figure 4-19 Surface production rate and downhole temperature

Table 4-4: Gas and formation properties (estimated at 1370 psi and 141.3^{0}F)

Viscosity $\mu\ at\ P_{avg}\ \&\ T_i\ [cP]$	0.01373	Density of gas $\rho\ at\ P_{avg}\ \&\ T_i\ [lbm/ft^3]$	3.995
Specific gravity $S.G$	0.605	Porosity of formation ϕ	0.15
Thermal expansion coefficient of gas $\beta_T\ at\ P_{avg}\ \&\ T_i\ [°F^{-1}]$	0.0044	Specific heat capacity of the formation rock $\rho_r\ at\ P_{avg}\ \&\ T_i\ [Btu/(lbm°F)]$	219.74
Specific heat capacity of gas $\beta_T\ at\ P_{avg}\ \&\ T_i\ [Btu/(lbm°F)]$	682.14	Density of formation rock $at\ P_{avg}\ \&\ T_i\ [lbm/ft^3]$	156.07

TTA assumes a constant flowrate before and after the step rate change in question. The useable drawdown periods were selected based on their having a preceding period of constant flowrate (a well shut-in) and a sufficiently long drawdown flow period, so the effects of wellbore warm-up die-out while still providing sufficient data for TTA.

The transient temperature signal {Figure 4-20(a)} shows an initial warmup period during which the sensor temperature increases as hotter produced fluid arrives at its location above the producing zone. This warm-up effect dies-out after 6 hrs, after which the signal shows the same behaviour as observed in the ideal model case studies, a linear slope on a semilog plot.

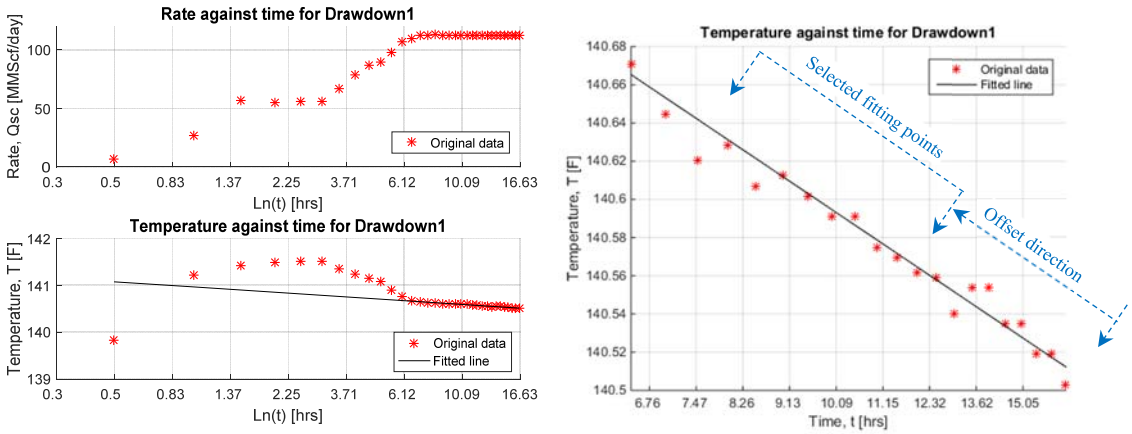

Figure 4-20: (a) Plot of surface production rate and downhole transient temperature drawdown period 1. (b) Plot of transient temperature showing fitting points and offset direction

It was shown earlier that, the effect on the slope of the transient temperature signal due to non-Darcy flow is relatively small even when Darcy's law is not valid. r_{nD}, the ratio of the additional pressure drop due to the non-Darcy effect to the Darcy pressure drop, describes the importance of this effect. Geertsma (1974) illustrated how to determine r_{nD} from Equation 4-25.

The non-Darcy effect results in underestimating *kh* because it increases the slope of the TTA signal. Numerical simulation indicated that the non-Darcy effect on the value of the TTA slope is approximately one tenth of the value of r_{nD}. The value of r_{nD} was found to be about 0.5 for this case, implying an error of about 5% in the slope of the transient temperature signal. The relative increase in slope due to the non-Darcy effect is thus relatively small in this case. Hence, it is possible can apply a "Darcy-based" workflow with sufficient accuracy for this illustration of TTA.

The accuracy of the *kh* value estimated from TTA data also depends on both the methodology used to choose the data points and the resulting number of data points available for analysis. The impact {Figure 4-20(b)} on the results from this real field case of two procedures for selecting the data points based on the following criteria was examined:

- Have the transient effects from the initial wellbore warmup and varying rates died-out before the first data point is selected?

- Is the flow still in the infinite acting regime?

- Is the transient temperature in the linear region and Equation 4-11 applicable?

Method 1 (a fixed number of fitting points and a variable end offset): The number of selected data points were kept constant and the data points are offset from the last data point. The slope is calculated for each offset.

Method 2 (zero end offset and a variable number of fitting points): the selected data points are not offset, but the number of selected data points is increased and the slope is calculated in each case.

Figure 4-21 and Table 4-5 summarise the results from the TTA of the mean permeability-thickness product and its variance using a different number of data points. The analysis was repeated with a fixed number of data points while offsetting the data points (i.e. changing the data points used for the analysis). The results of this study are shown in Figure 4-22 and Table 4-6.

The results obtained from the two methods are similar with a standard deviation of less than 10% from the mean value of the estimated permeability-thickness. However, the results from drawdown period 1 have a lower standard deviation, probably because the linear portion of the transient temperature signal is longer (~ 10 hr versus ~ 8.5 hr).

This demonstrates the potential of using TTA for gas well and reservoir characterization. Alternatively, if kh is known, this method can be used to estimate the production rate from one or more layers by using the transient sandface temperature measurement.

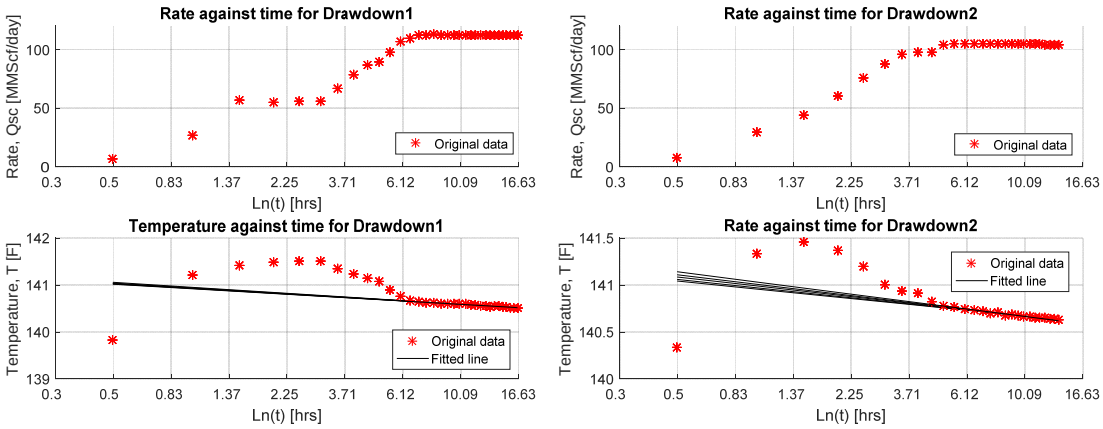

Figure 4-21: Plots of surface production rate, downhole transient temperature and fitted lines for different offsets and 12 data fitting points (a) Drawdown period 1 (b) Drawdown period 2

Table 4-5. TTA estimated kh for drawdowns 1 and 2

	Drawdown 1	**Drawdown 2**
Production rate (MM scf/day)	112	105
Estimated mean kh (mDft) with 12 fitting points (Incremental offset from 1 to 5 data points)	34,100	35,300
Standard deviation of estimated kh (mD. ft) using 12 data points	$\pm$ 1,690	$\pm$ 3,430

Table 4-6. TTA estimated kh for drawdowns 1 and 2

	Drawdown 1	**Drawdown 2**
Production rate (MM Scf/day)	112	105
Estimated mean kh (mD. ft) with zero offset (using 12 to 17 data points)	32,000	36,500
Standard deviation of estimated kh (mD. ft) using 12 data points	$\pm$ 795	$\pm$ 2210

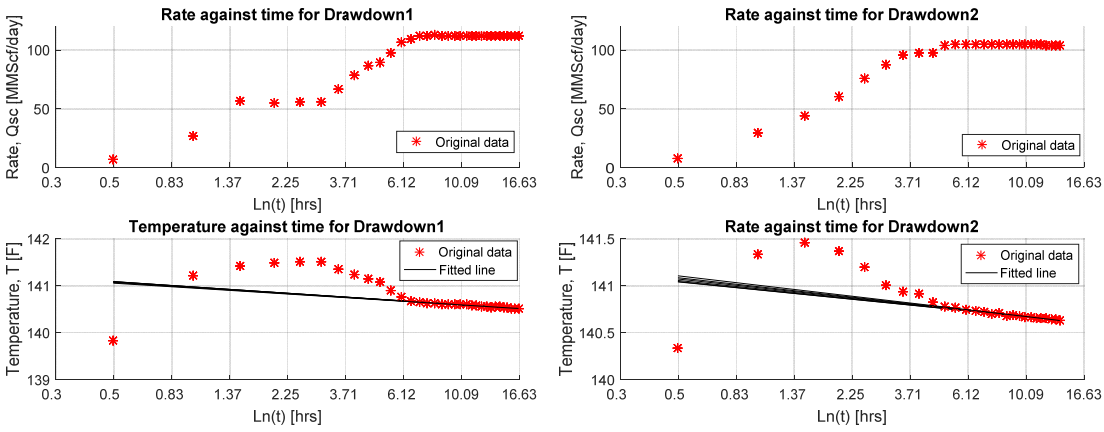

Figure 4-22: Surface production rate and downhole transient temperature for different numbers of data points, zero offset (a) Drawdown period 1 (b) Drawdown period 2

4.11.3 Validation of TTA Results

The above results from the TTA workflow have been compared with those from both pressure and rate transient analysis (RTA) using the Figure 4-23 data.

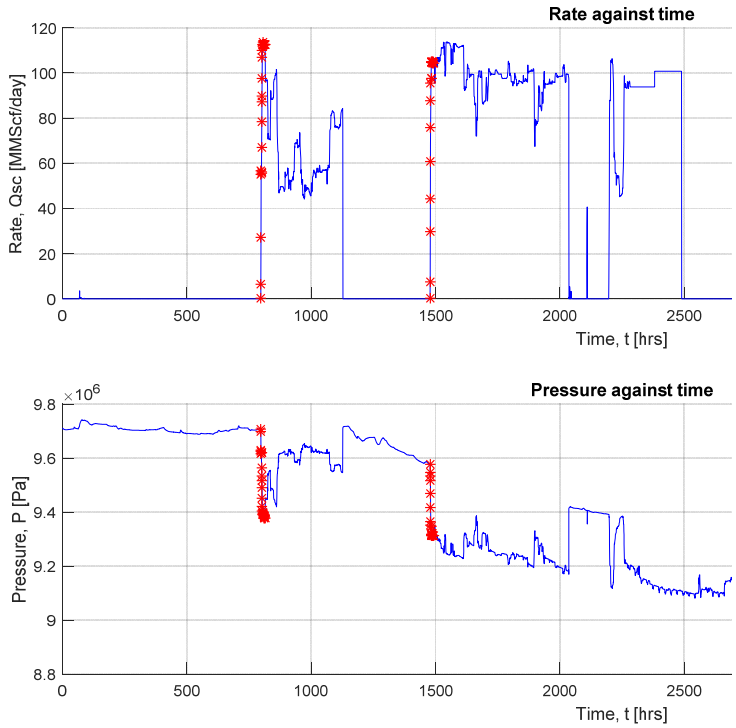

Figure 4-23 Surface production rate and downhole transient pressure in a vertical, gas well

4.11.3.1 Case Study No. 2: Pressure Transient Analysis

There are no distinct pressure build-up periods in the measured downhole pressure data (presumably because of non-ideal well shut-in); hence it is only possible to use the drawdown periods, the same ones as used for TTA. The PTA in a gas well uses the pressure drawdown solution for infinite acting radial inflow (Equation 4-4 or equivalent pressure drawdown solution). Equation 4-30 describes the semilog slope for the pressure. The PTA results for this particular case are quite inaccurate.

$$\frac{dP_{wf}(t)}{d[ln(t)]} = m = \frac{B\Gamma TQ_{sc}}{2kh} \qquad (4\text{-}30)$$

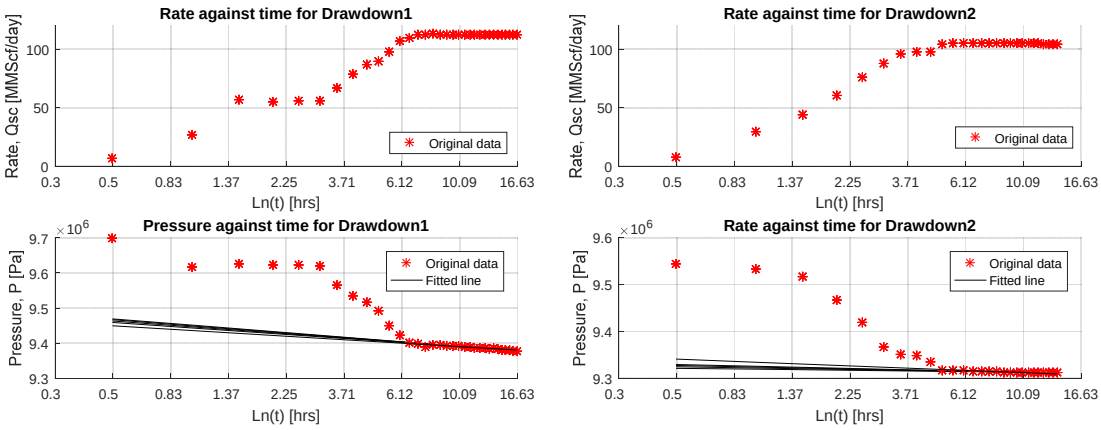

Figure 4-24 Surface production rate and downhole transient pressure in a vertical, gas well (a) Drawdown period 1 (b) Drawdown period 2

Table 4-7. PTA estimated kh for drawdowns 1 and 2

	Drawdown 1	**Drawdown 2**
Production rate (MM scf/day)	112	105
Estimated mean kh (mDft) with 12 fitting points (Incremental offset from 1 to 5 data points)	48,649	232,564
Standard deviation of estimated kh (mD. ft) using 12 data points	$\pm$ 5,571	$\pm$ 99,662
Estimated kh (95% confidence interval) (mD. ft)	37,507 – 59,791	33,240 – 431,888

4.11.3.2 Rate Transient Analysis

The value of kh was also estimated with commercial software using the same input data.

Table 4-8. RTA estimated kh for drawdowns 1 and 2

	Drawdown 1	**Drawdown 2**
Production rate (MM scf/day)	112	105
Estimate of kh from RTA $[mD.ft]$	40,900	55,400

The results obtained from TTA, PTA (Figure 4-24 and Table 4-7) and a more suitable RTA (rate-transient analysis) presented in Table 4-8 are close and are summarised in Table 4-9, though the estimate from drawdown 2 using PTA deviates from the other results. Also note that the TTA estimates are consistently lower than those from PTA and RTA, possibly due to the previously explained increasing (ramp-up) rate effect leading to an underestimate of the kh and an overestimation of the flow rate. The kh estimates from the two drawdown periods are more consistent with TTA, while PTA shows the largest discrepancy. The discrepancy between the two drawdowns in the PTA is due to the fact that the second drawdown is not starting from stabilized pressure. This can be verified from Figure 4-23; which shows a gradual reduction in pressure (despite the surface choke being shut) before the start of the second drawdown event. This decreasing pressure trend during the shut-in periods is probably due to the gas trapped in the wellbore loosing heat into the cooler surroundings and thus contracting. This results in the pressure change that can have two possible effects; on one hand it masks the 'ideal' buildup pressure data. On the other hand, cooling of the gas column in the wellbore leads to contraction which can result in some afterflow, which in turn affects the drawdown analysis after the shut-in period. A similar decreasing temperature trend has been observed by Izgec et al. (2007), they recommended placing the gauge close to the sandface to ensure sufficient data quality.

Table 4-9. Estimated kh for drawdowns 1 and 3 obtained using TTA, PTA and RTA

	Drawdown 1	**Drawdown 2**
Estimate of kh from TTA [$mD.ft$]	34,100	35,300
Estimate of kh from PTA [$mD.ft$]	48,649	232,564
Estimate of kh from RTA [$mD.ft$]	40,900	55,400

4.11.4 Uncertainty Estimation

The sensitivity of kh estimation to different input parameters has been considered in Section 4.8.2. It was observed that the thermal expansion coefficient, β_T, has the highest impact on the estimation of kh while gas density, ρ, the gas specific heat capacity, C_p, the pressure-pseudo pressure slope, B, and the TTA slope, a, rank after β_T in terms of importance. It can be observed from Equation. 4-20) that the fluid properties are all

lumped into 2 main terms, "ε" and "η^*". The impact of the uncertainty in these two properties has been investigated using the Monte-Carlo method.

The uncertainty in the value of the formation averaged adiabatic coefficient and Joule-Thomson coefficient was investigated by creating normal distributions with a standard deviation of 5% around the initial temperature and the average pressure (see Table 4-10 and a plot of the probability density function, Figure 4-25).

$$\mu_{\eta^*} = \eta^*(T_i, P_{avg}) \quad (4\text{-}31)$$

$$\sigma_{\eta^*} = 0.05\mu_{\eta^*} \quad (4\text{-}32)$$

$$\mu_{\varepsilon} = \varepsilon(T_i, P_{avg}) \quad (4\text{-}33)$$

$$\sigma_{\varepsilon} = 0.05\mu_{\varepsilon} \quad (4\text{-}34)$$

$$P_{avg} = \frac{P_i + P_s}{2} \quad (4\text{-}35)$$

Table 4-10. Normal distribution parameters for fluid thermal properties

	Drawdown 1	**Drawdown 2**
μ_{η^*}	1.1003×10^{-7}	1.1003×10^{-7}
σ_{η^*}	1.3754×10^{-8}	1.3709×10^{-8}
μ_{ε}	-2.6376×10^{-6}	-2.6448×10^{-6}
σ_{ε}	3.2970×10^{-7}	3.3060×10^{-7}
Sample size	5000	5000

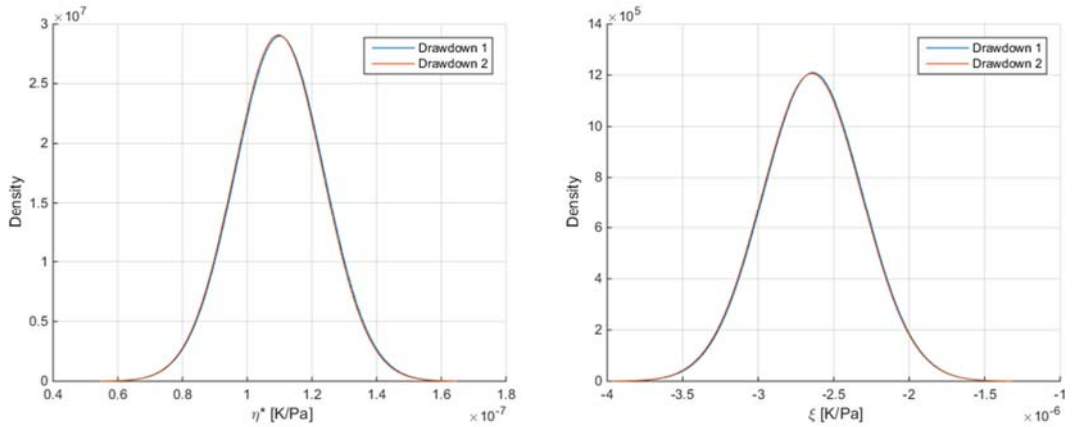

Figure 4-25 (a) Probability density of adiabatic expansion coefficient (b) Probability density of Joule-Thomson coefficient

Table 4-11: Distribution of kh estimate due to normal distribution in fluid thermal properties

	Drawdown 1	**Drawdown 2**
μ_{kh}	1.0538×10^{-11}	1.1806×10^{-11}
σ_{kh}	1.2689×10^{-12}	1.4045×10^{-12}
Sample size	5000	5000
kh (95% confidence)	0.8×10^{-11} to 1.3076×10^{-11}	0.8997×10^{-11} to 1.4615×10^{-11}

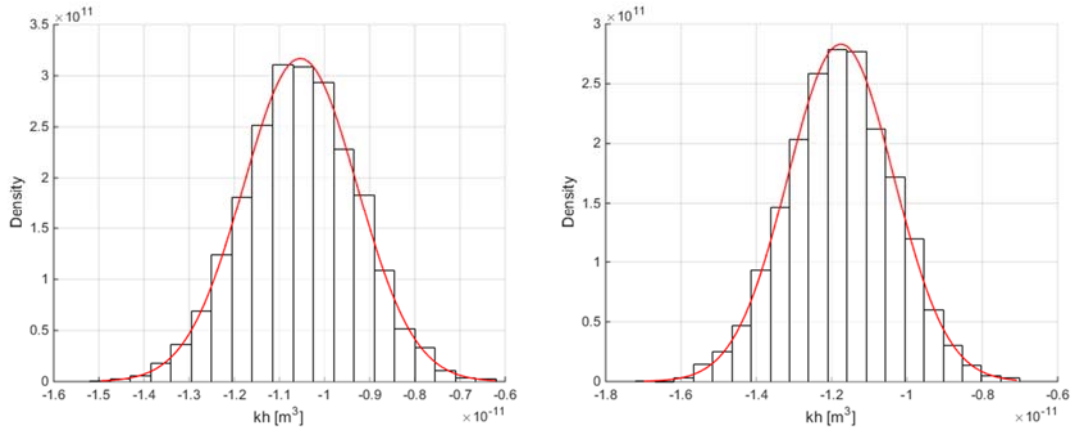

Figure 4-26 Distribution of kh estimate (a) Drawdown 1 (b) Drawdown 2

The probability density plot of kh obtained from the sampled values of η^* and ε is shown in Figure 4-26. A normal distribution function was also fitted to the results and the mean and standard deviation was estimated (Table 4-11). The standard deviation of the kh distribution is about 12% of the mean value, as opposed to the 5% standard deviation value for the input properties. This gives an indication of how much confidence can be placed on the estimated kh value and quantifies how less certain input data will lead to a much poorer estimation of the kh value.

4.12 Conclusion

This chapter has developed the mathematical background and a practical workflow for Temperature Transient Analysis in a vertical dry gas producing well. It is proven to:

- Be an effective alternative to the well-known Pressure Transient Analysis workflow in this type of well for determining the near-wellbore reservoir properties.

- Have the unique ability to identify the permeability and the depth of the near-wellbore formation damage.

This was achieved by:

1. Developing a (semi-log plot) linear form of the analytical solution transient sandface temperature in a vertical dry gas producing well. This linear analytical solution was subsequently incorporated in workflows for estimating the "permeability-thickness" of the producing layer, including determining the properties of a formation damage zone present in the near-wellbore region.

2. Verifying that a workflow based on Darcy flow can be confidently applied in many practical cases since the impact of non-Darcy effects on the slope of the transient temperature–time semi-log plot were minimal. The critical flow rate, above which the non-Darcy flow effects notably affect the temperature signal, is well and reservoir specific, but also depends on the (chosen) acceptable level of error.

3. Analysing the uncertainty in the results that is inherent in the workflow and the errors in the values of the input parameters.

4. Applying the developed workflow to both synthetically generated and field measured temperature data. The analysis of these data sets demonstrated the value of the proposed Temperature Transient Analysis workflow for estimating the properties of a gas producing layer when the flowrate is known or, alternatively, determining the flowrate when the properties of the producing reservoir are known.

4.13 Nomenclature

α: Defined in Equation 4-12 $[sec/m^2]$

β: Non-Darcy coefficient $[m^{-1}]$

β_T: Thermal expansion coefficient $[K^{-1}]$

γ: Euler-Mascheroni constant [ ]

δ: Deviation of analytical solution from logarithmic approximation [ ]

ε: Joule-Thomson coefficient $[K/Pa]$

η: Adiabatic coefficient $[K/Pa]$

η^*: Formation averaged adiabatic coefficient $[K/Pa]$

λ : Constant term [ ]

μ: Viscosity of fluid $[Pa.s]$

μ_{η^*}: Mean value of η^* $[K/Pa]$

μ_ε: Mean value of ε $[K/Pa]$

μ_{kh}: Mean value of kh $[m^3]$

ρ: Density of fluid $[kg/m^3]$

ρ_r: Density of rock $[kg/m^3]$

σ_{η^*}: Standard deviation of η^* $[K/Pa]$

σ_ε: Standard deviation of ε $[K/Pa]$

σ_{kh}: Standard deviation of kh $[m^3]$

ϕ: Porosity [ ]

ψ: Pseudo-pressure $[Pa^2/Pa.s]$

ψ_i: Pseudo-pressure at initial conditions $[Pa^2/Pa.s]$

Γ : Constant term $[Pa/K]$

c: Isothermal compressibility $[Pa^{-1}]$

d: Molar density $[mol/m^3]$

k: Permeability $[m^2]$

r: Radius $[m]$

r_{nD}: Ratio of non-Darcy pressure drop component to Darcy pressure drop component [ ]

r_T: Thermal radius of investigation $[m]$

t: Time $[s]$

t_j: Time at which transient temperature becomes linear $[s]$

v: Velocity $[m/s]$

A: Constant term in pressure pseudo-pressure relationship $[Pa]$

B: Coefficient in pressure pseudo-pressure relationship $[s]$

C: Ratio of gas heat capacity to averaged formation heat capacity.[ ]

C_p: Specific heat capacity of fluid $[J/kgK]$

C_{pr}: Specific heat capacity of rock $[J/kgK]$

C_t: Total formation volumetric heat capacity $[J/kgK]$

L_w: Length of well-reservoir contact $[m]$

P: Pressure $[Pa]$

Q_d: Dimensionless pressure [ ]

T: Temperature $[K]$

T_{nD}: Ratio of temperature change due to non-Darcy effect to temperature change due to Darcy effect [ ]

U_o : Velocity of convective heat transfer $[m^2/s]$

4.14 Subscripts

$crit$: Critical condition

d: Damage zone

i: Initial conditions

r: Rock

t: Time

sc: Surface conditions

$skin$: Damage region / skin region

T: Thermal

w: Well

wb: Wellbore

wf: Well flowing

Chapter 5: Analytical Solutions for Linear Flow

5.1 Introduction

The development of horizontal well technology is one of the most important developments in the Oil and Gas industry in the last 50 years. This development has made previously uneconomical resources viable and has also created added-value by increasing the rate of production and the oil and gas recovery (Pendleton 1991), reducing the payback period and increasing the NPV. Horizontal well technology has also introduced new challenges into fluid flow modelling, requiring new models to capture the flow in and around such wells. Models and analytical solutions for the analysis of pressure data have been developed and extensively used (Table 5-1), but this is not yet true for temperature modelling.

Many intelligent completions (i.e. with the completion that offer some degree of real-time, sandface monitoring and/or control) are installed in horizontal wells. Hence it is important to develop horizontal well TTA solutions to enable the full exploitation of the monitoring capabilities of these wells. However, there is currently only one analytical solution published for transient temperature in horizontal, oil wells (Muradov & Davies 2012a) and to the best of my knowledge there is no analytical or semi-analytical solutions for horizontal gas wells yet. This is because of the complexity of modelling transient temperature in horizontal wells due to the multiple flow regimes and the effect of anisotropy, coupled with the compressible nature of gas. Few attempts have been made to develop analytical TTA methods for horizontal wells aside from the work by Muradov & Davies (2012a) and Muradov & Davies (2013), with the work of others being based on numerical simulations, for example Bahrami & Siavoshi (2007).

The transient temperature is strongly dependent on pressure and its derivatives, hence its modelling always begins by deriving (or selecting, where available) an appropriate pressure solution for the flow regime in question. ‘Appropriate’ means a solution which is both sufficiently accurate while being mathematically simple so as to not overcomplicate the subsequent temperature model.

There are several, transient pressure solutions available for horizontal wells covering a range of flow and boundary conditions (Figure 5-1) that fall into this ‘appropriate’

category. Some of the existing pressure solutions, along with their boundary conditions, are listed in Table 5-1. They all represent a horizontal well either as a line sink or a planar sink (a.k.a. 'vertical fracture') in a horizontal, homogeneous reservoir.

Note that the 'vertical fracture' solutions can literally be immediately applied to the fractured wells.

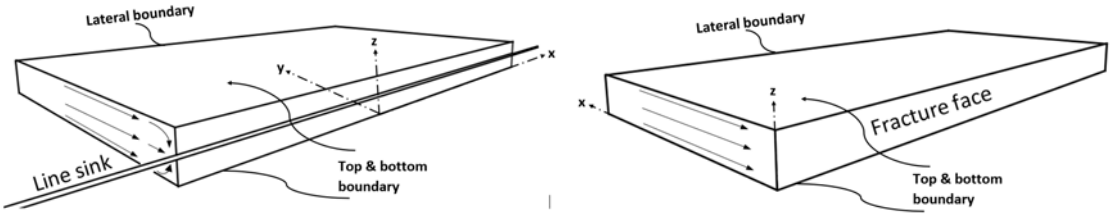

Figure 5-1: (a) Flow into a line sink. (b) Flow into a vertical fracture.

This work mostly uses the early time period semi-infinite acting pressure solutions, as these are sufficiently mathematically simple and investigate the near-wellbore formation, flow rate allocation and zonal monitoring of produced fluids of interest to TTA. The investigation of the reservoir boundaries, is most efficiently carried out using late-time pressure transient analysis (PTA) that would require a separate research if applied to TTA.

Table 5-1. Review of classical, transient pressure solutions for horizontal wells

Transient Pressure Solution	**Boundary Condition**		**Flow condition**	**Remarks**
	Top/Bottom	Lateral		
(Clonts & Ramey 1986)	No flow	Infinite acting	Constant rate, line sink	
(Odeh & Babu 1990)	No flow	Closed	Constant rate, line sink	
(Carslaw & Jaeger 1959)*	No flow	Infinite acting	Constant rate	Analogous solution from heat conduction theory
(Carslaw & Jaeger 1959)*	No flow	Constant pressure	Constant rate	Analogous solution from heat conduction theory

* This pressure solution is derived following the solution of heat conduction in solids solutions by Carslaw & Jaeger (1959)

5.2 Flow Regime Identification and TTA

Fluid flow in horizontal wells occur in different flow regimes, with each flow regime having different characteristics. This effect has been extensively discussed by Clonts & Ramey (1986), Goode (1987), Kuchuk et al. (1991), Odeh & Babu (1990) and Ozkan et al. (1987). The flow regimes (Figure 5-2) usually observed in a horizontal well are: the early time radial flow, the early time linear flow, the late pseudo-radial and the late linear (Odeh & Babu 1990).

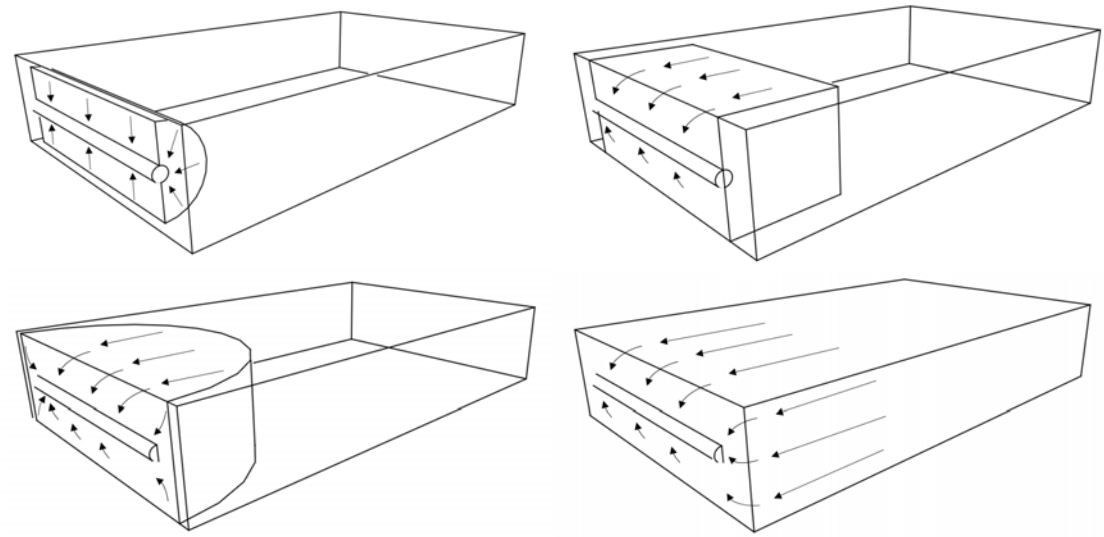

Figure 5-2: Horizontal well flow regimes (a) Early radial. (b) Early linear. (c) Late pseudo-radial. (d) Late linear

The early time radial flow occurs before the pressure wave (or disturbance) reaches the top, bottom and lateral boundaries of the reservoir. This flow regime is characterized by the change in pressure (ΔP) being a linear function of $log(t)$. This period begins at the start of production and ends at the time given by Equation 5-1. The pressure slope {i.e. its derivative to log(t)} during this period is a function of both the horizontal and vertical permeability (Odeh & Babu 1990). Therefore, this flow regime's pressure response in an anisotropic reservoir will therefore be different from an isotropic one. This fact is an important fact to be remembered later when carrying out TTA using temperature solutions derived assuming an isotropic reservoir.

$$t_{end} = min\left(\frac{0.0328L^2\phi\mu C_t}{k_y}, \frac{0.467\phi\mu C_t d_z^2}{k_z}\right) \qquad (5\text{-}1)$$

$$Where\, d_z = min(z_0, H - z_0) \qquad (5\text{-}2)$$

ϕ is the porosity of the formation, μ is the viscosity of the fluid, L is the length of the well, k_i is the permeability in the i direction ($i = x, y \; or \; z$), H is the thickness of the formation and z_0 is the vertical location of the well

The early time linear flow regime occurs shortly after the pressure wave has reached the top and bottom of the reservoir, but before it has reached the lateral boundaries. The change in pressure (ΔP) during this flow regime is a linear function of $\sqrt{t}$ and is independent of the vertical permeability of the reservoir. An anisotropic reservoir will thus have the same pressure response as an isotropic one. The start and end time of this flow regime is given by Equation 5-3 and Equation 5-4. There are situations where this flow regime does not exist, e.g. when $t_{start} \geq t_{end}$ (Odeh & Babu 1990).

$$t_{start} = \frac{0.467\phi\mu C_t D_z^2}{k_z} \qquad (5\text{-}3)$$

$$t_{end} = \frac{0.0422\phi\mu C_t L^2}{k_y} \qquad (5\text{-}4)$$

$$Where\, D_z = max(z_0, H - z_0) \qquad (5\text{-}5)$$

Ozkan et al. (1987) investigated the effect on the (very early) pressure response of the:

1. Wellbore radius. This can generally be neglected for TTA because the temperature transient's velocity is several orders of magnitude slower than that of the pressure wave. The early time pressure effect is thus virtually too fast to be noticeable by the temperature response.

2. Well location. This effect can be assessed using the dimensionless length defined by Equation 5-6.

$$L_D = \frac{L}{2H}\sqrt{\frac{k_z}{k}} \qquad (5\text{-}6)$$

The pressure response is insensitive to well location at the large values of L_D (i.e. >>1), as is the case for the majority of horizontal wells, where the line source pressure solution

approaches the vertical fracture pressure solution (Ozkan et al. 1987). This approximation works for transient pressure; but is not applicable to transient temperature as discussed in Section 5.6.

5.3 Governing Equations

The diffusivity equation is:

$$\frac{\partial}{\partial t}\Phi = D\nabla^2\Phi \qquad (5\text{-}7)$$

Where D is the diffusivity, and Φ is the dependent variable. It has been shown (Al-Hussainy et al. 1966) that the diffusivity equation for gas can be expressed using the gas pseudo-pressure equation (Equation 5-8).

$$\frac{\partial}{\partial t}\psi = \frac{k}{\phi\mu(P)c_g(P)}\nabla^2\psi \qquad (5\text{-}8)$$

Comparison of Equation 5-7 and Equation 5-8 provides Equation 5-9 for the diffusion coefficient D.

$$D = \frac{k}{\phi\mu(P)c_g(P)} \qquad (5\text{-}9)$$

This relationship makes it possible to apply existing solutions of the diffusivity equation for liquids to gas by using the gas pseudo-pressure (Equation 5-10).

$$\frac{\partial}{\partial t}\psi = D\nabla^2\psi \qquad (5\text{-}10)$$

The model for temperature change in porous media Equation 5-11 provided by Weibo Sui et al. (2008) is a combination of the temperature change due to transient fluid expansion (2nd term on Left hand side LHS), transient formation expansion (3rd term on LHS), heat convection (1st term on RHS), Joule-Thomson effect (2nd and 3rd terms on RHS) and conduction (4th term on RHS).

$$\overline{\rho C_P}\,\frac{\partial T}{\partial t} - \emptyset\beta T\frac{\partial P}{\partial t} - \emptyset C_f\left(P + \rho_r C_{Pr} T\right)\frac{\partial P}{\partial t} = -\rho \boldsymbol{v} C_P \cdot \nabla T + \beta T \boldsymbol{v} \cdot \nabla P - \boldsymbol{v} \cdot \nabla P + K\nabla^2 T \qquad (5\text{-}11)$$

Equation 5-11 can be rewritten with the transient temperature term on the LHS and all other terms are on the RHS. The transient temperature change is thus due to a combination of different effects (i.e. fluid expansion, Joule-Thomson effect, heat convection and conduction).

$$\overline{\rho C_P}\,\frac{\partial T}{\partial t} = \emptyset\beta T\frac{\partial P}{\partial t} + \emptyset C_f\left(P + \rho_r C_{Pr} T\right)\frac{\partial P}{\partial t} - \rho \boldsymbol{v} C_P \cdot \nabla T + \beta T \boldsymbol{v} \cdot \nabla P - \boldsymbol{v} \cdot \nabla P + K\nabla^2 T \qquad (5\text{-}12)$$

The solution of this equation is discussed in Section 5.4 along with the assumptions made.

All the terms are defined in Nomenclature.

5.3.1 Pressure Models and Solutions

Unlike the temperature solution being very sensitive to pressure, the pressure solution can generally be assumed independent of the temperature due to the reservoir temperature not changing strongly to sufficiently affect the fluid properties and therefore pressure in practical conditions. Hence a constant temperature can be reasonably assumed for the pressure solution when studying most of the oil and gas production tests. This allows the problem to be decoupled as shown in Chapter 3. Two pressure solutions of varying complexity and accuracy will be considered in this study: the 'planar' solution (for linear flow) and the 'line source' solution.

The planar pressure solution, which assumes linear flow to a fracture face {Figure 5-1(b)} was chosen for its simplicity. This allows deriving an analytical solution for temperature during the time period when the linear flow regime dominates the flow into a horizontal well. The effect of flow convergence to the wellbore wall is not included, resulting in errors when analysing the very early time (i.e. pre-linear flow regime) data.

The line source (or sink) solution, (Figure 5-1) assumes flow into a well of infinitesimal radius. This solution provides a better model of flow convergence into the wellbore. It will therefore be more accurate at early times, i.e. during the early radial flow regime. This solution has the advantage of accuracy, but makes the derivation of an analytical temperature solution non-trivial, requiring a numerical solution.

5.3.1.1 Planar Pressure Solution

The planar pressure solution used here is derived by taking a similar solution to that adopted by Muradov (2010) based on heat conduction solutions from Carslaw & Jaeger (1959).

Several solutions for temperature change T in a solid, finite slab of length *l* experiencing heat flow in x direction have been given by Carslaw & Jaeger (1959). Two of them presented below, were adopted to describe the change in pseudo-pressure of a gas in linear flow. Equation 5-13 is for the case with zero initial temperature disturbance (equivalent to the stabilised pressure case in the case of gas flow), constant flux F_o into the region at $x = l$. (Equivalent to producing gas at a constant mass flow rate), and $x = 0$ kept at zero temperature change {Equation. (6) Section 3.8 of (Carslaw & Jaeger 1959)} (which is equivalent to the reservoir pressure not changing at the drainage area boundary). Equation 5-14 is for the case with constant heat flux at x = 0, zero initial temperature and semi-infinite lateral boundaries {Section 2.9 of (Carslaw & Jaeger 1959)}.

$$T = \frac{2F_o(Dt)^{\frac{1}{2}}}{K}\sum_{n=0}^{\infty}(-1)^n\left[ierfc\left(\frac{2(n+1)l-x}{2(Dt)^{\frac{1}{2}}}\right) - ierfc\left(\frac{2(n+1)l+x}{2(Dt)^{\frac{1}{2}}}\right)\right] \qquad (5\text{-}13)$$

$$T = \frac{2F_o(Dt)^{\frac{1}{2}}}{K}ierfc\left(\frac{x}{2(Dt)^{\frac{1}{2}}}\right) \qquad (5\text{-}14)$$

Further consider the diffusivity equation for pseudo-pressure with a constant mass-flux inner boundary condition at $x = x_w$ to adopt the solutions Equation 5-13 and Equation 5-14 to the gas pressure case. The mass-flux is given by Equation 5-15:

$$\frac{\dot{m}}{A} = \boldsymbol{v}\rho \qquad (5\text{-}15)$$

or, assuming Darcy's law:

$$\frac{\dot{m}}{A} = \frac{\boldsymbol{k}}{RT} \cdot \frac{P}{\boldsymbol{\mu} Z} \nabla P \qquad (5\text{-}16)$$

For the linear flow case discussed here:

$$\nabla P = \frac{dP}{dx} \qquad (5\text{-}17)$$

Also, from the definition of pseudo-pressure by Al-Hussainy et al. (1966)

$$\psi = \int_{Pref}^{P} \left(\frac{2P}{\mu Z}\right) dp \qquad (5\text{-}18)$$

$$\frac{d\psi}{dP} = \frac{2P}{\mu Z} \qquad (5\text{-}19)$$

$$dP = \frac{\mu Z}{2P} d\psi \qquad (5\text{-}20)$$

Substituting Equation 5-17 & 5-20 into Equation 5-16 gives the mass-flux as a function of pseudo-pressure (Equation 5-21).

$$\frac{\dot{m}}{A} = \frac{\boldsymbol{k}}{2RT} \cdot \frac{d\psi}{dx} \qquad (5\text{-}21)$$

Equivalent to the heat flux Fo parameter in the original solutions by Carslaw & Jaeger (1959):

$$F_o = -K \frac{dT}{dx} \qquad (5\text{-}22)$$

Comparing Equation 5-21 with the Fourier's Law of conduction (Equation 5-22) it is evident that the mass flux $\frac{\dot{m}}{A}$ is mathematically analogous to the heat flux F_o, while $\frac{\boldsymbol{k}}{2RT}$ is analogous to the thermal conductivity K, and $\frac{d\psi}{dx}$ is analogous to the temperature gradient

$\frac{dT}{dx}$. Using this analogy and Equation 5-9 it is possible to rewrite $\frac{2F_o(Dt)^{\frac{1}{2}}}{K}$ as shown in Equation 5-23

$$\frac{2F_o(Dt)^{\frac{1}{2}}}{K} = \frac{2\left(\frac{\dot{m}}{A}\right)\left(\frac{kt}{\phi\mu c_g}\right)^{\frac{1}{2}}}{\left(\frac{k}{2RT}\right)} \tag{5-23}$$

$$\frac{2F_o(Dt)^{\frac{1}{2}}}{K} = \frac{4\dot{m}RT}{A}\sqrt{\frac{t}{\phi\mu k c_g}} \tag{5-24}$$

For the linear flow condition, the inflow area $A = HL_{well}$, hence:

$$\frac{2F_o(Dt)^{\frac{1}{2}}}{K} = \frac{4\dot{m}RT}{HL_{well}}\sqrt{\frac{t}{\phi\mu k c_g}} \tag{5-25}$$

In a similar manner $(Dt)^{\frac{1}{2}}$ can be rewritten by substituting Equation 5-9

$$(Dt)^{\frac{1}{2}} = \sqrt{\frac{kt}{\phi\mu c_g}} \tag{5-26}$$

The pseudo-pressure solution is obtained for the linear gas flow at the constant pressure boundary condition in the finite drainage area (Equation 5-27), as well as for the infinite reservoir (Equation 5-28) by substituting Equation 5-25 and Equation 5-26 into Equation 5-13 and Equation 5-14 and then changing the coordinates of Equation 5-13 such that the constant flow boundary is at $x = 0$ and the constant pressure boundary is at $x = l$.

$$\psi_i - \psi(x,t) = \frac{4\dot{m}RT}{HL_{well}}\sqrt{\frac{t}{\phi\mu k c_g}}\sum_{n=0}^{\infty}(-1)^n\left\{ierfc\frac{2nl+x}{2}\sqrt{\frac{\phi\mu c_g}{kt}}\right\} - \frac{4\dot{m}RT}{HL_{well}}\sqrt{\frac{t}{\phi\mu k c_g}}\sum_{n=0}^{\infty}(-1)^n\left\{ierfc\frac{2(n+1)l-x}{2}\sqrt{\frac{\phi\mu c_g}{kt}}\right\} \tag{5.27}$$

$$\psi_i - \psi(x,t) = \frac{4\dot{m}RT}{HL_{well}}\sqrt{\frac{t}{\phi\mu k c_g}}ierfc\left(\frac{x}{2}\sqrt{\frac{\phi\mu c_g}{kt}}\right) \tag{5-28}$$

Equation 5-27 was derived for the case with constant pressure at the lateral boundary case and Equation 5-28 for an infinite lateral boundary.

Finally, the pseudo-pressure ψ in Equation 5-27 and Equation 5-28 can be converted to pressure using the Equation 5-29 relationship where A and B are gas specific as shown in Chapter 3. This seemingly simplified linear approximation, has been proven to be both accurate and practical for gas wells with detailed workflows and case studies presented in Chapters 3 and 4.

$$P = A + B\psi \qquad (5\text{-}29)$$

5.3.1.2 Line Source Pressure Solution for Anisotropic Media

Linear flow is one of several flow regimes taking place around horizontal wells. The early radial and early linear flow regimes are sufficiently well captured by the line source pressure solution (Odeh & Babu, 1990; Clonts & Ramey, 1986; Goode, 1987 and Ozkan et al., 1987). These solutions can be used at early times instead of the planar pressure solution. A summary of some of some existing solutions is presented in Table 5-2.

Table 5-2. Line source pressure solutions for horizontal wells

	Solution	**Boundary condition**
1	(Odeh & Babu 1990)	Closed lateral boundary
2	(Clonts & Ramey 1986)	Infinite lateral boundary

The early radial and linear flow regime pressure solution by Clonts & Ramey (1986) was chosen due to its simplicity.

$$s(x,t) = \frac{1}{2}\left[erf\left(\frac{\frac{x_f}{2}+(x-x_w)}{2\sqrt{\eta_x t}}\right) + erf\left(\frac{\frac{x_f}{2}-(x-x_w)}{2\sqrt{\eta_x t}}\right)\right] \qquad (5\text{-}30)$$

$$s(y,t) = \frac{exp\left(-\frac{(y-y_w)^2}{4\eta_y t}\right)}{2\sqrt{\pi\eta_y t}} \qquad (5\text{-}31)$$

$$s(z,t) = \frac{1}{H}\left[1 + 2\sum_{n=1}^{\infty} exp\left(-\frac{n^2\pi^2\eta_z t}{H^2}\right) cosn\pi\frac{z_w}{H} cosn\pi\frac{z}{H}\right] \quad (5\text{-}32)$$

$$\psi_i - \psi = A1\int_0^t s(x,t)s(y,t)s(z,t)\,d\tau \quad (5\text{-}33)$$

Where

$$A1 = \frac{\dot{m}RT}{4\pi L\sqrt{k_x k_z}} \quad (5\text{-}34)$$

The pseudo-pressure line source solution, Equation 5-33 can be converted to pressure in a similar manner as that used for Equation 5-14. The solution of Equation 5-34 can be obtained numerically by, for example, using quadrature rules by Gander & Gautschi (2000).

5.4 Temperature Solution

5.4.1 Simplification of the Thermal Model

The thermal model Equation 5-12 includes the effects of heat conduction and convection, fluid expansion and Joule-Thomson heating or cooling. The following several reasonable assumptions were made at this stage to simplify the thermal model, in order to find its solution:

1. *Fluid flow is linear*. The applicability limits of this assumption are investigated later by considering the flow convergence effect.

2. *Pseudo-pressure relationship to pressure can be approximated using a linear relationship.* This has been shown in Chapters 3 and 4 to be reasonably accurate for a given range of pressure change.

3. *The effects of heat conduction can be ignored at the early-time period.* This was justified in Section 5.5.

4. *Effect of fluid expansion and Joule-Thomson (gas) cooling can be separated.* It is shown in this section (Section 5.4.1) that the former dominates the temperature signal at the very early time period, whereas the latter is the major effect at later time.

5. *The pressure drop in the wellbore can be ignored.* The typical, conventional wellbore has a very high conductivity compared to the reservoir, with the heel-to-toe effect being lower-order of magnitude during transient processes. This chapter deals with such cases.

6. *Darcy flow is assumed.* The flow of gas at high velocities is better modelled by the Forchheimer equation which captures the non-Darcy inertial flow behaviour. However, Darcy flow is assumed for the derivations because (1) it makes the derivation possible and, more importantly (2) the flow velocity of the gas is generally lower compared to a vertical well due to the greater wellbore reservoir contact in a horizontal well.

These assumptions reduce the problem to a simpler, linear problem which can be solved by separating the expansion effect from the others followed by solving them separately.

The analytical solution for transient sandface temperature in liquid producing horizontal wells was developed by Muradov (2010) and Muradov & Davies (2012a). They confirmed during their derivation of this solution that the major cause of the temperature change at early time is the (transient) fluid expansion. This expansion-dominated period is observed for a relatively short period of time, followed by the major cause of the temperature change due to the Joule-Thomson effect. However, as will be observed, the duration of the expansion-dominated period is relatively longer in a horizontal gas well where it continues to play an important role as long as the flow remains in the infinite acting regime (i.e. before the pressure signal reaches the lateral, constant pressure reservoir boundaries).

Table 5-3: Case study description for investigation of different effects in a thermal model

Property	**Symbol**	**Value**	**Unit**
Thermal conductivity	K_T	3.338	W/mK
Porosity	ϕ	0.15	
Specific heat capacity of gas	Cp_f	2967	J/kgK
Specific gas constant	R	519.66	J/kgK
Specific heat capacity of rock	Cp_r	920	J/kgK
Density of rock	ρ_r	2500	kg/m^3
Specific gravity of gas	$S.G_f$	0.605	
Pseudo-pressure at initial reservoir pressure	ψ_i	16×10^{18}	$Pa^2/Pa.s$
Viscosity at initial reservoir pressure	μ_i	1.467×10^{-5}	$Pa.s$
Total formation compressibility at initial condition	Cf_i	7×10^{-8}	Pa^{-1}
Gas mass flow rate	$\dot{m}$	23.28	kg/s
Pressure at standard conditions	P_{sc}	101325	Pa
Temperature at standard conditions	T_{sc}	289	K
Initial reservoir pressure	P_i	1.4×10^7	Pa
Initial reservoir temperature	T_i	322	K
Reservoir permeability	k	10×10^{-15}	m^2
Reservoir thickness	h	2	m
Fracture face	x_f	1.0×10^{-7}	m
Reservoir lateral boundary	x_e	50	m
Thermal expansivity of gas	β_T	0.0048995	K^{-1}
Well length	L_w	1000	m

Table 5-3 lists the properties of a synthetic, numerical, non-isothermal model of fluid flow into a horizontal well from a homogenous reservoir. The simulation was done in OpenFOAM. These properties were selected for the study of the early linear and late linear flow regimes. The early radial and late pseudo-radial will not be studied because this model is for flow into a vertical fracture, where these effects are either not observed (the former one) or are observed at a relatively later time (the latter one).

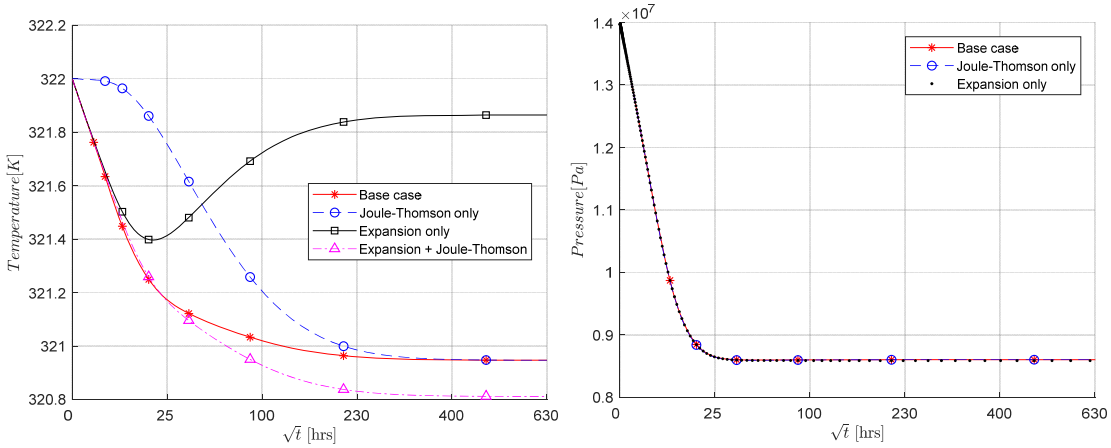

Figure 5-3: (a) Effect of different physics on the wellbore temperature. (b) Effect of different physics on the wellbore pressure.

Figure 5-3 plots the wellbore temperature and pressure response resulting from the effect of fluid expansion and Joule-Thomson. The cases are:

1. The base case or "full physics" model with all effects modelled.

2. Only fluid expansion is modelled (obtained by setting the Joule-Thomson term in Equation 5-12 to zero).

3. The Joule-Thomson effect is modelled together with heat convection and conduction (while setting the expansion term in Equation 5-12 to zero).

4. The combined temperature change obtained by summing cases 2 and 3.

Figure 5-3 (b) shows the plots of pressure for the first three cases confirming that the pressure response is essentially independent of temperature due to the latter changing only within a few degrees Kelvin. The temperature plots {Figure 5-3(a)} show that the

combined effects of Joule-Thomson and adiabatic fluid expansion (case 4) matches the base case accurately for the early time period t< 25 hours (which is the time before the pressure signal reached the lateral boundary).

The solution method employed here is similar to that used by Muradov & Davies (2012a). The different temperature change effects are separated by assuming that the dominant effect at early time is due to fluid expansion, and at later times due to the Joule-Thomson effect. Their solution approach has been modified to solve the models for fluid expansion and for Joule-Thomson separately over the entire time period considered. The results of the two solutions are then combined. Mathematically speaking these two solutions are not strictly complementary, but they can be combined to give a reasonable solution applicable to the whole time period being considered since they dominate at different times.

The thermal model (Equation 5-12) can be reduced to Equation 5-35 when conduction in the direction of flow is neglected. Heat transfer between the formation and the surroundings is included as term 5 on the RHS of Equation 5-35.

$$\overline{\rho C_P}\,\frac{\partial T}{\partial t} = \emptyset\beta T\frac{\partial P}{\partial t} - \rho \boldsymbol{v} C_P \cdot \nabla T + \beta T \boldsymbol{v} \cdot \nabla P - \boldsymbol{v} \cdot \nabla P + \frac{2U}{H}(T - T_i) \quad (5\text{-}35)$$

Equation 5-35 can be split into two as Equation 5-36: (the temperature change due to the transient fluid expansion) and Equation 5-37 (the temperature change due to the Joule-Thomson effect, convection and conduction between the formation and the surroundings).

$$\overline{\rho C_P}\,\frac{\partial T}{\partial t}_{Exp} = \emptyset\beta T\frac{\partial P}{\partial t} \quad (5\text{-}36)$$

$$\overline{\rho C_P}\,\frac{\partial T}{\partial t}_{JT} = -\rho \boldsymbol{v} C_P \cdot \nabla T + \beta T \boldsymbol{v} \cdot \nabla P - \boldsymbol{v} \cdot \nabla P + \frac{2U}{H}(T - T_i) \quad (5\text{-}37)$$

The final sandface temperature (Equation 5-38) is a combination of these solutions where ΔT_{exp} is derived from the solution of Equation. 5-36) and ΔT_{JT} from the solution of Equation 5-37.

$$T_{wb}(t) = T_i - \Delta T_{exp} - \Delta T_{JT} \quad (5\text{-}38)$$

5.4.2 Planar Flow Solution for Expansion-Dominated Temperature Change

The change in temperature due to the expansion effect, i.e. Equation 5-36 is solved by integration to yield (Equation 5-39):

$$(T - T_i)_{Exp} = -\frac{\emptyset\beta T}{\overline{\rho C_P}}(P_i - P) \qquad (5\text{-}39)$$

5.4.3 Planar Flow Solution for Temperature Change Due to Joule-Thomson, Convection and Heat Conduction to Surroundings

Equation 5-37 is a first order quasilinear PDE. Its solution uses the method of characteristics.

First rewrite Equation 5-37 as shown in Equation 5-40

$$\frac{\partial T}{\partial t}_{JT} = -\frac{\rho \boldsymbol{v} C_P}{\overline{\rho C_P}} \cdot \nabla T + \frac{\beta T \boldsymbol{v}\cdot\nabla P - \boldsymbol{v}\cdot\nabla P}{\overline{\rho C_P}} + \frac{2U}{\overline{\rho C_P} H}(T - T_i) \qquad (5\text{-}40)$$

The velocity and the pressure and temperature gradients can be expressed as shown below.

$$\boldsymbol{v} = -\frac{\boldsymbol{k}}{\mu}\frac{\partial P}{\partial x} \qquad (5\text{-}41)$$

$$\nabla P = \frac{\partial P}{\partial x} \qquad (5\text{-}42)$$

$$\nabla T = \frac{\partial T}{\partial x} \qquad (5\text{-}43)$$

Equation 5-44 is obtained by substituting Equation 5-41, Equation 5-42 and Equation 5-43 into Equation 5-40,

$$\frac{\partial T}{\partial t}_{JT} = \frac{\rho C_P \boldsymbol{k}}{\mu \overline{\rho C_P}}\frac{\partial P}{\partial x}\cdot\frac{\partial T}{\partial x} - \frac{(\beta T - \mathbf{1})}{\overline{\rho C_P}}\frac{\boldsymbol{k}}{\mu}\left(\frac{\partial P}{\partial x}\right)^2 + \frac{2U}{\overline{\rho C_P} H}(T - T_i) \qquad (5\text{-}44)$$

Equation 5-44 can be expressed as Equation 5-45.

$$\frac{\partial T}{\partial t}_{JT} - \frac{\rho C_P \boldsymbol{k}}{\mu \overline{\rho C_P}} \frac{\partial P}{\partial x} \cdot \frac{\partial T}{\partial x} = - \frac{(\beta T - \mathbf{1})}{\overline{\rho C_P}} \frac{\boldsymbol{k}}{\mu} \left(\frac{\partial P}{\partial x}\right)^2 + \frac{2U}{\overline{\rho C_P} H} (T - T_i) \qquad (5\text{-}45)$$

K1, K2, K3 and K4 are defined as:

$$K1 = \overline{\rho C_P} = \phi \rho C_p + (1 - \phi) \rho_r C_{pr} \qquad (5\text{-}46)$$

$$K2 = \frac{\rho C_p k}{\mu} \qquad (5\text{-}47)$$

$$K3 = \frac{(\beta T - 1) k}{\mu} \qquad (5\text{-}48)$$

$$K4 = \frac{2U}{H} \qquad (5\text{-}49)$$

Equation 5-45 can be expressed as Equation 5-50.

$$\frac{\partial T}{\partial t}_{JT} - \frac{K2}{K1} \frac{\partial P}{\partial x} \cdot \frac{\partial T}{\partial x} = - \frac{K3}{K1} \left(\frac{\partial P}{\partial x}\right)^2 + \frac{K4}{K1} (T - T_i) \qquad (5\text{-}50)$$

U is the overall heat transfer coefficient between the formation and the surroundings (i.e. overburden and underburden). The parameters K1 & K3 depend on the gas and reservoir properties, but their values are relatively unchanged for the typical pressure and temperature changes observed at typical production conditions (for proof see Chapter 3)., They can be assumed constant for the purpose of this paper, but U was shown to vary with time (Zolotukhin 1979), but over very long time periods in the order of months or years. The value of U and consequently K4 can be assumed constant, for most production cases at early time periods in the order of hours or a few days. Finally, assume the parameter K2 to be constant when its value is calculated at the average fluid properties (see Chapter 3).

This makes it possible to apply the method of characteristics to Equation 5-50; let $t = t(\tau)$ and $x = x(\tau)$

$$\frac{\partial t}{\partial \tau} = 1 \qquad (5\text{-}51)$$

$$\frac{\partial x}{\partial \tau} = -\frac{K2}{K1}\frac{\partial P}{\partial x} \qquad (5\text{-}52)$$

Equation 5-50 can be written in the form below.

$$\frac{\partial T}{\partial t}\frac{\partial t}{\partial \tau} + \frac{\partial T}{\partial r}\frac{\partial r}{\partial \tau} = \frac{\partial T}{\partial \tau} = -\frac{K3}{K1}\left(\frac{\partial P}{\partial x}\right)^2 + \frac{K4}{K1}(T - T_i) \qquad (5\text{-}53)$$

Solving Equation 5-53 along the charactersitics obtained from Equation 5-51 and Equation 5-52 gives the transient temperature solution. This solution depends on the pressure solutions used to obtain the pressure gradient in these equations.This is discussed in Section 5.3.1.

If the effect of conduction to the surroundings is assumed negligible (as was shown in Chapter 3), it is possible to find solutions for the transient sandface temperature using a modified form of Equation 5-53 given in Equation 5-54

$$\frac{\partial T}{\partial t}\frac{\partial t}{\partial \tau} + \frac{\partial T}{\partial r}\frac{\partial r}{\partial \tau} = \frac{\partial T}{\partial \tau} = -\frac{K3}{K1}\left(\frac{\partial P}{\partial x}\right)^2 \qquad (5\text{-}54)$$

Substitute Equation 5-51 and Equation 5-52 into Equation 5-54

$$\frac{\partial T}{\partial \tau} = \frac{K3}{K2}\frac{\partial P}{\partial \tau} \qquad (5\text{-}55)$$

$$\frac{K3}{K2} = \frac{(\beta T - 1)}{\rho C_p} = -\varepsilon \qquad (5\text{-}56)$$

$$\frac{\partial T}{\partial \tau_{JT}} = -\varepsilon\frac{\partial P}{\partial \tau} \qquad (5\text{-}57)$$

$$\left(T_{wb}(t) - T_i(t)\right)_{JT} = -\varepsilon\left[P_{(x=s)} - P_{wf}(t)\right] \qquad (5\text{-}58)$$

The solution of Equation 5-58 requires solving for the pressure along the characteristics $P_{(x=s)}$ (Equation 5-51 and 5-52). The characteristic pressure solution in this study refers to the two boundary conditions investigated in Sections 5.3:

1. Semi-infinite lateral boundary and

2. Constant pressure lateral boundary

Solution for Semi-Infinite Lateral Boundary; No Heat Conduction

Solution of Equation 5-58 obtained using the pressure solution for the semi-infinite boundary condition (Equation. 5-28) can first be obtained by numerically solving it for the characteristics (Equation 5-51 and Equation 5-52). The temperature solution can be obtained by solving the system of ODEs (Equation 5-51, Equation 5-52 & Equation 5-53) using an ODE solver (e.g fourth order Runge-Kutta, implemented as ODE45 in Matlab), or by substituting the solution of Equation 5-51 into Equation 5-52 and solving the resulting ODE to determine the characteristic curve at a given value of x (in this case $x \approx 0$, i.e. at the fracture face). This can be done by iteratively solving the resulting ODE for s at different values of t, by using Newton-Raphson for the iteration, and the fourth order Runge-Kutta method for the solution of the ODE.

First Approach: Numerical

This involves solving the system of 3 ODEs (Equation 5-51, Equation 5-52 & Equation 5-53) using fourth order Runge-Kutta (implemented in Matlab as ODE45). The system of 3 ODEs can be reduced to a system of 2 ODEs by solving Equation 5-51 using the initial conditions $t(0) = 0$ and $x(0) = s$. The solution of Equation 5-51 is given by Equation 5-59

$$t = \tau \qquad (5\text{-}59)$$

Therefore Equation 5-52 and Equation 5-53 can be expressed as shown in Equation 5-60 and Equation 5-61 by neglecting the effect of heat conduction with the surroundings.

$$\frac{\partial X}{\partial \tau} = -\frac{K2}{K1}\frac{\partial P}{\partial x} \quad (5\text{-}60)$$

$$\frac{\partial T}{\partial \tau} = -\frac{K3}{K1}\left(\frac{\partial P}{\partial x}\right)^2 \quad (5\text{-}61)$$

Or alternatively as Equation 5-62 and Equation 5-63; if the solution of Equation 5-51 i.e. Equation 5-59, is substituted into Equation 5-60 and Equation 5-61

$$\frac{\partial X}{\partial t} = -\frac{K2}{K1}\frac{\partial P}{\partial x} \quad (5\text{-}62)$$

$$\frac{\partial T}{\partial t} = -\frac{K3}{K1}\left(\frac{\partial P}{\partial x}\right)^2 \quad (5\text{-}63)$$

Let

$$\frac{\partial X}{\partial t} = f(t, x, T) = -\frac{K2}{K1}\frac{\partial P}{\partial x} \quad (5\text{-}64)$$

$$\frac{\partial T}{\partial t} = g(t, x, T) = -\frac{K3}{K1}\left(\frac{\partial P}{\partial x}\right)^2 \quad (5\text{-}65)$$

With initial conditions

$$f(0) = x_0 \quad (5\text{-}66)$$

$$g(0) = T_i \quad (5\text{-}67)$$

The equations above can be written as a matrix

$$w(t) = \begin{bmatrix} x \\ T \end{bmatrix} \quad (5\text{-}68)$$

$$G(t, w) = \begin{bmatrix} f(t, w_1, w_2) \\ g(t, w_1, w_2) \end{bmatrix} \quad (5\text{-}69)$$

$$w(0) = \begin{bmatrix} x_0 \\ T_i \end{bmatrix} \qquad (5\text{-}70)$$

This system of equations (Equation 5-69) with initial conditions (Equation 5-70) can be solved using an appropriate ODE solver, for example, by using Matlab's ODE45, which is based on an explicit Runge-Kutta (4,5) formula (Shampine & Reichelt 1997). The pressure gradient is obtained from the appropriate analytical pressure solution.

Second Approach: Approximate Analytical

The pressure gradient equation (Equation 5-71) derived from the planar pressure solution with semi-infinite lateral boundary is substituted into Equation 5-52 to obtain Equation 5-72.

$$\frac{\partial P}{\partial x} = \frac{B4\dot{m}RT}{HkL_{well}} erfc\left(\frac{x}{2}\sqrt{\frac{\phi\mu c_g}{kt}}\right) \qquad (5\text{-}71)$$

$$\frac{\partial x}{\partial \tau} = -\frac{K2}{K1}\frac{B4\dot{m}RT}{HkL_{well}} erfc\left(\frac{x}{2}\sqrt{\frac{\phi\mu c_g}{kt}}\right) \qquad (5\text{-}72)$$

Substituting Equation 5-59 into Equation 5-72 above gives Equation 5-73 below.

$$\frac{\partial x}{\partial \tau} = -\frac{K2}{K1}\frac{B4\dot{m}RT}{HkL_{well}} erfc\left(\frac{x}{2}\sqrt{\frac{\phi\mu c_g}{k\tau}}\right) \qquad (5\text{-}73)$$

Equation 5-74 is derived by substituting the initial conditions $t(0) = 0$ and $x(0) = s$ into Equation 5-73

$$\frac{\partial x}{\partial \tau} = -\frac{K2}{K1}\frac{B4\dot{m}RT}{HkL_{well}} erfc\left(\frac{s}{2}\sqrt{\frac{\phi\mu c_g}{k\tau}}\right) \qquad (5\text{-}74)$$

This ODE (Equation 5-74) is solved iteratively to minimize the error between s and any given value of x (where $x \approx 0$ for the sandface temperature solution) at time t. This gives

a characteristic curve $s = f(x,t)$. This curve was observed to be linear (i.e. $s = x + at$) for small values of x (i.e. $x \approx 0$)

The following steps to obtain the characteristic curve were followed:

1. Select a value of x

2. For each point in time carry out the following steps:

    a. Assume an initial value of s.

    b. Solve the ODE (Equation 5-74) for x.

    c. Find the residual of x {this is the difference between the value of x obtained from step 2.a and the selected value of x in step. 1}

    d. Return to step 2.a if the residual is greater than the threshold, else return the value of s and proceed to the next point in time.

The numerical solution of this characteristic curve for very small values of x, i.e. $x \cong 0$ can be approximated by the analytical Equation 5-75

$$s = x + at \qquad (5\text{-}75)$$

This approximation may be validated by finding the limit of $\lim_{x\to 0}\left(\frac{\partial X}{\partial \tau}\right)$ from the planar pressure solution with a semi-infinite lateral boundary (Equation 5-28).

$$\lim_{x\to 0}\left(\frac{\partial x}{\partial \tau}\right) = -\frac{K2}{K1}\frac{B4\dot{m}RT}{HkL_{well}} = \Omega \qquad (5\text{-}76)$$

At the fracture face where x is sufficiently close to zero, , the derivative is:

$$\frac{\partial x}{\partial \tau} = \Omega \qquad (5\text{-}77)$$

$$x = \Omega\tau + C(s) \qquad (5\text{-}78)$$

Where $C(s)$ is a constant term, which is a function of the variable s.

Using initial conditions $t(0) = 0$ and $x(0) = s$ the solution of the characteristics (Equation 5-51 and Equation 5-77) are given in Equation 5-79 and Equation 5-80 below.

$$t = \tau \qquad (5\text{-}79)$$

$$x = \Omega\tau + s \qquad (5\text{-}80)$$

The change in temperature $[(T_{wb}(t) - T_i(t))_{JT}]$ is obtained from Equation 5-58. Figure 5-4, a plot of Equation 5-80 shows the linear nature of the characteristic curve $s = f(x \approx 0, t)$. The Table 5-4) case differs from the Table 5-3) one by the greater distance to the lateral boundary which allows the flow in the infinite acting region to continue for a longer time, the formation thickness is also greater in this case. All other parameters are the same as in Table 5-3).

Table 5-4: Case study parameters for the linear case with semi-infinite lateral boundary that differ from Table 5-3) values.

Property	**Symbol**	**Value**	**Unit**
Reservoir thickness	h	10	m
Reservoir lateral boundary	x_e	500	m
A		6.1805×10^6	Pa
B		4.9012×10^{-13}	s

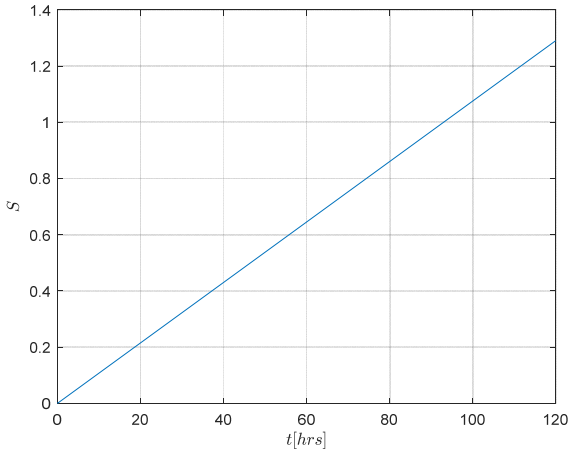

Figure 5-4: (a) Plot of characteristics showing the linear approximation for $x \cong 0$ the data used was from the case study defined in Table 5-3 and Table 5-4

Solution for Constant Pressure Lateral Boundary; No Heat Conduction

Alternatively, the solution of Equation 5-58 can be found by using the pressure gradient solution with constant pressure at the reservoir boundaries (Equation 5-82, the derivative of Equation 5-27 w.r.t x). The characteristics may also be obtained numerically or, as above, approximated by the linear approximation Equation 5-80.

$$\frac{\partial \psi}{\partial x} = \frac{2\dot{m}RT}{kHL_{well}}\left[\sum_{n=0}^{\infty}(-1)^n\left\{erfc\frac{2nl+x}{2}\sqrt{\frac{\phi\mu c_g}{kt}}\right\} + \sum_{n=0}^{\infty}(-1)^n\left\{erfc\frac{2(n+1)l-x}{2}\sqrt{\frac{\phi\mu c_g}{kt}}\right\}\right] \quad (5\text{-}81)$$

$$\frac{\partial P}{\partial x} = \frac{2B\dot{m}RT}{kHL_{well}}\left[\sum_{n=0}^{\infty}(-1)^n\left\{erfc\frac{2nl+x}{2}\sqrt{\frac{\phi\mu c_g}{kt}}\right\} + \sum_{n=0}^{\infty}(-1)^n\left\{erfc\frac{2(n+1)l-x}{2}\sqrt{\frac{\phi\mu c_g}{kt}}\right\}\right] \quad (5\text{-}82)$$

5.4.4 Complete Solution of Transient Temperature for Planar Flow

The complete solution (i.e. the wellbore temperature) is the combination of the temperature change due to Joule-Thomson, convection and Expansion effects Equation 5-83.

$$T_{wb}(t) = T_i - \Delta T_{exp} - \Delta T_{JT} \quad (5\text{-}83)$$

$$\Delta T_{JT} = (T_{wb}(t) - T_i)_{JT} = -\varepsilon\left[P_{(x=s)} - P_{wf}(t)\right] \quad (5\text{-}84)$$

$$\Delta T_{exp} = (T_{wb}(t) - T_i)_{Exp} = -\frac{\emptyset\beta T}{\overline{\rho C_p}}\left(P_i - P_{wf}(t)\right) \quad (5\text{-}85)$$

Where ε is the Joule-Thomson coefficient, $P_{wf}(t)$ is the well bottomhole flowing pressure, $P_{(x=s)}$ is the presssure at the characteristic $x = s$, P_i is the initial pressure

The transient sandface presure is obtained from Equation 5-29 $\{ P = A + B\psi \}$ and as for the value of ψ, the transient pseudo-pressure, this can be obtained for the semi-infiinite case (Equation 5-28) or the case with constant pressure at the lateral boundaries (Equation 5-27).

5.4.4.1 Complete Solution of Transient Temperature for Planar Flow With Semi-Infinite Lateral Boundary

For the semi-infinite lateral boundary case, the transient pressure solution (Equation 5-86) is obtained

$$P_{wf}(t) = A + B\left[\psi_i - \frac{4\dot{m}RT}{HL_{well}}\sqrt{\frac{t}{\phi\mu kc_g}}ierfc\left(\frac{x}{2}\sqrt{\frac{\phi\mu c_g}{kt}}\right)\right] \quad (5\text{-}86)$$

For the pressure at the characteristics $s = x - \Omega\tau$

$$P_{(x=s)} = A + B\left[\psi_i - \frac{4\dot{m}RT}{HL_{well}}\sqrt{\frac{t}{\phi\mu kc_g}}ierfc\left(\frac{(x-\Omega\tau)}{2}\sqrt{\frac{\phi\mu c_g}{kt}}\right)\right] \quad (5\text{-}87)$$

$$P_i = A + B\psi_i \quad (5\text{-}88)$$

$$\Delta T_{exp} = -\frac{\emptyset\beta T}{\overline{\rho C_p}}\left[\frac{B4\dot{m}RT}{HL_{well}}\sqrt{\frac{t}{\phi\mu kc_g}}ierfc\left(\frac{x}{2}\sqrt{\frac{\phi\mu c_g}{kt}}\right)\right] \quad (5\text{-}89)$$

$$\Delta T_{JT} = -\varepsilon \frac{B4\dot{m}RT}{HL_{well}} \sqrt{\frac{t}{\phi\mu kc_g}} \left[ierfc\left(\frac{x}{2}\sqrt{\frac{\phi\mu c_g}{kt}}\right) - ierfc\left(\frac{(x-\Omega\tau)}{2}\sqrt{\frac{\phi\mu c_g}{kt}}\right)\right] \quad (5\text{-}90)$$

Figure 5-5 is the complete temperature solution, obtained from Equation 5-83, 5-89, and 5-80. The plot also shows the Joule-Thomson and expansion effect-domintaed solutions, as well as the complete analytical solution as a sum of these two. There is a relatively good match between the analytical solution and the full numerical solution. This solution applies to the early time period before the pressure signal reaches the reservoir's lateral boundaries.

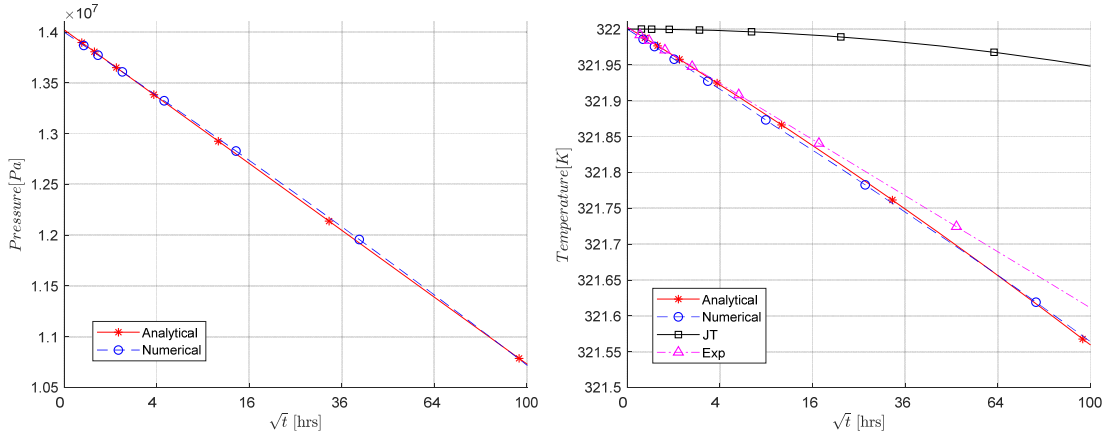

Figure 5-5: Plots based on the Table 5-4 parameters case (a) The transient pressure for analytical and numerical solutions (b) The different temprature solutions compared

5.4.4.2 Complete Solution of Transient Temperature for Planar Flow With Constant Pressure Lateral Boundary

The temperature solution for the constant pressure lateral boundary case can be obtained in a similar manner to that described in Section 5.4.4.1. The pseudo-pressure solution can be obtained from Equation 5-27, and then substituted into the pressure-pseudo pressure relationship (Equation 5-29) for the well flowing pressure (Equation. 5-91) and the pressure at the characteristics (Equation. 5-92).

$$P_{wf}(t) = A + B\left[\psi_i - \left(\frac{4\dot{m}RT}{HL_{well}}\sqrt{\frac{t}{\phi\mu kc_g}}\sum_{n=0}^{\infty}(-1)^n\left\{ierfc\,\frac{2nl+x}{2}\sqrt{\frac{\phi\mu c_g}{kt}}\right\} - \right.\right.$$

$$\left.\left.\frac{4\dot{m}RT}{HL_{well}}\sqrt{\frac{t}{\phi\mu kc_g}}\sum_{n=0}^{\infty}(-1)^n\left\{ierfc\,\frac{2(n+1)l-x}{2}\sqrt{\frac{\phi\mu c_g}{kt}}\right\}\right)\right] \quad (5\text{-}91)$$

For the pressure at the characteristics $s = x - \Omega\tau$

$$P_{(x=s)} = A + B\left[\psi_i - \left(\frac{4\dot{m}RT}{HL_{well}}\sqrt{\frac{t}{\phi\mu kc_g}}\sum_{n=0}^{\infty}(-1)^n\left\{ierfc\frac{2nl+(x-\Omega\tau)}{2}\sqrt{\frac{\phi\mu c_g}{kt}}\right\} - \frac{4\dot{m}RT}{HL_{well}}\sqrt{\frac{t}{\phi\mu kc_g}}\sum_{n=0}^{\infty}(-1)^n\left\{ierfc\frac{2(n+1)l-(x-\Omega\tau)}{2}\sqrt{\frac{\phi\mu c_g}{kt}}\right\}\right)\right] \quad (5\text{-}92)$$

$$P_i = A + B\psi_i \quad (5\text{-}93)$$

$$\Delta T_{exp} = -\frac{\emptyset\beta T}{\overline{\rho C_P}}\left[\frac{B4\dot{m}RT}{HL_{well}}\sqrt{\frac{t}{\phi\mu kc_g}}\sum_{n=0}^{\infty}(-1)^n\left\{ierfc\frac{2nl+x}{2}\sqrt{\frac{\phi\mu c_g}{kt}}\right\} - \frac{4\dot{m}RT}{HL_{well}}\sqrt{\frac{t}{\phi\mu kc_g}}\sum_{n=0}^{\infty}(-1)^n\left\{ierfc\frac{2(n+1)l-x}{2}\sqrt{\frac{\phi\mu c_g}{kt}}\right\}\right] \quad (5\text{-}94)$$

$$\Delta T_{JT} = -\varepsilon\frac{B4\dot{m}RT}{HL_{well}}\sqrt{\frac{t}{\phi\mu kc_g}}\left[\left(\sum_{n=0}^{\infty}(-1)^n\left\{ierfc\frac{2nl+(x-\Omega\tau)}{2}\sqrt{\frac{\phi\mu c_g}{kt}}\right\} - \sum_{n=0}^{\infty}(-1)^n\left\{ierfc\frac{2(n+1)l-(x-\Omega\tau)}{2}\sqrt{\frac{\phi\mu c_g}{kt}}\right\}\right) - \left(\sum_{n=0}^{\infty}(-1)^n\left\{ierfc\frac{2nl+x}{2}\sqrt{\frac{\phi\mu c_g}{kt}}\right\} - \sum_{n=0}^{\infty}(-1)^n\left\{ierfc\frac{2(n+1)l-x}{2}\sqrt{\frac{\phi\mu c_g}{kt}}\right\}\right)\right] \quad (5\text{-}95)$$

There is a short distance to the lateral boundary in the following case study designed to observe the boundary effect,. The Table 5-3 parameters are modified in Table 5-5 with a different reservoir thickness and gas mass flow rate.

The complete temperature solution for the planar flow case with a constant pressure lateral boundary is obtained from Equation 5-82, 5-93, and 5-94. Figure 5-6 compares the plot of the temperature solution with one generated by the full numerical solution. The derived analytical transient temperature solution matches both (1) the early linear flow period {before the pressure signal reaches the lateral boundary (between $t = 0$ hrs and $t \cong 20$ hrs)}, and (2) after the pressure signal reaches the lateral boundary (between $t \cong 90$ hrs and $t \cong 240$ hrs). There is a transition period between these two flow periods where the analytical slightly deviates from the numerical solution; and at the late time ($t > 240$ hrs) the solutions no longer match.

Table 5-5: Modifications to the Table 5-3 parameters for a case study with linear flow and constant pressure lateral boundary

Property	**Symbol**	**Value**	**Unit**
Gas mass flow rate	$\dot{m}$	7.76	kg/s
Reservoir thickness	h	6	m
Reservoir lateral boundary	x_e	50	m
A		6.1655×10^{6}	Pa
B		4.9013×10^{-13}	s

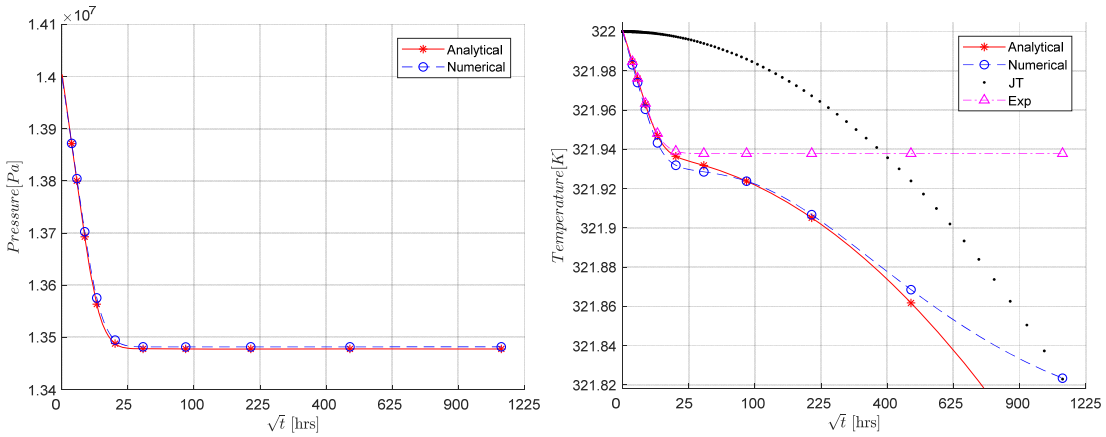

Figure 5-6: Comparison of analytical and numerical solutions for (a) Pressure and (b) Temperature

5.4.5 Simplified Solution for Planar Flow

It is also desirable to have a simplified solution in order to perform a fast and efficient TTA.

This section discusses simplified analytical solutions that are easy to solve analytically or can be represented by using a regression algorithm which will make it possible to rapidly and efficiently solve an inverse problem of estimating reservoir parameters from the observed temperature as part of TTA. Analytical solutions have been derived for the transient sandface temperature for planar flow with (1) a semi-infinite lateral boundary and (2) a constant pressure lateral boundary. As expected, the solutions provide similar

results for the time period during the 'infinite acting' flow regime prior to the pressure wave reaching the boundary.

5.4.5.1 Simplified Solution for Semi-Infinite Lateral Boundary

Temperature Change Due to Expansion Assuming Semi-Infinite Lateral Boundary

The transient temperature solution for planar flow consists of temperature changes due to fluid expansion and those due to Joule-Thomson and convection effects.

The change in temperature due to expansion can be approximated as a linear function of the square root of time, "$\sqrt{t}$", for small values of x.

$$\Delta T_{exp} = -\frac{\emptyset\beta T}{\overline{\rho C_P}}\left[\frac{B4\dot{m}RT}{HL_{well}}\sqrt{\frac{t}{\phi\mu kc_g}}ierfc\left(\frac{x}{2}\sqrt{\frac{\phi\mu c_g}{kt}}\right)\right] \qquad (5\text{-}96)$$

$$\lim_{x\to 0}\left[ierfc\left(\frac{x}{2}\sqrt{\frac{\phi\mu c_g}{kt}}\right)\right] = \frac{1}{\sqrt{\pi}} \qquad (5\text{-}97)$$

Therefore, at small values of x, i.e. at the sandface, the temperature {Figure 5-7(a)} change due to fluid expansion is given by Equation 5-98 and its derivative Equation 5-99.

$$\Delta T_{exp} = -\frac{\emptyset\beta T}{\overline{\rho C_P}}\left[\frac{1}{\sqrt{\pi}}\left(\frac{B4\dot{m}RT}{HL_{well}}\sqrt{\frac{t}{\phi\mu kc_g}}\right)\right] = \frac{4\,\emptyset\beta TB\dot{m}RT}{\overline{\rho C_P}\,HL_{well}\sqrt{\pi\phi\mu kc_g}}\sqrt{t} \qquad (5\text{-}98)$$

$$T\ slope = -\frac{4\,\emptyset\beta TB\dot{m}RT}{\overline{\rho C_P}\,HL_{well}\sqrt{\pi\phi\mu kc_g}} \qquad (5\text{-}99)$$

Temperature Change Due to Joule-Thomson and Convection Effect Assuming a Semi-Infinite Lateral Boundary

The change in temperature due to the Joule-Thomson and convection effect was observed to be a linear function of time "t". The temperature change close to the sandface due to

Joule-Thomson effect (Equation 5-100) was obtained from the complete solution (Equation 5-90) by assuming that x is very small.

$$\Delta T_{JT} = -\varepsilon \frac{B4\dot{m}RT}{HL_{well}} \sqrt{\frac{t}{\phi\mu k c_g}} \left[ierfc\left(\frac{x}{2}\sqrt{\frac{\phi\mu c_g}{kt}}\right) - ierfc\left(\frac{(x-\Omega t)}{2}\sqrt{\frac{\phi\mu c_g}{kt}}\right)\right] \quad (5\text{-}100)$$

$$\lim_{x\to 0}\left[ierfc\left(x\sqrt{\frac{\phi\mu c_g}{kt}}\right)\right] = \frac{1}{\sqrt{\pi}} \quad (5\text{-}101)$$

When the value of $x\sqrt{\frac{\phi\mu c_g}{kt}}$ is very close to zero, the integral complementary error function can be approximated by a linear curve passing through $\frac{1}{\sqrt{\pi}}$ when the argument $x\sqrt{\frac{\phi\mu c_g}{kt}}$ is zero. This approximation was derived from the definition of the integral complementary error function (Equation 5-102).

$$ierfc(z) = \frac{exp^{(-z^2)}}{\sqrt{\pi}} - z \cdot erfc(z) \quad (5\text{-}102)$$

Where the complementary error function is given by Equation 5-103

$$erfc(z) = 1 - erf(z) \quad (5\text{-}103)$$

Further, the error function can be expressed as a Maclaurin's series (Equation 5-104)

$$erf(z) = \frac{2}{\sqrt{\pi}}\sum_{n=0}^{\infty}\frac{(-1)^n z^{2n+1}}{n!(2n+1)} = \frac{2}{\sqrt{\pi}}\left(z - \frac{1}{3}z^3 + \frac{1}{10}z^5 - \frac{1}{42}z^7 + \cdots\right) \quad (5\text{-}104)$$

$erf(z)$ can be represented by the first term of the Maclaurin's series for small values of z and $exp^{(-z^2)}$ is approximately equal to unity.

$$erf(z) = \frac{2}{\sqrt{\pi}}z \quad (5\text{-}105)$$

$$exp^{(-z^2)} = 1 \quad (5\text{-}106)$$

$$\therefore ierfc(z) = \frac{1}{\sqrt{\pi}} - \left(z - \frac{2}{\sqrt{\pi}} z^2\right) \quad (5\text{-}107)$$

Ignoring the z^2 term results in a linear approximation for $ierfc(z)$

$$ierfc(z) = \frac{1}{\sqrt{\pi}} - z \quad (5\text{-}108)$$

$$\therefore \lim_{\left|x\sqrt{\frac{\phi\mu c_g}{kt}}\right| \to 0} \left[ierfc\left(\frac{x}{2}\sqrt{\frac{\phi\mu c_g}{kt}}\right) - ierfc\left(\frac{(x-\Omega t)}{2}\sqrt{\frac{\phi\mu c_g}{kt}}\right)\right] = -\frac{\Omega t}{2}\sqrt{\frac{\phi\mu c_g}{kt}} \quad (5\text{-}109)$$

Where Ω is defined as Equation 5-109

$$\Omega = \frac{4\rho C_P B\dot{m}RT}{\mu\overline{\rho C_P} H L_{well}} \quad (5\text{-}110)$$

Therefore Equation 5-109 can be approximated by Equation 5-111 when the value of $x\sqrt{\frac{\phi\mu c_g}{kt}}$ is close to zero

$$\left[ierfc\left(x\sqrt{\frac{\phi\mu c_g}{kt}}\right) - ierfc\left((x-\Omega t)\sqrt{\frac{\phi\mu c_g}{kt}}\right)\right] = -\frac{2\rho C_P B\dot{m}RTt}{\mu\overline{\rho C_P} H L_{well}}\sqrt{\frac{\phi\mu c_g}{kt}} \quad (5\text{-}111)$$

$$\Delta T_{JT} = \varepsilon\frac{B4\dot{m}RT}{HL_{well}}\sqrt{\frac{t}{\phi\mu k c_g}}\frac{4\rho C_P B\dot{m}RTt}{\mu\overline{\rho C_P} H L_{well}}\sqrt{\frac{\phi\mu c_g}{kt}} \quad (5\text{-}112)$$

$$\Delta T_{JT} = \frac{16\varepsilon\rho C_P B^2\dot{m}^2R^2T^2}{\mu\overline{\rho C_P} H^2 {L_{well}}^2\sqrt{k}}t \quad (5\text{-}113)$$

$$T\ slope = \frac{16\varepsilon\rho C_P B^2\dot{m}^2R^2T^2}{\mu\overline{\rho C_P} H^2 {L_{well}}^2\sqrt{k}} \quad (5\text{-}114)$$

Equation 5-113, the simplified description of the change in temperature due to the Joule-Thomson effect, is plotted in Figure 5-7(b).

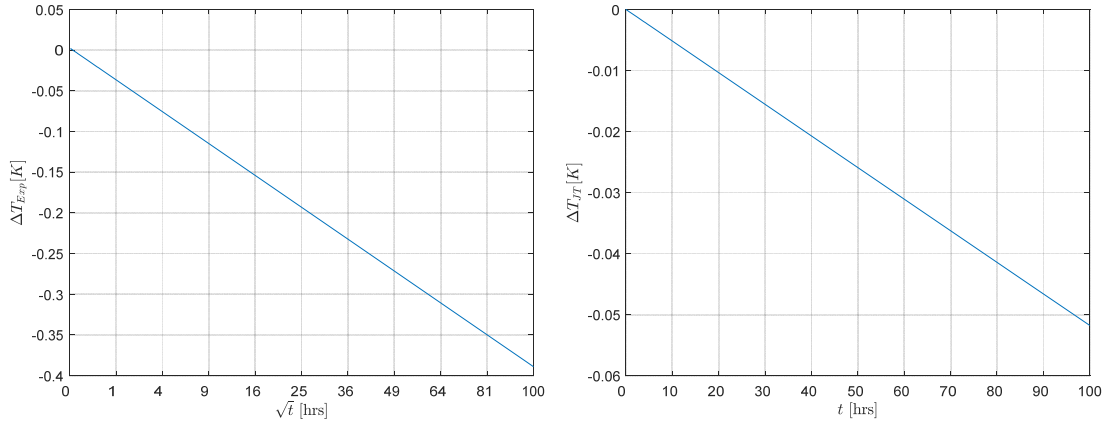

Figure 5-7: (a) The temperature change due to fluid expansion is as a linear function of $\sqrt{time}$ while (b) the temperature change due to the Joule-Thomson effect is a linear function of $time$

Equation 5-116 is the simplified solution for planar flow with semi-infinite lateral boundary. The plot of this equation, Figure 5-8(b) compares it with the complete transient temperature solution obtained from Equation 5-83, Equation 5-89 and Equation 5-90.

$$T_{wb}(t) = T_i - \Delta T_{exp} - \Delta T_{JT} \qquad (5\text{-}115)$$

$$T_{wb}(t) = T_i - \frac{4\,\emptyset\beta TB\dot{m}RT}{\overline{\rho C_p}\,HL_{well}\sqrt{\pi\phi\mu k c_g}}\sqrt{t} - \frac{16\varepsilon\rho C_P B^2\dot{m}^2R^2T^2}{\mu\overline{\rho C_P}H^2{L_{well}}^2\sqrt{k}}\,t \qquad (5\text{-}116)$$

The slope of the transient temprature signal can be approximated from the second and third term of Equation 5-116. The importance of this is that the slope of the transient temperature signal can be determined from these equations. The slope of the transient temperature (Equation 5-99) is a linear function of $\sqrt{t}$ when the expansion effect is dominant and when the Joule-Thomson effect is dominant, this slope becomes a linear function of t (Equation. 5-114)

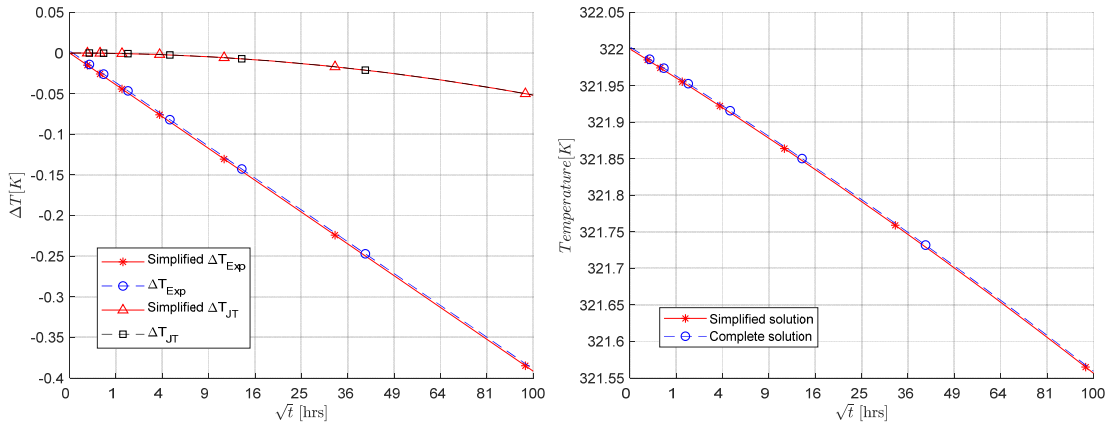

Figure 5-8: (a) $\sqrt{time}$ plot of the temperature change due to fluid expansion and Joule-Thomson effect (b) Comparison of the complete and simplified temperature solutions

5.4.6 Line Source Temperature Solution

The line source solutions better represents flow into a real horizontal well than the planar solutions derived in previous sections. The form of the line source pressure solution prohibits a full analytical solution for the temperature, instead the PDE is reduced to a system of ODEs which are subsequently solved numerically. The following assumptions are required:

1. The temperature solution is assumed linear and the pressure solution is described by the line source solution. This is because the line source pressure solution creates an additional pressure drop due to flow convergence into the wellbore, this effect that is not present in the pressure solution for planar flow. This pressure transient effect occurs at very early time and has virtually no impact on the slowly-propagating temperature; it is too fast to be noticeable on the temperature level. Hence it is reasonable to describe the temperature signal by linear flow.

2. The formation is assumed isotropic (i.e. vertical and horizontal permeabilities are equal). This is generally not true in real cases, but this work's solution for isotropic porous media may inform further research extending it to non-isotropic cases.

The system of ODEs (Equation 5-51. Equation 5-52 and Equation 5-53) is solved by the method of characteristics. Thus resulting reduced system of ODEs (obtained by substituting the solution of Equation 5-51 into Equation 5-52 and Equation 5-53) is given as Equation 5-117 and Equation 5-118

$$\frac{\partial X}{\partial t} = f(t,x,T) = -\frac{K2}{K1}\frac{\partial P}{\partial x} \quad (5\text{-}117)$$

$$\frac{\partial T}{\partial t} = g(t,x,T) = -\frac{K3}{K1}\left(\frac{\partial P}{\partial x}\right)^2 + \frac{K4}{K1}(T - T_i) \quad (5\text{-}118)$$

With the initial conditions:

$$f(0) = x_0 \quad (5\text{-}119)$$

$$g(0) = T_i \quad (5\text{-}120)$$

The above equations can be written in a matrix form as:

$$w(t) = \begin{bmatrix} x \\ T \end{bmatrix} \quad (5\text{-}121)$$

$$G(t,w) = \begin{bmatrix} f(t,w_1,w_2) \\ g(t,w_1,w_2) \end{bmatrix} \quad (5\text{-}122)$$

$$w(0) = \begin{bmatrix} x_0 \\ T_i \end{bmatrix} \quad (5\text{-}123)$$

The pressure gradient $\frac{\partial P}{\partial x}$ is obtained from the line source pressure solution (Equation 5-33). Equation 5-122 is then solved numerically using the Equation 5-123 initial conditions and the solution plotted in Figure 5-9. This figure compares the pressure and temperature solution obtained using the line source pressure solution with the numerical results. The individual fluid expansion and Joule-Thomson dominated components of the temperature signal are shown separately. The semi-analytical result matches the full numerical solution at early times.

Table 5-6: Table 5-3) modified parameters for the line-source pressure solution with semi-infinite pressure boundary

Property	**Symbol**	**Value**	**Unit**
Thermal conductivity	K_T	1.7	W/mK
Gas mass flow rate	$\dot{m}$	23.28	kg/s
Reservoir thickness	h	10	m
Well radius	r_w	0.12	m
A		6.0×10^6	Pa
B		8.5575×10^{-13}	s

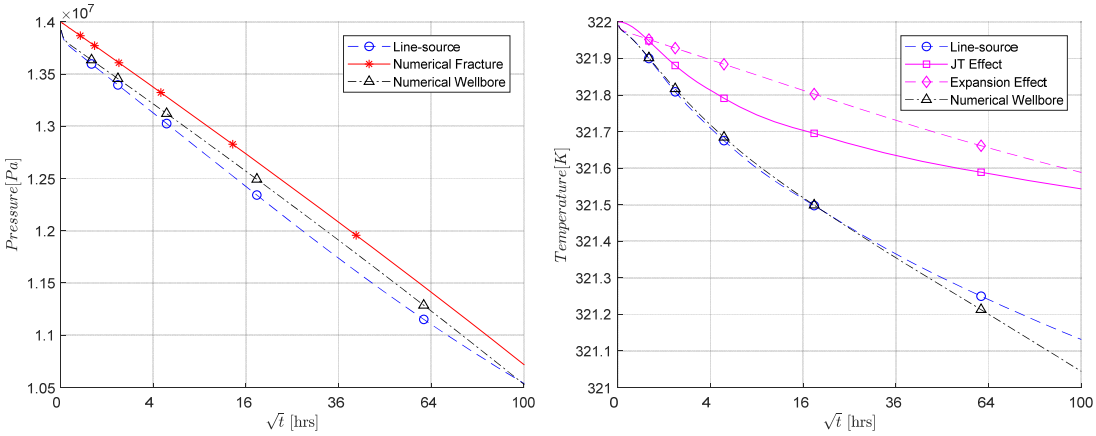

Figure 5-9: (a) The transient pressure for line-source solution, fracture flow and numerical solution for flow into a wellbore (b) Transient temperature for the line-source pressure solution, the numerical solution for flow into a wellbore and the individual fluid expansion and Joule-Thomson effects.

The linear assumption for the temperature solution produces accurate results at early time and can therefore be used to simplify the temperature solution, this is valid despite the flow into the wellbore being modelled as a line source. The planar solution does provide a fast method for estimating temperature change in a vertical fracture face; but the line source solution is a better representation of the actual temperature change in a real horizontal well. This will be discussed further in Section 5.6.

5.5 Effect of Heat Conduction

The above analytical solutions ignored the effect of heat conduction both within the reservoir and in the surrounding formations because it was expected to be very small for the early time periods relevant to TTA. This has been shown many times in multiple TTA studies providing early-time solutions. On top of this a numerical model was used in this work to confirm the above expectation by accurately capturing and studying this effect (for details see Chapter 3 and Appendix C). One important factor to be considered when modelling conduction is the thermal boundary condition of the overburden and underburden. App (2010) and Chevarunotai et al. (2015) used the concept of a time varying overall heat transfer coefficient {originally developed by (Zolotukhin 1979)} to model the heat transfer between the formation and the surroundings for a radial flow system. This approach provides a relatively simple analytical method for estimating the heat exchange between the formation and its surroundings. However, the boundary condition used to develop this solution is not representative of the real boundary condition and can lead to errors. These errors occur because the constant temperature boundary (at the top and bottom of the formation) assumption originally used by Zolotukhin (1979) for the steam injection wells study, implies that an unrealistically high temperature gradient is present at the boundary in the case of TTA. This, in turn, results in unrealistically high heat transfer between the formation and the surroundings when the heat transfer coefficient by Zolotukhin (1979) is directly used.

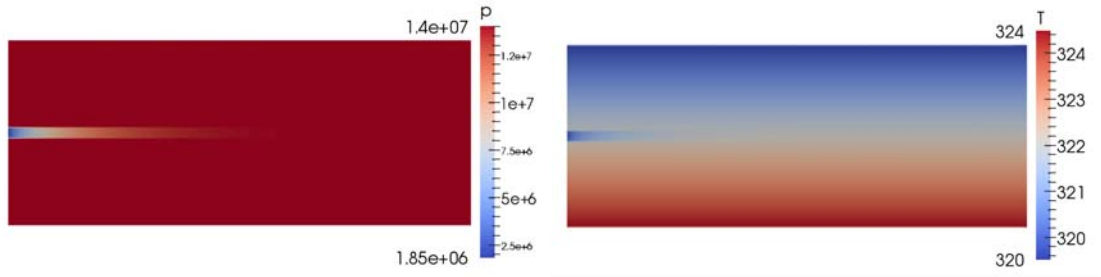

Figure 5-10: Surface plots of numerical results for planar flow, showing producing layer, overburden and underburden (a) Layer pressure, showing a lower pressure occurring in the producing layer (b) Layer temperature, showing geothermal gradient, and lower temperature due to production from the producing layer

An infinite boundary condition is the correct approach to model the thermal boundary at the top and bottom of the formation. This consists of a constant temperature boundary (equal to the geothermal temperature at any given depth) that is sufficiently far from the

producing layer, such that the temperature disturbance does not reach this boundary within the time of interest (Figure 5-10 and Figure 5-11)

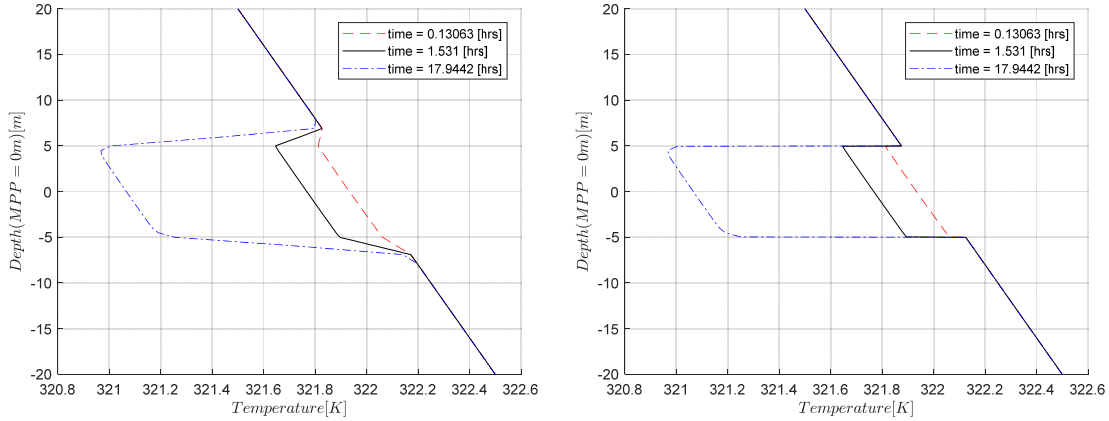

Figure 5-11: Vertical temperature profile at the sandface for (a) An infinite thermal boundary at the top and bottom of the producing layer. (b) A constant temperature boundary at the top and bottom of the producing layer.

The relative importance of heat conduction within the reservoir can also be estimated by using the Peclet's number (App & Yoshioka 2011) defined by Equation 5-124. They showed that this approach can give an apriori estimate of the importance of conduction, allowing the engineer to decide whether the solution is sufficiently accurate for the case being considered. The Peclet number was found to be between 100 and 350 for the above case studies modelled in this work, confirming that conduction is not important.

$$Pe = -\frac{ur}{\propto} \qquad (5\text{-}124)$$

$\propto$; Equation 5-125 is the thermal diffusivity of the formation

$$\propto = \frac{K}{\rho_r C_{Pr}} \qquad (5\text{-}125)$$

All the above studies have confirmed that the heat conduction effect is negligible during early-time TTA conditions discussed in this work and therefore need not be modelled.

5.6 Effect of Flow Convergence into the Wellbore

The pressure change for the flow converging into the wellbore is the same as for pure linear flow at early times (Figure 5-12) apart from the shift to the pressure profile. The transient temperature slope for the vertical fracture case is consistently different from the case with flow convergence into a wellbore (see Figure 5-12).

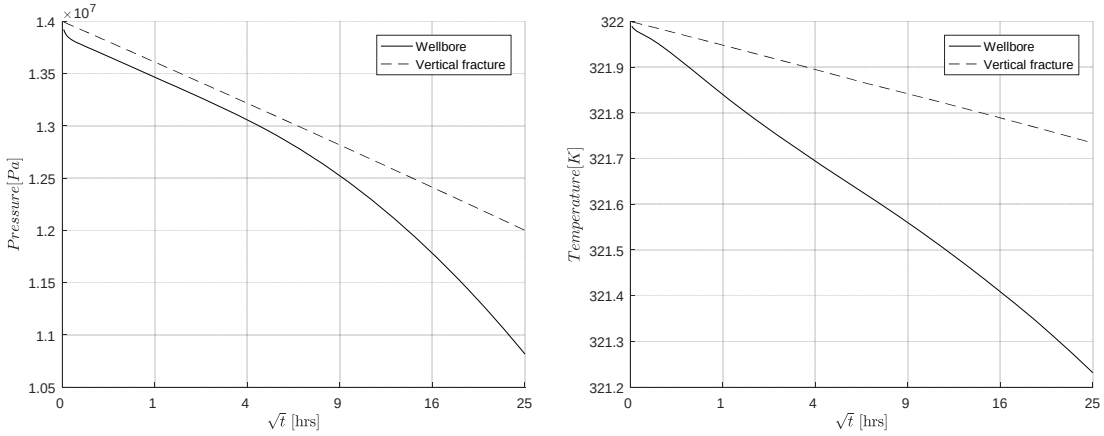

Figure 5-12: Numerical results for a well and vertical fracture (a) Transient pressure profile for vertical fracture and wellbore, showing equal slope during the early linear flow regime. (b) Transient temperature profile for a vertical fracture and a wellbore showing different slopes during the early linear flow regime

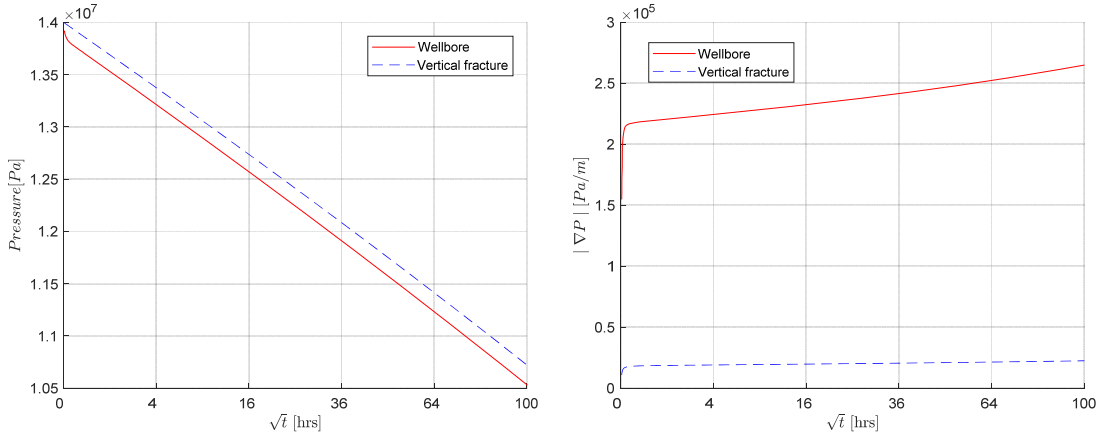

Figure 5-13: Numerical results for a well and vertical fracture comparing transient pressure and transient pressure derivative for the Table 5-4 and Table 5-6 cases (a) Transient pressure profile for vertical fracture and wellbore with a similar slope for early linear flow and a small shift in the pressure profiles. (b) Transient pressure derivative for a vertical fracture and wellbore showing the difference in slopes and the shift in the profiles.

The {Figure 5-12(b)} difference in the transient temperature slope between a vertical fracture (planar) flow and flow into a wellbore is due to the difference in pressure gradient near the wellbore {Figure 5-12(a)} where flow convergence occurs. This difference in pressure gradient can be quite significant, being about one order of magnitude {Figure 5-13(b)}. It depends on the ratio of wellbore radius to formation thickness. The temperature change due to the Joule-Thomson effect is a function of the pressure gradient and not the temperature derivative leading to a greater Joule-Thomson effect in the case of flow into a wellbore. Figure 5-14 compares the transient temperature, expansion effect and Joule-Thomson effect for planar flow (for the Table 5-4 and Table 5-6) case studies.

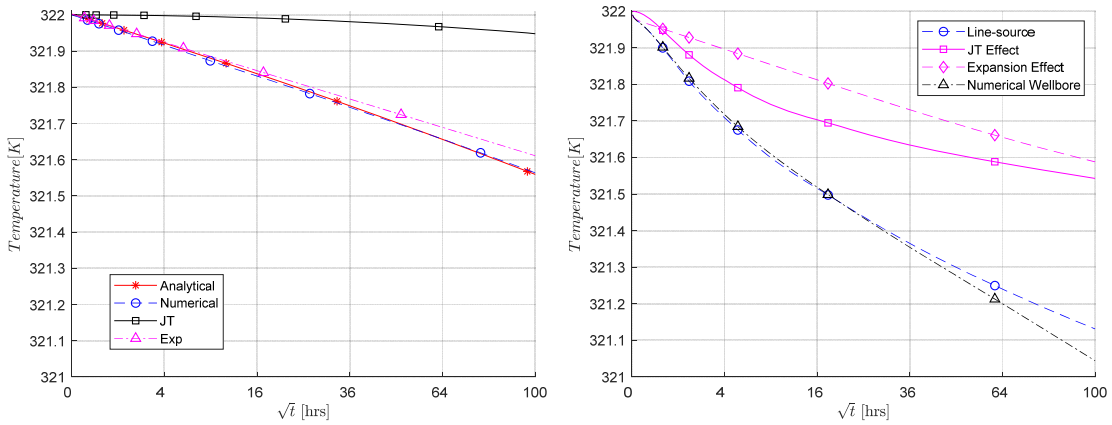

Figrue.5-14: Comparison of analytical and numerical solutions showing the expansion and Joule-Thomson temperature components of the transient temperature solution for (a) planar flow (b) flow into a wellbore

The transient temperature solution describing flow into a vertical fracture cannot be used to describe flow into a wellbore. The line source solution can either be used (1) to directly predict the transient sandface temperature, or (2) to determine the relative correction of the slope due to the flow convergence. This is required if it is preferred to use the planar solution to obtain an approximate solution for a horizontal well.

5.7 Conclusion

This work develops new analytical and semi-analytical solutions for transient sandface temperature in dry gas producing horizontal wells. Solutions for planar flow with semi-infinite lateral boundary and constant pressure boundary were developed. A semi-analytical transient temperature solution which takes into account the effect of flow convergence into the wellbore using the line-source pressure solution was also developed.

Note that the planar flow (or 'vertical fracture') solutions can literally be applied to the flow into fractured vertical wells, which indeed extends the application envelope of the solutions.

The developed solutions reproduced the numerical modelling results with a reasonable accuracy. The analytical solutions matched the numerical results well for the planar solution with semi-infinite boundaries. However, there is a transition region when the pressure signal reaches the boundary for the planar solution with constant pressure lateral boundaries. The analytical solution again matches the numerical results after this transition period.

A simplified analytical solution was developed for the planar flow (i.e. flow into a vertical fracture) with the semi-infinite acting lateral boundaries. The simplified solution was a combination of the fluid expansion effect (a linear function of the square root of time) and the Joule-Thomson effect (a linear function of time). The simplified solution matches the complete solution relatively well, and may also be used as a fundamental TTA solution for horizontal, gas production wells.

Finally, the effect of flow convergence into the horizontal wellbore was investigated using numerical simulations. It was confirmed that this effect does not have a great impact on the transient pressure signature, but does have a significant effect on the transient temperature profile because of the difference in the pressure gradient near the wellbore and the resulting impact on the magnitude of the Joule-Thomson temperature change. This can limit the application of the planar solution in real well situations. However, the planar solution can be made widely applicable to real wells by carrying out further studies to develop a correction for the flow convergence effect. While these solutions were developed using the pseudo-pressure for gas, these solutions can also be applied to liquids by replacing the pseudo-pressure with pressure. Finally, Table 5-7 summarizes the solutions and the boundary conditions for which they have been derived. All these solutions have been shown applicable to describe the early-time pressure and temperature transients in horizontal and fractured wells.

Table 5-7: Developed solutions and boundary conditions for which they are applicable.

Developed solution	**Section**	**Inflow boundary**	**External boundary**
Semi-infinite boundary, planar flow	4.4.1	Flow into a vertical fracture (i.e. a planar sink)	Semi-infinite boundary
Simplified semi-infinite boundary, planar flow	4.4.2		
Constant pressure boundary, planar flow	4.5	Flow into a vertical fracture (i.e. a planar sink)	Constant pressure
Line source flow	4.6	Flow into a wellbore (i.e. line sink)	Semi-infinite boundary

5.8 Nomenclature

Φ: Dependent variable of diffusivity equation

D: Diffusivity $[m^2/s]$

t: time $[s]$

ψ: Pseudo-pressure $[Pa^2/Pa.s]$

k: Permeability $[m^2]$

P: Pressure $[Pa]$

c_g: Gas isothermal compressibility $[Pa^{-1}]$

μ: Gas viscosity$[Pa.s]$

ϕ: Porosity [ ]

T: Temperature $[K]$

C_P: Specific heat capacity of gas $[J/kgK]$

C_{Pr}: Specific heat capacity of formation rock $[J/kgK]$

ρ: Density of gas $[kg/m^3]$

ρ_r: Density of formation rock $[kg/m^3]$

β: Thermal expansion coefficient of gas $[K^{-1}]$

C_f: Formation compressibility $[Pa^{-1}]$

$\boldsymbol{v}$**:** Velocity $[m/s]$

K_T: Thermal conductivity $[W/mK]$

F_o: Heat flux $[W/m^2]$

K: Thermal conductivity $[W/mK]$

l: Fracture half-length $[m]$

$\dot{m}$: Mass flow rate $[kg/s]$

R: Specific gas constant $[J/kgK]$

Z: Gas compressibility [ ]

A: Cross sectional area $[m^2]$

A: Intercept of pressure pseudo-pressure linear relationship $[Pa]$

B: Coefficient of pressure pseudo-pressure linear relationship $[s]$

x_f: X-position of fracture face $[m]$

η_i: $k_i/\phi\mu c_g$ where $i = x, y \text{ or } z$ $[m^2/s]$

C_t: Total compressibility $[Pa^{-1}]$

D_z: as defined by Equation.(33) $[m]$

L_{well}: Well length $[m]$

U: Overall heat transfer coefficient $[W/K]$

H: Formation thickness $[m]$

ε: Joule-Thomson coefficient $\left[[K/Pa]\right]$

5.9 Subscripts

ref: Reference value

x: x-direction

y: y-direction

z: z-direction

D: Dimensionless

t: Total

exp: Expansion effect

JT: Joule-Thomson effect

i: Initial condition

T: Thermal

wf: Well flowing

Chapter 6: Mitigation of the Remote Gauge Problem

6.1 Introduction

The reservoir-wellbore fluid production system is closely coupled, with changes in one affecting the other. The thermal effects in the wellbore do not have a significant effect on the reservoir, but changes in the temperature and pressure of the fluid in the wellbore greatly affect the measured fluid temperature, leading to significant differences between the sandface temperature and the remotely measured, gauge temperature. The wellbore effect must be accounted for when analyzing downhole transient temperature data using interpretation models that were developed for handling sandface temperature data. (N.B. Published TTA methods to-date have been based on the availability of sandface data).

This work concentrates on cases where a gauge is installed at a distance from the production zone. Ideally, in both modern, intelligent and conventional wells the gauge or sensor should be placed next to or across the tested interval. However, this is not always the case. The "remote gauge problem" has frequently been ignored in the past due to the lack of suitable workflows for data correction.

TTA involves relatively small temperature changes in the reservoir and at the sandface. This allows PTA to assume a constant temperature, but does require the installation of high precision gauges that can sufficiently accurately measure the temperature changes shown in Figure 6-1(a) for an oil well ($\Delta T < 1°C$) and in Figure 6-1(b) for a gas well ($\Delta T < 2°C$). Modern gauges are sufficiently sensitive to resolve these signals; making it possible to use the measured data for TTA. Figure 6-1(b) also shows that the duration of the useable transient temperature signal is about 16 hours. Measurement of TTA well test data is reasonably cost effective with measurement periods of less than one day. TTA has been successfully applied for characterizing the producing layer properties (Muradov et al., 2017; Onur & Çinar, 2016) for rate allocation (Muradov & Davies 2013) and for near wellbore analysis (Muradov et al., 2017 and Ramazanov et al., 2010). TTA is therefore a valuable complement to PTA as well as for stand-alone analysis. Some of the important TTA publications have been summarised in Table 4-1.

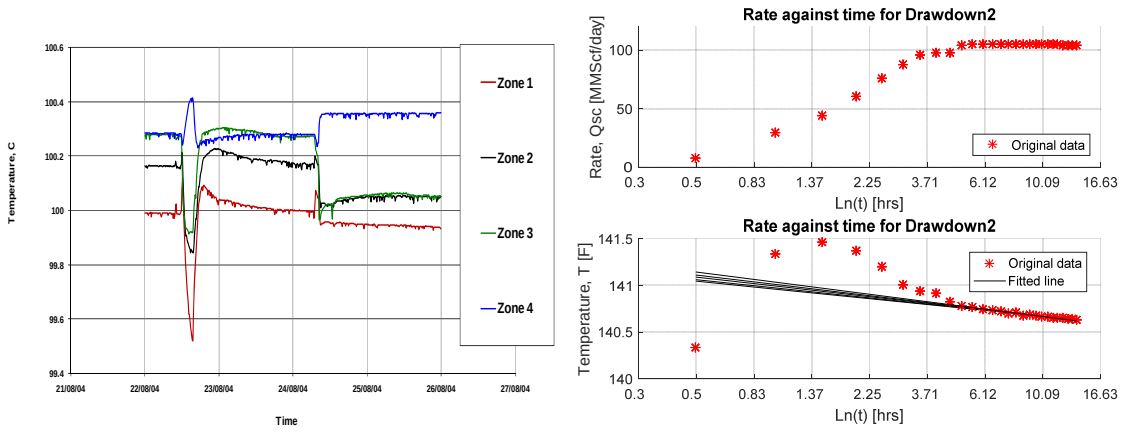

Figure 6-1: (a) Typical zonal temperature measurement in an advanced well (Muradov & Davies 2013) (b) Gas well transient temperature and flowrate data (Dada, Muradov & Davies 2017)

The wellbore effects can be classified as:

- *Wellbore storage*: Fluid expansion and compression in the wellbore affecting the flow and pressure.

- *Thermal wellbore storage*: Mixing of fluid inflow from the reservoir with fluid in the wellbore (Ramazanov et al. 2010) and heating/cooling due to adiabatic expansion/compression of the fluid in the wellbore when the wellbore pressure changes.

- *Heat transfer in wellbore*: Heat transfer between the fluid, the wellbore completion and the formation.

- *Other*: Include thermodynamics (phase changes – such as gas evolution, scaling, etc.); interactions between flowing phase; Joule-Thomson effect within the wellbore and across restrictions, etc. (These are assumed to be negligible in this work for single-phase flow from the reservoir to the gauge position without any significant flow restrictions between them.)

Wellbore storage results in a non-instantaneous sandface production rate change at well start-up and well shut-in (‘afterflow’) which affects the accuracy of both PTA and TTA since they normally assume a constant sandface flowrate. Therefore, it is important to be

able to correct for, or at least estimate, the impact of the wellbore storage effect on the accuracy of the transient analysis. Many methods have been developed for PTA. Muradov (2010) proposed a method for correcting for the mixing effects in the tubing downstream of an inflow control valve, an approach which should correct for most thermal wellbore storage effects. This work provides methods for correcting for signal attenuation resulting from heat transfer between the fluid in the wellbore, the wellbore completion and the formation.

An accurate, thermal, wellbore model able to predict both the fluid flow and thermal effects in the wellbore is required to correct for heat transfer effects in TTA. However, the thermal properties of the formation, fluid or wellbore are often not accurately known. Hence it is necessary to develop a method that can deduce the wellbore model parameters and subsequently calibrate the wellbore model.

Two approaches are suggested. The first one involves making simultaneous measurements at the sandface and the gauge. Such measurements can be acquired when carrying out a well test with a production logging tool positioned at the sandface while simultaneous measurements are being recorded by the permanent downhole gauge located at a distance from the tested interval. This approach provides relatively accurate data for characterizing the wellbore's thermal properties; but has the drawback of requiring a costly, and possibly risky, intervention, that may not always be possible. The second drawback is that the temperature data obtained from the logging tool has to be corrected for the movement of the tool, a process that could also introduce errors. Finally, due to the transient nature of the test, some wellbore properties will change during the production period. Hence, the information obtained at the time of production logging becoming increasingly inaccurate with time.

The second approach uses the wellbore warmup period after well start-up, i.e. the period before the reservoir fluid temperature front fully reaches the gauge location. The transient temperature data measured during the warm-up period when a shut-in well is brought into production only contains information about the wellbore, since the temperature front from the sandface has not yet arrived at the gauge location. Many permanent gauges are located at some distance from the sandface, making this a useful measurement for characterizing the wellbore and providing a more accurate model for sandface temperature reconstruction. This approach makes it possible to update the wellbore model prior to

each TTA. The warmup period for each event will reflect the current condition caused by all changes occurring in or around the wellbore during the well's productive life. The drawback to this approach is that it assumes an initial linear geothermal gradient in the well (which requires that the well has been shut-in for a sufficient length of time). Changes in the geothermal gradient during production will affect the accuracy of the solution. These two approaches will be discussed in detail, and illustrated with case studies.

There are several analytical transient thermal wellbore models (Izgec et al. 2007), (Duru & Horne 2010), (Hasan et al. 2005) and (Ramey Jr. 1962). Most of these models are based on Ramey Jr. (1962) and are very similar with only the model by Duru & Horne (2010) including the effect of a varying bottomhole (i.e. sandface or fluid inflow) temperature. All the other models are based on the constant bottomhole flowing temperature assumption. Of the models mentioned only Duru's model can be used to reconstruct the transient sandface temperature for TTA, Figure 6-2, where the variable bottomhole temperature (BHT) is not propagated in Ramey's model, while it is propagated in Duru's model.

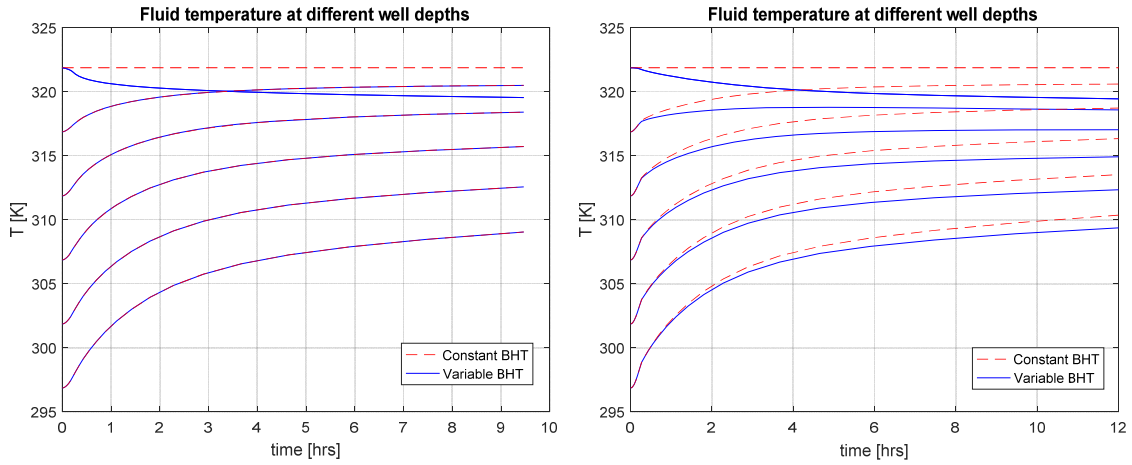

Figure 6-2: (a) Gauge temperature estimated at different gauge distances using Ramey, Izgec or Hassan's model (b) Gauge temperature estimated at different gauge distances using Duru's model

Numerical simulators capable of accurately modelling the transient wellbore temperature changes have been developed in recent years. However, unlike analytical models they are computationally expensive, difficult to couple to a linear regression routine and not as accessible to many engineers.

Duru's analytical model will be used in this work because of its inclusion of the effect of varying transient sandface temperature. Duru's model with a constant bottomhole flowing temperature is equivalent to Ramey's model. T_D is the time function, the importance of which will be discussed in detail in the following section. Hence, the estimation of the other parameters used in this equation is similar to that from the other models, where the fluid temperature is given as a function of depth and time $T_f(z,t)$ and depends on the difference between the bottomhole flowing temperature and the geothermal temperature at the bottomhole $(T_{fin} - T_{ein})$. C_p is the specific heat capacity of the fluid, g is the acceleration due to gravity, g_G is the geothermal gradient, T_{ei} is the initial geothermal temperature at the distance z and θ is the inclination of the well segment.

$$T_f(z,t) = T_{ei} + \frac{1-e^{-aL_R t}}{L_R}\left[\left(1 - e^{(z-L)L_R}\right)\left(g_G \sin\theta + \phi - \frac{g\sin\theta}{C_p}\right) - L_R e^{(z-L)L_R}\left(T_{fin} - T_{ein}\right)\right] \quad (6\text{-}1)$$

$$a = \frac{WC_p}{mC_p(1+C_T)} \quad (6\text{-}2)$$

Where W is the mass flow rate of the produced fluid, m is the mass of fluid per unit depth and C_T is the thermal storage parameter (Hasan et al. 2005). The relaxation distance is given by Equation 6-3 and k_e is the thermal conductivity of the earth (i.e. formation), r_{to} is outside radius of the tubing, U_{to} is the overall heat transfer coefficient based on the outer radius of the tubing and T_D is the dimensionless time function (also denoted by $f(t)$ in some situations).

$$L_R = \frac{2\pi r_{to} U_{to} k_e}{WC_p[k_e + r_{to} U_{to} T_D]} \quad (6\text{-}3)$$

The last lumped parameter ϕ is the Joule-Thompson temperature change due to the pressure gradient in the well (Equation (6-4). Where μ_{JT} is the Joule-Thompson coefficient of the fluid, and $\frac{\partial P}{\partial z}$ is the pressure gradient of the flowing fluid in the tubing.

$$\phi = \mu_{JT}\frac{\partial P}{\partial z} \quad (6\text{-}4)$$

6.2 Effect of Time Function Assumptions

As mentioned, most of the transient thermal wellbore models (Duru & Horne, 2010; Hasan et al., 2005 and Izgec et al., 2006) are based on Ramey's model (Ramey Jr. 1962). These models use the same basic assumption for modelling heat conduction from the casing into the formation surrounding the wellbore. The models use time functions $f(t)$ derived for solutions of radial heat conduction from an infinitely long cylinder into the formation at a constant temperature, a constant heat-flux line source and a cylinder losing heat under radiation (or convection) boundary condition (Ramey Jr. 1962). These solutions using different conditions were all found to converge at late time. The time function can be derived from Equation 6-5 if the transient conduction solution is known (Kutun et al. 2015).

$$f(t) = \frac{2\pi k_e}{q}(T - T_{ei}) \qquad (6\text{-}5)$$

Where T is the transient temperature at the outer surface of the casing; T_{ei} is the undisturbed geothermal temperature and q is the heat flow rate per unit length.

However, TTA is mostly concerned with early time transient solutions, i.e. those immediately after a well rate change event. Therefore, the solution zone of interest will often be in the region where the different solutions, based on the different time functions, give significantly different results.

The constant temperature and heat flux assumptions used to develop the time functions are simplifications which do not strictly speaking apply in reality, as the temperature and heat flux in the wellbore is continuously changing, especially during the early transient period. "*In the case of the general wellbore heat problem, neither heat flux nor temperature at the wellbore remains constant except in special cases*" (Ramey Jr. 1962). These two assumptions (constant temperature and heat flux) are simpler to implement than the radiation boundary condition, but they can also lead to errors that can then affect the TTA's reliability.

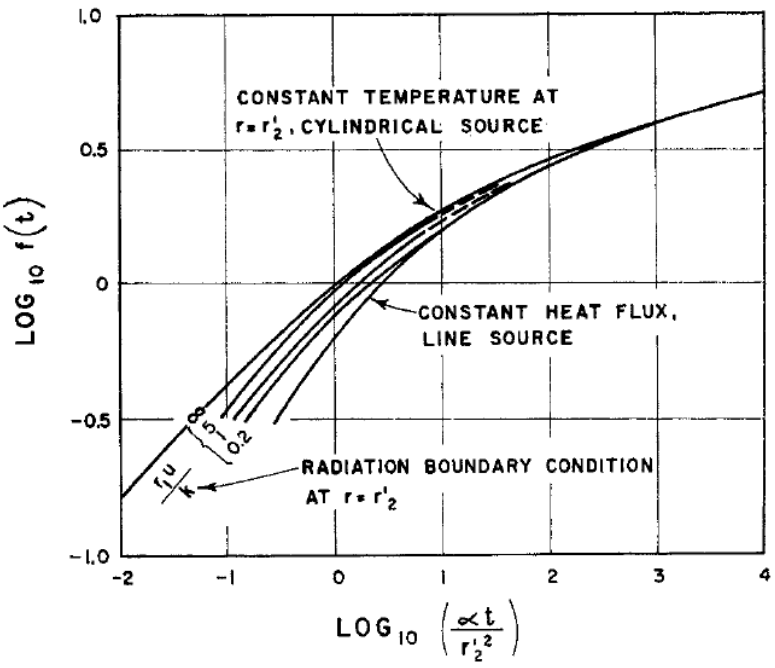

Figure 6-3: Transient heat conduction in an infinite radial system {Figure 1 of (Ramey Jr. 1962)}

Figure 6-3 {Figure 1 of (Ramey Jr. 1962)} shows that the time required for the different time functions $f(t)$ to converge is significant in comparison to TTA test durations (hours or usually 1-2 days). This is about 1.1 Fourier time, or about 24 hours, for a formation thermal conductivity of 5 W/mK, specific heat capacity of 920 J/kgK, density of 2500 kg/m^3.

By contrast, Ramey Jr. (1962) showed the different time functions converge when $log_{10}\left(\alpha t/r_{to}^2\right) \cong 3$ indicating a convergence time exceeding 3 days for typical for typical values of α and r_{to} . Selection of the correct time function for the wellbore heat transmission model is important for ensuring high solution accuracy.

The importance of time functions at early transient periods led to the evaluation of the different time functions by Kutun et al. (2015). The different time functions were compared with numerical solutions for the case with a constant temperature cylindrical source. The authors then proposed a simplified time function, $f(t) = ln(1 + 1.7\sqrt{t_D})$, for fitting Ramey's numerical $f(t)$ data. It gave the best match for all time periods.

An attempt was made also by Izgec et al. (2006), correcting for this effect by changing the formation temperature due to heat accumulation around the wellbore used in Hasan et al. (2005)'s model. This approach uses an average temperature over a formation volume element (between r_w to r_{ve}, where r_w is the inner radius, and $r_{ve}$is the outer radius of the specified volume element). It has the drawback of being sensitive to the thickness of the volume element around the wellbore. This observed change could vary from very high formation temperature change for a very small thickness to zero formation temperature change (i.e. geothermal) for a very large thickness.

Another issue with the work done by Izgec is that it is based on the Hasan's model which includes the undisturbed surrounding temperature (as the original Ramey model assumes infinite external boundary for heat transfer) and not the temperature adjacent to the wellbore. Updating this temperature would lead to significant errors in the obtained solution.

The next section reviews the different time functions. Note that we, similar to all authors, ignore the effects of heat exchange between wells and other heat sources/sinks, e.g. 'heat islands' in cluster well installations. In this case the remote gauge is located significantly deep in the well, so this effect can be ignored. Also multiple flow or heat sources between the sandface and the gauge are assumed to be absent. Thus any gas lift valves or pumps are installed above the gauge.

6.2.1 Time Functions for Wellbore Heat Transfer

A comparison of the different time functions used in the wellbore heat transmission model was carried out by Ramey Jr. (1962). The radiation boundary condition (i.e. the condition at which the heat loss from the wellbore is proportional to the temperature distribution around the wellbore) is recommended for early times (t < 1000 Fourier time), while at late times, the different time functions converge and the solution remains the same regardless of the time function used.

The time function is derived from the solution of the heat conduction in solids PDE for a wellbore formation system with the following initial and boundary conditions;

1. Initial condition: $\lim_{t\to 0} T_e = T_{ei}$ (the wellbore is in stabilisied equilibrium with surrounding formation).

2. Boundary condition at the well: this depends on the specified time function.

3. Boundary condition in the far region: no heat flow $\lim_{r\to\infty}\left(\frac{\partial T_e}{\partial r}\right) = 0$

The major difference between the different time functions is the boundary condition at the wellbore. Several time functions have been developed to match different wellbore boundary conditions. Some of these are discussed below.

Constant Temperature At Wellbore:

Boundary condition at the well:

$$T_e|_{r=r_w} = constant \qquad (6\text{-}6)$$

This boundary condition is achieved by simply setting a constant temperature at the wellbore. An analytical equation was developed for this boundary condition by Eppelbaum (2005) as reported by Kutun et al. (2015). This analytical equation was reported to give a good match (within 1%) with numerical results for a model with constant temperature at a cylindrical source.

Constant Heat Flux At Wellbore:

Boundary condition at the well:

$$2\pi k_e r \frac{\partial T_e}{\partial r}\Big|_{r=r_w} = constant \qquad (6\text{-}7)$$

This time function is obtained by setting a constant heat flux at the wellbore. Hasan & Kabir (2002) developed an analytical equation for the time function using this boundary

condition and a solution approach similar to the constant rate solution by Van Everdingen & Hurst (1949).

Hasan & Kabir (2002) reported, "*Ameen used the superposition principle to account for changing heat flux using a numerical approach. His solution showed that the assumption of constant heat flux introduced very little inaccuracy"*.

However, the level of inaccuracy and the spread over the different time periods was not discussed. This is an important element of any TTA study because it relies on analysis of the early time periods. Ramey Jr. (1962) showed that the constant heat flux condition is inaccurate at early times.

Radiation Boundary At Wellbore:

Boundary condition at the well:

$$-k\frac{\partial T}{\partial r}\Big|_{r=r_w} = U_2(T_1 - T_2) \qquad (6\text{-}8)$$

Where U_2 is the overall heat transfer coefficient from the outside radius of the casing and U is the overall heat transfer coefficient from the inside radius of tubing

$$U_2 = \frac{r_{ti}U}{r_w} \qquad (6\text{-}9)$$

This was recommended by Ramey as the most representative time function for early times. He (Ramey) further produced curves of this time function against Fourier time for different values of $\frac{r_1 U}{K}$. However, no analytical solution was provided for this time function in Ramey Jr. (1962) or in any later publications on wellbore heat transmission.

The importance of the time function was investigated to determine the suitable time function to be used for sandface temperature reconstruction. Duru & Horne (2010)'s use of the constant heat flux time function from Hasan & Kabir (2002) led to the observation that the constant temperature time function gave better results and (matches numerical

solution) than constant heat flux time function. The constant temperature time function will therefore be used with Duru's model for sandface temperature reconstruction.

6.3 Numerical Wellbore Models

There are several approaches to modelling the transient thermal effect in wellbores. Analytical models were discussed above. Commercial, numerical transient multiphase wellbore flow simulators, OLGA™ (Schlumberger 2012) and LedaFlow™ (LedaFlow 2017) can also be used. Analytical models excel in terms of computational speed, but numerical models provide more detail and accuracy. OLGA™ will be used in this study.

6.3.1 OLGA™ Numerical Model

The OLGA™ wellbore model was used to investigate the possibility of reconstructing the sandface temperature when the wellbore model is known. The possibility of deducing parameters of the wellbore model when the transient temperature at the sandface and gauge are known was also investigated.

The reservoir was modelled separately and then the fluid flow from the reservoir (into the wellbore) was imposed as a "source" term in OLGA™, since OLGA™ does not provide a fully coupled, thermal wellbore-reservoir system model. This approach made it possible to impose a transient sandface (or fluid) temperature at the inlet of the well such that OLGA solves the mass, momentum and energy conservation equations for each fluid component (in this case a single component, gas) in the wellbore coupled with heat transfer to the surrounding formation. Table F-1 of Appendix F gives details of the parameters used to setup the wellbore model in OLGA™.

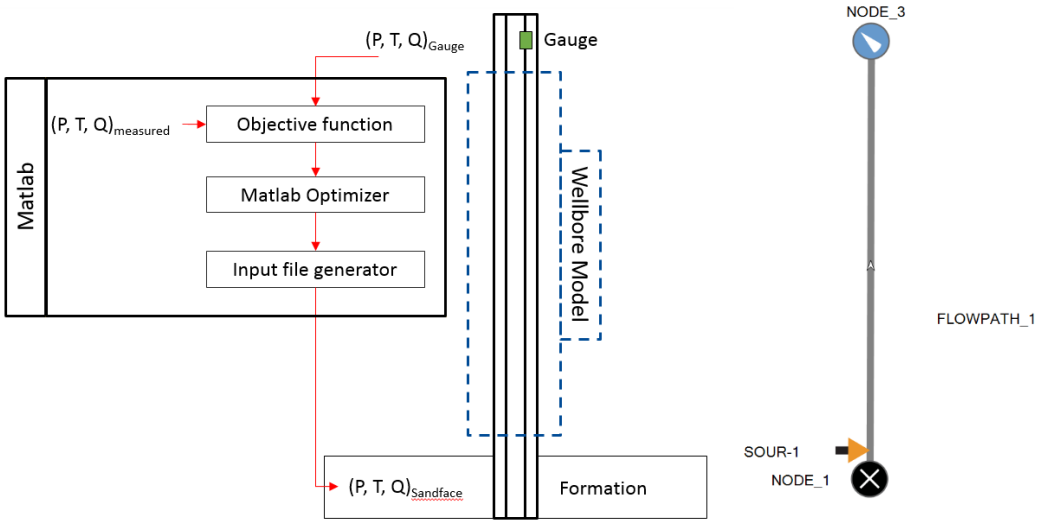

Figure 6-4: (a) Coupled optimizer and wellbore model for well characterization and sandface temperature reconstruction from gauge data; (b) OLGA™ wellbore model schematic view

However, there are difficulties with the approach of the source term defining the flow rate, temperature and pressure at the bottomhole. This approach is different from controlling a well by adjusting the choke (situated above the gauge) to achieve the required rate. This adjustment will also affect the bottomhole pressure. Adding a bottomhole source term can, for instance, lead to pressure spikes in the well if the surface choke is not opened wide enough.

It is possible to prevent this effect by using a proportional-integral-derivative (PID) controller at the wellhead choke to match the bottomhole pressure and flow-rate. However, fluctuations in the pressure and temperature are created, making it difficult to analyze the data produced from the simulation. This model is also difficult to invert, because the PID controller is tuned {e.g. using (Ziegler & Nichols 1942)} for a specific well condition. Changing the well or flow properties during optimization often makes the controller unstable.

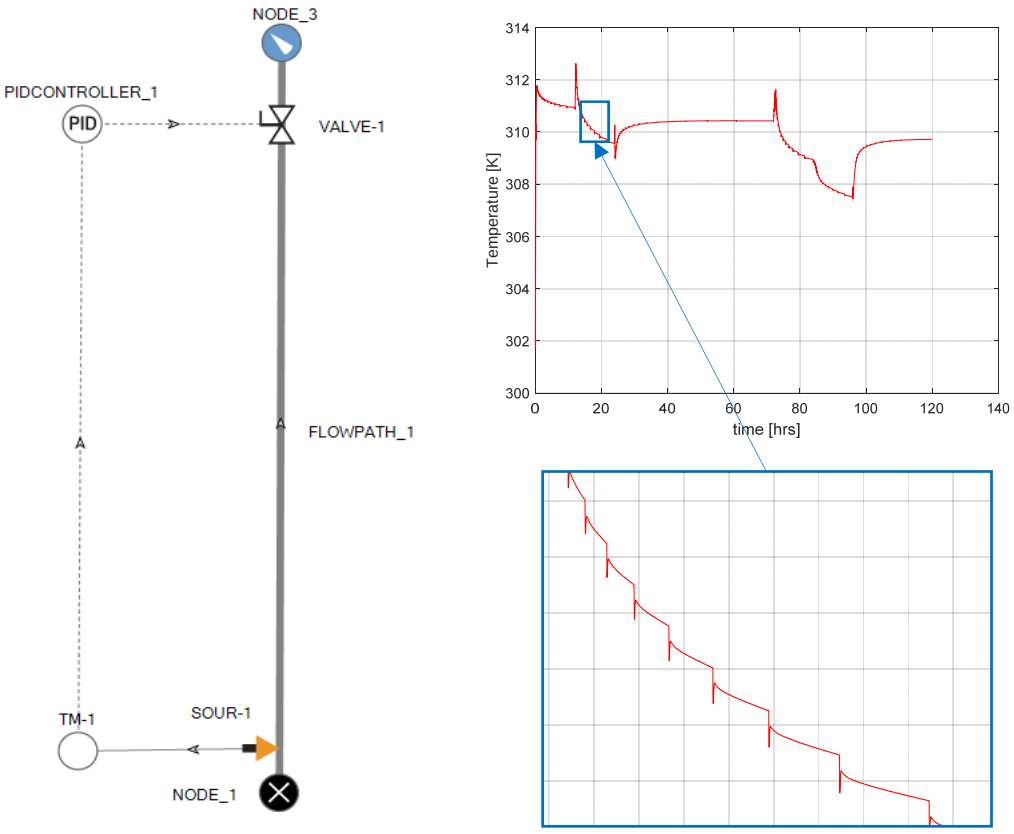

Figure 6-5: (a) OLGA™ wellbore model schematic with PID controller; (b) Plot of resulting transient temperature

6.3.2 Objective Functions for Linear Regression

The thermal characterization or sandface temperature reconstruction from the remote gauge data using a numerical wellbore flow model involves using a non-linear regression to minimize the error in the objective function.

The following options were considered for the objective function (Equation 6-10), based on the purpose of the optimization.

1. Wellbore characterization:

    a. Root mean squared error (RMSE) of the entire temperature signal

    b. RMSE of the warmup period of the temperature signal

c. RMSE of the time weighted temperature signal

2. Reconstruction of the sandface temperature:

a. RMSE of the entire temperature signal

b. RMSE of the time weighted temperature signal.

$$\sqrt{\frac{\sum_1^n[\boldsymbol{\Lambda}(\varepsilon^2)]}{n}} \qquad (6\text{-}10)$$

Where $\boldsymbol{\Lambda}$ is a vector of weights having the same length as the error vector, ε is the error vector, n is the length of the error vector. The weights vector ($\boldsymbol{\Lambda}$) is a logistic function of the scaled time vector (ts), and it is defined as Equation 6-11 and the constants C1, C2, C3 & C4 are tuning parameters which can be used to adjust the weight vector. Setting C2 and C4 equal zero, and C1 and C3 equal one results in a uniform weight of one for all times.

$$\boldsymbol{\Lambda} = \frac{C1}{C2+C3\cdot e^{(-C4\cdot ts)}} \qquad (6\text{-}11)$$

The scaled time vector is created such that its values range between zero and one. If the aim it to assign larger weights to the early time period, the scaled time vector is defined as Equation 6-12, and as Equation 6-13 if the aim is to assign larger weights to the late time period.

$$ts = \frac{t-t_i}{t_f-t_i} \qquad (6\text{-}12)$$

$$ts = \frac{t_f-t}{t_f-t_i} \qquad (6\text{-}13)$$

A weighted temperature signal error can be used to give priority to a particular portion of the signal. For example, then weights can be assigned to give the early time period greater priority if the zone of interest is the near wellbore analysis (Akindolu. Dada et al. 2017).

6.3.3 Optimization Parameters

A multi-parameter optimization was used to characterize the well or reconstruct the sandface temperature. The parameters to be optimized are the uncertain wellbore parameters in the case of wellbore characterization; while the individual data points in the sandface temperature signal are the optimization parameters for sandface temperature reconstruction. This leads to a large number of optimization parameters during sandface temperature reconstruction which greatly increases the time required for convergence.

One method of tackling this problem is to fit a model to the sandface temperature signal and then use the parameters of the model as the optimization parameters. The analytical transient temperature solution (Akindolu Dada et al. 2017) was fitted to the data points of the source (sandface) temperature and the parameters of this model was then used as the optimization parameters. This greatly reduced the number of optimization parameters to just seven. A similar approach can be applied using other models if the form of the transient sandface temperature signal is known. The parameters C1 to C7 are used as the optimization parameters in our work.

$$T_{wb}(t) = T_i + \frac{B\Gamma TQ_{sc}}{2kh}\left(\frac{1-\beta_T T}{C_p\rho}\left[ln\left(\frac{\left(r_w{}^2+2\left[\frac{C_p\rho B\Gamma TQ_{sc}}{\overline{\rho C_p}\mu h}\right]t\right)}{r_w^2}\right)\right]\right) + \frac{B\Gamma TQ_{sc}}{2kh}\left(\frac{\phi\beta_T T}{\overline{\rho C_p}}exp^{\left(-\frac{2\alpha C_p\rho B\Gamma TQ_{sc}}{\overline{\rho C_p}\mu h}\right)}\left[\gamma + ln\left(\frac{\varphi\mu C_t r_w^2}{4\lambda kt}\right)\right]\right) \quad (6\text{-}14)$$

$$C1 = \frac{B\Gamma TQ_{sc}}{2kh} \quad (6\text{-}15)$$

$$C2 = \frac{1-\beta_T T}{C_p\rho} \quad (6\text{-}16)$$

$$C3 = r_w{}^2 \quad (6\text{-}17)$$

$$C4 = 2\left[\frac{C_p \rho B \Gamma T Q_{sc}}{\overline{\rho C_p} \mu h}\right] \quad (6\text{-}18)$$

$$C5 = \frac{\phi \beta_T T}{\overline{\rho C_p}} \quad (6\text{-}19)$$

$$C6 = \frac{\varphi \mu C_t}{4\lambda k} \quad (6\text{-}20)$$

$$C7 = T_i \quad (6\text{-}21)$$

$$T_{wb}(t) = C7 + C1\left(C2\left[ln\left(\frac{(C3+C4\cdot t)}{C3}\right)\right]\right) + C1\left(C5 \cdot exp^{(-C6\cdot C4)}\left[\gamma + ln\left(\frac{C6\cdot C3}{t}\right)\right]\right) \quad (6\text{-}22)$$

The above terms are defined in Nomenclature at the end of this chapter.

6.4 Reconstruction of Sandface Temperature

The second approach involves reconstructing the sandface temperature by using existing analytical models as well as numerical models (see for example the analytical models discussed in Section 6.1). The Duru model which includes the effect of varying sandface temperature will be used in this study. As discussed previously the accuracy of the reconstructed sandface temperature depends on the accuracy of the wellbore model. Some of the parameters in the wellbore model can be estimated accurately, while others cannot be estimated sufficiently accurately apriori. This is because these properties change during the life of the well or the production period. Duru's thermal wellbore model is based on the Ramey's solution which made assumptions when developing the time functions. These time functions also affect the accuracy of the model and the reconstructed sandface temperature (as discussed in Section 6.2).

6.4.1 Thermal Characterization of Wellbore Using a Numerical Wellbore Simulator

Section 6.1 discussed how the parameters of the wellbore model are uncertain. However they can be deduced by using the warm-up period temperature measurement at the gauge or when simultaneous temperature measurements are taken at the sandface and gauge.

Known sandface and gauge temperature. This information is obtained by simultaneously measuring the sandface and gauge temperatures with a production logging tool and a permanent gauge. Alternatively, the warmup period (i.e. period before the temperature front reaches the gauge location, and the gauge temperature stabilises) temperature measured by the gauge can be used for this purpose. The accuracy of this approach is not as good as the pervious one, however, it can reduce the uncertainty in the wellbore model parameters.

Warm up period data can be very valuable, because the duration of this period increases with the distance of the gauge from the sandface. Therefore, a considerable warmup period is expected for situations where wellbore effects are significant and cannot be ignored.

The information contained in this period is independent of the sandface temperature; but it does depend on the flowrate and the formation thermal conductivity { Figure 6-6(c) and 6-6(d)}. The plots in Figure 6-6 are for a gauge is located 500 m from the sandface. The slope and the peak temperature of the warmup period is independent of the sandface temperature; while the peak temperature is affected by the formation thermal conductivity and the slope is only affected by the flow rate and geothermal gradient.

Important wellbore parameters that can be estimated include:

1. *Formation thermal conductivity*: this parameter is not normally available.

2. *Initial geothermal gradient*: the well shut-in temperature profile might change after a long period of production, biasing the value from the undisturbed geothermal condition.

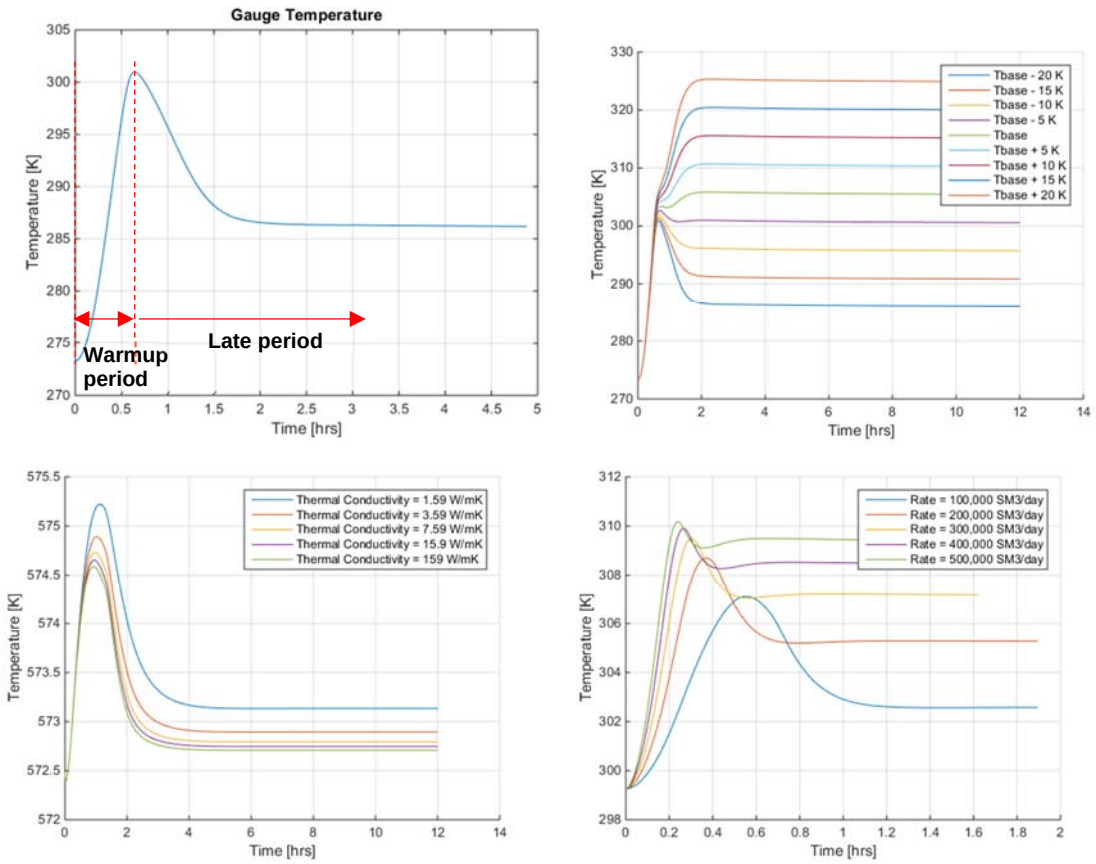

Figure 6-6: (a) Measured gauge signal showing warmup period (b) Effect of sandface temperature on warmup temperature signal (c) Effect of formation thermal conductivity on warmup temperature signal (d) Effect of flow rate on warmup temperature signal.

Figures 6-7 shows the results from two thermal characterizations using different well start-up flow rates (50,000 m^3/day and 800,000 m^3/day). The optimiser used was a simplex search method by (Lagarias et al. 1998) implemented in Matlab. The formation conductivity and geothermal gradient parameters were varied until the observed and the numerical gauge temperatures converge. Fast convergence after about 100 iterations was achieved regardless of the gas flow rate. The parameters also converge to the same values for the different flow rates. Figure 6-8 repeats the study with a fixed flow rate but with different sandface temperatures.

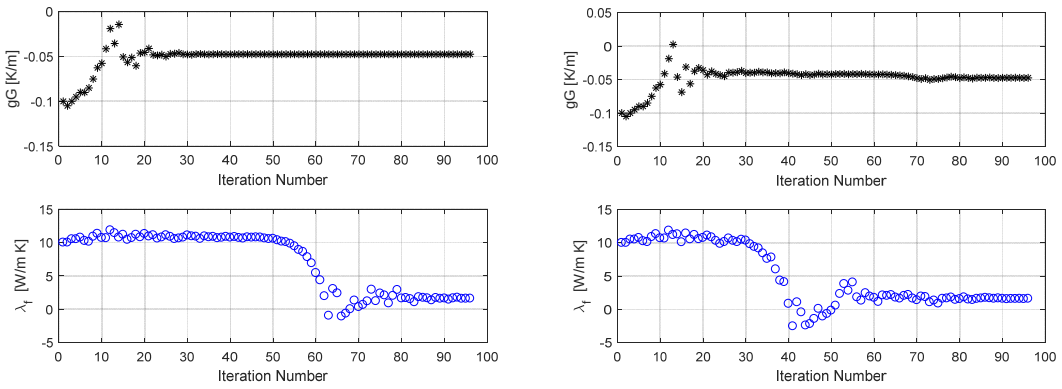

Figure 6-7: Plot showing estimation of geothermal gradient and formation thermal conductivity using the warmup period for (a) Qsc = 50,000 m^3/day (b) Qsc = 800,000 m^3/day

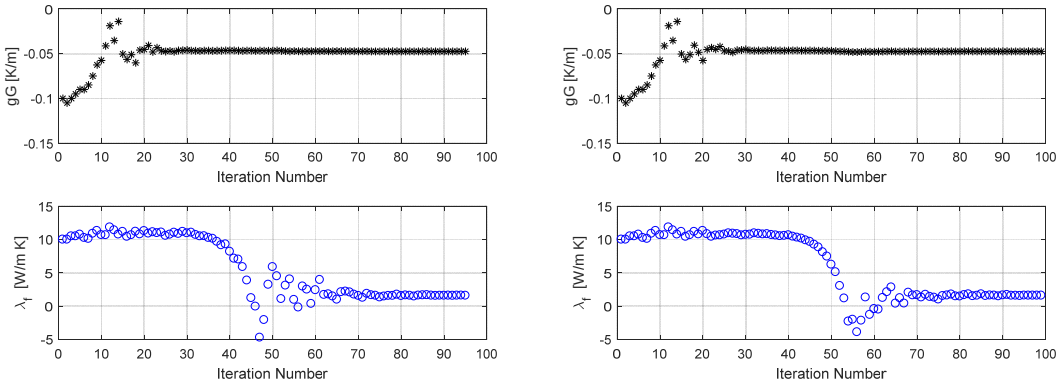

Figure 6-8: Plot showing estimation of geothermal gradient and formation thermal conductivity using the warmup period for Qsc = 200,000 m^3/day (a) Sandface temperature = $T_{base} - 10K$ (b) Sandface temperature = $T_{base} + 10K$

The result from the characterization is shown in Table 6-2 below. It shows that the value of the sandface temperature does not affect the thermal characterization of the wellbore with accurate results being obtained irrespective of the magnitude of the measured sandface temperature.

Characterizing the wellbore model makes it possible to invert this (now more accurate) wellbore model in order to reconstruct the sandface temperature when only the gauge temperature is known (measured). The inversion can either be carried out analytically or by use of a non-linear regression algorithm which minimizes the mismatch between the observation and the numerically or analytically modelled temperature. The various objective functions that can be used for the optimisation and their implications were

discussed in the previous section. The nonlinear regression approach will be considered in this work, first by using a transient thermal wellbore simulator as the wellbore model, and then by using the analytical wellbore heat transmission model by Duru.

Table 6-2: Result of wellbore characterization using warm-up period and different fluid inflow temperatures

Sandface Temperature	**Property**	**Value at start of optimization**	**Value at end of optimization**	**Actual value**
$T_{base} - 10K$	Geothermal gradient [K/m]	0.1	-0.0474	-0.0474
	Thermal conductivity [W/mK]	10	1.589	1.59
$T_{base} + 10K$	Geothermal gradient [K/m]	0.1	-0.0474	-0.0474
	Thermal conductivity [W/mK]	10	1.588	1.59

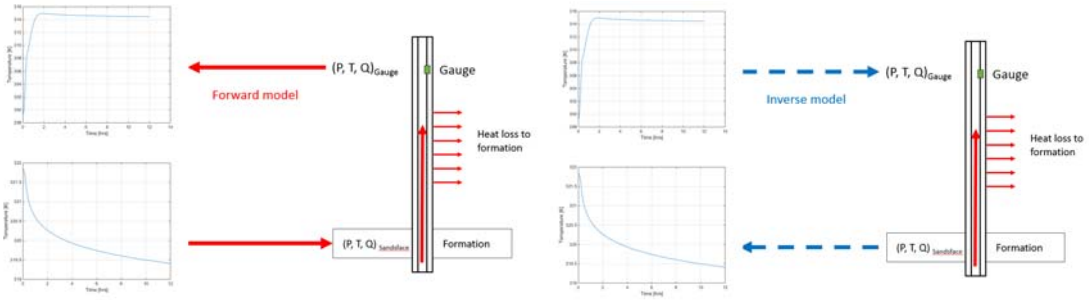

Figure 6-9: Schematic showing input and outputs of (a) Forward model (b) Inverse model

6.4.2 Reconstruction of Sandface Temperature Using a Numerical Wellbore Simulator

The method of reconstructing the sandface temperature is similar to that used for thermal characterization of the wellbore with the difference being that, the wellbore model is accurately defined while the sandface temperature is unknown.

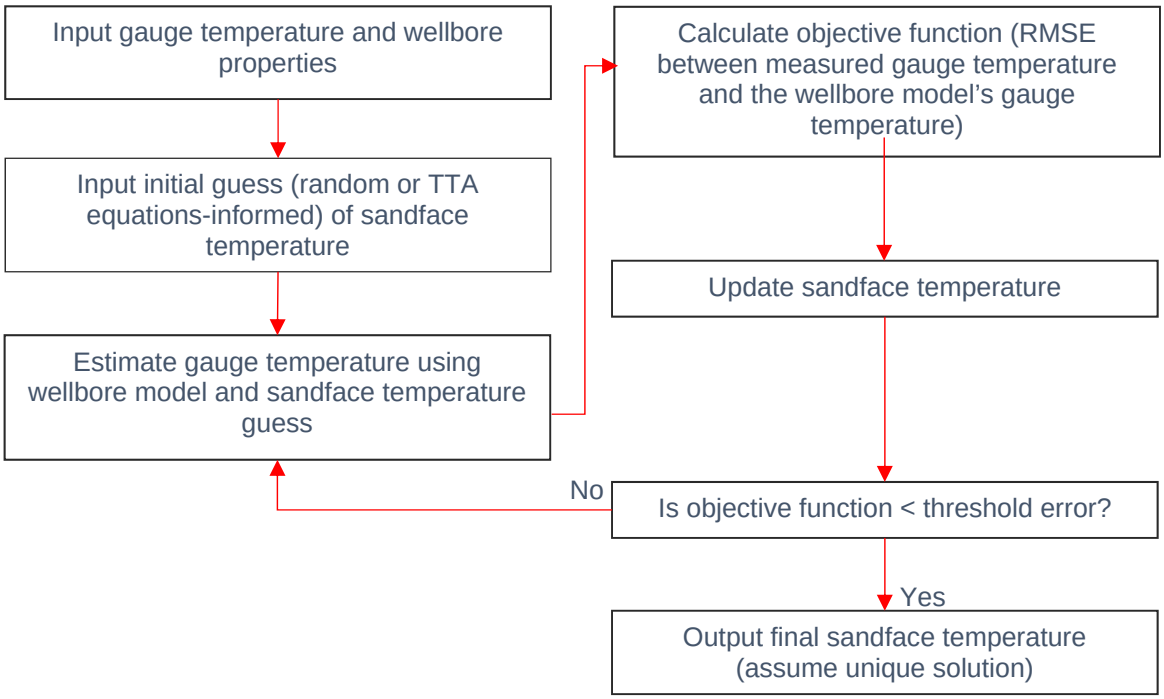

Figure 6-10: Flowchart for sandface temperature reconstruction.

The above workflow reconstructed the sandface temperature from a given gauge temperature. The slope of the reconstructed sandface temperature matched that of the actual sandface temperature. This is important because TTA, similar to PTA, makes extensive use of the derivative of the transient measurement. However, the reconstructed sandface temperature did not match the early time period accurately. This effect is still currently under investigation with the objective of being able to (1) accurately match the entire signal, (2) determine the uniqueness of the solution and (3) evaluate how accurately the wellbore model must be known for an accurate solution.

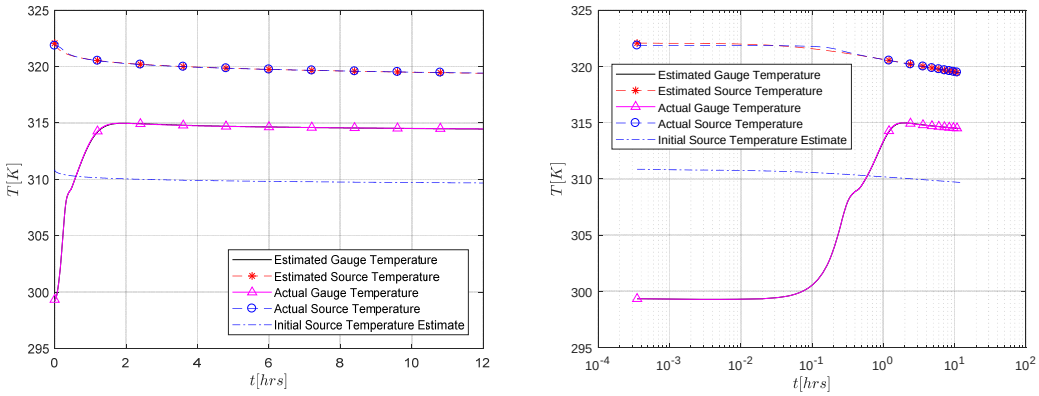

Figure 6-11: Reconstructed sandface temperature, gauge temperature and actual sandface temperature for (a) Normal time scale (b) Logarithmic time scale

6.4.3 Reconstruction of Sandface Temperature using Duru's Model

6.4.3.1 Analytical Inversion

The forward model by Duru & Horne (2010) can also be inverted to reconstruct the sandface temperature from the gauge temperature. The inversion of this model can be done analytically or numerically using a non-linear regression algorithm. The analytical inversion is a trivial process, but the inverse equation (Equation 6-23), has some limitations.

$$T_{fin} = T_{ein} + \left\{\left[1 - e^{(z-L)L_R}\right]\left[g_G \sin\theta + \psi - \frac{g\sin\theta}{C_p J g_c}\right] - \frac{(T_f - T_{ei})L_R}{1-e^{-aL_R t}}\right\} e^{(L-z)L_R}/L_R \qquad (6\text{-}23)$$

The first limitation is the sensitivity to the measured gauge temperature. Since Equation 6-23 indicates the sandface temperature is an exponential function of $(L-z)L_R$. So the formation properties-dependent relaxation distance, L_R, has an exponential effect on the reconstructed sandface temperature of up to several orders of magnitude. The result is a model that is intolerant to gauge measurement errors -something that cannot be avoided in reality. Figure 6-12 shows the sensitivity of the predicted sandface temperature to gauge errors (Equation 6-24).

$$\frac{\partial T_{fin}}{\partial T_f} = \frac{e^{(L-z)L_R}}{(1-e^{-aL_R t})} \qquad (6\text{-}24)$$

The second limitation is that the magnitude of the term $(e^{(L-z)L_R})$ exceeds the range of double precision floating point numbers (FP64); making it impossible to reconstruct the sandface temperature for large gauge distances at early time.

Finally, Duru's model, being based on Ramey's work, will overestimate the wellhead temperature during the early transient period with low values of Fourier time (Hagoort 2004). This difficulty in matching the early time temperature makes it impossible to use the early time temperature data for well characterization before reconstructing the sandface temperature.

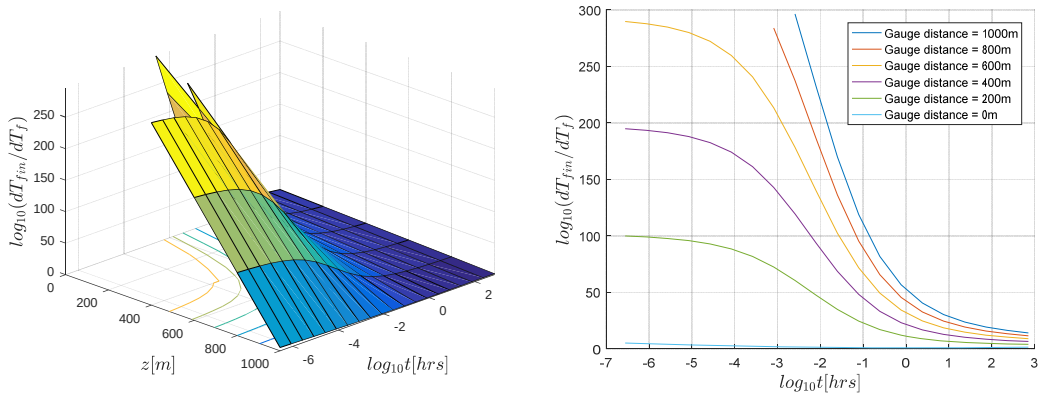

Figure 6-13: (a) Surface plot of $\frac{\partial T_{fin}}{\partial T_f}$ over different gauge distances and time (b) Line plot of $\frac{\partial T_{fin}}{\partial T_f}$ over different gauge distances and time

6.4.3.2 Numerical Inversion

Analytical inversion was shown above to be impractical because the reconstructed sandface temperature is highly sensitive to the errors in the measured gauge temperature, the floating-point number limit is exceeded and the early time overestimation of the wellbore temperature. The analytical equation can be inverted numerically, eliminating both the sensitivity and the floating-point limitations, though it does not eliminate the effect of the early time overestimation errors. The numerical inversion is more robust because it uses the forward model (Equation 6-1), which includes the term $e^{(z-L)L_R}(T_{fin} - T_{ein})(1 - e^{-aL_R t})$, resulting in a value that tends to zero for large gauge distances. By contrast, the inverse model includes the term $[(T_f - T_{ei})e^{(L-z)L_R}]/(1 - e^{-aL_R t})$ whose value tends to infinity for large gauge distances; resulting in undefined values for the inverse model.

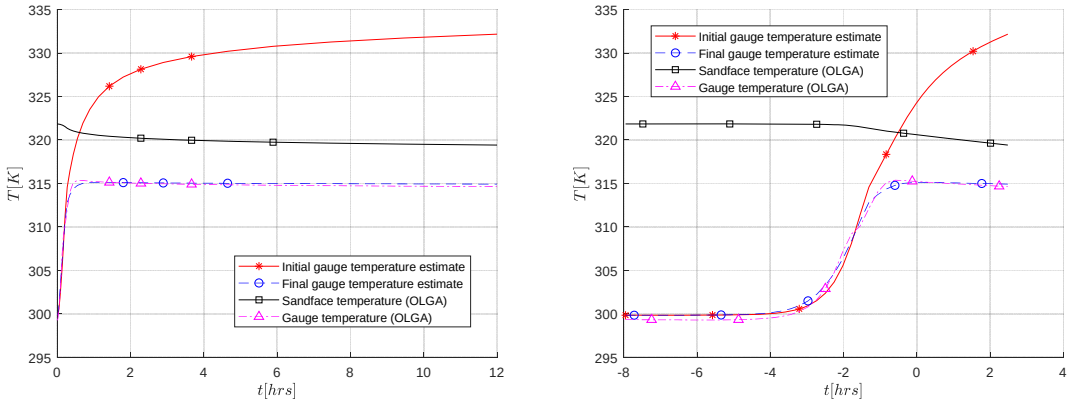

Figure 6-13: Result of wellbore model characterization (using Duru's model) showing gauge temperature based on the initial and final guess of wellbore model parameters (a) Normal time scale (b) Logarithmic time scale

The wellbore characterization used Duru's analytical wellbore model, while the sandface and gauge data were obtained from OLGA™. The result show that Duru's model was able to reproduce the OLGA™ gauge temperature accurately. The wellbore parameters obtained from this step (see Table 6-3) were then used for the sandface temperature reconstruction. While these values do not necessarily represent the actual values of the wellbore properties, they are however the combination of parameters that produce a thermal wellbore model which mimics the actual wellbore (in this case OLGA™).

Table 6-3: Result of wellbore characterization using Duru's analytical wellbore model and entire temperature signal

Parameter	**Initial estimate**	**Final estimate**	**Unit**
Formation thermal conductivity	5	65.5799	W/mK
Geothermal gradient	0.1	-0.6195	K/m
Specific heat capacity of formation	2000	1.6298e-8	J/kgK
Heat storage	3	0.2123	
Joule-Thomson coefficient of fluid	1e-5	-7.3374e-4	$/K$
Overall heat transfer coefficient of fluid	500	6.3099e3	W/m^2K

A similar approach to the previous section is used with Duru's model replacing the OLGA™ numerical simulator. This approach proved to be faster with Duru's model providing a good match for the slope (Similar to the sandface temperature reconstruction by OLGA™), but the early time period did not accurately match the actual sandface temperature (Figure 6-14). The first step in the sandface temperature reconstruction involved a wellbore characterization but, unlike the numerical case, the characterization was carried out using simultaneous sandface and gauge temperature measurements (see

results of characterization in Figure 6-13). This is because of the over estimation errors in the Duru's model at early time.

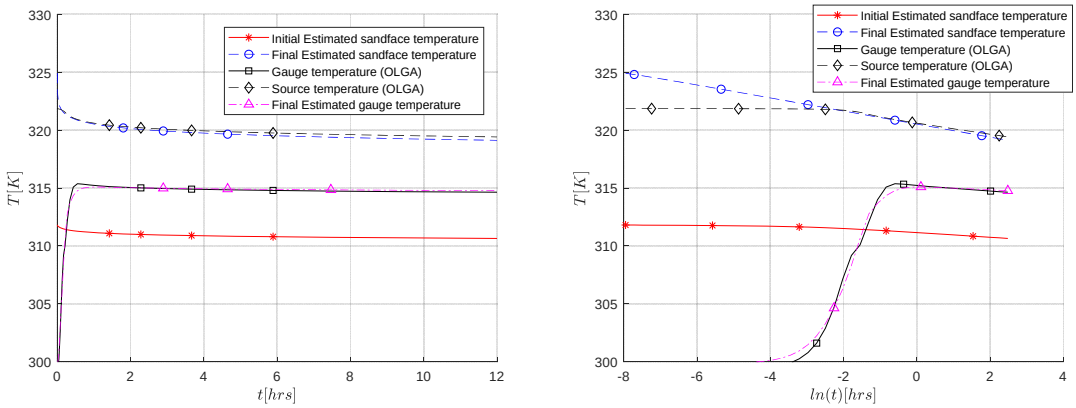

Figure 6-14: Result of sandface temperature reconstruction (using Duru's model) showing initial and final guess of sandface temperature (a) Normal time scale (b) Logarithmic time scale

The logarithmic slope of the reconstructed sandface temperature was found to be -0.5647 K/ln(s) While that of the original sandface temperature was -0.5162 K/ln(s) This shows a great improvement in accuracy when compared with the slope of the measured gauge transient temperature (-0.2286 K/ln(s).).

6.5 Guidelines for Minimizing Heat Transmission Effect

It is also possible to design or operate the well in a way that minimizes the heat transmission effect, therefore reducing the attenuation of the transient temperature signal. These two approaches are discussed below and guidelines for achieving this is also provided. While it might be impossible to eliminate the heat transmission effect completely, minimizing it such that it has a negligible effect on TTA is preferred to sandface temperature reconstruction. The gauge can be installed sufficiently close to the sandface for a given production rate and properties of the fluid, well completion and formation. Alternatively, the well can be operated at a production rate that minimizes the heat transmission effect for the installed gauge/sandface distance.

$$N_{Ra} = \frac{2\pi\lambda_f L}{C_P w} \qquad (6\text{-}25)$$

λ_f : Thermal conductivity of formation around wellbore $[W/mK]$

L : Distance from sandface to gauge $[m]$

C_P : Specific heat capacity of fluid $[kJ/kgK]$

w : Mass flowrate of fluid $[kg/s]$

Equation 6-25 is the dimensionless Ramey's number. This is a number that expresses the ratio of heat conducted away from the wellbore (into the formation surrounding the wellbore) to the heat convected by the fluid in the wellbore. This number is a direct indication of the degree of attenuation of the transient temperature signal. A low Ramey number indicates a low attenuation of the transient temperature signal and vice versa.

6.5.1 Estimation of Rate Required to Minimize Heat Transmission Effects

(Hagoort 2004) showed the effect of Ramey number on wellhead temperature shown in Figure 6-15, the plot of wellhead temperature against the dimensionless Fourier time (Equation 6-26) for different values of Ramey number. Based on this it is suggested that in situations where the Ramey number is less than 0.05, the effect of wellbore heat transmission can be neglected.

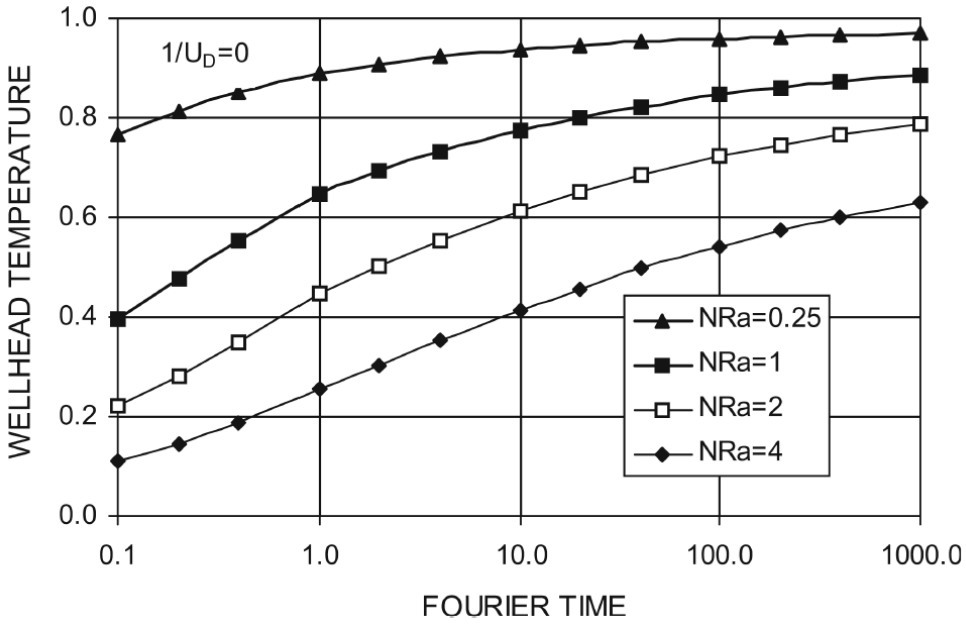

Figure 6-15 Plot of wellhead temperature against Fourier number for different values of Ramey Number (Hagoort 2004)

$$t_{DFo} = \frac{\lambda_f t}{\rho C_P {r_{cf}}^2} \qquad (6\text{-}26)$$

ρ : Density of the fluid $[kg/m^3]$

r_{cf} : Radius of formation inner boundary (at interface of cement zone and formation) $[m]$

t : Time$[s]$

When creating transients events for TTA, the following guidelines can be followed;

1. When creating a transient drawdown event from well shut-in, a high enough rate change should be created, as this would result in a reduced value of the Ramey number.

2. When creating a transient drawdown event from a producing well, the sum of the additional rate increase and the original rate should result in a total rate that achieves the desired Ramey number.

3. The rate change required to achieve the desired Ramey number can be estimated from Equation 6-25.

6.5.2 Estimation of Gauge Distance to Minimize Heat Transmission Effect

The maximum gauge distance required to minimize the heat transmission effect (i.e. Ramey number ≤ 0.05) can be estimated for the expected flowrate in the well by using Equation 6-25, i.e. a similar method as that used to estimate the rate required to minimize the heat transmission effect. This estimation is invaluable in the design of new well completions where TTA is planned.

6.6 Conclusion

Most TTA algorithms and workflows were developed using transient sandface solutions. However, the transient temperature is rarely measured at the sandface but at some distance from the sandface, which results in errors in the TTA or, at times, makes TTA impossible. This occurs because the measured temperature data includes the effects of wellbore heat transmission, which was not included in earlier TTA models. Accurate TTA requires that all effects due to wellbore heat transmission have to be accounted for or corrected for prior to carrying out the TTA.

This work investigated different methods of mitigating the "distant gauge problem". Guidelines have been developed that can be used to operate the well such that the heat transmission effect is minimized and the measured gauge temperature is as close as possible an approximation of the sandface temperature. Methods for reconstructing the sandface temperature from the measured gauge temperature have been fully described. These sandface temperature reconstruction methods will prove invaluable in situations where the analysis of the measured transient temperature signal using the current "sandface TTA" equations yield erroneous solution.

Case studies applying both numerical and analytical wellbore models for the sandface temperature reconstruction have been presented and the limitations and advantages of the different approaches were highlighted.

6.7 Nomenclature

$\boldsymbol{\Lambda}$: Vector of weights for scaling the error at each time [ ]

λ : Constant parameter [ ]

λ_f : Thermal conductivity of formation $[W/mK]$

ϕ : Porosity of formation [ ]

ρ : Fluid density $[kg/m^3]$

μ : Fluid viscosity [$Pa.s$]

ρ_e : Density of the formation around the wellbore [kg/m^3]

θ : Well inclination from horizontal [ ]

C_P : Specific heat capacity of fluid [J/kgK]

C_{pe} : Specific heat capacity of the formation around the wellbore [J/kgK]

g : Acceleration due to gravity [m/s^2]

$f(t)$: Time function [ ]

g_G : Geothermal gradient [K/m]

h : Formation thickness [m]

k : Permeability of formation [m^2]

k_e : Thermal conductivity of the formation (or earth) [W/mK]

L : Length of well [m]

L_R : Relaxation distance [m]

Q_{sc} : Surface production rate [m^3/s]

r_{cf} : Radius of cement-formation contact point [m]

r_{ti} : Internal radius of tubing [m]

r_w : Well radius $[m]$

t_{DFo} : Dimensionless Fourier number [ ]

ts : Scaled time vector $[s]$

T_D : Dimensionless time function [ ]

T_{ei} : Undisturbed earth temperature $[K]$

T_{ein} : Undisturbed earth temperature at location of inflow from reservoir $[K]$

T_f : Fluid temperature at specified depth in the wellbore $[K]$

T_{fin} : Fluid temperature at location of inflow from reservoir $[K]$

U : Overall heat transfer coefficient $[W/K]$

U_{to} : Overall heat transfer coefficient of the outer boundary of the tubing $[W/K]$

w : Mass flow rate in well $[kg/s]$

6.8 Abbreviations

BHT: Bottomhole temperature

PTA: Pressure transient analysis

PID: Proportional-integral-derivative

TTA: Temperature transient analysis

RMSE: Root mean squared error

FP64: 64 bits precision floating point number

Chapter 7: Discussions, Conclusions and Future Work

7.1 Conclusions

This work presents analytical solutions, interpretation workflows and models or guidelines for carrying out temperature transient analysis in dry gas producing wells. These results would make analysis of transient temperature in dry gas wells possible and is also a major advancement in the development of a full-fledged multiphase TTA method which can be applied to a wider category of wells including ones where the gauge is installed distant from the producing layer .The conclusions are summarised below for the major work carried out.

7.1.1 Transient Temperature Solutions for Vertical Dry Gas Producing Wells (Chapter 3)

An analytical solution was developed for predicting the sandface transient temperature in a vertical dry gas producing wells:

1. The analytical solution was developed by making reasonable assumptions (obtained by using a numerical simulator). The prediction from this analytical solution was compared against the results from a full numerical simulation with a reasonable match obtained between the two.

2. The derived solution is for an infinite acting radial flow regime, hence a deviation was observed between the numerical and analytical solutions when the pressure signal reaches the lateral boundary of the reservoir.

3. Appropriate pressure and temperature conditions for estimating the gas properties to be used in the analytical solution were also recommended. The initial temperature and an average pressure condition, obtained from the initial pressure and the stabilized pressure, was found to produce the most accurate result.

4. The effect of non-Darcy flow was considered and its limitations on the derived solution (based on the assumption of Darcy flow) was discussed.

5. Synthetic and real case studies were presented to demonstrate the application of the developed solutions.

7.1.2 TTA Workflows for Vertical Dry Gas Producing Wells (Chapter 4)

An analysis workflow was developed based on a simplified form of the derived analytical solution for vertical gas wells:

1. A (semi-log) linear form of the analytical solution derived in Chapter 3 was developed. An equation was also presented for estimating the time after which the transient temperature signal is effectively approximated by the linear equation.

2. Analysis workflows for estimating permeability-thickness, rate, fluid property and for near wellbore analysis were developed using the linear form of the analytical solution. Though the workflow developed is based on Darcy flow, it was demonstrated that it can be applied in many practical cases because the impact of non-Darcy effects on the transient temperature slope, which is used for TTA, are minimal.

3. The limitation in estimating the permeability-thickness (KH) of the virgin formation in the presence of near-wellbore damage was investigated. It was observed that the estimated virgin formation KH is an average of that of the near-wellbore damage zone and the virgin formation. This finding can provide some guidance when using the TTA methods in wells with near-wellbore damage.

4. The developed workflows were applied to synthetic and field transient temperature data, demonstrating the value of the proposed workflow for estimating the properties of the producing layer and for investigating the properties of the near wellbore region.

7.1.3 Transient Temperature Solutions for Horizontal Dry Gas Producing Wells (Chapter 5)

New analytical and semi-analytical solutions were developed for transient sandface temperature in dry gas producing horizontal wells:

1. Analytical solutions for transient temperature was developed for planar flow (i.e. flow into a vertical fracture) with semi-infinite and constant pressure lateral boundaries.

2. A simplified solution for transient sandface temperature was developed for the planar flow case with semi-infinite lateral boundary. This simplified solution would make application to TTA easier and faster.

3. The effect of flow convergence into a wellbore was investigated by comparing a semi-analytical solution for a line sink (with semi-infinite lateral boundaries) with the developed planar solutions. A significant difference was observed between the transient temperature slopes for both cases. The reason for this was found to be due to the difference in pressure gradients at the sandface, with the flow into the wellbore (or line sink) having a pressure gradient about one order of magnitude greater than the planar flow case.

4. Finally, the effect of heat conduction between the producing layer and the surroundings was considered and it was observed that, for the typical TTA duration, this effect can be neglected.

7.1.4 Mitigation of the Remote Gauge Problem in Temperature Transient Analysis (Chapter 6)

The effect of using transient temperature data measured by a gauge located at a remote location was investigated and method were proposed to either reduce this effect or correct the measured temperature for this effect:

1. Guidelines were presented that can be used to design or operate a well such that the distant gauge effect is minimized and the accuracy of the resulting TTA is acceptable.

2. Methods for correcting the measured gauge temperature for the thermal wellbore effects (i.e. reconstructing the sandface temperature) were presented. The sandface temperature reconstruction method relies heavily on the accuracy of the

thermal wellbore model. The sandface temperature reconstruction was demonstrated using both analytical and numerical thermal wellbore models.

3. A thermal wellbore characterization method for improving the accuracy of the thermal wellbore model was also presented. This is important when some of the thermal properties of the well are either not available or when they vary over the life of the well. This thermal wellbore characterization was observed to improve the results of the sandface temperature reconstruction.

7.2 Future Work

The development of a comprehensive TTA algorithm is of paramount importance in order to increase the value-added by advanced well completions. The results presented in this thesis are a significant contribution in achieving this (i.e. a comprehensive TTA algorithm). However, there is more to be done in order to achieve this goal, and some of these are proposed below:

1. Extensive application / testing of the developed workflows on real data. Although the results of the real case study presented in Chapters 3 and 4 are satisfactory it is still necessary to apply the developed methods to more real case scenarios. Doing this would give more credence to the methods, and also help in flagging potential challenges which engineers might face while applying the workflows.

2. (Mao & Zeidouni 2017a) proposed a method for correcting for non-Darcy effect by adjusting the gas property for the additional pressure drop due to the non-Darcy effect. Investigate the possibility of using this method to correct for the non-Darcy effect in TTA for gas wells.

3. Section 4.7 identified a limitation in the estimation of the permeability-thickness of the virgin formation in the presence of near wellbore damage. Therefore, it would be necessary to develop a method for extracting the actual virgin formation properties from the effective formation properties. Having such would increase the accuracy of estimating the properties of the virgin formation in different scenarios and also increase the certainty of the results obtained from such analysis.

4. The effect of flow convergence into the wellbore of a horizontal well was mentioned in Chapter 5 (Section 5.6) this effect has to be properly investigated and methods developed for correcting the TTA method for this effect.

5. The effect of anisotropy also needs to be investigated and solutions and analysis workflows capable of handling anisotropic reservoirs should be developed.

6. The effect of heterogeneity should be investigated. Since the TTA methods presented here (and in most publications) assume a homogeneous reservoir, it is important to determine if the homogenous assumption is a good approximation for the temperature response in a heterogeneous reservoir.

7. All the developed workflows assume a homogenous reservoir, which is far from the case in reality. However, the heterogeneity might have a homogenous response in some cases, making it possible to use a homogenous model for the TTA of such reservoirs. A detailed study which considers the impact of heterogeneity on TTA and also develops correlations which can be used to reduce a heterogeneous reservoir response to an analogous homogenous one would also be necessary.

8. The developed workflows focused on dry gas producing wells. Since there are already existing models and workflows for liquid wells, it is necessary to integrate these two (i.e. liquid and gas TTA methods) to produce a TTA method capable of analysing transient temperature data from a well producing liquid and gas phases.

9. The wellbore characterization and sandface temperature reconstruction has been tested using numerical wellbore models, but these also need to be tested using real well data to validate its potential to reconstruct the sandface temperature in a real production well. This might require building more detailed and sophisticated wellbore models if necessary.

References

Abou-Kassem, J.H. & Dranchuk, P.M., 1982. Isobaric Heat Capacities of Natural Gases at Elevated Pressures and Temperatures. In *Proceedings of SPE Annual Technical Conference and Exhibition*. Society of Petroleum Engineers.

Ahmed, T., 2006. *Reservoir Engineering Handbook* 3rd ed., Gulf Professional Publishing.

Al-Hadhrami, a. K., Elliott, L. & Ingham, D.B., 2003. A new model for viscous dissipation in porous media across a range of permeability values. *Transport in Porous Media*, 53(1), pp.117–122.

Al-Hussainy, R., Ramey Jr., H.J. & Crawford, P.B., 1966. The Flow of Real Gases Through Porous Media. *Journal of Petroleum Technology*, 18(5), pp.624–636.

Al-Khelaiwi, F.T.M., 2013. *A comprehensive approach to the design of advanced well completions (vol 1)*. Heriot-Watt University.

Al-Shammari, H.H., 2014. Intelligent Well Completions Performance and Reliability in the Northern Fields of Saudi Aramco. In *International Petroleum Technology Conference*. International Petroleum Technology Conference.

App, J.F., 2010. Nonisothermal and Productivity Behavior of High-Pressure Reservoirs. *SPE Journal*, 15(01), pp.50–63.

App, J.F., Energy, C. & Company, T., 2013. SPE 166298 Influence of Hydraulic Fractures on Wellbore/Sandface Temperatures During Production. In *SPE Annual Technical Conference and Exhibition*. Society of Petroleum Engineers, pp. 1–14.

App, J.F. & Yoshioka, K., 2011. Impact of Reservoir Permeability on Flowing Sandface Temperatures; Dimensionless Analysis. In *SPE Annual Technical Conference and Exhibition*. Society of Petroleum Engineers.

Bahrami, H. & Siavoshi, J., 2007. Application of Temperature Transient Analysis In Well Test Interpretation For Gas Wells. In *Proceedings of Asia Pacific Oil and Gas Conference and Exhibition*. Society of Petroleum Engineers.

Bellarby, J., 2009. *Well completion design*, Elsevier.

Benedict, M., Webb, G.B. & Rubin, L.C., 1942. An empirical equation for thermodynamic properties of light hydrocarbons and their mixtures: II. Mixtures of methane, ethane, propane, and n-butane. *The Journal of Chemical Physics*, 10(12), pp.747–758.

Birchenko, V.M., 2010. *Analytical modelling of wells with inflow control devices.* Heriot-Watt University.

Bird, R.B., Lightfoot, E.N. & Stewart, W.E., 2007. *Transport phenomena*, John Wiley & Sons.

Bostick III, F.X., 2003. Commercialization of Fiber Optic Sensors for Reservoir Monitoring. In *Offshore Technology Conference*. Offshore Technology Conference.

Brekke, K. & Lien, S.C., 1994. New and Simple Completion Methods for Horizontal Wells Improve the Production Performance in High-Permeability, Thin Oil Zones. *SPE Drilling & Completion*, 9(03), pp.205–209.

Carr, N.L., Kobayashi, R. & Burrows, D.B., 1954. Viscosity of Hydrocarbon Gases

Under Pressure. *Journal of Petroleum Technology*, 6(10), pp.47–55.

Carslaw, H.S. & Jaeger, J.C., 1959. *Conduction of heat in solids* 2nd ed., Oxford: Clarendon Press.

Chekalyuk, E.B., 1965. Thermodynamics of oil formation. *Nedra, Moscow*, 1(1).

Chen, Y., Ma, G. & Wang, H., 2018. Heat extraction mechanism in a geothermal reservoir with rough-walled fracture networks. *International Journal of Heat and Mass Transfer*, 126, pp.1083–1093.

Chevarunotai, N., Hasan, A.R. & Kabir, C.S., 2015. Transient Flowing-Fluid Temperature Modeling in Oil Reservoirs for Flow Associated with Large Drawdowns. In *SPE Annual Technical Conference and Exhibition*. Society of Petroleum Engineers.

Clonts, M.D. & Ramey, H.J., 1986. Pressure Transient Analysis for Wells With Horizontal Drainholes. In *SPE California Regional Meeting*. Society of Petroleum Engineers.

CMG GEM, 2012. GEM User's Guide.

Courant, R., Friedrichs, K. & Lewy, H., 1967. On the Partial Difference Equations of Mathematical Physics. *IBM Journal of Research and Development*, 11(2), pp.215–234.

Dada, A. et al., 2017. Numerical and analytical modelling of sandface temperature in a dry gas producing well. *Journal of Natural Gas Science and Engineering*, 40, pp.189–207.

Dada, A., Muradov, K. & Davies, D., 2017. Temperature transient analysis models and workflows for vertical dry gas wells. *Journal of Natural Gas Science and Engineering*, 45, pp.207–229.

Dada, A.O., Muradov, K.M. & Davies, D.R., 2016. Novel Solutions and Interpretation Methods for Transient, Sandface Temperature in Vertical, Dry Gas Producing Wells. In *SPE Intelligent Energy International Conference and Exhibition*. Society of Petroleum Engineers.

Dranchuk, P.M. & Abou-Kassem, J.H., 1975. Calculation of Z Factors for Natural Gases Using Equations of State. *Journal of Canadian Petroleum Technology*, 14(3), pp.34–36.

Duru, O. & Horne, R., 2008. Modeling Reservoir Temperature Transients and Matching to Permanent Downhole Gauge Data for Reservoir Parameter Estimation. In *Proceedings of SPE Annual Technical Conference and Exhibition*. Society of Petroleum Engineers.

Duru, O. & Horne, R., 2010. Modeling Reservoir Temperature Transients and Reservoir-Parameter Estimation Constrained to the Model. *SPE Reservoir Evaluation & Engineering*, 13(6), pp.873–883.

EerNisse, E.P., 2001. Quartz Resonators vs Their Environment: Time Base or Sensor? *Japanese Journal of Applied Physics*, 40(Part 1, No. 5B), pp.3479–3483.

EerNisse, E.P., Ward, R.W. & Wiggins, R.B., 1988. Survey of quartz bulk resonator sensor technologies. *IEEE Transactions on Ultrasonics, Ferroelectrics and Frequency Control*, 35(3), pp.323–330.

Elfrink, E.B., Sandberg, C.R. & Pollard, T.A., 1949. A New Compressibility

Correlation for Natural Gases and Its Application to Estimates of Gas-In-Place. *Journal of Petroleum Technology*, 1(08), pp.219–223.

Eltaher, E.K. et al., 2014. Autonomous Inflow Control Valves - their Modelling and Added Value. In *SPE Annual Technical Conference and Exhibition*. Society of Petroleum Engineers.

Eltaher, E.M.K., 2017. *Modelling and applications of autonomous flow control devices*. Heriot-Watt University.

ERCB, 1979. *Gas Well Testing , Theory and Practice*, Alberta: Energy Resources Conservation Board.

Van Everdingen, A.F. & Hurst, W., 1949. The Application of the Laplace Transformation to Flow Problems in Reservoirs. *Journal of Petroleum Technology*, 1(12), pp.305–324.

Firoozabadi, A., 1979. An Analysis of High-Velocity Gas Flow Through Porous Media. *Spe*, 31(February), pp.211–216.

Franco, A. & Vaccaro, M., 2014. Numerical simulation of geothermal reservoirs for the sustainable design of energy plants: A review. *Renewable and Sustainable Energy Reviews*, 30, pp.987–1002.

Gander, W. & Gautschi, W., 2000. Adaptive Quadrature—Revisited. *BIT Numerical Mathematics*, 40(1), pp.84–101.

Geertsma, J., 1974. Estimating the Coefficient of Inertial Resistance in Fluid Flow Through Porous Media. *Society of Petroleum Engineers Journal*, 14(5), pp.445–450.

van Gisbergen, S.J.C.H.M. & Vandeweijer, A.A.H., 1999. Reliability analysis of permanent downhole monitoring systems. In *Offshore Technology Conference*. Offshore Technology Conference.

Going, W.S., Anderson, A.B. & Vachon, G.P., 2006. Intelligent Well Technology-The Evolution to Closed-Loop Control. In *Offshore Technology Conference*. Offshore Technology Conference.

Goode, P. a., 1987. Pressure Drawdown and Buildup Analysis of Horizontal Wells in Anisotropic Media. *Spe*, 2(December), pp.683–697.

Grebenkin, I.M., 2013. *A new optimisation procedure for uncertainty reduction by intelligent wells during field development planning*. Heriot-Watt University.

Gringarten, A.C. & Ramey, H.J., 1973. The Use of Source and Green's Functions in Solving Unsteady-Flow Problems in Reservoirs. *Society of Petroleum Engineers Journal*, 13(05), pp.285–296.

Hagoort, J., 2004. Ramey's Wellbore Heat Transmission Revisited. *SPE Journal*, 9(4), pp.465–474.

Hasan, A.R. & Kabir, C.S., 2002. *Fluid flow and heat transfer in wellbores*, Society of Petroleum Engineers.

Hasan, A.R., Kabir, C.S. & Lin, D., 2005. Analytic Wellbore Temperature Model for Transient Gas-Well Testing. *SPE Reservoir Evaluation & Engineering*, 8(03), pp.240–247.

Haug, B.T., 1992. The Second Long-Term Horizontal Well Test in Troll: Successful Production From a 13-in. Oil Column With the Well Partly Completed in the

Water Zone. In *SPE Annual Technical Conference and Exhibition*. Society of Petroleum Engineers.

Hubbert, M.K., 1957. Darcy's Law and The Field Equations of The Flow of Underground Fluids. *International Association of Scientific Hydrology. Bulletin*, 2(1), pp.23–59.

Ibeh, C. et al., 2015. The Agbami Digital Oilfield Solution and Reliability Assessment of Intelligent Well Completions. In *Offshore Technology Conference*. Offshore Technology Conference.

Izgec, B. et al., 2007. Placement of Permanent Downhole Pressure Sensors in Reservoir Surveillance. In *EUROPEC/EAGE Conference and Exhibition*. Society of Petroleum Engineers.

Izgec, B. et al., 2006. Transient Fluid and Heat Flow Modeling in Coupled Wellbore/Reservoir Systems. In *SPE Annual Technical Conference and Exhibition*. Society of Petroleum Engineers.

Jasak, H., 1996. *Error Analysis and Estimation for the Finite Volume Method with Applications to Fluid Flows*. Imperial College London (University of London).

Jasak, H., Jemcov, A. & Tukovic, Z., 2007. OpenFOAM : A C ++ Library for Complex Physics Simulations. In *International Workshop on Coupled Methods in Numerical Dynamics*. pp. 1–20.

Juretic, F., 2004. *Error analysis in finite volume CFD*. Imperial College London (University of London).

Konopczynski, M., Ajayi, A. & Russell, L.-A., 2003. Intelligent Well Completion: Status and Opportunities for Developing Marginal Reserves. *Nigeria Annual International Conference and Exhibition*.

Kopaygorodsky, E.M., Krantz, W.B. & Guliants, V. V, 2001. Scaling Analysis–A Valuable Technique in Engineering Teaching and Practice. In *2001 ASEE Annual Conference and Exposition Proceedings*. Citeseer, pp. 24–27.

Kragas, T.K., Turnbull, B.F. & Francis, M.J., 2002. Permanent Fiber Optic Monitoring at Northstar: Pressure/Temperature System and Data Overview. In *SPE Western Regional/AAPG Pacific Section Joint Meeting*. Society of Petroleum Engineers.

Krantz, W., Krantz, W.B. & Manasseh, I., 2007. Scaling analysis as a pedagogical tool in teaching transport and reaction processes.

Kuchuk, F.J. et al., 1991. Pressure-Transient Behavior of Horizontal Wells With and Without Gas Cap or Aquifer. *SPE Formation Evaluation*, 6(01), pp.86–94.

Kutun, K., Tureyen, O. & Satman, A., 2015. Analysis of wellhead production temperature derivatives. *Proceedings, 40th Workshop*.

Lagarias, J.C. et al., 1998. Convergence Properties of the Nelder--Mead Simplex Method in Low Dimensions. *SIAM Journal on Optimization*, 9(1), pp.112–147.

LedaFlow, 2017. LedaFlow advanced transient multiphase flow simulator.

Lien, S.C. et al., 1991. The First Long-Term Horizontal-Well Test in the Troll Thin Oil Zone. *Journal of Petroleum Technology*, 43(08), pp.914–973.

Malakooti, R., 2015. Novel methods for active reservoir monitoring and flow rate allocation of intelligent wells.

Mangani, L., 2008. *Development and Validation of an Object Oriented CFD Solver for Heat Transfer and Combustion Modelling in Turbomachinery Aplications*. Universita degli Studi di Firenze.

Mao, Y. & Zeidouni, M., 2017a. Accounting for Fluid Property Variations in Temperature Transient Analysis. In *SPE Intelligent Oil and Gas Symposium*. Society of Petroleum Engineers.

Mao, Y. & Zeidouni, M., 2017b. Analytical Solutions for Temperature Transient Analysis and Near Wellbore Damaged Zone Characterization. In *SPE Reservoir Characterisation and Simulation Conference and Exhibition*. Society of Petroleum Engineers.

Mao, Y. & Zeidouni, M., 2017c. Near Wellbore Characterization from Temperature Transient Analysis: Accounting for Non-Darcy Flow Effect. In *SPE Symposium: Production Enhancement and Cost Optimisation*. Society of Petroleum Engineers.

Muradov, K., 2010. *Temperature modelling and real-time flow rate allocation in wells with advanced completion*. Heriot-Watt University.

Muradov, K. et al., 2017. Transient Pressure and Temperature Interpretation in Intelligent Wells of the Golden Eagle Field. In *SPE Europec featured at 79th EAGE Conference and Exhibition*. Society of Petroleum Engineers.

Muradov, K. & Davies, D., 2012a. Early-time Asymptotic, Analytical Temperature Solution for Linear Non-adiabatic Flow of a Slightly Compressible Fluid in a Porous Layer. *Transport in Porous Media*, 91(3), pp.791–811.

Muradov, K. & Davies, D., 2013. Some case studies of temperature and pressure transient analysis in Horizontal, multi-zone, intelligent wells. In *EAGE Annual Conference & Exhibition incorporating SPE Europec*. Society of Petroleum Engineers.

Muradov, K. & Davies, D., 2012b. Temperature transient analysis in horizontal wells: Application workflow, problems and advantages. *Journal of Petroleum Science and Engineering*, 92–93, pp.11–23.

NI, 2011. Overview of Fiber Optic Sensing Technologies. Available at: http://www.ni.com/white-paper/12953/en/ [Accessed November 8, 2017].

Odeh, A.S. & Babu, D.K., 1990. Transient Flow Behavior of Horizontal Wells: Pressure Drawdown and Buildup Analysis. *SPE Formation Evaluation*, 5(1), pp.7–15.

Onur, M. & Çinar, M., 2016. Temperature Transient Analysis of Slightly Compressible, Single-Phase Reservoirs. In *SPE Europec featured at 78th EAGE Conference and Exhibition*. Society of Petroleum Engineers.

OpenFOAM Foundation, 2018. OpenFOAM C++ Source Guide. Available at: https://cpp.openfoam.org/v6/ [Accessed August 7, 2018].

OpenFOAM Foundation, 2015. OpenFOAM Progarmmer's Guide. *OpenFOAM Foundation*. Available at: http://foam.sourceforge.net/docs/Guides-a4/ProgrammersGuide.pdf [Accessed July 16, 2015].

OpenFOAM Foundation, 2014. OpenFoam User Guide. *OpenFOAM Foundation*, (December), p.222. Available at: http://www.openfoam.org/docs/ [Accessed July 16, 2015].

Ozkan, E., Raghavan, R. & Joshi, S.D., 1987. Horizontal Well Pressure Analysis. In *SPE California Regional Meeting*. Society of Petroleum Engineers.

P M Dranchuk, R A Purvis & D B Robinson, 1973. Computer Calculation of Natural Gas Compressibility Factors Using the Standing and Katz Correlation. In *Annual Technical Meeting*. Edmonton: Petroleum Society of Canada.

Pendleton, L.E., 1991. Horizontal Drilling Review. In *Archie Conference on Reservoir Definition and Description*. Society of Petroleum Engineers.

Pruess, K., Oldenburg, C.M. & Moridis, G.J., 1999. TOUGH2 user's guide version 2.

Ramazanov, A. et al., 2010. Thermal Modeling for Characterization of Near Wellbore Zone and Zonal Allocation. In *SPE Russian Oil and Gas Conference and Exhibition*. Society of Petroleum Engineers.

Ramey Jr., H., 1962. Wellbore Heat Transmission. *Journal of Petroleum Technology,*, 14(April), pp.427–435.

Reid, R.C., Prausnitz, J.M. & Sherwood, T.K., 1977. *The properties of gases and liquids* 3rd ed., McGraw-Hill.

Sage, B.H. & Lace, W.N., 1941. The Prediction Of The Properties Of Hydrocarbons At Elevated Pressures. *Drilling and Production Practice*.

Schlumberger, 2014. Eclipse technical description 2014.

Schlumberger, 2012. OLGA Dynamic Multiphase Flow Simulator.

Schlumberger, 2008. WellWatcher Real-Time Reservoir and Production Monitoring. Available at: http://www.slb.com/~/media/Files/completions/others/wellwatcher_timeline.pdf.

Shampine, L.F. & Reichelt, M.W., 1997. The MATLAB ODE Suite. *SIAM Journal on Scientific Computing*, 18(1), pp.1–22.

Shaw, J., 2011. Comparison of Downhole Control System Technologies for Intelligent Completions. In *Canadian Unconventional Resources Conference*. Society of Petroleum Engineers.

Standing, M.B. & Katz, D.L., 1942. Density of Natural Gases. *Trans. AIME*, 146, pp.140–149.

Sui, W. et al., 2008. Determining Multilayer Formation Properties From Transient Temperature and Pressure Measurements. In *Petroleum Science and Technology*. Society of Petroleum Engineers, pp. 672–684.

Sui, W. et al., 2010. Determining Multilayer Formation Properties From Transient Temperature and Pressure Measurements in Commingled Gas Wells. In *Petroleum Science and Technology*. Society of Petroleum Engineers, pp. 672–684.

Sui, W. et al., 2008. Model for Transient Temperature and Pressure Behavior in Commingled Vertical Wells. In *SPE Russian Oil and Gas Technical Conference and Exhibition*. Society of Petroleum Engineers.

Sutton, R.P., Hamman, J.G. & Company, M.O., 2009. SPE 124971 Accuracy of Fluid Property Estimates for Calculating Seismic Properties. In *SPE Annual Technical Conference and Exhibition*. Society of Petroleum Engineers, pp. 4–7.

Wang, X. & Economides, M., 2009. *Advanced Natural Gas Engineering*, Texas: Gulf Publishing Company.

Weller, H.G. & Tabor, G., 1998. A tensorial approach to computational continuum mechanics using object-oriented techniques. *Computers in Physics*, 12(6), pp.620–

631.

Yoneda, Y., 1979. Estimation of the Thermodynamic Properties of Organic Compounds in the Ideal Gas State - 1. Acyclic Compounds and Cyclic Compounds With a Ring of Cyclopentane, Cyclohexane, Benzene, or Naphthalene. *Bulletin of the Chemical Society of Japan*, 52(5), pp.1297–1314.

Yoshioka, K., Zhu, D. & Hill, A., 2006. Detection of Water or Gas Entries in Horizontal Wells from Temperature Profiles. *SPE Europec/EAGE Annual Conference and Exhibition, 12-15 June, Vienna, Austria*.

Zhu, Z., Gerritsen, M.G. & Thiele, M.R., 2009. Thermal Streamline Simulation for Hot Water Flooding. *SPE Reservoir Simulation Symposium*.

Ziegler, J.. (Taylor I.C. & Nichols, N.. (Taylor I.C., 1942. Optimum Settings for Automatic Controllers. *Transactions of the ASME*, 64, pp.759–768.

Zolotukhin, A.B., 1979. Analytical Definition Of The Overall Heat Transfer Coefficient. In *SPE California Regional Meeting*. Society of Petroleum Engineers.

Appendix A: Derivation of Thermal Model

The thermal model is based on the energy balance equation by (Bird et al. 2007) as shown in Equation (A.1) below.

$$\underset{\substack{rate\ of\ increase\\ of\ internal\\ energy\ per\ unit\\ volume}}{\frac{\partial}{\partial t}\rho\widehat{U}} = \underset{\substack{net\ rate\ of\ addition\\ of\ internal\ energy\\ by\ convective\ transport\\ per\ unit\ volume}}{-\left(\nabla\cdot\ \rho\widehat{U}\boldsymbol{v}\right)} \underset{\substack{rate\ of\ internal\\ energy\ addition\\ per\ unit\ of\ volume\\ by\ heat\ conduction}}{-(\nabla\cdot q)} \underset{\substack{reversible\ rate\ of\\ internal\ \ energy\ increase\\ per\ unit\ volume\\ by\ compression}}{-P(\nabla\cdot\boldsymbol{v})} \underset{\substack{irreversible\ rate\ of\\ internal\ \ energy\ increase\\ per\ unit\ volume\\ by\ viscous\ dissipation}}{-(\tau\colon\nabla\boldsymbol{v})} \qquad (A.1)$$

The first term on the right hand side is the advection of the internal energy $\widehat{U}$, the viscous dissipation is given by $(\tau\colon\nabla v)$ and the thermal conduction term is given as $\nabla.q = -K_T\nabla T$. The mean internal energy of both formation and fluid can be expressed as:

$$\rho\widehat{U} = \phi\rho\widehat{U} + (1-\phi)\rho_r\widehat{U}_r \qquad (A.2)$$

Therefore Equation. (A.1) can be rewritten as:

$$\frac{\partial}{\partial t}\left[\phi\rho\widehat{U} + (1-\phi)\rho_r\widehat{U}_r\right] = -\nabla\cdot\left(\rho\widehat{U}v\right) - P\nabla.v - (\tau\colon\nabla v) + K_T\nabla^2T \qquad (A.3)$$

But $(\tau\colon\nabla v) = (v\cdot\nabla P)$ according to (Al-Hadhrami et al. 2003) therefore

$$\frac{\partial}{\partial t}\left[\phi\rho\widehat{U} + (1-\phi)\rho_r\widehat{U}_r\right] = -\nabla\cdot\left(\rho\widehat{U}v\right) - P\nabla.v - (v\cdot\nabla P) + K_T\nabla^2T \qquad (A.4)$$

Enthalpy of a fluid is defined as

$$\widehat{H} = \widehat{U} + PV = \widehat{U} + \frac{P}{\rho} \quad (A.5)$$

$$d\widehat{H} = C_P dT + \left(\frac{\partial H}{\partial P}\right)_T dP \quad (A.6)$$

$$\left(\frac{\partial H}{\partial P}\right)_T = \frac{1}{\rho}(1 - \beta_T T) \quad (A.7)$$

$$d\widehat{H} = C_P dT + \frac{1}{\rho}(1 - \beta_T T) dP \quad (A.8)$$

Substitute Equation. (A.5) into (A.6)

$$\frac{\partial}{\partial t}\left[\phi\rho\widehat{H} - \phi P + (1-\phi)\rho_r \widehat{U}_r\right] = -\nabla \cdot \left(\rho\widehat{H}v - PV\right) - P\nabla . v - (v \cdot \nabla P) + K_T \nabla^2 T \quad (A.9)$$

$$\frac{\partial}{\partial t}\left[\phi\rho\widehat{H} - \phi P + (1-\phi)\rho_r \widehat{U}_r\right] = -\nabla \cdot \left(\rho\widehat{H}v\right) + K_T \nabla^2 T \quad (A.10)$$

The change in energy of the rock is mainly due to temperature change as the rock is assumed incompressible

$$d\widehat{U}_r = C_{Pr} dT_r \quad (A.11)$$

$$\phi\rho\frac{\partial \widehat{H}}{\partial t} + \widehat{H}\frac{\partial(\phi\rho)}{\partial t} - \phi\frac{\partial P}{\partial t} - P\frac{\partial \phi}{\partial t} + (1-\phi)\rho_r C_{Pr}\frac{\partial T_r}{\partial t} - \rho_r C_{Pr} T_r \frac{\partial \phi}{\partial t} = -\rho v \cdot \nabla\widehat{H} - \widehat{H}\nabla \cdot \rho v + K_T \nabla^2 T \quad (A.12)$$

The continuity equation is given as

$$\frac{\partial(\phi\rho)}{\partial t} = -\nabla \cdot \rho v \quad (A.13)$$

$$\phi\rho\frac{\partial \widehat{H}}{\partial t} - \phi\frac{\partial P}{\partial t} - P\frac{\partial \phi}{\partial t} + (1-\phi)\rho_r C_{Pr}\frac{\partial T_r}{\partial t} - \rho_r C_{Pr} T_r \frac{\partial \phi}{\partial t} = -\rho v \cdot \nabla\widehat{H} + K_T \nabla^2 T \quad (A.14)$$

The formation compressibility is given as $C_f = \frac{1}{\phi}\frac{\partial \phi}{\partial P}$

$$\partial \phi = \phi C_f \partial P \qquad (A.15)$$

$$\phi\rho\frac{\partial \hat{H}}{\partial t} - \phi\frac{\partial P}{\partial t} - \phi C_f(P + \rho_r C_{Pr} T_r)\frac{\partial P}{\partial t} + (1-\phi)\rho_r C_{Pr}\frac{\partial T_r}{\partial t} = -\rho v \cdot \nabla \hat{H} + K_T \nabla^2 T \qquad (A.16)$$

Substitute Equation (A.8) into Equation (A.16)

$$\phi\rho C_P\frac{\partial T}{\partial t} - \phi\beta_T T\frac{\partial P}{\partial t} - \phi C_f(P + \rho_r C_{Pr} T_r)\frac{\partial P}{\partial t} + (1-\phi)\rho_r C_{Pr}\frac{\partial T_r}{\partial t} = -\rho v C_P \nabla T + (\beta_T T - 1) v \cdot \nabla P + K_T \nabla^2 T \qquad (A.17)$$

Since the rock and the fluid can be assume to come to thermal equilibrium fast:

$$T = T_r$$

$$[\phi\rho C_P + (1-\phi)\rho_r C_{Pr}]\frac{\partial T}{\partial t} - \phi\beta_T T\frac{\partial P}{\partial t} - \phi C_f(P + \rho_r C_{Pr} T_r)\frac{\partial P}{\partial t} = -\rho v C_P \nabla T + (\beta_T T - 1) v \cdot \nabla P + K_T \nabla^2 T \qquad (A.18)$$

Appendix B: Gas Properties and Equations-Of-State

The properties of gas are strongly dependent on pressure and temperature. To properly model the transient temperature changes, this pressure-temperature dependence of its properties has to be taken into account. Correlations and EOS are normally used. Some of the traditionally used correlations are applied in this work to realistically capture the gas behaviour.

Density

For gases at high pressure the relationship between density, pressure and temperature is given as:

$$\rho = \frac{P}{ZRT} \qquad (B.1)$$

where $Z = f(P, T)$. The Z-factor is used to capture the non-ideal behaviour of the gas as a function of pressure and temperature, and it also varies with the composition of the gas.

Z-Factor

Z-factor is usually determined experimentally, and correlations are developed based on fitting experimental data to equations.

The Benedict Webb Rubin (BWR) EOS was used instead of correlations for simplicity and consistency, as the molal volume (determined from BWR EOS) was used in determining the thermal properties of the gas. The Z-factor estimated using BWR EOS was in close agreement with that from correlations by Dranchuk & Abou-Kassem (1975).

Molal Density

The molal volume of the gas was calculated using the BWR EOS, similar to Benedict et al. (1942), this is shown in Equation. (B.2) below. The equation can be solved iteratively to determine the molal density "d". Newton's iteration method was used, and rapid convergence of the solution was achieved. The values of the parameters are as given in Benedict et al. (1942).

$$P = \left(B_o RT - A_o - {C_o}/{T^2}\right) d + (bRT - a)d^3 + a\alpha d^6 + \frac{cd^3}{T^2}[(1 + \gamma d^2)exp(-\gamma d^2)] \quad (B.2)$$

$B_o = 0.0426000; A_o = 1.85500; C_o = 0.0225700 \times 10^6; b = 0.00338004$;

$a = 0.0494000; \alpha = 0.000124359; c = 0.00254500 \times 10^6; \gamma = 0.0060000$;

Viscosity
The correlation used in this case is that of (Carr et al. 1954).

Thermal-Expansion-Coefficient
The thermal expansion coefficient is given by:

$$\beta_T = \frac{1}{V}\left(\frac{\partial V}{\partial T}\right)_P \quad (B.3)$$

Using the cyclic relationship $\left(\frac{\partial P}{\partial T}\right)_V \left(\frac{\partial T}{\partial V}\right)_P \left(\frac{\partial V}{\partial P}\right)_T = -1$

$$\left(\frac{\partial V}{\partial T}\right)_P = -\frac{\left(\frac{\partial P}{\partial T}\right)_V}{\left(\frac{\partial P}{\partial V}\right)_T} \quad (B.4)$$

$$\therefore \beta_T = -\frac{1}{V}\frac{\left(\frac{\partial P}{\partial T}\right)_V}{\left(\frac{\partial P}{\partial V}\right)_T} \quad (B.5)$$

Where $\left(\frac{\partial P}{\partial T}\right)_V$ & $\left(\frac{\partial P}{\partial V}\right)_T$ can be determined from BWR's EOS.

Specific Heat Capacity
The specific heat capacity of natural gas is dependent on pressure and temperature. To determine the specific heat capacity, the specific heat capacity at ideal conditions (atmospheric pressure) has to be determined, and then the "heat capacity departure" at the high pressure existing in the reservoir is estimated. The method used was similar to Abou-Kassem & Dranchuk (1982)

$$C_p = (C_p - C_v) + (C_v - C_{vo}) + C_{po} - R = (C_p - C_{po}) + C_{po} \qquad (B.6)$$

$(C_p - C_{po})$ is the "isobaric heat capacity departure"for the real gas

C_v is the specific heat capacity at constant volume for the real gas

C_{vo} is the specific heat capacity at constant volume for the ideal gas

C_{po} is the specific heat capacity at constant pressure for the ideal gas

$$(C_p - C_v) = -T\left(\frac{\partial P}{\partial T}\right)_V^2 \Big/ \left(\frac{\partial P}{\partial V}\right)_T \qquad (B.7)$$

$$\left(\frac{\partial C_v}{\partial V}\right)_T = T\left(\frac{\partial^2 P}{\partial T^2}\right)_V \qquad (B.8)$$

The derivatives $\left(\frac{\partial P}{\partial T}\right)_V$, $\left(\frac{\partial P}{\partial V}\right)_T$ & $\left(\frac{\partial^2 P}{\partial T^2}\right)_V$ can be determined from the BWR's EOS. Integrating Equation. (B.8) gives $C_v - C_{vo}$.

$$C_v - C_{vo} = \int_{vo}^{v} T\left(\frac{\partial^2 P}{\partial T^2}\right)_V dV \qquad (B.9)$$

Since $V = \frac{1}{d}$, where: V is the molal volume of the gas and d is the molal density.

Therefore the BWR's EOS can be written as:

$$P = \left(B_o RT - A_o - {C_o}/{T^2}\right)V^{-1} + (bRT - a)V^{-3} + a\alpha V^{-6} + \frac{cV^{-3}}{T^2}[(1 + \gamma V^{-2})exp(-\gamma V^{-2})] \qquad (B.10)$$

The procedure for calculating the specific heat capacity of the real gas at elevated pressures and temperatures is described below.

1. Using the BWR's EOS, determine $\left(\frac{\partial P}{\partial T}\right)_V$, $\left(\frac{\partial P}{\partial V}\right)_T$ & $\left(\frac{\partial^2 P}{\partial T^2}\right)_V$

2. Determine $C_v - C_{vo} = \int_{vo}^{v} T\left(\frac{\partial^2 P}{\partial T^2}\right)_V$

3. Determine $\left(C_p - C_v\right) = -T\left(\frac{\partial P}{\partial T}\right)_V^{\ 2} \Big/ \left(\frac{\partial P}{\partial V}\right)_T$

4. Determine C_{po} from correlations

5. Substitute$\left(C_p - C_v\right)$, $\left(C_v - C_{vo}\right)$ & C_{po} into Equation.(B.6)

The correlation used to determine C_{po} is taken from Reid et al. (1977). The ideal heat capacity of the hydrocarbon was calculated using Yoneda's group contribution method (Yoneda 1979), and then corrections were made for non-hydrocarbon components according to Equation.(26, 27 & 28) of the work published by Sutton et al. (2009)

Joule-Thomson Coefficient

The equation for calculating the Joule-Thompson coefficient is derived from the definition of the Joule-Thomson coefficient.

$$\mu_{JT} = \left(\frac{\partial T}{\partial P}\right)_H \qquad (B.11)$$

$$dH = \left(\frac{\partial H}{\partial T}\right)_P dT + \left(\frac{\partial H}{\partial P}\right)_T dP \qquad (B.12)$$

But at constant enthalpy,

$$dH = \left(\frac{\partial H}{\partial T}\right)_P dT + \left(\frac{\partial H}{\partial P}\right)_T dP = 0 \qquad (B.13)$$

Dividing through by dP and rearranging gives

$$\left(\frac{\partial T}{\partial P}\right)_H = -\frac{\left(\frac{\partial H}{\partial P}\right)_T}{\left(\frac{\partial H}{\partial T}\right)_P} \quad (B.14)$$

$$C_P = \left(\frac{\partial H}{\partial T}\right)_P \quad (B.15)$$

$$\therefore\ \mu_{JT} = -\frac{\left(\frac{\partial H}{\partial P}\right)_T}{C_P} \quad (B.16)$$

$$\left(\frac{\partial H}{\partial P}\right)_T = V - T\left(\frac{\partial V}{\partial T}\right)_P = V\left[1 - \frac{T}{V}\left(\frac{\partial V}{\partial T}\right)_P\right] \quad (B.17)$$

$$but\ \ \frac{T}{V}\left(\frac{\partial V}{\partial T}\right)_P = \beta_T \quad (B.18)$$

$$\left(\frac{\partial H}{\partial P}\right)_T = V[1 - \beta_T] = \frac{1}{\rho}[1 - \beta_T] \quad (B.19)$$

$$\therefore \mu_{JT} = \frac{(\beta_T T - 1)}{\rho C_P} \quad (B.20)$$

To determine the gas properties over the range of pressure and temperature in the reservoir, the following properties (Table B-1) were used.

Table B-1: Natural gas properties

Property	**Symbol**	**Value**	**Unit**
Pseudo critical temperature	T_{pc}	190.6	K
Pseudo critical pressure	P_{pc}	4.6624×10^{6}	Pa
Thermal conductivity	K_T	1.7	W/mK
Molal specific heat capacity of natural gas sample at ideal conditions	Cp_o	33.8901	$J/mol.K$
Universal gas constant	$\tilde{R}$	8.3145	$kJ/mol.K$
Specific gas constant	R	519.6563	$J/kg.K$
Specific gravity of gas	$S.G_f$	0.605	
Viscosity at initial reservoir pressure	μ_i	1.52×10^{-5}	$Pa.s$
Mass fraction of H_2S in natural gas		0	
Mass fraction of CO_2 in natural gas		0	
Mass fraction of N_2 in natural gas		0	

Appendix C: Numerical Model in OpenFOAM

A numerical solver was developed by modifying an existing solver in OpenFOAM. The base solver chosen was the rhoPimpleFOAM solver because it handles transient compressible flow, and this is similar to the problem being solved except that it was not developed for porous media flow. The modifications described here are to adapt the rhoPimpleFOAM solver to handle porous media flow.

OpenFOAM contains an extensive library of routines and these would be used where possible while developing add-ons where necessary. The descriptions here apply to the parts of the OpenFOAM library or rhoPimpleFOAM solver that have been modified, the OpenFOAM documentation (OpenFOAM Foundation, 2014; OpenFOAM Foundation, 2015 and OpenFOAM Foundation, 2018) should be consulted for the other unmodified relevant code, equations, or libraries.

The gas properties tables were generated using the Benedict-Webb-Rubin Equation of State (BWR EOS). These properties were calculated for the entire range of pressure and temperature expected in the reservoir. Doing this saved simulation time, as there was no need to carry-out the iterative process necessary to calculate the gas property at every time step. The property was determined from the table using simple 2-dimensional interpolation.

In order to use the property tables, a library was created which interpolates for the gas property at a given temperature and pressure.

This Appendix first discusses the equations implemented in OpenFOAM, the numerical schemes used in the models, the performance of a sample simulation, and then the modified codes are presented and discussed.

Implementation of Modifications in OpenFOAM

Partial differential equation of the Forchheimer equation	Expression in OpenFOAM
$-\nabla P = \frac{\mu}{k}\boldsymbol{v} + \rho\beta\lvert\boldsymbol{v}\rvert\boldsymbol{v}$	tmp<fvVectorMatrix> UEqn (fvm::Sp((mu/k),U) + fvm::Sp((rho*forch*mag(U)),U));
Partial differential equation of the continuity equation	Expression in OpenFOAM

$\frac{\partial}{\partial t}(\phi\rho) + \nabla\cdot(\rho\boldsymbol{V}) = 0$	{
	solve(fvm::ddt(poro,rho) + fvc::div(phi));
	}

Partial differential equation of the thermal model	Expression in OpenFOAM
$\overline{\rho C_P}\,\frac{\partial T}{\partial t} - \emptyset\beta T\frac{\partial P}{\partial t} - \emptyset C_f\left(P + \rho_r C_{Pr} T\right)\frac{\partial P}{\partial t} = -\rho\boldsymbol{v}C_P\cdot\nabla T + \beta T\boldsymbol{v}\cdot\nabla P - \boldsymbol{v}\cdot\nabla P + K_T\nabla^2 T$	fvScalarMatrix TEqn (fvm::ddt(rhocPMean,T) - fvm::SuSp(poro*betaT*dpdt,T) - (poro*rockComp*p*dpdt) - fvm::SuSp((poro*rockComp*rhoRock * cPRock*dpdt), T) + Cp*fvm::div(phi,T) - fvm::SuSp(((gradP&U)*betaT),T) + (U&gradP) - fvm::laplacian(kTRock,T));
Partial differential equation of pressure	Expression in OpenFOAM
pressure equation (as derived by(Jasak 1996))was also modified by including the porosity of the rock	fvScalarMatrix pEqn (fvm::ddt((poro*psi), p) + fvc::div(phiHbyA) - fvm::laplacian(rhorAUf, p));

Further details of the equations and how they are implemented in OpenFOAM can be found in Jasak (1996), Juretic (2004), Mangani (2008), Weller & Tabor (1998) and Jasak et al. (2007).

Discretization Schemes Used in the Simulation

The following discretization schemes are used for the simulations. However, OpenFOAM has options for other numerical schemes and these can be easily changed.

Table C-1: Discretization schemes used in the simulation

Operator	**Discretization scheme**	**Details**
$\frac{\partial}{\partial t}$	Euler	Implicit, first order and transient
∇	Gauss linear	Second order, unbounded with linear interpolation
$\nabla \cdot$	Gauss linear	Second order, unbounded with linear interpolation
∇^2	Gauss linear orthogonal	

A detailed description of the developed OpenFOAM solver and its implementation is presented below.

Description of the Main Solver File (gasPorousFoamV2Hetero.C, Code listing 1)

The header files included on lines 40, 41, 42, 43, 44 includes the necessary core OpenFOAM libraries. The header file included on line 45 i.e. "gasProperties.H" includes the library required to evaluate the gas properties for the domain during the simulation. The evaluation of the gas properties is done by reading a pressure and temperature dependent property table and then interpolating for the gas property over the entire domain using pressure and temperature field of the domain.

The include statement on the lines 51, 52 and 53 are also part of the core library of OpenFOAM and are used to initialize the case, create the time object and also the mesh object. The mesh object defines the spatial discretization of the domain, which would then be used to set-up the other domain variables.

The pimple object is created on line 55 using the mesh object as its input and the value returned by pimple.nCorrPIMPLE() is initialized. The pimple object carries out the pressure velocity coupling by a hybrid of the Pressure Implicit with Splitting of Operators (PISO) and the Semi-Implicit Method with Pressure Linked Equations (SIMPLE) methods.

The include file on line 57 creates the scalar and vector fields for the simulation, while the include statement on line 58, includes the library (also part of the core library of OpenFOAM) used to initialize the continuity errors to zero.

The include file on line 66 checks if the simulation is setup to use adjustable time-steps, line 67 calculates the courant number and line 68 adjusts the time step based on the courant number. It is important to note here that there is the internal simulation time-step, and this is adjusted based on the courant number, while the simulation result time-step (i.e. the time at which simulation results are written to disk) is a constant value set by the user and is not affected by the time-step adjustment.

Line 74 to 77 ensures that the continuity equation is solved at least once each time step (or more, if the number of pimple correctors specified in the simulation setup).

The PIMPLE pressure-velocity correction is carried out between line 80 to 91. The while loop continues to execute as long as pimple.loop() returns a true value, i.e. until the residuals of pressure, velocity and temperature become smaller than the specified tolerance value or the maximum number of iterations is exceeded.

pimple.Loop() checks if the number of corrections has been carried out or if convergence has been attained for that time steps and then returns a true or false value as required.

The PIMPLE pressure velocity coupling is implemented in OpenFOAM, in each PIMPLE loop the velocity equation (or momentum equation, which is the Forchheimer's law in this case) and the energy equation (which is the temperature equation in this case) are solved n times in the outer loop, where the value of n is defined by the nOuterCorrectors defined in the fvSolution dictionary. The pressure equation is solved in the inner correction loop depending on the value of the nCorrectors and nNonOrthogonalCorrectors defined in the fvSolution dictionary. For example, if nOuterCorrectors is 2, nCorrectors is 2 and nNonOrthogonalCorrectos is 1; the momentum and energy equations are solve twice, while the pressure equation is solved eight times, twice in the non-orthogonal correction loop, twice in the inner corrector loop and twice in the outer corrector loop.

```
Outer corrector loop:
{
      Solve momentum equation
      Solve Energy equation
      Inner corrector loop:
      {
            Non orthogonal corrector loop:
            {
                  Solve pressure equation
            }
            End Non orthogonal corrector loop
      }
      End Inner corrector loop
}
End outer corrector loop
```

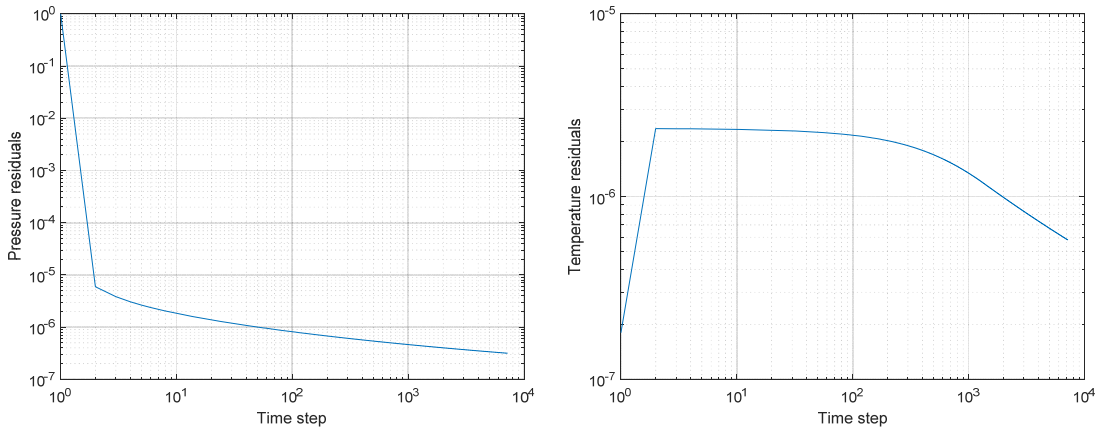

Figure C.2: (a) Plot of pressure residuals, (b) Plot of temperature residuals.

Description of Simulation Time-Step Control (Code listing 4)

The time-step control is carried out to ensure that the Courant number is always less than one. This is done to ensure the Courant–Friedrichs–Lewy condition (Courant et al. 1967) is met. The plots of the Courant number during a simulation is shown in Fig C.2 The mean and maximum values of the Courant number is less than 1, thereby ensuring the computational speed is not faster than the physics.

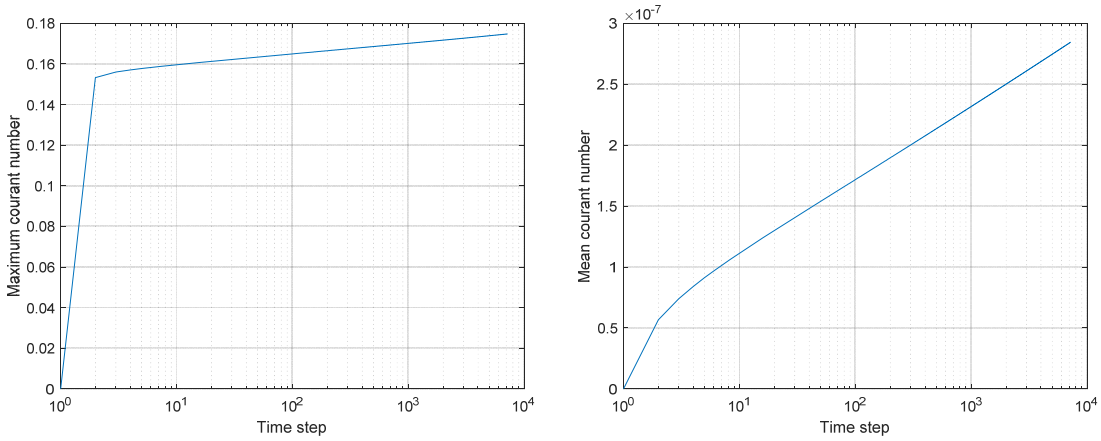

Figure C.2: (a) Plot of maximum Courant number, (b) Plot of mean Courant number.

Description of the Continuity, Momentum and Energy Equation (rhoEqn.H Code Listing 5; UEqn.H Code Listing 6; TEqn.H Code Listing 7)

The continuity equation was modified from to handle porous media flow by including the effect of porosity in the equation as described in Equation. 3-2) of Section 3.2.1. The temperature equation (analogous to the energy equation) is presented in Code Listing 7 this equation is the same as Equation.3-8) of Section 3.2.2 while the momentum equation is replaced by the Forchheimer's equation, Equation.3-102) and the OpenFOAM code is presented in Code Listing 6.

Description of Compressible Continuity Errors (compressibleContinuityErrors.H Code Listing 9)

The compressible continuity errors is a measure of the errors in mass conservation, and should be consistently low for conservation of mass to be met. The continuity errors are consistently low as shown in Fig. (C.3).

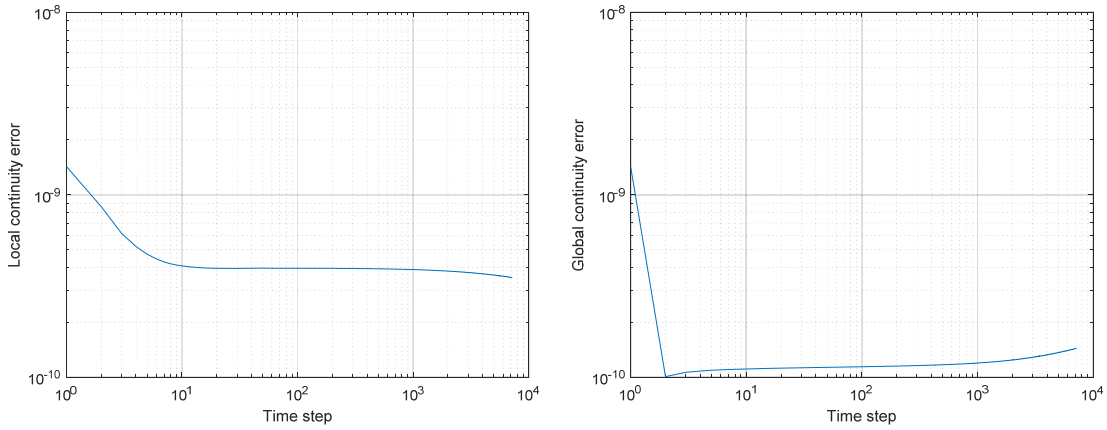

Figure C.3: (a) Plot of local continuity errors, (b) Plot of global continuity errors.

Description of Gas Property Estimator (gasProperties.H Code Listing 10; gasProperties.C Code Listing 11)

The gas properties are read from a lookup table, the code described in Code Listing 10 and 11 reads the gas property tables and then interpolates for the gas property at each cell, based on the pressure and temperature of the cell.

Code Listings

Code listing 1: Modified OpenFOAM solver for transient compressible non-isothermal flow of gas in porous media.

```
001    /*---------------------------------------------------------------------------*\
002      =========                 |
003      \\      /  F ield         | OpenFOAM: The Open Source CFD Toolbox
004       \\    /   O peration     |
005        \\  /    A nd           | Copyright (C) 2011-2013 OpenFOAM Foundation
006         \\/     M anipulation  |
007    -------------------------------------------------------------------------------
008    License
009        This file is part of OpenFOAM.
010
011        OpenFOAM is free software: you can redistribute it and/or modify it
012        under the terms of the GNU General Public License as published by
013        the Free Software Foundation, either version 3 of the License, or
014        (at your option) any later version.
015
016        OpenFOAM is distributed in the hope that it will be useful, but WITHOUT
017        ANY WARRANTY; without even the implied warranty of MERCHANTABILITY or
018        FITNESS FOR A PARTICULAR PURPOSE.  See the GNU General Public License
019        for more details.
020
021        You should have received a copy of the GNU General Public License
022        along with OpenFOAM.  If not, see <http://www.gnu.org/licenses/>.
023
024    Application
```

```
025         rhoPimpleFoam
026
027     Description
028         Transient solver for laminar or turbulent flow of compressible fluids
029         for HVAC and similar applications.
030
031         Uses the flexible PIMPLE (PISO-SIMPLE) solution for time-resolved and
032         pseudo-transient simulations.
033
034     This packaged PIMPLEFOAM OpenFOAM solver was modified by Akindolu Dada (2014-
2018)
035     to:
036      1. Simulate gas flow in porous media
037      2. Read the required gas properties from a text file
038     \*---------------------------------------------------------------------------*/
039
040     #include "fvCFD.H"
041     #include "psiThermo.H"
042     #include "bound.H"
043     #include "pimpleControl.H"
044     #include "fvIOoptionList.H"
045     #include "gasProperties.H"
046
047     // * * * * * * * * * * * * * * * * * * * * * * * * * * * * * * * * * * * * * //
048
049     int main(int argc, char *argv[])
050     {
051         #include "setRootCase.H"
052         #include "createTime.H"
053         #include "createMesh.H"
054
055         pimpleControl pimple(mesh);
056
057         #include "createFields.H"
058         #include "initContinuityErrs.H"
059
060         // * * * * * * * * * * * * * * * * * * * * * * * * * * * * * * * * * * * * * //
061
062         Info<< "\nStarting time loop\n" << endl;
063
064         while (runTime.run())
065         {
066             #include "readTimeControls.H"
067             #include "compressibleCourantNo.H"
068             #include "setDeltaT.H"
069
070             runTime++;
071
072             Info<< "Time = " << runTime.timeName() << nl << endl;
073
074             if (pimple.nCorrPIMPLE() <= 1)
075             {
076                 #include "rhoEqn.H"
077             }
078
079             // --- Pressure-velocity PIMPLE corrector loop
080             while (pimple.loop())
081             {
082                 #include "UEqn.H"
083                 #include "TEqn.H"
084
085                 // --- Pressure corrector loop
086                 while (pimple.correct())
087                 {
088                     #include "pEqn.H"
089                 }
090
091             }
092
093             runTime.write();
094
095             Info<< "ExecutionTime = " << runTime.elapsedCpuTime() << " s"
096                 << "  ClockTime = " << runTime.elapsedClockTime() << " s"
097                 << nl << endl;
098         }
099
100         Info<< "End\n" << endl;
101
102         return 0;
103     }
```

```
104
105
106    // ************************************************************************* //
107
```

Code listing 2: Code for creating the initializing the field variables for the computational domain.

```
001    /*
002    ------------------------------------------------------------
003    This section creates the transport properties.
004    The transport properties are scalr variables that are read
005    from the transportProperties dictionary
006    ------------------------------------------------------------
007    */
008        Info<< "Reading transportProperties\n" << endl;
009
010        IOdictionary transportProperties
011        (
012            IOobject
013            (
014                "transportProperties",
015                runTime.constant(),
016                mesh,
017                IOobject::MUST_READ_IF_MODIFIED,
018                IOobject::NO_WRITE
019            )
020        );
021
022        dimensionedScalar beta
023        (
024            transportProperties.lookup("beta")
025        );
026
027        dimensionedScalar kTRock
028        (
029            transportProperties.lookup("kTRock")
030        );
031
032
033        dimensionedScalar cPRock
034        (
035            transportProperties.lookup("cPRock")
036        );
037
038        dimensionedScalar rhoRock
039        (
040            transportProperties.lookup("rhoRock")
041        );
042
043    dimensionedScalar rockComp
044        (
045            transportProperties.lookup("rockComp")
046        );
047
048        dimensionedScalar forch
049        (
050            transportProperties.lookup("forch")
051        );
052
053
054        dimensionedScalar poro
055        (
056            transportProperties.lookup("poro")
057        );
058
059
060    dimensionedScalar Runi
061        (
062            transportProperties.lookup("Runi")
063        );
064
065    dimensionedScalar MMass
066        (
```

```
067             transportProperties.lookup("MMass")
068         );
069
070     dimensionedScalar SG_g
071         (
072             transportProperties.lookup("SG_g")
073         );
074
075     dimensionedScalar MF_H2S
076         (
077             transportProperties.lookup("MF_H2S")
078         );
079
080     dimensionedScalar MF_CO2
081         (
082             transportProperties.lookup("MF_CO2")
083         );
084
085     dimensionedScalar MF_N2
086         (
087             transportProperties.lookup("MF_N2")
088         );
089
090     dimensionedScalar TcH2S
091         (
092             transportProperties.lookup("TcH2S")
093         );
094
095     dimensionedScalar TcCO2
096         (
097             transportProperties.lookup("TcCO2")
098         );
099
100     dimensionedScalar TcN2
101         (
102             transportProperties.lookup("TcN2")
103         );
104
105     dimensionedScalar PcH2S
106         (
107             transportProperties.lookup("PcH2S")
108         );
109
110     dimensionedScalar PcCO2
111         (
112             transportProperties.lookup("PcCO2")
113         );
114
115     dimensionedScalar PcN2
116         (
117             transportProperties.lookup("PcN2")
118         );
119
120     dimensionedScalar mySwitch1
121         (
122             transportProperties.lookup("mySwitch1")
123         );
124
125     dimensionedScalar mySwitch2
126         (
127             transportProperties.lookup("mySwitch2")
128         );
129
130     // create gasProperties object
131     gasProperties gas(Runi, MMass, SG_g, MF_H2S, MF_CO2, MF_N2, TcH2S, TcCO2, TcN2,
PcH2S, PcCO2, PcN2);
132
133     /*
134     ------------------------------------------------------------
135     This section creates the scalar and vector field variables.
136     These field variables are the spatially varying values in the
137     domain
138     ------------------------------------------------------------
139     */
140     //------------------------------------------------------------------------------
------------------------------
141
142         // create the permeability field,
143         // the inital values would be read from file
144     Info<< "Reading field k\n" << endl;
```

```
145     volScalarField k
146         (
147             IOobject
148             (
149                 "k",
150                 runTime.timeName(),
151                 mesh,
152                 IOobject::MUST_READ,
153                 IOobject::AUTO_WRITE
154             ),
155             mesh
156         );
157 
158         // create the pressure field,
159         // the inital values would be read from file
160     Info<< "Reading field p\n" << endl;
161     volScalarField p
162         (
163             IOobject
164             (
165                 "p",
166                 runTime.timeName(),
167                 mesh,
168                 IOobject::MUST_READ,
169                 IOobject::AUTO_WRITE
170             ),
171             mesh
172         );
173 
174         // create the temperature field,
175         // the inital values would be read from file
176     Info<< "Reading field T\n" << endl;
177     volScalarField T
178         (
179             IOobject
180             (
181                 "T",
182                 runTime.timeName(),
183                 mesh,
184                 IOobject::MUST_READ,
185                 IOobject::AUTO_WRITE
186             ),
187             mesh
188         );
189 
190         // create the velocity field,
191         // the inital values would be read from file
192         Info<< "Reading field U\n" << endl;
193         volVectorField U
194         (
195             IOobject
196             (
197                 "U",
198                 runTime.timeName(),
199                 mesh,
200                 IOobject::MUST_READ,
201                 IOobject::AUTO_WRITE
202             ),
203             mesh
204         );
205 
206         // create the psi field, psi =
207         // the inital values would be read from file
208     Info<< "Reading field psi\n" << endl;
209     volScalarField psi
210         (
211             IOobject
212             (
213                 "psi",
214                 runTime.timeName(),
215                 mesh,
216                 IOobject::READ_IF_PRESENT,
217                 IOobject::AUTO_WRITE
218             ),
219             mesh,
220             dimensionedScalar("psi", dimensionSet(0,-2,2,0,0,0,0),0)
221         );
222     Info << "psi dimension = " << psi.dimensions() << endl;
223 
224         // create the density field,
```

```
225         // the inital values would be calculated based on P and T
226         volScalarField rho
227         (
228             IOobject
229             (
230                 "rho",
231                 runTime.timeName(),
232                 mesh,
233                 IOobject::READ_IF_PRESENT,
234                 IOobject::AUTO_WRITE
235             ),
236             mesh,
237             dimensionedScalar("rho", dimensionSet(1,-3,0,0,0,0,0),0)
238         );
239     Info << "rho dimension = " << rho.dimensions() << endl;
240 
241         // Calculate the flux field
242         #include "compressibleCreatePhi.H"
243 
244         dimensionedScalar rhoMax(pimple.dict().lookup("rhoMax"));
245         dimensionedScalar rhoMin(pimple.dict().lookup("rhoMin"));
246 
247         // create the viscosity field,
248         // the inital values would be calculated based on P and T
249         volScalarField mu
250         (
251             IOobject
252             (
253                 "mu",
254                 runTime.timeName(),
255                 mesh,
256                 IOobject::READ_IF_PRESENT,
257                 IOobject::AUTO_WRITE
258             ),
259             mesh,
260             dimensionedScalar("mu", dimensionSet(1,-1,-1,0,0,0,0),0)
261         );
262     Info << "mu dimension = " << mu.dimensions() << endl;
263 
264 
265         // create the specific gas constant field,
266         // Rgas = Runi/MMass
267     Info<< "Creating field Rgas\n" << endl;
268     volScalarField Rgas
269         (
270             IOobject
271             (
272                 "Rgas",
273                 runTime.timeName(),
274                 mesh,
275                 IOobject::READ_IF_PRESENT,
276                 IOobject::AUTO_WRITE
277             ),
278             mesh,
279             dimensionedScalar("Rgas", (Runi/MMass))
280         );
281 
282         // create the Z-factor field,
283         // the inital values would be calculated based on P and T
284     Info<< "Creating field Zfact\n" << endl;
285     volScalarField Zfact
286         (
287             IOobject
288             (
289                 "Zfact",
290                 runTime.timeName(),
291                 mesh,
292                 IOobject::READ_IF_PRESENT,
293                 IOobject::AUTO_WRITE
294             ),
295             mesh,
296             dimensionedScalar("Zfact", dimensionSet(0,0,0,0,0,0,0),0)
297         );
298 
299 
300         // create the thermal conductivity field,
301         // the inital values would be calculated based on P and T
302     Info<< "Creating field Kappa\n" << endl;
303         volScalarField kappa
304         (
```

```
305             IOobject
306             (
307                 "kappa",
308                 runTime.timeName(),
309                 mesh,
310                 IOobject::READ_IF_PRESENT,
311                 IOobject::AUTO_WRITE
312             ),
313             mesh,
314             dimensionedScalar("kappa", dimensionSet(1,1,-3,-1,0,0,0),0)
315         );
316
317         // create the specific heat capacity field for gas,
318         // the inital values would be calculated based on P and T
319     Info<< "Creating field Cp\n" << endl;
320         volScalarField Cp
321         (
322             IOobject
323             (
324                 "Cp",
325                 runTime.timeName(),
326                 mesh,
327                 IOobject::READ_IF_PRESENT,
328                 IOobject::AUTO_WRITE
329             ),
330             mesh,
331             dimensionedScalar("Cp", dimensionSet(0,2,-2,-1,0,0,0),0)
332         );
333
334         // create the pressure derivative field,
335         // this is estimated at each time step of the simulation
336         Info<< "Creating field dpdt\n" << endl;
337         volScalarField dpdt
338         (
339             IOobject
340             (
341                 "dpdt",
342                 runTime.timeName(),
343                 mesh,
344                     IOobject::READ_IF_PRESENT,
345                 IOobject::AUTO_WRITE
346             ),
347             mesh,
348             dimensionedScalar("dpdt", p.dimensions()/dimTime, 0)
349         );
350
351         // create the temperature derivative field,
352         // this is estimated at each time step of the simulation
353     Info<< "Creating field dTdt\n" << endl;
354         volScalarField dTdt
355         (
356             IOobject
357             (
358                 "dTdt",
359                 runTime.timeName(),
360                 mesh,
361                     IOobject::READ_IF_PRESENT,
362                 IOobject::AUTO_WRITE
363             ),
364             mesh,
365             dimensionedScalar("dTdt", T.dimensions()/dimTime, 0)
366         );
367
368         // create the thermal expansion coefficient field for gas,
369         // the inital values would be calculated based on P and T
370     Info<< "Creating field betaT\n" << endl;
371         volScalarField betaT
372         (
373             IOobject
374             (
375                 "betaT",
376                 runTime.timeName(),
377                 mesh,
378                     IOobject::READ_IF_PRESENT,
379                 IOobject::AUTO_WRITE
380             ),
381             mesh,
382             dimensionedScalar("betaT", dimensionSet(0,0,0,-1,0,0,0), 0)
383         );
384
```

```
385        // create the pressure gradient field,
386        // this is estimated at each time step of the simulation
387        Info<< "Creating field gradP\n" << endl;
388        volVectorField gradP
389        (
390            IOobject
391            (
392                "gradP",
393                runTime.timeName(),
394                mesh,
395                    IOobject::READ_IF_PRESENT,
396                IOobject::AUTO_WRITE
397            ),
398            mesh,
399            dimensionedVector("gradP", p.dimensions()/dimLength, Foam::vector(0,0,0))
400        );
401
402
403     //create and update gas properties in the gas properties object
404     gas.update( p,  T, mu, Cp, betaT, psi, rho);
405
406        // Calculate the volumetric heat capacity
407        Info<< "Creating field mean heat capacity rhocPMean\n" << endl;
408        volScalarField rhocPMean("rhocPMean", ((poro*rho*Cp) + ((1-
poro)*rhoRock*cPRock)));
409
410
```

Code listing 3: Code for calculating Courant number

```
01    /*---------------------------------------------------------------------------*\
02      =========                 |
03      \\      /  F ield         | OpenFOAM: The Open Source CFD Toolbox
04       \\    /   O peration     |
05        \\  /    A nd           | Copyright (C) 2011 OpenFOAM Foundation
06         \\/     M anipulation  |
07    -------------------------------------------------------------------------------
08    License
09        This file is part of OpenFOAM.
10
11        OpenFOAM is free software: you can redistribute it and/or modify it
12        under the terms of the GNU General Public License as published by
13        the Free Software Foundation, either version 3 of the License, or
14        (at your option) any later version.
15
16        OpenFOAM is distributed in the hope that it will be useful, but WITHOUT
17        ANY WARRANTY; without even the implied warranty of MERCHANTABILITY or
18        FITNESS FOR A PARTICULAR PURPOSE.  See the GNU General Public License
19        for more details.
20
21        You should have received a copy of the GNU General Public License
22        along with OpenFOAM.  If not, see <http://www.gnu.org/licenses/>.
23
24    Global
25        CourantNo
26
27    Description
28        Calculates and outputs the mean and maximum Courant Numbers.
29
30    \*---------------------------------------------------------------------------*/
31
32    scalar CoNum = 0.0;
33    scalar meanCoNum = 0.0;
34
35    if (mesh.nInternalFaces())
36    {
37        scalarField sumPhi
38        (
39            fvc::surfaceSum(mag(phi))().internalField()
40          / rho.internalField()
41        );
42
43        CoNum = 0.5*gMax(sumPhi/mesh.V().field())*runTime.deltaTValue();
44
45        meanCoNum =
```

```
46            0.5*(gSum(sumPhi)/gSum(mesh.V().field()))*runTime.deltaTValue();
47    }
48
49    Info<< "Courant Number mean: " << meanCoNum
50        << " max: " << CoNum << endl;
51
52    // ************************************************************************* //
53
```

Code listing 4: Code for calculating the time step

```
01    /*---------------------------------------------------------------------------*\
02      =========                 |
03      \\      /  F ield         | OpenFOAM: The Open Source CFD Toolbox
04       \\    /   O peration     |
05        \\  /    A nd           | Copyright (C) 2011 OpenFOAM Foundation
06         \\/     M anipulation  |
07    -------------------------------------------------------------------------------
08    License
09        This file is part of OpenFOAM.
10
11        OpenFOAM is free software: you can redistribute it and/or modify it
12        under the terms of the GNU General Public License as published by
13        the Free Software Foundation, either version 3 of the License, or
14        (at your option) any later version.
15
16        OpenFOAM is distributed in the hope that it will be useful, but WITHOUT
17        ANY WARRANTY; without even the implied warranty of MERCHANTABILITY or
18        FITNESS FOR A PARTICULAR PURPOSE.  See the GNU General Public License
19        for more details.
20
21        You should have received a copy of the GNU General Public License
22        along with OpenFOAM.  If not, see <http://www.gnu.org/licenses/>.
23
24    Global
25        setDeltaT
26
27    Description
28        Reset the timestep to maintain a constant maximum courant Number.
29        Reduction of time-step is immediate, but increase is damped to avoid
30        unstable oscillations.
31
32    \*---------------------------------------------------------------------------*/
33
34    if (adjustTimeStep)
35    {
36        scalar maxDeltaTFact = maxCo/(CoNum + SMALL);
37        scalar deltaTFact = min(min(maxDeltaTFact, 1.0 + 0.1*maxDeltaTFact), 1.2);
38
39        runTime.setDeltaT
40        (
41            min
42            (
43                deltaTFact*runTime.deltaTValue(),
44                maxDeltaT
45            )
46        );
47
48        Info<< "deltaT = " <<  runTime.deltaTValue() << endl;
49    }
50
51    // ************************************************************************* //
52
```

Code listing 5: Code for the continuity equation

```
01
02    // Creates and solves the continuity equation for porous media
03    // This equation is a modified form as that implemented in the
04    // OpenFOAM source code.
```

```
05    {
06     solve(fvm::ddt(poro,rho) + fvc::div(phi));
07    }
08
09    // ************************************************************************* //
10
11
```

Code listing 6: Code for. the momentum equation

```
01
02    // create and solve the Forchheimer's equation
03    // This equation is equivalent to the momentum equation
04    tmp<fvVectorMatrix> UEqn
05    (
06        fvm::Sp((mu/k),U) + fvm::Sp((rho*forch*mag(U)),U)
07    );
08
09    UEqn().relax();
10
11    if (pimple.momentumPredictor())
12    {
13        solve(UEqn() == -fvc::grad(p));
14    }
15
```

Code listing 7: Code for the energy equation expressed in terms of temperature

```
01
02    // Create and solve the Temperature equation
03    // This equation is equivalent to and derived from the energy equation
04    {
05
06        fvScalarMatrix TEqn
07        (
08            fvm::ddt(rhocPMean,T) - fvm::SuSp(poro*betaT*dpdt,T)
09        - mySwitch1*(poro*rockComp*p*dpdt)
10        - mySwitch2*fvm::SuSp((poro*rockComp*rhoRock*cPRock*dpdt), T)
11          + Cp*fvm::div(phi,T) - fvm::SuSp(((gradP&U)*betaT),T)
12        + (U&gradP) - fvm::laplacian(kTRock,T)
13        );
14
15        TEqn.relax();
16
17        TEqn.solve();
18    }
19
```

Code listing 8: Code for the pressure equation

```
01    rho = gas.getRho(p, T);
02    rho = max(rho, rhoMin);
03    rho = min(rho, rhoMax);
04    rho.relax();
05
06    volScalarField rAU(1.0/UEqn().A());
07    surfaceScalarField rhorAUf("rhorAUf", fvc::interpolate(rho*rAU));
08
09    volVectorField HbyA("HbyA", U);
10    HbyA = rAU*UEqn().H();
11
12    if (pimple.nCorrPISO() <= 1)
13    {
14        UEqn.clear();
15    }
```

```
16
17    {
18        surfaceScalarField phiHbyA
19        (
20            "phiHbyA",
21            (
22                (fvc::interpolate(rho*HbyA) & mesh.Sf())
23              + rhorAUf*fvc::ddtCorr(rho, U, phi)
24            )
25        );
26
27        //fvOptions.makeRelative(fvc::interpolate(rho), phiHbyA);
28
29        while (pimple.correctNonOrthogonal())
30        {
31            // Pressure corrector
32            fvScalarMatrix pEqn
33            (
34                fvm::ddt((poro*psi), p)
35              + fvc::div(phiHbyA)
36              - fvm::laplacian(rhorAUf, p)
37            );
38
39            //fvOptions.constrain(pEqn);
40
41            pEqn.solve(mesh.solver(p.select(pimple.finalInnerIter())));
42
43            if (pimple.finalNonOrthogonalIter())
44            {
45                phi = phiHbyA + pEqn.flux();
46            }
47        }
48    }
49
50    #include "rhoEqn.H"
51    #include "compressibleContinuityErrs.H"
52
53    // Explicitly relax pressure for momentum corrector
54    p.relax();
55
56    // Recalculate density from the relaxed pressure
57    rho = gas.getRho(p, T);
58    rho = max(rho, rhoMin);
59    rho = min(rho, rhoMax);
60    rho.relax();
61
62    U = HbyA - rAU*fvc::grad(p);
63    U.correctBoundaryConditions();
64
65    // Calculate volumetric heat capacity
66    rhocPMean = ((poro*rho*Cp) + ((1-poro)*rhoRock*cPRock));
67
68    // Calculate the pressure derivative
69    dpdt = fvc::ddt(p);
70
71    // Calculate the pressure gradient
72    gradP = fvc::grad(p);
73
74    // Calculate the temperature derivative
75    dTdt = fvc::ddt(T);
76
77    // Update gas properties
78    gas.update( p,  T, mu, Cp, betaT, psi, rho);
79
```

Code listing 9: Code for calculating the compressible continuity error

```
01    /*---------------------------------------------------------------------------*\
02      =========                 |
03      \\      /  F ield         | OpenFOAM: The Open Source CFD Toolbox
04       \\    /   O peration     |
05        \\  /    A nd           | Copyright (C) 2011 OpenFOAM Foundation
06         \\/     M anipulation  |
07    -------------------------------------------------------------------------------
08    License
```

```
09        This file is part of OpenFOAM.
10
11        OpenFOAM is free software: you can redistribute it and/or modify it
12        under the terms of the GNU General Public License as published by
13        the Free Software Foundation, either version 3 of the License, or
14        (at your option) any later version.
15
16        OpenFOAM is distributed in the hope that it will be useful, but WITHOUT
17        ANY WARRANTY; without even the implied warranty of MERCHANTABILITY or
18        FITNESS FOR A PARTICULAR PURPOSE.  See the GNU General Public License
19        for more details.
20
21        You should have received a copy of the GNU General Public License
22        along with OpenFOAM.  If not, see <http://www.gnu.org/licenses/>.
23
24    Global
25        continuityErrs
26
27    Description
28        Calculates and prints the continuity errors.
29
30    \*---------------------------------------------------------------------------*/
31
32    {
33        dimensionedScalar totalMass = fvc::domainIntegrate(rho);
34
35        scalar sumLocalContErr =
36            (fvc::domainIntegrate(mag(rho - gas.getRho(p, T)))/totalMass).value();
37
38        scalar globalContErr =
39            (fvc::domainIntegrate(rho - gas.getRho(p, T))/totalMass).value();
40
41        cumulativeContErr += globalContErr;
42
43        Info<< "time step continuity errors : sum local = " << sumLocalContErr
44            << ", global = " << globalContErr
45            << ", cumulative = " << cumulativeContErr
46            << endl;
47    }
48
49    // ************************************************************************* //
50
```

Code listing 10: Code for gas property reader header file

```
01    #ifndef gasProperties_H
02    #define gasProperties_H
03
04    #include "fvCFD.H"
05    #include <iostream>
06    #include <fstream>
07    #include <string>
08
09    class gasProperties
10    {
11    private:
12      scalar Rgas;
13      scalar Rmol;
14      scalar MMass;
15      scalar SG_g;
16
17      scalar MF_H2S;
18      scalar MF_CO2;
19      scalar MF_N2;
20
21      scalar TcH2S;
22      scalar TcCO2;
23      scalar TcN2;
24
25      scalar PcH2S;
26      scalar PcCO2;
27      scalar PcN2;
28
29      string lineString;
30      std::ifstream gasPPTYFile;
```

```
31      int PLength;
32      int TLength;
33      double PTRange [6];
34      double *Pdata;
35      double *Tdata;
36      double **gasPPTYData ;
37
38    public:
39
40    // class constructor
41    gasProperties
42    (
43      dimensionedScalar, dimensionedScalar, dimensionedScalar,
44      dimensionedScalar,  dimensionedScalar, dimensionedScalar,
45      dimensionedScalar, dimensionedScalar, dimensionedScalar,
46      dimensionedScalar, dimensionedScalar, dimensionedScalar
47    );
48
49    // read gas properties from file
50    void readPropertyData(const string &);
51
52    // interpolate for scalar value
53    scalar scalarInterpolate(const scalar &, const scalar &, const int);
54
55    // interpolate for volScalarField values
56    volScalarField scalarFieldInterpolate(const volScalarField &, const volScalarField
&, const int);
57
58
59    // calculate the viscosity of gas based on pressure and temperature
60    volScalarField getMu(const volScalarField & , const volScalarField &);
61
62    // calculate the viscosity of gas based on pressure and temperature
63    void updateMu(const volScalarField & , const volScalarField &, volScalarField & );
64
65    //update Cp based on temperature, pressure and updated values of Z, Z-derivatives
and Cpom
66    void updateCp(const volScalarField & , const volScalarField & , volScalarField &
);
67
68    // calculate the thermal expansion coefficient of gas based on pressure and
temperature
69    volScalarField getBetaT(const volScalarField & , const volScalarField &);
70
71    //update betaT based on temperature, Z and first derivative of Z w.r.t temperature
72    void updateBetaT(const volScalarField & , const volScalarField & , volScalarField
&);
73
74    // calculate psi of gas based on pressure and temperature
75    volScalarField getPsi(const volScalarField & , const volScalarField &);
76
77    // calculate psi of gas based on pressure and temperature
78    void updatePsi(const volScalarField & , const volScalarField &, volScalarField &
);
79
80    // calculate the density of gas based on pressure and temperature
81    volScalarField getRho(const volScalarField & , const volScalarField &);
82
83    //update the density of gas based on pressure and value of psi
84    void updateRho(const volScalarField & , const volScalarField & , volScalarField
&);
85
86    // update all gas properties based on pressure and temperature
87    void update
88    (
89    const volScalarField &, const volScalarField &, volScalarField &,
90    volScalarField &, volScalarField &, volScalarField &, volScalarField &
91    );
92
93    };
94    #endif
95
```

Code listing 11: Code for gas property reader

```
001    #include "gasProperties.H"
002    // class gasProperties Constructor
003    gasProperties::gasProperties
004    (
005     dimensionedScalar R, dimensionedScalar MM, dimensionedScalar SG,
006     dimensionedScalar MH2S, dimensionedScalar MCO2, dimensionedScalar MN2,
007     dimensionedScalar TH2S, dimensionedScalar TCO2, dimensionedScalar TN2,
008     dimensionedScalar PH2S, dimensionedScalar PCO2, dimensionedScalar PN2
009    )
010    {
011     Rmol = R.value();
012     MMass = MM.value();
013     Rgas = R.value()/MM.value();
014     SG_g = SG.value();
015
016     // mass fraction of H2S, CO2 & N2
017     MF_H2S = MH2S.value();
018     MF_CO2 = MCO2.value();
019     MF_N2 = MN2.value();
020
021     // critical temperatures of H2S, CO2 & N2
022     TcH2S = TH2S.value();
023     TcCO2 = TCO2.value();
024     TcN2 = TN2.value();
025
026     // critical pressures of H2S, CO2 & N2
027     PcH2S = PH2S.value();
028     PcCO2 = PCO2.value();
029     PcN2 = PN2.value();
030
031     // read the gas property data from file
032     readPropertyData("gasPPTY");
033
034
035
036    }
037
038    //---------------------------------------------------------------------------
--------------
039    //---------------------------------------------------------------------------
--------------
040    // Read gas property data from file
041    void gasProperties::readPropertyData(const string &fileName)
042    {
043
044     // read gas property data header
045     gasPPTYFile.open (fileName.c_str());
046     if (gasPPTYFile.is_open())
047             {
048             int count = 0;
049             while ( (std::getline (gasPPTYFile,lineString)) && (count <= 2) )
050             {
051                     if (count == 2)
052                     {
053                             std::cout << lineString << '\n';
054                             std::cout << "this is what i want to extract" << '\n';
055
056                             std::string delim = "\t";
057                             std::size_t last = 0;
058                             std::size_t next = 0;
059                             int ii = 0;
060                             while ((next = lineString.find(delim, last)) !=
string::npos)
061                             {
062                                     PTRange[ii] = atof(lineString.substr(last, next-
last).c_str()) ;
063                                     std::cout << PTRange[ii] << '\n';
064                                     last = next + delim.length();
065                                     ii++ ;
066                             }
067                             PTRange[5] = atof(lineString.substr(last).c_str());
068                             std::cout << PTRange[5] << '\n';
069                     }
070                     else
071                     {
072                             std::cout << lineString << '\n';
073                             std::cout << "check" << '\n';
074                     }
075                     count++;
076             }
```

```
077             gasPPTYFile.close();
078             }
079
080             else cout << "Unable to open file";
081
082     // initialize gasPPTYData array, based on the range of pressure and temperature
083     PLength = ((int)((PTRange[2] - PTRange[0])/PTRange[1])) + 1;       // number of
pressure values
084     TLength = ((int)((PTRange[5] - PTRange[3])/PTRange[4])) + 1;       // number of
temperature values
085
086     int rows = TLength*7;
087     int columns = PLength;
088
089     // memory allocated for elements of rows.
090     gasPPTYData = new double *[rows];
091
092     // memory allocated for elements of each column.
093     for( int i = 0; i < rows; i++)
094     {
095             gasPPTYData [i] = new double [columns];
096     }
097
098     // create array for Temperature and pressure values in the range used for the
property data
099     Pdata = new double [columns];
100     Tdata = new double [rows];
101
102     for( int i = 0; i < columns; i++)
103     {
104             Pdata [i] = PTRange[0] + (i*PTRange[1]);
105     }
106
107     for( int i = 0; i < rows; i++)
108     {
109             Tdata [i] = (PTRange[3] + (i*PTRange[4])) - ((floor(i/TLength))*TLength);
110     }
111
112     for (int ii = 0; ii < rows; ii++)
113     {
114             std::cout << "ii = " << ii << " Tdata = " << Tdata[ii] << '\n';
115     }
116
117     for (int ii = 0; ii < columns; ii++)
118     {
119             std::cout << "ii = " << ii << " Pdata = " << Pdata[ii] << '\n';
120     }
121
122     std::cout << "rows = " << rows << '\n';
123     std::cout << "columns = " << columns << '\n';
124
125     // read gas property data
126     gasPPTYFile.open (fileName.c_str());
127     if (gasPPTYFile.is_open())
128             {
129             int count = 0;
130             while ( (std::getline (gasPPTYFile,lineString)) && ((count >= 0)&&(count
<=(rows+3))) )
131             {
132                     if (count >= 4)
133                     {
134                             //std::cout << lineString << '\n';
135                             //std::cout << "this is what i want to extract" << '\n';
136
137                             std::string delim = "\t";
138                             std::size_t last = 0;
139                             std::size_t next = 0;
140                             int ii = 0;
141                             while ((next = lineString.find(delim, last)) !=
string::npos)
142                             {
143                                     gasPPTYData[count-4][ii] =
atof(lineString.substr(last, next-last).c_str()) ;
144                                     //std::cout << gasPPTYData[count-4][ii] << '\n';
145                                     last = next + delim.length();
146                                     ii++ ;
147                             }
148                             //std::cout << "ii     =            " << ii << '\n';
149                             gasPPTYData[count-4][ii] =
atof(lineString.substr(last).c_str());
```

```
150                         //std::cout << gasPPTYData[count][5] << '\n';
151                 }
152                 count++;
153                 //std::cout << "count  =      " << count << '\n';
154             }
155             std::cout << "count final  = " << count << '\n';
156             gasPPTYFile.close();
157 
158             std::cout << "first element of gasPPTYData = " << gasPPTYData[0][0] <<
'\n';
159             std::cout << "last element of gasPPTYData = " << gasPPTYData[rows-
1][columns-1] << '\n';
160             std::cout << "last element of gasPPTYData = " << gasPPTYData[1000][1] <<
'\n';
161             std::cout << "last element of gasPPTYData = " << gasPPTYData[1000][50] <<
'\n';
162             std::cout << "last element of gasPPTYData = " << gasPPTYData[1000][99] <<
'\n';
163             //std::cout << "last element of gasPPTYData = " <<
gasPPTYData[rows][columns] << '\n';
164             }
165 
166             else cout << "Unable to open file";
167 
168     }
169 
170     //-------------------------------------------------------------------------------
--------------
171     //-------------------------------------------------------------------------------
--------------
172     // interpolate for scalar value
173     scalar gasProperties::scalarInterpolate(const scalar & P, const scalar & T, int
pptyFlag)
174     {
175      // calculate the index for the location of given pressure and temperature in
table
176      // note: pptyFlag varies from 0 to N-1, where N = number of properties in
dataTable
177      scalar Pi = (P - PTRange[0])/PTRange[1] ;
178      scalar Ti = ((T - PTRange[3])/PTRange[4]) + (pptyFlag*TLength) ;
179 
180      scalar Qa, Qb, Qc;
181 
182      int floorPi = floor(Pi);
183      int ceilPi = ceil(Pi);
184      int floorTi = floor(Ti);
185      int ceilTi = ceil(Ti);
186 
187      if (floorTi == ceilTi)
188      {
189             Qa = gasPPTYData[floorTi][floorPi];
190             Qb = gasPPTYData[floorTi][ceilPi];
191      }
192      else
193      {
194             Qa = ((gasPPTYData[ceilTi][floorPi] - gasPPTYData[floorTi][floorPi]) /
(Tdata[ceilTi] - Tdata[floorTi])
195                          * (T - Tdata[floorTi])) + gasPPTYData[floorTi][floorPi];
196 
197             Qb = ((gasPPTYData[ceilTi][ceilPi] - gasPPTYData[floorTi][ceilPi]) /
(Tdata[ceilTi] - Tdata[floorTi])
198                          * (T - Tdata[floorTi])) + gasPPTYData[floorTi][ceilPi];
199      }
200 
201      if (floorPi == ceilPi)
202      {
203             Qc = Qa;
204      }
205      else
206      {
207             Qc = ((Qb - Qa) / (Pdata[ceilPi] - Pdata[floorPi]) * (P -
Pdata[floorPi])) + Qa;
208      }
209 
210      return Qc;
211     }
212 
213     //-------------------------------------------------------------------------------
--------------
```

```
214    //---------------------------------------------------------------------------
--------------
215    // interpolate for volScalarField values
216    volScalarField gasProperties::scalarFieldInterpolate(const volScalarField & P,
const volScalarField & T, int pptyFlag)
217    {
218     dimensionedScalar PUnits ("PUnits", P.dimensions(),1);
219     volScalarField ppty = (P-P)/PUnits;
220
221     scalarField& pptyCells = ppty.internalField();
222     const scalarField& PCells = P.internalField();
223        const scalarField& TCells = T.internalField();
224
225        forAll(pptyCells, cellI)
226        {
227            pptyCells[cellI] = scalarInterpolate(PCells[cellI], TCells[cellI],
pptyFlag);
228        }
229
230        forAll(ppty.boundaryField(), patchI)
231        {
232            fvPatchScalarField& pppty = ppty.boundaryField()[patchI];
233            const fvPatchScalarField& pP = P.boundaryField()[patchI];
234            const fvPatchScalarField& pT = T.boundaryField()[patchI];
235
236            forAll(pppty, faceI)
237            {
238                pppty[faceI] = scalarInterpolate(pP[faceI], pT[faceI], pptyFlag);
239            }
240        }
241
242     return ppty;
243    }
244
245    //---------------------------------------------------------------------------
-----------
246    //---------------------------------------------------------------------------
-----------
247    // calculate the viscosity of gas based on pressure and temperature
248    volScalarField gasProperties::getMu(const volScalarField & p, const
volScalarField & T)
249    {
250     dimensionedScalar muUnits ("muUnits", dimensionSet(1,-1,-1,0,0,0,0), 1);
251     volScalarField mu = scalarFieldInterpolate(p, T, 4) * muUnits;
252     return mu;
253    }
254
255    //---------------------------------------------------------------------------
-----------
256    //---------------------------------------------------------------------------
-----------
257    // calculate the viscosity of gas based on pressure and temperature
258    void gasProperties::updateMu(const volScalarField & p, const volScalarField & T,
volScalarField & _mu)
259    {
260     volScalarField mu = getMu(p, T);
261     _mu = mu;
262    }
263
264    //---------------------------------------------------------------------------
-----------
265    //---------------------------------------------------------------------------
-----------
266    // calculate the specific heat capacity of gas based on pressure and temperature
267    volScalarField gasProperties::getCp(const volScalarField & p, const
volScalarField & T)
268    {
269     dimensionedScalar CpUnits ("CpUnits", dimensionSet(0,2,-2,-1,0,0,0),1);
270     volScalarField Cp = scalarFieldInterpolate(p, T, 2) * CpUnits;
271     return Cp;
272    }
273
274    //---------------------------------------------------------------------------
-----------
275    //---------------------------------------------------------------------------
-----------
276    // update the specific heat capacity of gas based on pressure and temperature
277    void gasProperties::updateCp(const volScalarField & p, const volScalarField & T,
volScalarField & _Cp)
278    {
```

```
279     volScalarField Cp = getCp(p, T);
280     _Cp = Cp;
281     }
282
283     //--------------------------------------------------------------------------------
-----------
284     //--------------------------------------------------------------------------------
-----------
285     // calculate the specific heat capacity of gas based on pressure and temperature
286     volScalarField gasProperties::getBetaT(const volScalarField & p, const
volScalarField & T)
287     {
288     dimensionedScalar betaTUnits ("betaTUnits", dimensionSet(0,0,0,-1,0,0,0), 1);
289     volScalarField betaT = scalarFieldInterpolate(p, T, 5) * betaTUnits;
290     return betaT;
291     }
292
293     //--------------------------------------------------------------------------------
-----------
294     //--------------------------------------------------------------------------------
-----------
295     // update the specific heat capacity of gas based on pressure and temperature
296     void gasProperties::updateBetaT(const volScalarField & p, const volScalarField &
T, volScalarField & _betaT)
297     {
298     volScalarField betaT = getBetaT(p, T);
299     _betaT = betaT;
300     }
301
302     //--------------------------------------------------------------------------------
-----------
303     //--------------------------------------------------------------------------------
-----------
304     // calculate the specific heat capacity of gas based on pressure and temperature
305     volScalarField gasProperties::getPsi(const volScalarField & p, const
volScalarField & T)
306     {
307     dimensionedScalar psiUnits ("psiUnits", dimensionSet(0,-2,2,0,0,0,0),1);
308     volScalarField psi = scalarFieldInterpolate(p, T, 0) * psiUnits;
309     return psi;
310     }
311
312     //--------------------------------------------------------------------------------
-----------
313     //--------------------------------------------------------------------------------
-----------
314     // update the specific heat capacity of gas based on pressure and temperature
315     void gasProperties::updatePsi(const volScalarField & p, const volScalarField & T,
volScalarField & _psi)
316     {
317     volScalarField psi = getPsi(p, T);
318     _psi = psi;
319     }
320
321     //--------------------------------------------------------------------------------
-----------
322     //--------------------------------------------------------------------------------
-----------
323     // calculate the specific heat capacity of gas based on pressure and temperature
324     volScalarField gasProperties::getRho(const volScalarField & p, const
volScalarField & T)
325     {
326     dimensionedScalar rhoUnits ("rhoUnits", dimensionSet(1,-3,0,0,0,0,0),1);
327     volScalarField rho = scalarFieldInterpolate(p, T, 1) * rhoUnits;
328     return rho;
329     }
330
331     //--------------------------------------------------------------------------------
-----------
332     //--------------------------------------------------------------------------------
-----------
333     // update the specific heat capacity of gas based on pressure and temperature
334     void gasProperties::updateRho(const volScalarField & p, const volScalarField & T,
volScalarField & _rho)
335     {
336     volScalarField rho = getRho(p, T);
337     _rho = rho;
338     }
339
340
```

```
341
342     // update all gas properties based on pressure and temperature
343     void gasProperties::update
344     (
345     const volScalarField & p, const volScalarField & T,
346     volScalarField & _mu, volScalarField & _Cp, volScalarField & _betaT,
347     volScalarField & _psi, volScalarField & _rho
348     )
349     {
350      //update mu
351      updateMu(p, T, _mu);
352
353      //update Cp
354      updateCp(p, T, _Cp);
355
356      //update betaT
357      updateBetaT(p, T, _betaT);
358
359      //update K
360      //updateK(p, T, _K);
361
362      //update psi
363      updatePsi(p, T, _psi);
364
365      //update rho
366      updateRho(p, T, _rho);
367     }
368
369
370
```

Appendix D: Case Study Data for Chapter 3

Table D-1: Case study for numerical simulation and analytical solutions

Property	**Symbol**	**Value**	**Unit**
Thermal conductivity	K_T	1.7	W/mK
Porosity	ϕ	0.15	
Specific heat capacity of gas	Cp_f	3030	J/kgK
Ratio of specific heat		1.31	
Specific gas constant	R	519.6563	J/kgK
Specific heat capacity of rock	Cp_r	920	J/kgK
Density of rock	ρ_r	2500	kg/m^3
Specific gravity of gas	$S.G_f$	0.605	
Pseudo-pressure at initial reservoir pressure	ψ_i	16×10^{18}	$Pa^2/Pa.s$
Viscosity at initial reservoir pressure	μ_i	1.52×10^{-5}	$Pa.s$
Total formation compressibility at initial condition	Cf_i	8.724×10^{-8}	Pa^{-1}
Gas flow rate at standard conditions	Qsc	2.3013	m^3/s
Pressure at standard conditions	P_{sc}	101325	Pa
Temperature at standard conditions	T_{sc}	289	K
Initial reservoir pressure	P_i	1.4×10^7	Pa
Initial reservoir temperature	T_i	322	K
Reservoir permeability	k	10×10^{-15}	m^2
Reservoir thickness	h	12	m
Well radius	r_w	0.125	m
Reservoir boundary radius	r_e	304.8	m
Thermal expansivity of gas	β_T	0.00522	K^{-1}
Constants in pressure solution (ERCB 1979)	Γ	111.888	Pa/K
	λ	1	

The case study used here describes a typical gas producing well and is taken from ERCB (1979)

Table D-2: Case study for numerical simulation and analytical solutions

Property	**Symbol**	**Case study 1**	**Case study 2**	**Case study 3**	**Unit**
Thermal conductivity	K_T	1.7	1.7	1.7	W/mK
Porosity	ϕ	0.15	0.15	0.15	
Specific heat capacity of gas	Cp_f	3030	3030	3030	J/kgK
Ratio of specific heat		1.31	1.31	1.31	
Specific gas constant	R	519.6563	519.6563	519.6563	J/kgK
Specific heat capacity of rock	Cp_r	920	920	920	J/kgK
Density of rock	ρ_r	2500	2500	2500	kg/m^3
Specific gravity of gas	$S.G_f$	0.605	0.605	0.605	
Pseudo-pressure at initial reservoir pressure	ψ_i	16	16	16	$\times 10^{18}\ Pa^2/Pa.s$
Viscosity at initial reservoir pressure	μ_i	1.52	1.52	1.52	$\times 10^{-5}\ Pa.s$
Total formation compressibility at initial condition	Cf_i	8.724	8.724	8.724	$\times 10^{-8}\ Pa^{-1}$
Gas flow rate at standard conditions	Qsc	2.3013	16.109	34.5195	m^3/s
Pressure at standard conditions	P_{sc}	101325	101325	101325	Pa
Temperature at standard conditions	T_{sc}	289	289	289	K
Initial reservoir pressure	P_i	1.4	1.4	1.4	$\times 10^7\ Pa$
Initial reservoir temperature	T_i	322	322	322	K
Reservoir permeability	k	10	100	100	$\times 10^{-15}\ m^2$
Reservoir thickness	h	30	30	60	m
Well radius	r_w	0.125	0.125	0.125	m

Reservoir boundary radius	r_e	304.8	304.8	304.8	m
Thermal expansivity of gas	β_T	0.00522	0.00522	0.00522	K^{-1}
Constants in pressure solution (ERCB 1979)	Γ	111.888	111.888	111.888	Pa/K
	λ	1	1	1	

Table D-3: Gas properties used to analytically model the 3 synthetic case studies described in Section 3.6.1

Property	**Symbol**	**Case Study 1**	**Case Study 2**	**Case Study 3**	**Unit**
Stabilized pressure	P_{stab}	1.2891	1.3230	1.3174	$\times 10^7\ Pa$
Viscosity at average condition (i.e. Ti and Pstab)	μ_{avg}	1.4911	1.4968	1.4954	$\times 10^{-5}\ Pa.s$
Density at average condition (i.e. Ti and Pstab)	ρ_{avg}	91.1318	92.1897	91.9344	kg/m^3
Specific heat capacity at average condition (i.e. Ti and Pstab)	Cp_{avg}	3078.9	3086.8	3084.9	J/kgK
Thermal expansion coefficient at average condition (i.e. Ti and Pstab)	β_{Tavg}	5.16063	5.17286	5.16991	$\times 10^{-3}\ K^{-1}$
Slope of pressure pseudo-pressure relationship	B	4.6337	4.5640	4.5724	$\times 10^{-13}\ s$
Intercept of pressure pseudo-pressure relationship	A	6.5613	6.6749	6.6602	$\times 10^6\ Pa$

Table D-4: Gas and formation properties used for the analytical solution in the real case study described in Section 3.6.2

Property	**Symbol**	**Value**	**Unit**
Stabilized pressure	P_{stab}	9.379×10^{6}	Pa
Viscosity at average condition (i.e. Ti and Pstab)	μ_{avg}	1.373×10^{-5}	$Pa.s$
Specific gravity of gas	$S.G$	0.605	
Density at average condition (i.e. Ti and Pstab)	ρ_{avg}	60.73	kg/m^3
Specific heat capacity at average condition (i.e. Ti and Pstab)	Cp_{avg}	2840	J/kgK
Thermal expansion coefficient at average condition (i.e. Ti and Pstab)	β_{Tavg}	4.355×10^{-3}	K^{-1}
Specific heat capacity of rock	Cp_r	920	J/kgK
Density of rock	ρ_r	2500	kg/m^3
Slope of pressure pseudo-pressure relationship	B	5.0×10^{-13}	s
Intercept of pressure pseudo-pressure relationship	A	6.0×10^{6}	Pa

Appendix E: Case Study Data for Chapter 4

To determine the gas properties over the range of pressure and temperature in the reservoir, the following properties (Table E-1) were used along with the Benedict-Webb-Rubin (BWR) EOS.

Table E-1: Natural gas properties

Property	**Symbol**	**Value**	**Unit**
Pseudo critical temperature	T_{pc}	-116.59	$°F$
Pseudo critical pressure	P_{pc}	676.22	Psi
Thermal conductivity	K_T	0.982	Btu/(hr.ft^2-°F/ft)
Molal specific heat capacity of natural gas at ideal conditions	Cp_o	8.1	Btu/(lb.mol°F)
Universal gas constant	$\tilde{R}$	1.987	Btu/(lb.mol°F)
Specific gas constant	R	124.12	Btu/(lbm°F)
Specific gravity of gas	$S.G_f$	0.605	
Viscosity at initial reservoir pressure	μ_i	0.0152	cP
Mass fraction of H_2S in natural gas		0	
Mass fraction of CO_2 in natural gas		0	
Mass fraction of N_2 in natural gas		0	

Table E-2: Case study for numerical simulation and analytical solutions

Property	**Symbol**	**Value**	**Unit**
Thermal conductivity	K_T	0.982	Btu/(hr.ft^2-°F/ft)
Porosity	ϕ	0.15	
Specific heat capacity of gas	Cp_f	723.70	Btu/(lbm°F)
Ratio of specific heat		1.31	
Specific gas constant	R	124.12	Btu/(lbm°F)
Specific heat capacity of rock	Cp_r	219.74	Btu/(lbm°F)
Density of rock	ρ_r	156.07	lbm/ft^3
Specific gravity of gas	$S.G_f$	0.605	
Pseudo-pressure at initial reservoir pressure	ψ_i	3.366×10^{14}	Psi^2/cP
Viscosity at initial reservoir pressure	μ_i	0.0152	Cp
Total formation compressibility at initial condition	Cf_i	6.015×10^{-4}	/Psi
Gas flow rate at standard conditions	Qsc	7.0216	MMScf/day
Pressure at standard conditions	P_{sc}	14.7	Psi
Temperature at standard conditions	T_{sc}	60.53	°F
Initial reservoir pressure	P_i	2030.5	Psi
Initial reservoir temperature	T_i	119.93	°F
Reservoir permeability	k	10	mD
Reservoir thickness	h	39	ft
Well radius	r_w	0.39	ft
Reservoir boundary radius	r_e	1000	ft
Thermal expansion coefficient of gas	β_T	0.009396	/°F
Constants in pressure solution (ERCB 1979)	Γ	0.0292	Psi/°F
	λ	1	

Table E-3: Case study for non-Darcy effect

		Q_{sc} $[MM\ scf/day]$	k $[mD]$	$\beta[1/m]$
$r_{nD} = 0.1$	Darcy	1.513	10	0
	Non-Darcy	1.513	10	4.21×10^9
$r_{nD} = 0.2$	Darcy	3.026	10	0
	Non-Darcy	3.026	10	4.21×10^9
$r_{nD} = 0.3$	Darcy	4.540	10	0
	Non-Darcy	4.540	10	4.21×10^9
$r_{nD} = 0.4$	Darcy	6.053	10	0
	Non-Darcy	6.053	10	4.21×10^9
$r_{nD} = 0.5$	Darcy	7.567	10	0
	Non-Darcy	7.567	10	4.21×10^9

Estimating the Rate and Permeability*Thickness Values

These case studies use the data provided in Table E-2 of Appendix E, with different surface production rate, permeability and thickness values input in the simulation. The values used in the simulation (Cases 2 and 3)are given in Table E-4, while the result from the rate and permeability*thickness product estimation are given in Table E-5, and also plotted in Figures 4-12(a), E-1(a) & E-1(b). Case 1 is the base case described in the paper, and is presented here for comparison.

Table E-4: Case study description for rate and permeability thickness estimation

Property	**Symbol**	**Case1**	**Case2**	**Case3**	**Unit**
Gas flow rate at standard conditions	Qsc	7.0216	7.0216	105.3	MMScf/day
Permeability	k	10	10	100	mD
Formation thickness	h	39	98	196	ft

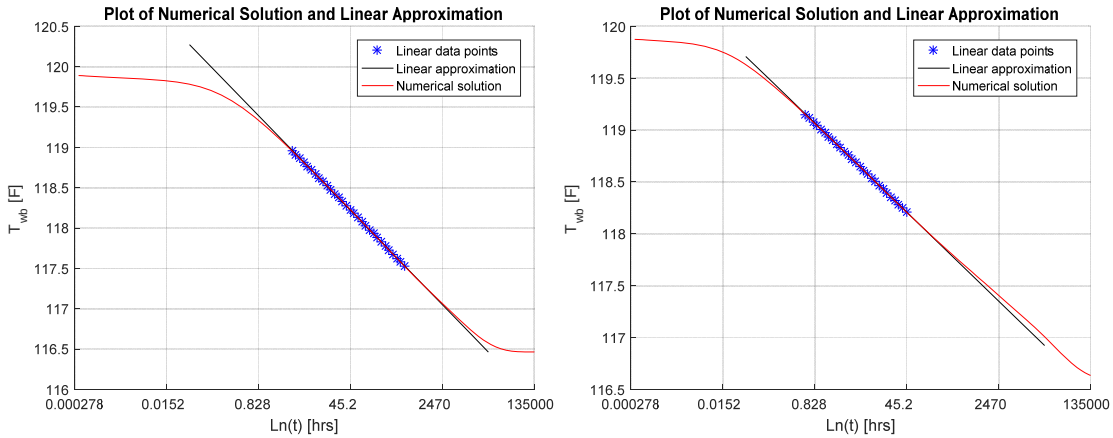

Figure E-1: Surface production rate and downhole temperature for Case 2 (left) and Case 3 (right)

Table E-5: Case study results for rate and permeability thickness estimation

Property	**Symbol**	**Case 1**	**Case 2**	**Case 3**	**Unit**
Stabilized pressure	P_{stab}	1635.38	1869.73	1910.72	psi
Gas viscosity at average condition (i.e. T_i, P_{avg})	μ_{avg}	0.01463	0.01494	0.014998	cP
Gas density at average condition (i.e. T_i, P_{avg})	ρ_{avg}	5.3654	5.7273	5.7904	lb/ft^3
Gas specific heat capacity at average condition (i.e. T_i, P_{avg})	Cp_{avg}	725.83	736.47	738.27	$Btu/(lbm^oF)$
Gas thermal expansion coefficient at average condition (i.e. T_i, P_{avg})	$\beta_{T,avg}$	0.009168	0.009302	0.009323	$/°F$

Slope of pressure pseudo-pressure relationship	B	5.0535	4.8302	4.7521	$\times 10^{-13} s$
Semilog slope of linear portion	a	-0.8489	-0.2930	-0.2141	$°F/ln(sec)$
Estimated gas flow rate at standard conditions	Qsc	7.369	6.926	103.63	$MMScf/day$
Estimated permeability thickness	kh	380.4	1011.8	20288	$mD.ft$

As can be seen from Tables E-1 and E-2, the kh estimation error in these three cases is less than 4%.

Estimating Parameters of the Near-Wellbore Damage Zone

These case studies use the data provided in Table E-2 of Appendix E, while a near-wellbore zone of lower permeability is included in the simulation model. The damage zone radius is denoted as r_d while the permeability of the damage zone is k_{skin}. The values for the two simulated cases (Cases 2 and 3) are given in Table E-6, while the result from the near-wellbore analyses is given in Table E-7, and also plotted in Figures 4-12(b), E-2(a) & E-2(b). Case 1 is the base case described in the paper, and is presented here for comparison. As can be seen from Tables E-6 and E-7, the damage zone kh estimation error in these three cases is less than 15%.

Table E-6: Case study description for near-wellbore analysis

Property	Symbol	Case1	Case2	Case3	Unit
Radius of damage zone	r_d	3.28	1.64	3.28	ft
Permeability of damage zone	k	5	5	3	mD
Formation thickness	h	39	39	39	ft

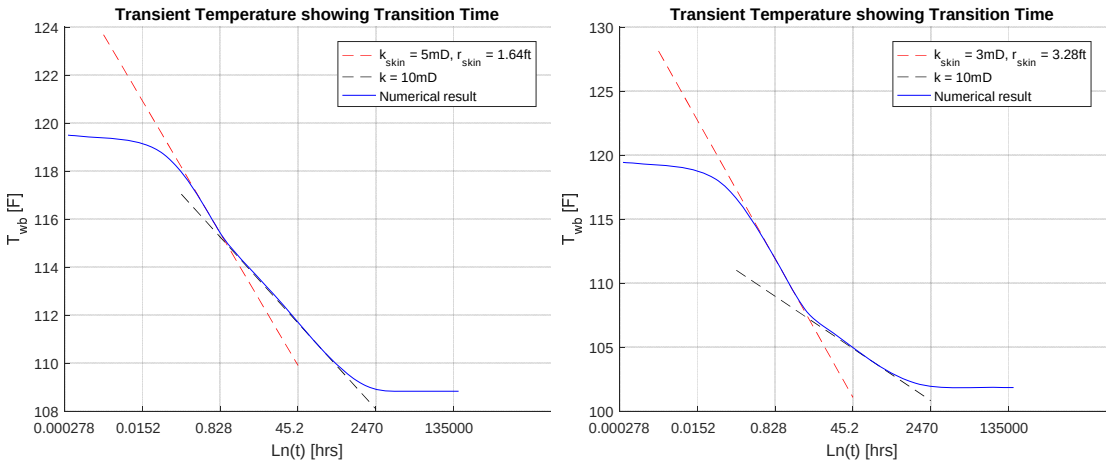

Figure E-2: Transient temperature signal and the slopes corresponding to the damage zone and the clean formation in Case 2 (left) and Case 3 (right)

Table E-7: Case study results for near-wellbore analysis

Property	**Symbol**	**Case1**	**Case2**	**Case3**	**Unit**
Transition time	t_d	3.886	1.16	4.697	hr
Pressure at transition time	P_{td}	1650.45	1718.72	1504.49	psi
Gas viscosity at average condition (i.e. T_i, P_{avg})	μ_{avg}	0.01465	0.01474	0.01446	cP
Gas density at average condition (i.e. T_i, P_{avg})	ρ_{avg}	5.3929	5.4988	5.1664	lb/ft^3
Gas specific heat capacity at average condition (i.e. T_i, P_{avg})	Cp_{avg}	726.73	729.95	719.85	$Btu/(lbm^oF)$
Gas thermal expansion coefficient at average condition (i.e. T_i, P_{avg})	$\beta_{T,avg}$	0.009189	0.009233	0.009096	$/°F$
Slope of pressure pseudo-pressure relationship	B	5.0	5.0	5.0	$\times 10^{-13}s$
Semilog slope of linear portion	a_{skin}	-1.5754	-0.7653	2.7054	$°F/ln(sec)$
Estimated, damage zone radius	r_d	3.08	1.73	3.32	ft
Estimated, damage zone permeability thickness	kh_{skin}	202.41	228.93	120.78	$mD.ft$

Appendix F: Case Studies for Chapter 6

Table F-1: Parameters for setting up OLGA wellbore model

Property	**Value**	**Unit**
Well length	500	m
Number of sections	10	
Diameter	0.254	m
Roughness	5×10^{-5}	m
Location of source	Section 1	
Thermal conductivity of casing	50	W/mK
Density of casing	7850	kg/m^3
Specific heat capacity of casing	500	J/kgK
Thickness of casing	12.7	mm
Thermal conductivity of formation	1.59	W/mK
Density of formation	2243	kg/m^3
Specific heat capacity of formation	1256	J/kgK
Specific gravity of gas	0.605	
Watercut	0	
Liquid gas ratio	0	
GOR model	LASATER	
Initial outlet temperature	298.15	K
Initial outlet pressure	120	bar
Initial inlet temperature	321.85	K
Initial inlet pressure	140	bar
Mass flow	1.55	kg/s
Standard flow rate	200,000	m^3/s
Phase	Gas	
Top node (NODE_3) type	Pressure	

Top node (NODE_3) temperature	298.15	K
Top node (NODE_3) pressure	98	bar
Bottom node (NODE_3) type	Closed	